An Investigation of the Heterogeneity of Mitochondrial Protein Biogenesis in Wheat (*Triticum aestivum* L.)

Janet M. Paterson

A thesis submitted to the University of St Andrews for the degree of Doctor of Philosophy in the School of Biology.

July 2001

CONTENTS

ABSTRACT

The natural developmental gradient of wheat (*Triticum aestivum* L., cv. Maris Huntsman) primary leaves was used as a model to investigate mitochondrial protein development. In monocot leaves, new cells originate in the basal intercalary meristem and are displaced away from the leaf base as they mature, creating a gradient of cell age from base to tip. Cell age was calculated and related to the position of cells relative to the basal meristem. Age-related changes in physiology (photosynthesis and respiration) and cell ultrastructure (cellular and subcellular compartmentation) were determined using stereological methods.

Immunocytochemical techniques were utilised to investigate the development of mitochondrial pyruvate dehydrogenase complex (PDC) and glycine decarboxylase complex (GDC). Using specific antibodies, the E1α, E1β, E2 and E3 subunits of PDC and the P- and L-proteins of GDC were localised in tissue from a range of developmental stages along the leaf. Initially, this was done by probing protein extracts from tranverse leaf sections, using a slot blot technique. Following this, proteins were detected using immunogold localisation, and the number of gold particles per unit mitochondrial area in mesophyll and phloem companion cells were counted on tissue sections. Since total mitochondrial volume per cell was found to remain constant throughout leaf development, the counts represented a measurement of relative mitochondrial and cellular protein concentration.

Both techniques revealed a heterogeneity in mitochondrial protein development, and immunogold analysis indicated a difference in development between the two cell types examined. PDC E1α and E1β development showed similarities with respiratory development in both cell types, while development of PDC E2 and E3 in mesophyll cells, paralleled that of photosynthesis. In companion cells, E2 and E3 exhibited developmental patterns similar to respiratory development in certain regions of the leaf. In mesophyll cells, development of GDC P- and L-proteins was similar to photosynthetic development, while in companion cells, the opposite trend was observed. Results are discussed in relation to protein function and the development of leaf cell metabolism.

DECLARATIONS

I, Janet M. Paterson, hereby certify that this thesis, which is approximately 40,000 words in length, has been written by me, that it is the record of work carried out by me and that it has not been submitted in any previous application for a higher degree.

date ..... signature .....

I was admitted as a research student in May 1997 and as a candidate for the degree of PhD in May 1997; the higher study for which this is a record was carried out in the University of St Andrews between 1997 and 2001.

date ..... signature .....

DECLARATION OF SUPERVISOR

I hereby certify that the candidate has fulfilled the conditions of the Resolution and Regulations appropriate for the degree of PhD in the University of St Andrews and that the candidate is qualified to submit this thesis in application for that degree.

date ..... signature .....

Dr Alyson K. Tobin

COPYRIGHT

DEDICATION

This thesis is dedicated to the memory of my great-grandmother Janet Johnston, who having been denied an education due to poverty and discrimination, became well known in Lanarkshire for encouraging local people, especially women, to continue at school and attend University.

ACKNOWLEDGEMENTS

I would like to thank my supervisor, Dr Alyson K. Tobin for her guidance and patience over the last 4 years, and for the opportunity of working in the fields of plant mitochondrial development and metabolism. Thanks also to Harry Hodge, Ray Stevenson, and the other technicians in the Department, and for Harry's constant stream of fabricated stories, e.g. the one about the transgenic greenhouse being turned into a seal tank, and the one about Alyson being awarded a grant to grow transgenic watermelons. Many thanks to EM technician John Mackie who provided invaluable instruction and advice in the use of the electron microscope. Thanks to my mum, dad, and brothers James and Thomas, with special thanks to Thomas for maintaining my computer and literally rebuilding it every time the screen went blank. I would like to thank my friends in the Plant Science Laboratory, past and present: Pam, Kirsty, David, Urte, Juliet, Mark, Laura and Jonathan, my flatmates Karen, Jenny and Marion, and my other friends in St Andrews and Glasgow. Finally, many thanks and lots of love to Michael.

ABBREVIATIONS

2-D	2-dimensional
3-D	3-dimensional
A_A	areal fraction
acetyl CoA	acetyl coenzyme A
ANOVA	analysis of variance
APAAP	alkaline phosphatase-anti-alkaline phosphatase
ATP	adenosine triphosphate
BCIP	bromochloroindoylphosphate
BSA	bovine serum albumin
CAM	Crassulacean acid metabolism
CCD	charge-coupled device
CoA-SH	coenzyme A
cv.	cultivar
d	day(s)
dicot	dicotyledon
DNA	deoxyribonucleic acid
ECL	enhanced chemiluminescence
EDTA	ethylene diamine tetraacetic acid
EM	electron microscope/microscopy
FAD	flavin adenine dinucleotide
$FADH_2$	reduced flavin adenine dinucleotide
g	relative centrifugal force
GDC	glycine decarboxylase complex
GFP	green fluorescent protein
h	hour(s)
HRP	horseradish peroxidase
Ig	immunoglobulin
kDa	kiloDaltons
LM	light microscope/microscopy
min(s)	minute(s)
monocot	monocotyledon
NAD^+	nicotinamide adenine dinucleotide

NADH	reduced nicotinamide adenine dinucleotide
NADPH	reduced nicotinamide adenine dinucleotide phosphate
NBT	nitroblue tetrazolium
N_V	numerical density
OAA	oxaloacetic acid
OPP	oxidative pentose phosphate
PAGE	polyacrylamide gel electrophoresis
PAP	peroxidase-anti-peroxidase
PAR	photosynthetically active radiation (400-700nm)
PCO	photosynthetic carbon oxidation
PDC	pyruvate dehydrogenase complex
PDH	pyruvate dehydrogenase
RNA	ribonucleic acid
r.p.m.	revolutions per minute
RSE	relative segmental elongation
Rubisco	ribulose 1,5-biphosphate carboxylase/oxygenase
Rubisco-LSU	ribulose 1,5-biphosphate carboxylase/oxygenase, large subunit
RuBP	ribulose 1,5-biphosphate
SDS	sodium dodecyl sulphate
SER	segmental elongation rate
SHMT	serine hydroxymethyltransferase
S_V	surface density
TA	transverse area
TBS	Tris-buffered saline
TCA	tricarboxylic acid
TEM	transmission electron microscope/microscopy
TEMED	N, N, N', N' tetramethylethylenediamine
THF	tetrahydrofolate
TPP	thiamine pyrophosphate
Tris	tris (hydroxymethyl) methylamine
Tween-20	polyoxyethylenesorbitan
UV	ultraviolet
v/v	volume/volume
V_D	velocity of displacement
V_V	volume fraction
w/v	weight/volume

LIST OF FIGURES

LIST OF TABLES

CHAPTER 1: INTRODUCTION

1.1 Plant Growth and Development

1.1.1 General Background and Definitions

The study of plant growth and development is of great interest to plant biologists, and there are few areas of plant science in which an understanding of these processes is not advantageous. By definition, growth can be described as an irreversible increase in volume of cells, organs or the whole plant in general. Development or morphogenesis, however, collectively refers to all the processes and events by which a zygote is transformed into a mature and functioning plant, and growth is intrinsically associated with this (Wareing & Phillips, 1981; Salisbury & Ross, 1992).

Although much is known regarding the biochemical and physiological events which occur during plant growth and development, continuing active research in this huge field indicates that much remains to be investigated. Many of the events occurring throughout plant development are well characterised, but how these events come about, i.e. what ultimately determines and regulates specific gene transcription to produce specific proteins at a given time, remains largely unanswered. To fully understand plant growth and development, it must be investigated from several different perspectives, involving research at the physiological, biochemical, genetic and molecular levels (Fosket, 1994; Van Volkenburgh, 1999). In addition, it must be noted that plant development is only partly genetically determined and is strongly influenced by environmental factors such as light and temperature (Terry, Waldron & Taylor, 1983; Tardieu *et al.*, 2000). Being sedentary organisms, plants must be capable of adapting to changing environmental conditions which may affect their function and survival.

Plant growth and development is ultimately governed by three basic processes - cell division, cell enlargement and cell differentiation (Dale, 1988).

Cell division occurs only in specific zones - meristems- within the plant. Primary meristems (formed in the embryo) are located in the root and shoot apices, while secondary meristems (formed after germination) occur in the vascular cambium, above the leaf nodes in monocots, and at the leaf bases in the Gramineae (Lyndon, 1990a). Since cells do not increase in size as a result of cell division, this process is not in itself growth. However, as there is a limit on the final size of all cell types, division is vital to plant

growth and development as a provider of new cells which may then proceed to enlarge and differentiate. The plane in which cells divide, determines the position of daughter cells within the body of the plant. Cell division within meristems is ultimately controlled by the complex events of the cell cycle, an ordered sequence of events spanning the time at which a cell divides to the time at which the resulting daughter cells divide again (Francis, 1992). Precise regulation of this co-ordinates plant growth and development in response to changes in the environment (Doerner, 1994).

Cell enlargement in plants occurs mainly by water uptake by the vacuole and cytoplasm via turgor-pressure driven expansion of the temporarily more elastic cell wall (Ray, Green & Cleland, 1972). Enlargement is usually highly polarised and cells tend to elongate in one dimension rather than expand in several directions, due to the orientation of cell wall cellulose fibres in one direction (Dale, 1988). In a stem or root, for example, this elongation occurs longitudinally, resulting in overall shoot or root elongation, without an equivalent increase in girth. Cell elongation occurs in a relatively defined elongation zone (according to species) immediately adjacent to the meristem, where cells attain their maximum size. Hence, cell enlargement is restricted to meristems and associated elongation zones, and elongating cells are displaced away from the meristem due to the formation of new cells there. It should be noted that reversible elastic deformation, a process by which plant cells change size via water uptake in response to temporary changes in turgor pressure, is separate from the irreversible process of growth (Proseus, Ortega & Boyer, 1999).

Following elongation, cells may then proceed to differentiate, i.e. become structurally specialised in some way to perform a particular function in the plant. This process usually starts with undifferentiated cells, although some specialised cells are capable of dedifferentiation into another cell type. The property of totipotency possessed by all plant cells means that some unspecialised cells with identical genes can differentiate to acquire different morphologies and functions as required, and in fact, a whole new plant can be produced from a single cell under suitable environmental conditions (Lyndon, 1990b). The variety of ways in which cells divide, elongate and differentiate account for the amazing range of specialised cells, tissues and organs that constitute a mature plant, and ultimately for the remarkable range and diversity of living plant species.

1.1.2 Leaf Development

Regardless of the final shape and size of leaves, all have similar origins as primordia - masses of dividing cells - which develop near the surface of shoot apices and eventually form visible outgrowths. The whole shoot and leaves of a plant originate from such activity in the apical meristem (Lyndon, 1983). Leaf primordia develop around the apex in a characteristic pattern (phyllotaxis) according to species, reflecting the distinct leaf architecture possessed by different plants (Dengler & Kang, 2001). Cell division continues at the primordia tip until a rudimentary leaf forms, and the extent and direction of cell division and expansion in primordia controls the shape of developing leaves. After this, meristematic activity occurs throughout the length of the primordia before altering again, according to species.

In dicots, most cell division ceases typically before the leaf has attained half its final size, the remaining growth occurring as a result of cell expansion (Lyndon, 1983). In the Gramineae however, cell division terminates at the leaf tip and then continues to cease down the leaf and eventually remains only in the leaf base as an intercalary meristem (Nelson & MacAdam, 1989). Such intercalary meristems (so-named as the meristematic tissue is intercalated or inserted between regions of older tissue) can remain potentially active for long periods of time so that grass which is constantly grazed or mown, will re-grow (Salisbury & Ross, 1992). Of course, successful leaf formation is vital to plant survival since leaves are - with some exceptions such as cacti - the major light intercepting structures of the plant.

1.1.3 Studies of Wheat Primary Leaf Development

There has been extensive study of the growth and development of *Triticum aestivum* (wheat), and of the development of cereals and the Gramineae in general, since they are especially suitable for leaf developmental studies.

In developing leaves of dicotyledon (dicot) plants, there are several meristematic zones located across the lamina, making it difficult to identify cells of a particular age and corresponding developmental stage. In monocotyledon (monocot) plants such as wheat however, all cell division in the young leaf occurs near the base within the basal intercalary meristem. This generates a developmental gradient along the leaf from base to tip, and provides a useful model for leaf developmental studies. The youngest cells are located just above the meristem with cells increasing in age distal to this, and with the

most functionally mature cells occurring at the leaf tip (Nelson & MacAdam, 1989; Tobin & Rogers, 1992). This means that developmental studies conducted at any point along the leaf, are concerned with cells of known age. In wheat for example, primary leaves are best studied when approximately seven days old (as in the present study), since at this time, the developmental gradient along the leaf is at its greatest (Tobin, Ridley & Stewart 1985).

1.1.4 Ultrastructural Development of Wheat Leaf Cells

The ultrastructure of higher plant cells is well documented and reflects the complex metabolic networks operating within the cell, which are essential for plant function and survival. Various levels of compartmentation within the cell contribute to metabolic control along with factors such as enzyme regulation, so that metabolism is regulated in both space and time (Robards, 1970; Beevers, 1991). The developmental gradient which exists along the wheat primary leaf (see Section 1.1.3) provides an excellent model for investigating ultrastructural changes taking place in plant cells throughout development. These changes in ultrastructure occur according to changes in metabolic role - immature heterotrophic cells recently produced via cell division in the basal intercalary meristem, develop into mature autotrophic cells as they migrate away from the leaf base (Tobin *et al.*, 1988). Plant organelle biogenesis has been studied mainly with reference to chloroplasts, with comparatively little information available regarding mitochondrial development, and even less concerning other cellular organelles. Current knowledge regarding chloroplastic development in wheat is outlined as follows, and wheat leaf mitochondrial structural development is discussed in Section 1.2.3.

Considerable changes take place in chloroplastic structure and population in mesophyll cells of developing wheat leaves. All higher plant plastids arise as tiny unspecialised proplastids with elementary internal membrane structure, within meristematic cells at the leaf base. Proplastids go through three stages of development, terminating in an ameboid stage prior to the formation of immature chloroplasts (Whatley, 1974). In the course of these stages, proplastids increase in size, followed by the synthesis and subsequent degeneration of starch grains within the organelles. In wheat, as the meristematic cells divide, the proplastids divide accordingly by fission, maintaining an equal number per cell. As cells are displaced from the meristem, the thylakoid membranes and other elements necessary for photosynthesis develop within

the plastids, e.g. the number of granal sacs per granum increase during cell development (Leech, Rumsby & Thomson, 1973). If plastid development occurs in the absence of light, pigmentless etioplasts are formed (Leech & Baker, 1983). The whole cycle from proplastid to functional chloroplast takes approximately six days in wheat, and chloroplasts are photosynthetically functional early in their development.

Above the meristem in wheat leaves, young chloroplasts usually continue to divide, especially in the presence of light. As a result, as cells leave the meristem and develop, chloroplasts increase in number as well as in size (Possingham, 1980; Tobin, Ridley & Stewart, 1985). This results in an increase in the % fractional cell volume (V_v) occupied by chloroplasts, with leaf cell development (Tobin & Rogers, 1992; Leech, 1984; Boffey *et al.*, 1979). In wheat, the V_v represented by mesophyll cell chloroplasts increases from 5.7% close to the leaf base, to 17.0% in mature mesophyll tissue near the leaf tip; and no other component of the cell changes in volume in this way except the cytosol, which decreases in volume with cell development as a direct result of increasing chloroplast volume (Ellis & Leech, 1985). Increasing chloroplast V_v and the changes in internal chloroplastic structure in developing wheat leaf mesophyll cells, can be correlated with the development of the photosynthetic capacity of cells as they are displaced away from the leaf base. Such metabolic changes with wheat leaf cell development are discussed below.

1.1.5 Metabolic Development of Wheat Leaf Cells

As leaf cells develop, ultrastructural changes take place to accommodate changes in metabolic activity. In the primary leaf of wheat, the developmental gradient from leaf base to tip represents a change from heterotrophy to fully autotrophic cells with photosynthetic and respiratory capacity (Moore *et al.*, 1992) and this provides a model for investigating the development of cellular metabolic activity (Tobin *et al*, 1992). Immature cells at the primary leaf base obtain nutrition from the seed and more mature regions of the leaf until they are capable of synthesising carbohydrates via photosynthesis. As with organelle structural biogenesis, studies of metabolic development have focused on plastids, and a substantial amount of information has been gathered with regard to these organelles. Development of metabolic activity in mitochondria, however, has received comparatively little attention despite the interdependence of the reactions of chloroplasts and mitochondria. This may be partly due to the difficulty in isolating and manipulating

mitochondria. Nonetheless, this presents opportunities for the elucidation of metabolic development of these organelles. The metabolic development of chloroplasts in wheat leaves is outlined below, while mitochondria are discussed in Section 1.2.4.

Measurements of light-dependent and CO_2-dependent O_2 production in developing leaves have shown that rate of photosynthesis increases with leaf cell development (Miranda, Baker & Long, 1981). This is evident in the primary wheat leaf, where cells develop a greater photosynthetic capacity as they are displaced further away from the intercalary meristem (Tobin *et al.*, 1988). In addition to changes in chloroplast ultrastructure and population, this can be related to changes in the activity of photosynthetic enzymes. Changes occur in the activity of ribulose 1,5-biphosphate carboxylase/oxygenase (Rubisco) for example. Rubisco activity and amount per cell has been found to increase with increasing cell age in barley (Viro & Kloppstech, 1980) and wheat (Dean & Leech, 1982a). These findings are supported by the observation of a similar increase in expression of RNA transcripts encoding both the large and small subunits of Rubisco (Topping & Leaver, 1990). Other photosynthetic enzymes show an increase in activity with cell development (Suzuki *et al.*, 1987). Photorespiratory enzymes also develop in parallel with photosynthetic enzymes (Tobin *et al.*, 1988). As cells in the developing leaf become autotrophic, photophosphorylation provides a new source of ATP and reductant in addition to that generated via aerobic respiration in the mitochondria. This is likely to affect other metabolic pathways in the cell, e.g. the reactions of the mitochondria. For a review, see Krömer, 1995.

1.2 Development of Plant Mitochondria

1.2.1. Mitochondrial Structure

Mitochondria have been known of since the late 19th century when light microscopy revealed the presence of individual organelles within the cytoplasm of plant and animal cells. Typically oblong with dimensions of approximately 1-2 μm long and 0.5-1 μm wide, they are the site of aerobic respiration in eukaryote cells. Spherical, filamentous or irregularly-shaped mitochondria also exist, e.g. worm-like mitochondria have been observed in plant vascular cells (Logan & Leaver, 2000). Mitochondria are bound by two specialised membranes. The smooth outer membrane allows passage of molecules into the fluid-filled intermembrane space via the large channel-forming protein, porin. The inner membrane has a higher protein content than the outer and forms a series of invaginations into the inner cavity (matrix) of the mitochondrion (Tzagoloff, 1982). These invaginations (cristae) are very distinctive, distinguishing mitochondria from other organelles such as plastids and are complex and visually intriguing structures, as first viewed under the electron microscope (Palade, 1953). It is now accepted that the standard baffle model for cristae structure - accepted for years - is inaccurate. Recently, electron microscopic tomography has revealed cristae resembling simple tubular structures – particularly in plant cells - to more complex lamellar structures merging with the inner mitochondrial membrane (Frey & Mannella, 2000).

Various proteins involved in the tricarboxylic acid cycle (TCA cycle) and oxidative phosphorylation (two of the three main stages of aerobic respiration) are located in the inner mitochondrial membrane. Spherical particles of adenosine triphosphate (ATP) synthetase are attached to the inner surface, and other proteins such as succinic dehydrogenase form an integral part of the membrane. Other enzymes involved in respiration are present in soluble form in the matrix (the fluid within the stroma). The elaborate internal structure of mitochondria created by the cristae is closely related to function - a large surface area is essential for maximum activity of respiratory enzymes (Munn, 1974). The form and amount of cristae varies depending on cell type, e.g. cells with particularly high energy requirements tend to have comparatively large amounts of highly-folded condensed cristae (Tzagoloff, 1982).

A notable feature of mitochondria is the presence of a distinct genome within the matrix which plays a vital role in mitochondrial biogenesis as well as encoding certain respiratory enzymes. This genome is one of three in plant cells - the other two being in the

nucleus and the chloroplasts - and some form of co-ordinated gene expression must occur between the three (Giege & Brennicke, 2001). Around 12 components of respiratory chain proteins are encoded by mitochondrial DNA, though the largest proportion are nuclear-encoded and imported into the mitochondria from the cytosol. Around 90% of the information required for mitochondrial biogenesis is also encoded by the nucleus and imported - the remaining proteins are encoded by mitochondrial genes. Mitochondrial biogenesis therefore relies on the controlled and integrated expression of genes derived from both genomes (Hawkesford & Leaver, 1987). The size and form of the mitochondrial genome varies considerably among eukaryotes. In plants it is comparatively large (10 to 100 times larger than in mammals), varying e.g. from 187 kbp in the liverwort *Marchantia polymorpha*, 372 kbp in *Arabidopsis thaliana* (the genomes of these two species have been completely sequenced: Oda *et al*, 1992; Unseld *et al*, 1997), to 2400 kbp in *Cucumis melo* (muskmelon). This variation means that the precise set of genes encoded by mitochondrial DNA varies among eukaryotes, though a 'master' set of mitochondrial genes are present in nearly all eukaryotes (Bonen & Gray, 1997). In higher plants and fungi, the mitochondrial genome exists in a circular forms, though linear forms can exist depending on species (Schuster & Brennicke, 1994). Hanson & Folkerts (1992) present a review of the higher plant mitochondrial genome, and Moore, Wood & Watts (1994) review protein import into plant mitochondria. Similarities between the mitochondrial genome and bacterial systems forms the basis of the endosymbiont theory of mitochondrial evolution (Margulis, 1970).

Unlike the situation in animal cells, plant mitochondria appear to have no particular spatial arrangement within the cytoplasm, although they are often more numerous near cell wall ingrowths, while not actually being in contact with the plasmalemma. It is evident however, that interactions occur between mitochondria and other organelles such as chloroplasts (for exchange of metabolites for instance), which explains the close proximity that the two organelle types often have within plant cells, and the cytoplasmic streaming of mitochondria towards and away from plastids. Recent work observing mitochondria labelled with green fluorescent protein (GFP) has revealed the dynamic movements of mitochondria within the cytoplasm of living plant cells, and has shown chloroplasts surrounded by mitochondria, indicating close interaction. This work has also shown that individual mitochondria can rapidly change shape in a matter of seconds (Köhler *et al.*, 1997; Logan & Leaver, 2000). Mitochondrial numbers per unit

volume of cytoplasm vary considerably depending on cell type, stage of cell development, and cell energy requirements, and there is evidence of a mitochondrial population heterogeneity in higher plants, in terms of structure and function (Dai *et al.*, 1998; Bowsher & Tobin, 2001).

1.2.2 Mitochondrial Metabolism

Plants consume carbohydrates generated autotrophically to produce ATP for cellular work via aerobic respiration. Hence, mitochondria are essential to plant survival as sites of the TCA cycle and oxidative phosphorylation, two of the three main stages of aerobic respiration. The other main phase of aerobic respiration is carbohydrate oxidation, which occurs outside the mitochondrion in the cytosol, via glycolysis and the less-dominant oxidative pentose phosphate (OPP) pathway. This carbohydrate breakdown provides substrates for the TCA cycle and oxidative phosphorylation, and the resulting energy production within mitochondria (ap Rees, 1985).

In brief, glycolysis involves the breakdown of glucose to form glyceraldehyde phosphate (via ATP consumption) which is then oxidised to eventually produce pyruvate, NADH, and a small amount of ATP. In the presence of oxygen (O_2), pyruvate enters mitochondria where it breaks down and attaches to coenzyme A (CoA-SH) to form acetyl coenzyme A (acetyl CoA), the entry compound to the TCA cycle. This is catalysed by the multienzyme pyruvate dehydrogenase complex (PDC) (Wiskich & Dry, 1985). Plaxton (1996), presents a review of the organisation and regulation of glycolysis in plants.

In plants, glycolysis also plays a major role in providing intermediates for the biosynthesis of complex molecules such as proteins, organic acids and lipids. Unlike animals, plants can synthesise all compounds required for growth and development, and it is therefore not surprising that a large proportion of carbon flow in the plant is concerned with this, and that intermediates from other pathways are used for this purpose (Kruger, 1997). In order to provide carbon for biosynthesis in plastids, glycolysis often takes place in plastids, catalysed by isoenzymes of the cytosolic forms. The OPP pathway of carbohydrate oxidation exists in intimate association with glycolysis and is also heavily involved in the production of biosynthetic intermediates (ap Rees, 1988).

The TCA cycle can be summarised as a series of eight oxidative steps, each catalysed by a specific enzyme in the mitochondrial matrix. The cycle functions to generate energy which is conserved as electrons in NADH (and some in $FADH_2$), and a

summary is shown in Figure 1.1. Electrons produced by the TCA cycle and glycolysis drive oxidative phosphorylation to produce most of the ATP in respiration (although in one step, ATP is produced via substrate-level phosphorylation). Oxidative phosphorylation is driven by the electron transport chain, a complex system of multiprotein carriers embedded in the inner mitochondrial membrane. Electrons pass down the chain from NADH and $FADH_2$ (attracted by increasing stability with each step) until they are finally received by O_2 which then combines with hydrogen ions in the matrix to form water. The TCA cycle itself generates a limited amount of ATP (Wiskich & Dry, 1985; Hill, 1997). In 1961, Peter Mitchell proposed a mechanism by which the transfer of electrons down the electron transport chain was coupled to ATP production. His 'chemiosmotic coupling' theory won him the Nobel prize and is well established today. In brief, the electron transport chain pumps H^+ ions across the inner mitochondrial membrane into the intermembrane space, creating a proton gradient (proton motive force) across the membrane. The ions move passively back down the proton gradient to the matrix via ATP synthase, which harnesses the energy to phosphorylate ADP to ATP (Mitchell, 1985).

There are distinct differences between the metabolic pathways within plant and animal mitochondria. For example, the role of the TCA cycle differs fundamentally - in mammalian cells, the TCA cycle represents a point of convergence of catabolic pathways, whereas the cycle is a point of divergence of anabolic pathways in plant cells as a provider of carbon intermediates for biosynthesis. During respiration, mammalian cells largely utilise protein and lipid substrates consumed heterotrophically, whereas in plants, photosynthetically-synthesised carbohydrates such as sucrose and starch are the main respiratory substrates. During germination, a certain amount of amino acids are partially processed in the TCA cycle, but this involvement is more a bi-product of their metabolism and not specifically for the purpose of energy production (Lambers, 1997). Lipids are only rarely a respiratory substrate in plants, though part of the TCA cycle plays an essential role in converting lipids to sugars via the glyoxylate cycle (Mettler & Beevers, 1980).

A more complex electron transport chain exists in cells of plants and some fungi, than in other Eukaryotes, e.g. at least four extra NAD(P)H dehydrogenases exist in the inner mitochondrial membrane (Rasmusson, Fredlund & Møller, 1993). A notable difference in plant cells is that in addition to the standard cytochrome pathway, a cyanide-resistant alternative electron transport pathway also exists which catalyses the reduction

of oxygen to water and is not energy-conserving (Affourtit, Krab & Moore, 2001). Another feature of plant cell respiration is that malate may enter the TCA cycle as an additional or alternative substrate to pyruvate. Malate is shuttled to the mitochondria from chloroplasts to replace carbon lost in the TCA cycle to anabolic processes elsewhere in the cell (Gottlob-M^{c}Hugh *et al.*, 1992).

Finally, the mitochondrion is one of the sites of photorespiration in the cells of C3 plants, an alternative respiratory pathway to 'dark' respiration. Light-dependent and occurring along with photosynthesis, the process involves O_2 uptake and CO_2 production and occurs when the enzyme Rubisco accepts O_2 rather than CO_2 to add to RuBP (the latter would be the case with photosynthesis) (Lorimer, 1981; Tolbert, 1997). The process is increased when hot, dry environmental conditions cause stomatal closure during the day and a consequent depletion of CO_2 in the leaf mesophyll air spaces due to photosynthesis - Rubisco has a higher affinity for O_2 than CO_2. CO_2 is then produced via the photosynthetic carbon oxidation (PCO) cycle. This involves the synthesis of glycolate which leaves the Calvin cycle in the chloroplast and enters the peroxisome. Glycolate is broken down in a co-ordinated series of reactions in the peroxisome to form glycine which enters the mitochondrion. In the mitochondrion, glycine is oxidised by the glycine decarboxylase enzyme complex (GDC), with the production of CO_2 (Douce *et al.*, 2001).

It is fascinating to contemplate the level of control required for the development and co-ordination of a metabolic pathway between three different organelles (reviews: Ogren, 1984; Canvin & Salon, 1997). Photorespiration does not generate any ATP and is therefore often viewed as wasteful by decreasing photosynthetic output. C4 and CAM (Crassulacean acid metabolism) plants have evolved mechanisms for the minimisation of the process (Canvin & Salon, 1997).

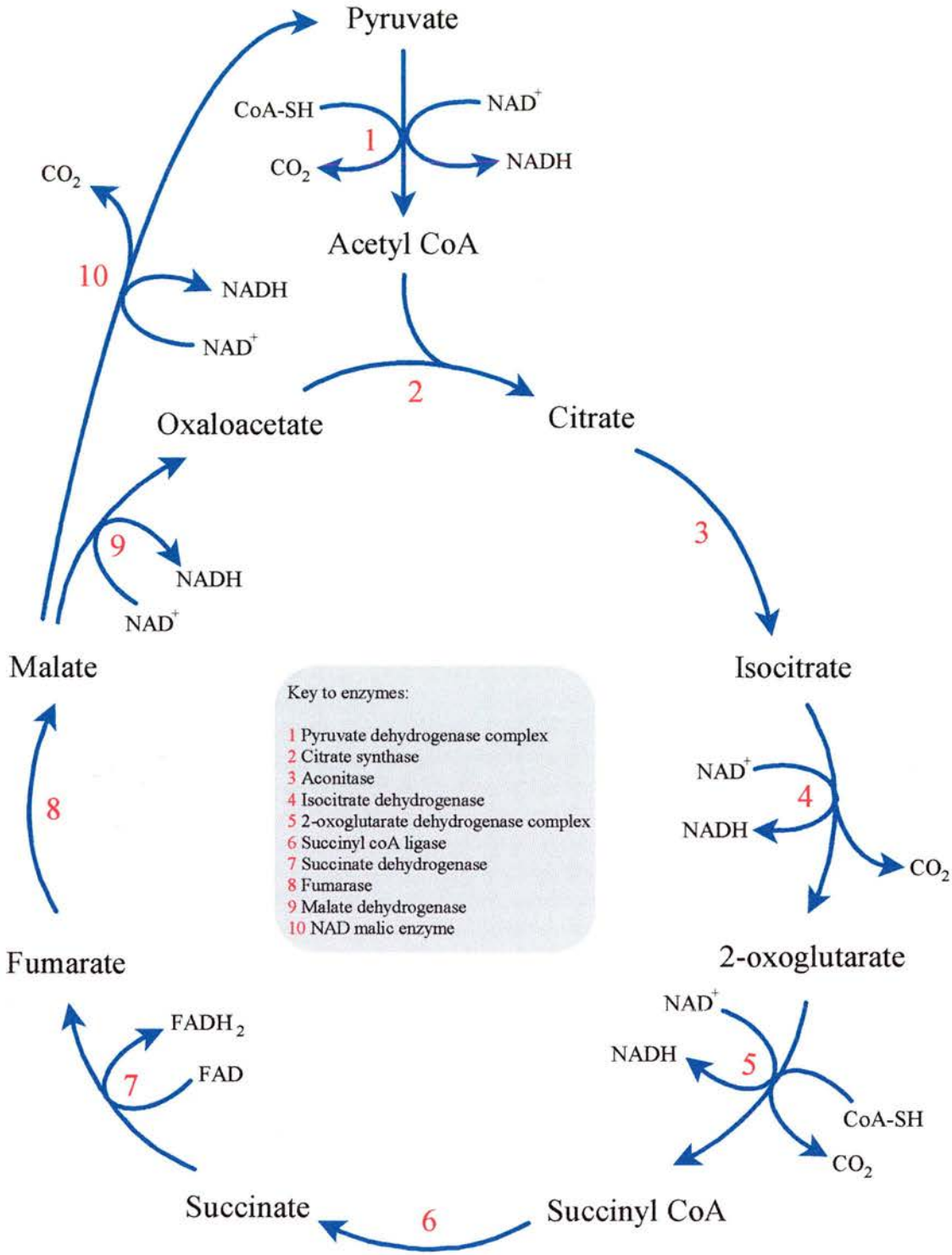

Figure 1.1 Summary of the Tricarboxylic Acid (TCA) Cycle in Plant Mitochondria. See section 1.2.2. In the respiratory pathway, pyruvate produced in the cytosol via glycolysis enters the mitochondria and attaches to coenzyme A (CoA-SH) to form acetyl CoA, catalysed by the pyruvate dehydrogenase complex (PDC). Acetyl CoA is the entry compound to the energy-generating TCA cycle which consists of eight oxidative steps, each catalysed by a different enzyme, as summarised above.

1.2.3 Structural Development of Plant Mitochondria

Compared to plastids, there have been few studies of the changes in the structure and cell population levels of mitochondria during leaf development. However, studies on wheat have revealed certain changes which take place in mesophyll cell mitochondria during growth and development of the primary leaf. In the basal intercalary meristem of wheat, mitochondria multiply via division, and observations of dumb-bell shaped mitochondria confirm this (Bagshaw, Brown & Yeoman, 1969; Köhler *et al.*, 1997). This occurs by inward invagination of the mitochondrial membranes at opposite sides followed by fission, to produce two separate organelles. As cells expand in the elongation zone, this division continues such that mean mitochondrial size and % fractional cell volume (V*v*) occupied by these organelles remains constant (Tobin & Rogers, 1992). Once cells have reached their maximum size, individual mitochondria then increase in size, while decreasing in number per cell. This occurs such that the V*v* occupied by mitochondria remains constant at 0.6 % at all stages of mesophyll cell development (Tobin *et al.*, 1992). Further changes tend to occur in older, mature leaf mesophyll cells - mitochondria continue to increase in size, while the total cell population decreases. Again, the V*v* occupied by mitochondria remains constant, and mitochondria appear to fuse together as mesophyll cells age. Decreasing cytoplasmic volume as a result of rising chloroplast populations in maturing leaf cells, may stimulate such mitochondrial fusion (Tobin & Rogers, 1992). Final mitochondria numbers in mature functioning cells varies depending on cell type, e.g. transfer cells contain large amounts compared to cell types with lower energy requirements (Tzagoloff, 1982).

1.2.4 Metabolic Development of Plant Mitochondria

It is clear that changes must take place in the metabolic activity of mitochondria in association with mitochondrial ultrastructural changes, and with changes in other metabolic pathways in the cell, as leaf cells develop. Mitochondria are involved in a substantial proportion of total cell metabolism, and understanding the changes in the activity, role and interaction of mitochondria with other organelles during leaf cell development presents a challenge. Immature cells at the base of the primary wheat leaf lack photosynthetic capacity (see Section 1.1.5). Initially, mitochondria must provide ATP for developing plastids. As cells become autotrophic, photosynthesis provides an additional source of ATP and reductants, suggesting that the metabolic role of

mitochondria changes from purely bioenergetic to more biosynthetic as cells age. This may occur due to a decreasing need for mitochondrial ATP synthesis, in addition to an increasing requirement for mitochondrial glycine oxidation due to rising rates of photorespiration (Tobin *et al.*, 1988).

General rates of respiration (as indicated by O_2 uptake) have been shown to decline with leaf development in a variety of species (Azcón-Bieto, Lambers & Day, 1983). There is also evidence of an individual decline in glycolysis with leaf development - it has been suggested that glycolysis is the dominant mode of carbohydrate degradation in young leaves, and that the OPP pathway becomes more important in mature leaf tissue (Croxdale & Pappas, 1987). The overall decline in respiration occurs at the same time as the onset of photosynthetic capacity in leaf cells, reflecting the transition from heterotrophy to autotrophy.

In order to investigate changes in mitochondrial metabolism throughout leaf cell development, various studies have involved the measurement of changes in levels and activity of mitochondrial enzymes. For example, there are two different patterns of development of mitochondrial enzymes in the primary wheat leaf. In mesophyll cells, enzymes involved in 'dark' respiration such as cytochrome oxidase and glutamate dehydrogenase are present in relatively high levels in immature cells at the leaf base, and increase in activity distal to this, reaching a maximum level at about 5 cm from the base (Tobin *et al.*, 1988). On the other hand, photorespiratory enzymes such as glycine decarboxylase (GDC), glutamine synthetase and glycollate oxidase develop in parallel with various photosynthetic enzymes such as Rubisco. Changes in the expression of certain mitochondrial genes reflect changes in enzyme levels and activities. For example, the relative abundance of genes encoding subunits I and II of cytochrome-c oxidase, decrease five to ten-fold between the leaf base and 1cm distal to this (Topping & Leaver, 1990).

1.3 Major Techniques Used in this Study

1.3.1 Immunocytochemistry

1.3.1.1 Definitions

Immunocytochemistry is the use of labelled antibodies as specific reagents for the localisation of tissue constituents *in situ* (Polak & Van Noorden, 1997), and originates from the early 1940s when an antibody was labelled with a fluorescent dye (Coons, Creech & Jones, 1941), and was then used successfully to identify tissue components (Coons & Kaplan, 1950). The antibodies are raised against the molecules to be localised, so that the latter act as antigens in specific antibody-antigen reactions.

1.3.1.2 Antibodies

Antibodies are animal proteins produced in response to the presence of foreign molecules (antigens) in the organism's body. They are immunoglobulin (Ig) proteins and consist of one or more copies of a characteristic Y-shaped molecule, each of which have two identical antigen binding sites. The most abundant of the five Ig classes are the IgG proteins, the most widely used in immunocytochemical techniques. Antibodies recognise and bind to specific sites (epitopes) on the antigen surface, forming very specific antibody-antigen bonds. However, bond fit (affinity) and strength (avidity) vary, and affect overall antibody specificity and usefulness (Harlow & Lane, 1988).

Specific antibodies for molecules of interest are produced by immunising mammals such as rabbits with pure antigen, to produce an antiserum in the host containing antibodies specific for the antigen. This may include a variety of antibodies against different epitopes present on the antigen, which is advantageous due to signal amplification, but disadvantageous where some of the same epitopes are present on other molecules, leading to a cross-reaction. The antiserum also contains antibodies specific to any antigen-carrier molecules, and antibodies present in the host prior to immunisation. To account for this it is useful to remove serum from the animal prior to immunisation for use as a control (pre-immune serum). Antibodies containing these various components are described as polyclonal (Johnstone & Thorpe, 1996). A monoclonal antibody, on the other hand, is specific for a single epitope on an antigen molecule, and is produced by immunising mice with pure antigen to produce a polyclonal serum, then removing antibody-producing B-lymphocyte cells from the animals. These are fused with myeloma tumour cells from other mice to produce

hybridomas. A clone is cultured from a single selected hybridoma cell to produce an infinite supply of the desired antibody, specific to a single epitope (Köhler & Milstein, 1975). As well as being highly specific, identical batches of monoclonals can be produced, whereas no two batches of polyclonal antiserum can be exactly the same. Immunisation is only one step in antibody production, and subsequent purification and testing must follow. Antibody choice depends on suitability for a particular purpose, and monoclonals are not necessarily more effective than polyclonals (Beesley, 1993). In the present study, both antibody types were used.

1.3.1.3 Direct and Indirect Immunocytochemical Techniques

Immunocytochemical techniques are often categorised as two types - direct and indirect localisation. In direct localisation (Coons & Kaplan, 1950), an antigen-specific antibody - labelled in some way for visualisation - binds directly to the antigen, indicating the location of the latter. A more frequently used technique however, and the method used in the present study, is indirect localisation (Coons, Leduc & Connolly, 1955). Here, an unlabelled antigen-specific antibody binds to the antigen, and then itself acts as an antigen for a labelled secondary antibody (raised against the Ig of the animal species which donated the primary antibody, in a different species), indicating the location of the antigen. Indirect localisation has a number of advantages over the direct method. For example, it is more sensitive since each primary antibody molecule has two antibody binding sites, and can therefore be recognised by two secondary antibody molecules, amplifying the amount of label for visualisation. Also, secondary antibodies are widely available and can be used to detect any number of primary antibodies specific for different antigens, providing that the secondary is raised against the animal species donating the primary (Polak & Van Noorden, 1997).

Molecules of interest may be located in whole cells or tissue sections, from fixed fresh, frozen or embedded samples. Where tissue is embedded (in paraffin wax or resin), pre-embedding or post-embedding immunostaining of tissue is employed. For electron microscopical observation, resin-embedded material is usually used as it allows the production of very thin sections. With plant tissue, post-sectioning (i.e. therefore post-embedding) immunostaining of tissue sections is almost exclusively used (as in the present study), since with few exceptions, the cellulose cell wall of plant cells renders them impermeable to antibodies and some probes (pers. com., C. Hawes, Oxford

Brookes University).

In order to visualise the end-product of an immunocytochemical reaction, some component of the reaction must be labelled. Fluorescent dyes and radioisotopes are possibilities; but the two label types used in the present study were enzymes (where reactions produce coloured end-products) and colloidal gold (Faulk & Taylor, 1971), visible as discrete particles under the transmission electron microscope. The two most popular enzyme labels used today, and in the present study, are horseradish peroxidase (Avrameas & Uriel, 1966) and alkaline phosphatase (Mason & Sammons, 1978).

Variations on the basic two-layer indirect method also exist. The peroxidase-anti-peroxidase (PAP) and alkaline phosphatase-anti-alkaline phosphatase (APAAP) methods involve a third layer consisting of labelled PAP and APAAP complexes (Sternberger *et al.*, 1970). These methods are highly sensitive due to the large chromagen aggregates which accumulate at the site of the antigen. Avidin-biotin techniques are also popular (Coggi, Dell'Orto & Viale, 1986). The simplest form involves antigen recognition by a primary antibody coupled to biotin, a group B vitamin. Incubation in enzyme-labelled avidin (a glycoprotein) reveals the location of the antigen due to the strong affinity of avidin for biotin.

1.3.2 Stereology

1.3.2.1 Definitions

First derived by the geologist Delesse in 1847 for analysing the composition of rocks, the fundamental principles of stereology allow the quantitative 3-dimensional (3-D) interpretation of 2-dimensional (2-D) images such as sections. The notion of measuring an object with respect to a reference system is fundamental to this. The best reviews of the subject area include Elias, Henning & Schwartz, 1971; Briarty, 1975; and Weibel, 1969, 1979. Where stereological principles are applied to the study of the relative proportions of different components of a body, the process is often termed morphometry (Weibel, 1969; Bolender, 1978a; Toth, 1982).

1.3.2.2 Volume Fraction (V*v*)

Three fundamental parameters of stereology and morphometry include surface density, S*v* (the surface area of a component per unit containing volume); numerical density, N*v* (the number of particles or features per unit containing volume); and

volume fraction, V*v* (the ratio of the volume of a component of a 3-D structure to the containing volume). The V*v* principle states that the relative area (areal fraction, A_A) of a component profile on random sections of a 3-D structure, is an unbiased estimate of the V*v* of that component (Delesse, 1847). The reasoning behind this can be outlined as follows. If a cube of tissue containing a component whose V*v* is to be measured is cut completely into thin serial sections of constant thickness *t*, the slices of tissue will obviously contain slices of the component. For each section, the area of the component profile (*a*) and the area of the section (A) can be measured. Adding all the component profiles then multiplying by *t* will give the volume of the component. Adding all the section areas then multiplying by *t* will give the volume of the cube of tissue. The two can then be divided to give the volume fraction of the component. Slice thickness, *t*, cancels out, leaving the ratio of the sum of the profile area to the sum of the section area, or the areal fraction, A_A:

$$Vv = (\Sigma a).t / (\Sigma A).t = A_A$$

The full mathematical derivation of the principle can be found in various sources such as Underwood (1969) and Weibel (1969). Hence, the V*v* of 3-D cells and organelles for example, can be calculated from A_A measurements taken from random 2-D transmission electron or light micrographs of tissue sections:

$$\mathbf{Area}_{\text{component}} / \mathbf{Area}_{\text{containing volume}} = \mathbf{Volume}_{\text{component}} / \mathbf{Volume}_{\text{containing volume}}$$

$$\mathbf{A_A = Vv}$$

The resulting value can then be multiplied by 100 to express the volume of the component as a % of the containing volume, as in the present study.

V*v* has conventionally been calculated via planimetry, usually involving tracing component profiles onto paper, then cutting and weighing them (Sorby, 1856: see Rhines, 1968). Slightly less laborious planimetric techniques are linear integration (Rosiwal, 1898: see Briarty, 1975) and point counting (Glagolev, 1933). These techniques are still used today, though more recently V*v* measurements have been made using the more rapid and efficient computer-aided image analysis, as in the present study.

1.3.2.3 Sampling for Stereological Investigations

Stereological methods are statistical in nature, and require the use of rigorous sampling procedures. As in any scientific study to be evaluated statistically, sampling should be independent and unbiased. Systematic random sampling (such as the use of lattice grids superimposed on sections) ensures that no overlapping or clustered sampling occurs, and has been found to produce smaller errors than simple random sampling (Ebbeson & Tang, 1967). However, there are a number of other factors which must be considered with specific reference to sampling of tissue sections under the transmission electron microscope (TEM) for stereological analysis.

Firstly, the tissue or cell type of interest may not be homogeneously distributed in the sample, a common situation in biological material, so that systematic random sampling on sections may not yield enough samples of the areas of interest. Here, the sampling method can be modified so that only selected parts of the tissue are sampled (Toth, 1982). For example, in the present study, mitochondrial V_v was measured by taking electron micrographs only from the mesophyll cell cytoplasm, since the majority of cell profiles examined consisted largely of vacuole. The data could be related back to the volume of the whole cell since cytoplasmic V_v with reference to total cell volume, was also measured.

Secondly, the use of low magnifications in order to sample as much tissue as possible may mean that smaller structures and organelles are not adequately resolved. A common solution is to separate the study into a hierarchy of magnifications of the same sections, so that smaller structures can be observed separately, but still allowing the data to be linked to the more macroscopic levels of the investigation such as individual cells (Weibel, 1979). Adequate systematic sampling must of course be carried out at each level as normal. In the present study, regions of cytoplasm were selected on EM grids by taking micrographs only from the top right hand corners of grid squares. In addition, only one section was used per embedded tissue block to ensure no repetition - the risk of sampling the same area would defeat the purpose of systematic sampling from EM grids when taking micrographs.

A third consideration in stereological studies at the EM level, is the question of how many micrographs per sample (each representing such small areas of tissue) should be analysed to faithfully represent the true situation in the organism. One way of achieving this is to empirically evaluate the sampling errors inherent in the stereological

methods used, by plotting the cumulative standard errors for an increasing number of micrographs (Bolender, 1978a; Gundersen & Østerby, 1980). The point at which the graph plateaus indicates the number of micrographs required to be examined to meet the equivalent level of confidence on the y-axis, e.g. the amount of micrographs required to reduce the standard error to ≤ 10% of the mean (Blouin, Bolender & Weibel, 1977; Bolender, 1978b). This must of course be done individually for each parameter measured, e.g. mitochondrial and chloroplastic V_v would be plotted separately. This method of plotting cumulative standard errors was used in the present study to estimate the number of micrographs to be examined for measurement of mitochondrial transverse area (TA) and V_v, and immunogold labelling studies.

As in all biological studies, the inherent variation present in organisms must be accounted for. So, although adequate numbers of micrographs must be examined in stereological studies, variations at the microscopic level of sampling must not be examined at the expense of variations at the level of the organism. For example, it is more efficient to take a few micrographs from each of many tissue sections, than to take 100 micrographs from a few sections, i.e. 'do more less well' as Weibel recommends (see: Gundersen & Østerby, 1980). This apparently obvious point is easily overlooked when working at the EM level. This also makes sense on a completely practical level, where time and expense in the laboratory is not infinite.

1.3.2.4 Sources of Error in Stereological Transmission Electron Microscopy Studies

There are a number of sources of error which might affect stereological TEM studies. For example, over-representation of opaque structures and under-representation of translucent structures may occur (Holmes effect). This can be corrected for by using formulae designed for the purpose, which is only necessary if the ratio of section thickness to the diameter of the structures being measured is <10% (Weibel, 1973).

Another problem may result from compression of sections during cutting, though dimensionless parameters such as V_v remain unaffected assuming that compression is uniform throughout the section. Tissue shrinkage due to fixation and embedding is another potential difficulty, but again V_v measurements are unaffected (Toth, 1982).

1.3.3 Immunogold Labelling

1.3.3.1 Definitions

Immunogold labelling is currently the most important and widely used method for the *in situ* localisation of cellular macromolecules using electron microscopy and the post-embedding technique. Colloidal gold - a solution of insoluble gold particles which remain evenly dispersed within the medium - has been used for centuries in Chinese and Indian medicine (Mahdihassan, 1984) and was first reported as a 'staining reagent' in the 17th century, when Kunkel produced ruby glass by adding colloidal gold to molten glass (see: Roth, 1983). In 1857, Faraday examined the metallic nature of colloidal gold, and his observations of its particulate nature were later confirmed by the first comprehensive TEM study into the nature of the substance by Theissen in 1942 (see Roth, 1983). Interestingly, colloidal gold was used in one of the first biological applications of electron microscopy, in a study of viruses (Kausche & Ruska, 1939: see Roth, 1983); though the modern development of immunocytochemical colloidal gold applications began with the work of Faulk & Taylor (1971) who successfully localised *Salmonella* surface antigens with an antibody conjugated to 5nm gold particles. Since then, the use of colloidal gold conjugated to various probe molecules in the localisation of cellular constituents has expanded enormously.

The current wide-spread use of immunogold labelling techniques is not surprising due to the various attributes of the technique. These are outlined as follows:

- Gold colloids can be made easily and reproducibly in a range of predefined sizes providing a very flexible system. Preparation methods are based on the controlled reduction of an aqueous tetrachloroauric acid solution (Roth, 1983; De Mey, 1986).
- A variety of macromolecular probes can be absorbed onto gold particles, including antibodies (as in the present study), protein A, lectins, toxins, hormones, and avidin. Most of these conjugates can be produced easily in the laboratory, and many are available commercially in a range of particle sizes from 1 to 80nm, or larger.
- Gold conjugates remain stable stored at -20°C with 20% glycerol, and retain most of the antigenicity of the original unlabelled probe molecule.
- Due to its high atomic number, gold is extremely electron-dense and colloidal particles appear as characteristic black circles under the TEM, easily distinguishable from biological structures and common TEM artifacts.

• Individual gold particles can be counted per unit area on tissue sections, providing a more accurate and direct approach than other immunocytochemical methods.
• Gold labelling produces a very low level of background staining compared to many other immunolabelling methods.
• Gold conjugates can be used for TEM (Faulk & Taylor, 1971); scanning EM (Horisberger, Rosset & Bauer, 1975); light microscopy (Geoghegan, Scillian & Ackerman, 1978), and non-microscopical techniques such as immunoblotting and immunoprecipitation (Schurer, Hoedemaeker & Molenaar, 1977).
• Gold conjugates can be used in multiple-labelling studies involving different particle sizes (Horisberger & Rosset, 1977), or in combination with other immunolocalisation methods such as enzyme labelling or immunofluorescence (Wang & Larsson, 1985).

1.3.3.2 Quantification of Immunogold Labelling

One of the most important advantages of immunogold labelling is that it allows a more accurate estimation of labelling density than many other immunostaining methods, since individual gold particles can be resolved under the TEM. However, although absolute numbers of gold particles can be counted per unit area on tissue sections, absolute quantification of tissue antigen concentration cannot presently be achieved with this technique (Hayat, 1992; Polak & Van Noorden, 1997). This is due to a number of factors.

Firstly, it is unlikely - and difficult if not impossible to prove - that antigen survival in processed tissue sections is 100% of that present in living tissue. Fixation, embedding, sectioning and immunostaining may all contribute to loss of antigenicity in samples. So, even if the antibodies used were known to be highly specific for the target molecule, no absolute quantification could be made from an antigen presence which was possibly reduced from that present in the original living tissue. Even at optimum labelling densities, it cannot be assumed that one gold particle indicates the presence of one antigen molecule (Howell *et al.*, 1987).

Secondly, the relationship between antigen concentration and labelling density is complex, and it is difficult to control the various factors which influence this association. Variations in factors such as tissue processing, antibody dilutions used, section surface relief, and gold particle size can produce different degrees of labelling intensity in identical tissue samples. There are a variety of reasons why it is preferable

to use the smallest possible particle size, as discussed by Kellenberger and Hayat (1991). One increasing problem with increasing particle size is steric hindrance, where one antibody-gold complex on a tissue section physically hinders the attachment of others to closely located antigens (Horisberger, 1981; Griffiths & Hoppeler, 1986). Gold probes are available with diameters from 1-80nm, and the smallest possible particle size should be used. Subsequent silver staining can be utilised to expand the size of gold particles if necessary (Holgate *et al.*, 1983). It has been suggested that particles of 15nm and less are suitable for most purposes (Polak & Van Noorden, 1997).

Although absolute quantification of tissue antigen concentration cannot be achieved using immunogold labelling, comparative quantification is of course possible, and here the technique is a useful tool. Providing that all samples are treated in exactly the same way, a comparison of the relative labelling densities between different tissue samples can be made, assuming the existence of a linear relationship between labelling density and antigen presence. Such comparisons can be very accurate since gold particles can be individually counted; and because it is widely believed that labelling is confined to the surface of the tissue only (Stierhof, Schwarz & Gordon, 1986), uneven antibody penetration into the section is avoided. It is vital that all samples are treated simultaneously and in the same way throughout all stages of the procedure, and rigorous standardisation of protocols is therefore required. Computerised image analysis contributes greatly to the rapid production of accurate and unbiased results (McBride, 1995). One problem with comparative quantification, however, may arise where labelling densities on different tissue types or structures are being compared, and it should be noted that labelling efficiency can vary between e.g. different organelles present in the same tissue section, regardless of antigen content, although this has mainly been reported in cryosections (Slot *et al.*, 1989), with variation in the density of the tissue sample usually given as the reason for this. In the present study, this was not a concern, since only mitochondria are being directly compared.

In order to observe gold labelling on particular structures on a tissue section, labelling density must be optimum, with background labelling reduced sufficiently. However, complete removal of background labelling is unnecessary and often undesirable for comparative quantification of immunogold labelling where zero background is accompanied by zero labelling in some of the structures of interest. If the latter occurred, the scale of any differences observed between different samples might

be lost since two different samples showing no labelling might show different labelling densities following experimental procedures that allowed much higher labelling. So, background labelling must not be reduced to the point where all labelling on any of the structures of interest is completely removed. Antibodies should be used at their lowest effective concentration determined following preliminary experiments, and no comparisons between samples can be made unless a linear relationship is established between labelling density and antigen presence in the tissue (Read & Rhodes, 1993). Despite all these considerations, any immunogold labelling procedure is only as good as the specificity of the primary antibodies used.

1.4 Proteins Under Investigation in this Study

This study investigated the development of enzymes from two major mitochondrial protein complexes, pyruvate dehydrogenase complex (PDC) and glycine decarboxylase complex (GDC). Six different proteins were under investigation: the E1α, E1β, E2 and E3 subunits of PDC, and the P-protein and L-protein subunits of GDC. PDC and GDC are described below, along with the reasons they were chosen for study.

1.4.1 Pyruvate Dehydrogenase Complex (PDC)

Mitochondrial PDC is a large multi-enzyme complex located within the mitochondrial matrix, which catalyses the oxidative decarboxylation of pyruvate to form acetyl CoA and NADH:

$$\text{pyruvate} + NAD^+ + \text{CoA-SH} = \text{acetyl CoA} + NADH + H^+ + CO_2$$

The complex core consists of three different enzymatic components: pyruvate dehydrogenase (E1); dihydrolipoamide transacetylase (E2); and dihydrolipoamide dehydrogenase (E3). The E1 enzyme consists of two subunits, E1α and E1β (Hill, 1997). PDC from mammals (Gopalakrishnan *et al.*, 1989), yeast (Behal *et al.*, 1989) and perhaps plants (Taylor, Cogdell & Lindsay, 1992) also contains a fourth enzymatic component - component X (E3 binding protein) - which shares some structural, immunological and functional similarities with E2, and has a structural role in E3 binding and the assembly of the E2 core (Millar, Leaver & Hill, 1999).

Current knowledge of the molecular structure of plant mitochondrial PDC is mostly via analogy with PDC from mammals, fungi and bacteria. Mammalian and yeast PDC have a central core of E2 subunits with E1 and E3 subunits arranged around this. The relative numbers of subunits vary with species (Patel & Roche, 1990; Stoops *et al.*, 1997). Attempts to identify the structural arrangement in plant PDC have been made using antibodies raised to plant and mammalian PDCs (Millar, Leaver & Hill, 1999).

Specifically, the E1 enzyme catalyses the decarboxylation of pyruvate and the transfer of the remaining acetyl moiety to the cofactor thiamine pyrophosphate (TPP). E2 catalyses the transfer of the acetyl moiety from TPP to coenzyme A, with the reduction of a covalently bound lipoamide cofactor; while the E3 subunit reoxidises the

lipoamide residue and converts NAD^+ into its reduced form, via a bound flavin adenine nucleotide cofactor (Hill, 1997) (see Figure 1.2). In pea, the E3 subunit of PDC is the same dihydrolipoamide dehydrogenase as that of the L-protein of glycine decarboxylase complex (GDC) and of the α-oxo acid dehydrogenase complexes (Bourguinon *et al.*, 1996), and it is possible that this is the case in other plant species.

PDC activity is regulated by metabolites, ions, and product inhibition (Patel & Roche, 1990); but the most notable regulatory mechanism is reversible phosphorylation by two associated regulatory enzymes (Randall *et al.*, 1995). PDH-kinase catalyses the ATP-dependent phosphorylation of E1α and concomitant inactivation and loss of catalytic activity; and the Mg^{2+}-stimulated phospho-PDH-phosphatase catalyses the dephosphorylation reaction (Thelen, Miernyk & Randall, 1998). There is evidence that this reversible phosphorylation is, in part, light-dependent, due to the association of mitochondria with the photorespiratory pathway (Gemel & Randall, 1992).

Plants also contain a plastidic PDC isoform, which has a similar composition to mitochondrial PDC, but is immunologically distinct and is not regulated by reversible phosphorylation. This is located in the plastidic stroma and is involved in the production of acetyl CoA for fatty acid biosynthesis (Leuthy, Miernyk & Randall, 1996).

PDC is located at a key point, namely the intersection of several metabolic pathways, making it an important site for regulation of carbon metabolism (Miernyk, Thelen & Randall, 1998). As the committed step of carbon entry into the TCA cycle, it is potentially important in understanding the control of respiratory metabolism (Millar, Knorpp, Leaver & Hill, 1998). The important role of PDC in mitochondrial metabolism, and the need for more information on the development of the complex in plants, are the main reasons that this complex was chosen for the present study.

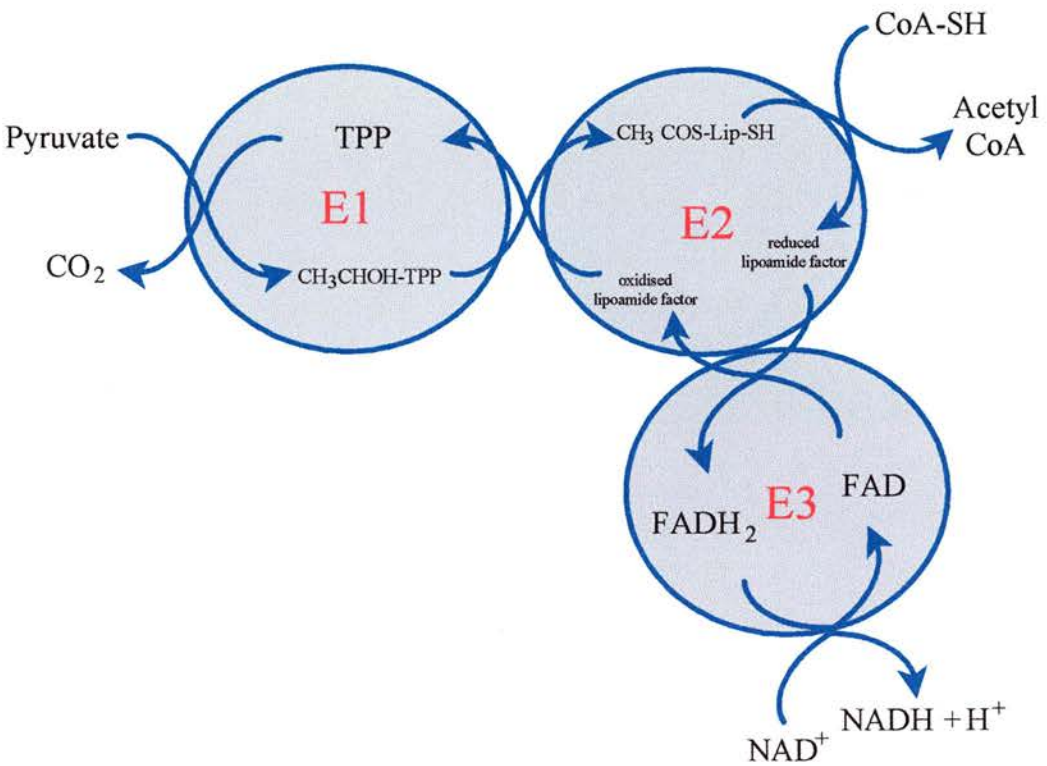

Figure 1.2 Reactions Catalysed by Mitochondrial Pyruvate Dehydrogenase Complex (PDC). See Section 1.4.1. PDC has three subunits (E1, E2 and E3), each involved in a different part of the overall reaction resulting in the formation of acetyl coenzyme A (acetyl CoA), the entry compound to the TCA cycle, in the respiratory pathway. Thyamine pyrophosphate (TPP), coenzyme A (CoA-SH). From Hill (1997).

1.4.2 Glycine Decarboxylase Complex (GDC)

GDC is a large multienzyme complex of the mitochondrial matrix, and consists of four subunits, the P-, H-, T- and L-proteins (Walker & Oliver, 1986). The main function of GDC is to oxidise glycine received from peroxisomes, in the photorespiratory pathway. Glycine is converted to serine via the sequential reactions of GDC and the enzyme serine hydroxymethyltransferase (SHMT). GDC oxidises glycine to form CO_2, NH_3, and methylene tetrahydrofolate (methylene THF). This reacts with a second glycine molecule in a reaction catalysed by SHMT, producing serine (Douce *et al.*, 2001):

GDC reaction: Glycine + NAD^+ + THF = methylene THF + CO_2 + NH_3 + NADH

SHMT reaction: Glycine + methylene-THF + H_2O = serine + THF

Specifically, the GDC P-protein decarboxylates glycine; the H-protein acts as carrier for methylamine and electrons; the T-protein transfers the methyl group to THF, releasing NH_3; and the L-protein transfers the electrons to NAD^+ to form NADH (Canvin & Salon, 1997). The H-protein plays a pivotal role in commuting between the other three proteins (Douce *et al.*, 2001). In pea, the L-protein of GDC is the same dihydrolipoamide dehydrogenase as that of the L-protein of PDC and of the α-oxo acid dehydrogenase complexes (Bourguinon *et al.*, 1996), and it is possible that this is the case in other plant species. All four sub-units are required for glycine decarboxylation, and absence of one component will inhibit the whole process, e.g. transgenic potato plants with reduced P-protein content, exhibit low levels of leaf glycine decarboxylation (Heineke *et al.*, 2001). The reactions catalysed by the complex are shown in Figure 1.3.

GDC is inhibited by NADH and serine: NADH is competitive with NAD^+ and serine with glycine (Oliver & Sarojini, 1987). Inhibition of GDC activity is prevented by a serine/glycine translocator in the inner mitochondrial membrane (Oliver, 1987); and by NADH oxidation via the electron transport chain to produce ATP, or via reduction of oxaloacetic acid (OAA) to malate (catalysed by malate dehydrogenase), coupled with the action of an OAA/malate transporter in the inner membrane (Ebbighausen, Jia & Heldt, 1985). GDC and SHMT together constitute nearly half of the total soluble protein in plant mitochondria isolated from photosynthetic tissue (Douce *et al.*, 1994, 2001).

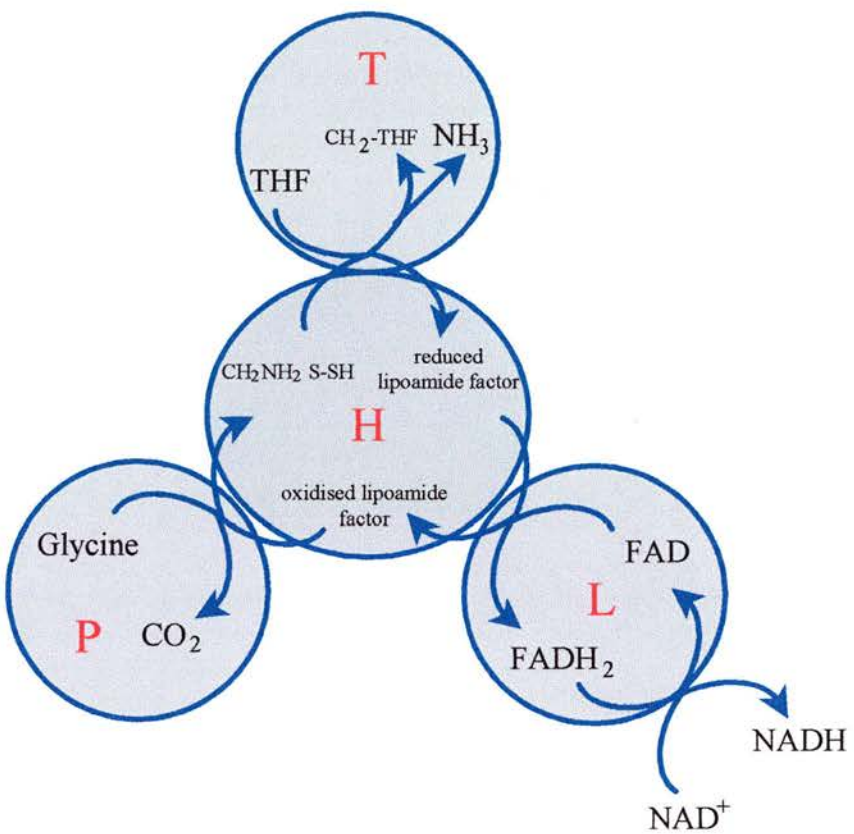

Figure 1.3 Reactions Catalysed by Mitochondrial Glycine Decarboxylase Complex (GDC). See Section 1.4.2. GDC has four subunits, each involved in a different part of the overall reaction resulting in the oxidation of glycine in the photorespiratory pathway. Tetrahydrofolate (THF). Adapted from Oliver (1994).

1.5 Aims of Study

The aim of this study was to investigate the metabolic development of higher plant mitochondria, by investigating the development of particular mitochondrial proteins, namely the pyruvate dehydrogenase complex (PDC) and glycine decarboxylase complex (GDC). This was done using wheat primary leaves, which are ideal for developmental studies due to the presence of a gradient of increasing cell age between the leaf base and tip. The study comprised the following elements:

(i) The identification and characterisation of the developmental gradient between the base and tip of wheat primary leaves, under the particular growth conditions of this study; to provide a basis for the study of mitochondrial protein development. This involved measurements of leaf growth and measurements of changes in leaf tissue and cell compartment sizes with increasing cell age.

(ii) An investigation of the general metabolic development of wheat primary leaves, via the measurement of major metabolic processes and soluble protein content throughout leaf cell development.

(iii) An investigation of the development of the E1α, E1β, E2 and E3 subunits of PDC, and the P-protein and L-protein subunits of GDC, by observing any changes in the relative concentrations of these proteins in crude leaf tissue protein extracts, with increasing cell age.

(iv) Further investigation of the development of the E1α, E1β, E2 and E3 subunits of PDC, and the P-protein and L-protein subunits of GDC with increasing cell age, at the microscopical level. The use of immunogold labelling and electron microscopy allowed observation of any changes in mitochondrial protein composition at the ultrastructural level, i.e. protein concentration per unit mitochondrial area was investigated. This enabled changing protein composition to be related to changing ultrastructural compartmentation, with increasing cell age. This technique also allowed the comparison of the development of the proteins between mesophyll and vascular cells.

CHAPTER 2: MATERIALS AND METHODS

2.1 Plant Material and Growth Conditions

Winter wheat (*Triticum aestivum* L. cv. Maris Huntsman) seedlings were used in all experiments. Seeds (Plant Breeding International, Cambridge, U.K.) were imbibed in aerated tap water for 18h at 20°C; sown on approximately 4cm of Levingtons M2 medium nutrient potting compost (Levington Horticulture Ltd., Ipswich, U.K.) at a density of 25g (pre-imbibition weight) per 30 × 44cm tray; and covered with a thin layer of fine grade vermiculite (Dupre, Hertford, U.K.). Plants were grown in a Fisons Series II Model 140G2 controlled environment chamber (Fisons Scientific Apparatus, Loughborough, U.K.) providing a 16h photoperiod (07:00 to 23:00 hours - seeds were sown at 09:00 hours) and 70% constant relative humidity. Light and dark period temperatures were 20°C and 10°C respectively. Irradiation was supplied by 16× 24" Life-Glo fluorescent 20W lamps (Hagen Ltd., Castleford, U.K.) and was monitored regularly using a photometer (Macam Photometrics Ltd., Livingston, U.K.). Quantum flux density at soil level ranged between 220-420 μmol $m^{-2}s^{-1}$ photosynthetically active radiation (PAR, λ 400-700nm).

2.2 Harvesting of Plant Tissue

In all experiments, 7d old primary leaves with a length of 90 ± 5mm about the mean were used. Seedlings were harvested 2h into the photoperiod at 7d post-imbibition, and the roots, seeds, any secondary leaves, and the primary leaf basal intercalary meristems removed, leaving the primary leaves. Leaves were transferred to a beaker of water for immediate use, or frozen in liquid N_2 and stored at −80°C until required.

2.3 Experimental Sampling and Statistical Analysis

Electron microscopy and light microscopy procedures were replicated three times, and all other procedures were replicated five times. Each replicate was taken from a different batch of plants. Statistical analysis was performed via one-way analysis of variance (ANOVA) using the Minitab programme (Minitab Inc., Pennsylvania, U.S.A.).

2.4 Chemicals Used

All laboratory chemicals used were of Analytical Grade, except those used for transmission electron microscopy (TEM), which were of EM Grade. Unless stated otherwise, chemicals were obtained from the following companies: Sigma Chemical Company Ltd., Poole, Dorset, U.K.; BDH Laboratory Supplies, Poole, Dorset, U.K.; Bio-Rad Laboratories Ltd., Hemel Hempstead, Hertfordshire, U.K.

2.5 Primary Leaf Growth Analysis

2.5.1 Leaf Length Measurements

The lengths of the primary leaves of 30 seedlings were measured daily in mm with a ruler, from 4d to 11d post-imbibition. Leaf length was taken as the distance between the point of attachment of the leaf to the seed, and the leaf tip.

2.5.2 Leaf Fresh and Dry Weight Measurements

The fresh weights of ten primary leaves were recorded in g daily using a fine balance, from 4d to 11d post-imbibition. Leaves were then placed in absorbent paper envelopes in a 60°C oven for 72h, and reweighed to obtain dry weight measurements.

2.5.3 Leaf Elongation Measurements

A modified method of Schnyder and Nelson (1988) was used to determine Segmental Elongation Rate (SER), the elongation rate of a specified leaf segment relative to elongation of the whole leaf; and Velocity of Displacement (V_D), the velocity at which a specified leaf segment is displaced away from the leaf base.

The primary leaves of 30 seedlings were pierced through the intact coleoptile, 6d post-imbibition and 2h into the photoperiod. Piercing was carried out using a 'comb' bearing eight pins of equal length made from 200μm diameter steel wire, positioned at 2mm intervals. The pinholes were made from approximately 2mm distal to the basal intercalary meristem to approximately 16mm distal to this and marked the leaves into seven segments. Plants were returned to the growth cabinet for 24h after which pierced leaves were removed from the seedlings and mounted flat onto paper with clear tape. Distances between pinholes were then measured in mm with a ruler under a dissection microscope at ×20 magnification. The primary leaf lengths of the 30 pierced seedlings and 30 unpierced control seedlings were also measured before and after piercing (6d

and 7d post-imbibition respectively) in order to detect any possible reduction in leaf growth caused by piercing. SER and V_D were calculated using the following equations:

Relative Segmental Elongation (RSE):

$$\mathbf{RSE_i = 2\ (D_{i,\ tn} - D_{i,\ to})\ (\ D_{i,\ tn} + D_{i,\ to})^{-1}}$$

i = particular leaf segment under analysis

$D_{i,\ to}$ = initial length of leaf segment i (i.e. 2mm)

$D_{i,\ tn}$ = length of leaf segment i after time (n) after piercing (i.e. 24h)

Segmental Elongation Rate (SER) (mm.mm leaf length^{-1}.h^{-1}):

$$\mathbf{SER_i = LER\ (RSE_i)\ (RSE_1 + RSE_2 + \ldots\ldots\ RSE_n)^{-1}\ (L^{-1})}$$

i = particular leaf segment under analysis

RSE_1, RSE_2 = RSE for first and second leaf segments from basal meristem

RSE_n = RSE for furthest leaf segment from basal meristem

LER = leaf elongation rate (mm.h^{-1}) of unpierced control leaves between 6d and 7d post-imbibition

L = initial length of leaf segment i (i.e. 2mm)

Velocity of Displacement ($\mathbf{V_D}$) (mm.h^{-1}), calculated for the midpoint of segment i:

$$\mathbf{V_{Di} = L\ (SER_1 + SER_2 + \ldots\ldots\ SER_{i-1}) + 0.5\ (L)\ (SER_i)}$$

i = particular leaf segment under analysis

Problems experienced with this method were the occasional failure to pierce the plant with all eight pinholes, and the placing of the first pinhole too close to or too far away from the basal meristem; but there was no way of improving the method in this respect due to the presence of the coleoptile.

2.5.4 Cell Age Determination along Leaf

A gradient of cell age along the primary leaf was calculated from V_D data (see Section 2.5.3) (Silk & Wagner, 1980). From V_D values (mm.h^{-1}), relative cell displacement from the leaf base towards the tip can be calculated for any given time, t (where t = 0h when cells are positioned approximately 2mm distal to the basal meristem, i.e. at the first pinhole) within leaf segment i. The procedure is as follows:

a) Multiply V_{Di} for segment i (start at the first segment adjacent to the leaf base, approximately 2-4mm distal to the basal meristem) by a set time interval, n (h). Add the resulting value to the current total distance distal to the basal meristem (the starting total is the position of the pinhole at the bottom of the first segment adjacent to the basal meristem, i.e. approximately 2mm distal to the basal meristem) to obtain a new cumulative total.

b) Continue to add ($V_{Di} \times n$) to the cumulative total until it is ≥ the segment midpoint (e.g. approximately 3mm distal to the basal meristem for the first segment adjacent to the leaf base).

c) Substitute V_{Di} for the V_D for the next adjacent segment (e.g. the second segment from the leaf base, approximately 4-6 mm distal to the basal meristem) and repeat a) and b) for all remaining segments.

d) Plot the resulting growth trajectory of cell age, i.e. distance from the basal meristem (mm) verses time (h). From this, cell age at any particular distance from the basal meristem can be determined. Use of a time increment of n = 0.25h in this procedure gives a fairly accurate determination of cell displacement distally from the leaf base. Beyond the zone of cell elongation, cell displacement becomes constant and linear and it is therefore sufficient to use a time increment of 1h from this point.

2.6 Photosynthesis Measurements in Sequential Primary Leaf Sections

Rates of oxygen evolution/consumption along the primary leaf were measured using a Hansatech DW1 leaf-disc electrode and control box (Hansatech, Norfolk, U.K.) linked to a Kogyo Rikadenki chart recorder (Kogyo Company, Tokyo, Japan). The apparatus was assembled according to the manufacturer's instructions and connected to a circulating water bath (Grant Cambridge Ltd., Hertfordshire, U.K.), maintaining a constant temperature of 20°C within the leaf-disc chamber. Before each measurement was made, the electrode was calibrated: the voltage output in mV (R1) displayed on the control box was recorded, then 1ml of air was transferred into the leaf-disc chamber using a syringe. The new voltage output (R2) generated following this was then recorded. The difference between these two readings (R1-R2) was used to calculate the relationship between voltage output on the chart recorder and O_2 concentration. At 20°C and standard pressure, 1ml of air (of which 21% is O_2) contains 8.73μmoles O_2 (Brown & LeMay, 1988). Hence, 8.73μmoles O_2 produces a voltage of (R1-R2)mV, so

8.73/(R1-R2)μmoles O_2 would generate a 1mV change on the chart recorder.

Immediately before use, transverse sections were freshly cut from ten leaves with a razor blade on a cold glass plate, at 5mm intervals starting at 0mm distal to the basal meristem, up to the leaf tip. The fresh weight of each individual set of ten sequential leaf sections was measured in mg on a fine balance, then the sections placed in the leaf-disc chamber. To provide a CO_2 concentration of 5%(v/v), 500μl of 1M potassium bicarbonate was added to the chamber, and the chamber sealed. After calibration, the sections were illuminated with red light (lamp emitting 410-740 μmol m^{-2} s^{-1} PAR) and a trace recorded until a linear trend was obtained.

2.7 Dark Respiration Measurements in Sequential Primary Leaf Sections

A leaf-disc electrode was used to measure rates of oxygen uptake in the dark in a similar procedure to that described for photosynthetic measurements, except without illumination with red light (Section 2.6).

2.8 Protein Analysis in Sequential Primary Leaf Sections

2.8.1 Protein Extraction from Leaf Tissue

Transverse sections were cut from ten leaves with a razor blade on a cold glass plate, at 5mm intervals starting at 0mm distal to the basal meristem, up to the leaf tip. The fresh weight of each set of ten sections was recorded in mg before protein extraction. Each set of sections was frozen in liquid N_2 and ground in an eppendorf tube with protein extraction buffer (72mM Na_2HPO_4, 28mM NaH_2PO_4, 0.5mM EDTA, 1μM leupeptin, 0.007% (v/v) β-mercaptoethanol) at a ratio of 1g fresh tissue to 5ml extraction buffer, for 2mins, using a hand-held homogeniser (Scotlab, Coatbridge, U.K.). Initially, the tissue was ground with approximately half the required volume of extraction buffer, then the homogeniser was washed with the remaining volume, and the washings combined with the crude extract. The samples were then vortex-mixed and centrifuged at 10,000*g* in an MSE Microcentaur bench-top centrifuge (MSE Ltd., Loughborough, U.K.) for 4mins at 4°C. The resulting supernatant was collected and stored on ice for immediate use or frozen in liquid N_2 and stored at -80°C until required.

2.8.2 Soluble Protein Determination in Sequential Leaf Sections

The soluble protein content of transverse sections taken at 5mm intervals

along the leaf (Section 2.8.1), was measured for ten leaves using the Bio-Rad protein microassay, detecting 0-25μg.ml^{-1} soluble protein per sample. The assay is based on that of Bradford (1976) and allows the quantitative measurement of the soluble protein content of a sample by measuring the corresponding colour change of a dye bound to the protein. This is possible since the absorbance maximum for acidic solutions of the dye (Coomassie Brilliant Blue G-250) moves from 465nm to 595nm when dye-protein binding occurs. Protein content of the tissue extracts (μg.ml^{-1}) was determined by extrapolation from a thyroglobulin (porcine thyroid glands, Sigma) protein standard calibration curve (1.25-25.0μg.ml^{-1}) (see Figure 2.1) - all tissue extracts were diluted to within a range of 5-20 μg.ml^{-1}. Triplicates of appropriately diluted 800μl protein samples (extracted as in Section 2.8.1) were vortex-mixed with 200μl Bio-Rad dye reagent concentrate, and the colour left to develop for 15mins. Absorbances at 595nm were measured on a Unicam Heλios Spectrophotometer (Unicam UV-Visible Spectrometry, Cambridge, U.K.).

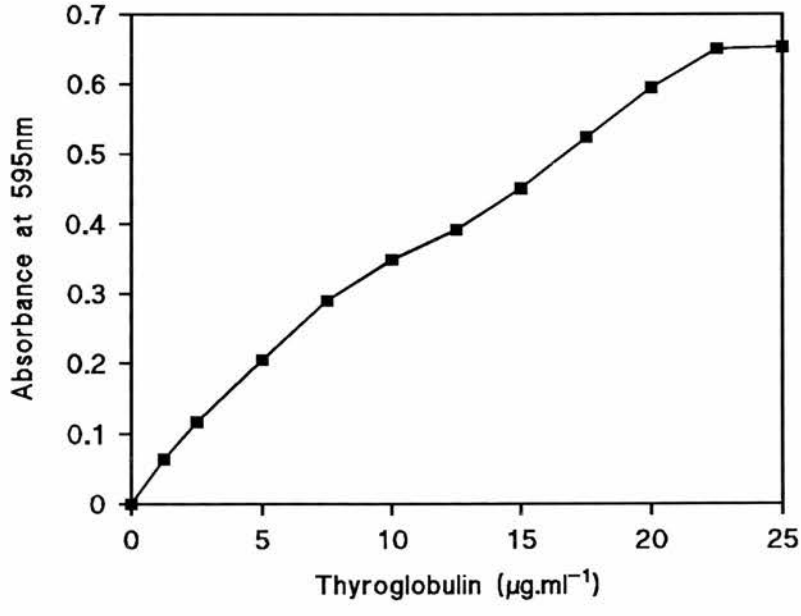

Figure 2.1 Typical Standard Curve used to Estimate Soluble Protein Content along Wheat Primary Leaves. See Section 2.8.2. The Bio-Rad protein microassay was used to estimate protein content in sequential 5mm transverse sections along the leaf. Thyroglobulin (1.25-25.0 μg.ml^{-1}) was used as the protein standard, and samples were zeroed against protein-free blanks.

2.8.3 Mesophyll Cell Number Counts in Sequential Leaf Sections

In order to express protein content along the primary leaf on a per cell basis, mesophyll cell numbers were determined using a modified method of Dean and Leech (1982). Transverse sections were cut from five leaves with a razor blade on a cold glass plate, at 5mm intervals starting at 0mm distal to the basal meristem, up to the leaf tip, and the fresh weight of each set of five sections recorded in mg. Each set of sections was transferred to 500µl of 5% (w/v) chromium trioxide, and stored in an eppendorf tube in the dark at 4°C for 7d. Following this, cells were released by gently pipetting the solutions, then vortex-mixing. Mesophyll cells were then counted using a Weber 1/16mm^2 0.2mm-depth haemocytometer (Weber Scientific International Ltd., Lancing, U.K.) viewed under a Nikon light microscope (Nikon U.K. Ltd., Telford, Salop, U.K.) at ×40 magnification. Cell counts were made within a 1mm^2 area, equating to a volume of 0.2µl each time. Six counts per leaf section were recorded per replicate, and the results expressed as cell number per g leaf tissue fresh weight.

2.9 Detection of Mitochondrial Proteins in Crude Extracts from Sequential Primary Leaf Sections

2.9.1 SDS- Polyacrylamide Gel Electrophoresis (SDS-PAGE)

Protein extracts from sequential primary leaf sections were fractionated on 12.5% (w/v) acrylamide gels using Hoefer mini-gel apparatus (Hoefer Scientific Instruments, San Francisco, U.S.A.), based on the method of Laemmli (1970).

Two gels were cast simultaneously in a Hoefer Mighty Small™ dual gel caster SE 245. Two notched alumina plates, two glass plates, four 1mm thick spacers and two 1mm thick Bio-Rad combs (Hoefer combs were found to be completely unsatisfactory) were washed in detergent, dH_2O and 50% (v/v) ethanol, and then air-dried. For each gel, two 1mm thick spacers were clamped in the gel caster between an alumina plate and a glass plate according to the manufacturer's instructions. Resolving gel solution (377mM Tris-HCl pH 8.8, 31% (w/v) acrylamide-bisacrylamide solution [40%:0.8% w/v] giving an overall acrylamide concentration of 12.5% (w/v), 0.1% (w/v) SDS, 0.05% (w/v) ammonium persulphate, 0.05% (v/v) TEMED) was pipetted between the plates to approximately 2/3 the height of the plates, then overlayed with water-saturated butanol to form a straight edge on the gel solution. Gels were left to polymerise for approximately 20mins, after which the butanol was poured off and the top of the gels

rinsed thoroughly with dH_2O and then stacking gel buffer (0.5M Tris-HCl, pH 6.8). Stacking gel solution (125mM Tris-HCl pH 6.8, 9.7% (v/v) acrylamide-bisacrylamide solution [40%:0.8% w/v] giving an overall acrylamide concentration of 3.9% (w/v), 0.1% (w/v) SDS, 0.05% (w/v) ammonium persulphate, 0.05% (v/v) TEMED) was then pipetted between the plates right to the top of the gel sandwiches. A 1mm thick 15-well comb was immediately inserted into the top of each gel between the plates, so that the bottom of the comb was approximately 1cm from the top of the resolving gel. Gels were left to polymerise for approximately 1h, after which the combs were carefully removed, and the gel sandwiches removed from the gel caster.

Polymerised gels were placed in a Hoefer Mighty Small™ gel electrophoresis unit SE 250 according to the manufacturer's instructions, and the inner buffer chambers filled with reservoir buffer (0.1% (w/v) SDS, 192mM glycine, 25mM Tris, pH 8.4) until the wells of the gels were completely covered with solution. Appropriately diluted primary leaf protein extracts (prepared as described in Section 2.8.1) were mixed with sample buffer (62.5mM Tris pH 6.8, 10% (v/v) glycerol, 2% (w/v) SDS, 0.01% (w/v) bromophenol blue, 5% (v/v) β-mercaptoethanol) at a ratio of four parts protein extract to one part sample buffer, boiled for 5mins to denature the proteins, cooled to room temperature and then loaded onto the gels using a Hamilton syringe ('ready to load' leaf protein samples were usually prepared in advance and stored at -20°C or -80°C). Protein content of the extracts was previously determined (as described in Section 2.8.2), and from preliminary experiments testing a range of concentrations, it was found that 50μg of leaf protein loaded per well was an ideal amount to produce satisfactory polypeptide bands after electrophoresis (equating to total volume of between 10 and 15μl per well, depending on the protein concentration of the tissue extract). For experiments measuring Rubisco-LSU concentration in the primary leaf (Section 4.2.1.2), 16μg leaf protein loaded per well since was optimum for subsequent immunostaining of Rubisco-LSU polypeptide bands (in the Rubisco-LSU experiments, pure Rubisco-LSU protein was also loaded onto the gels in amounts of 0.1μg, 1μg and 5μg). The outer chambers were then filled with a total of 200ml reservoir buffer. Prestained molecular weight markers (10μl per well), previously boiled in the same way as the protein extracts (Sigma prestained SDS-PAGE standard solution, molecular weight range 35-120 kDa), were loaded into one well per gel. Electrophoresis was carried out using a Pharmacia EPS 3500XL power supply (Pharmacia LKB

Biotechnology AB, Uppsala, Sweden) at 100V constant voltage and 250mA, and took approximately 2.5h.

Where gels were not required for Western blotting (Section 2.9.2), they were stained with Coomassie Brilliant Blue R250 to visualise the polypeptide bands. Gels were incubated in fixative (10% (v/v) acetic acid, 40% (v/v) methanol) for 15mins, then in Coomassie stain (0.05% (w/v) Coomassie Brilliant Blue R250, 8% (v/v) acetic acid, 25% (v/v) methanol) for 4h or overnight on a rotator. Gels were then incubated in destaining solution (8% (v/v) acetic acid, 25% (v/v) methanol) on a rotator for approximately 4h or until optimum visibility of the bands was obtained against a clear background. Where destained gels were stored, they were kept in 7% (v/v) acetic acid at 4°C. Alternatively, gels were placed between two sheets of Bio-Rad GelAir cellophane support, which had been soaked in water, and dried using a Bio-Rad GelAir gel dryer. Here, 1% (v/v) glycerol was added to the final destaining solution to prevent gel cracking during drying.

2.9.2 Western Blotting

Western blotting was carried out after the method of Towbin, Staehelin & Gordon (1979) using a Hoefer Mighty Small™ TE 22 Transphor Tank transfer unit. Immediately following SDS-PAGE (Section 2.9.1), two gels and two Bio-Rad Trans-Blot Transfer Medium nitrocellulose 0.45 μm membranes cut to the size of the gels, were soaked in chilled transfer buffer (20% (v/v) methanol, 15.6mM Tris, 120mM glycine, pH 8.3) for at least 30mins at 4°C. Each gel was placed against a nitrocellulose membrane, and then placed between four sheets of Whatman 3MM chromatography filter paper (Whatman International Ltd., Maidstone, U.K.). The resulting sandwich was placed between two sponge pads. Care was taken to ensure that no air bubbles were trapped between any of the layers, which might otherwise inhibit protein transfer. The filter paper and sponge pads were previously soaked in transfer buffer as before. The resulting sandwiches were then assembled in plastic cassettes within the transfer unit ensuring that the nitrocellulose was situated between the gel and the anode, according to the manufacturer's instructions. The transfer unit was filled with chilled transfer buffer and attached to a cold water-cooling system. Protein transfer was carried out using a Pharmacia EPS 3500XL power supply at 4°C at 50V constant voltage and 250mA, for 3h. The buffer within the unit was stirred throughout.

To check that adequate protein transfer had taken place, gels were incubated in Coomassie stain (0.05% (w/v) Coomassie Brilliant Blue R250, 8% (v/v) acetic acid, 25% (v/v) methanol) for 4h or overnight on a rotator, and usually only faint polypeptide bands were visible. Nitrocellulose blots were incubated in 0.25 (w/v) Ponceau S in 3% trichloroacetic acid (TCA) for a few minutes to temporarily stain the polypeptide bands, and ensure that transfer had taken place. The stain was removed by incubating the blots in dH_2O with agitation. Ponceau S staining apparently has no effect on protein antigenicity, and blots could then be used for immunostaining (Section 2.9.4).

2.9.3 Slot Blotting

A Bio-Rad Trans-Blot Transfer Medium nitrocellulose 0.45 μm membrane was cut to the correct size and soaked in wash buffer (25mM Tris, 192mM glycine, pH 8.3) for 5mins. The membrane was then placed in a Hoefer 48-well PR 648 Slot Blot, assembled according to the manufacturer's instructions. A vacuum (0.45-0.85Bar) was then applied, drawing the membrane down towards the base of the apparatus. The vacuum was removed, each well was loaded with 100μl wash buffer, and the vacuum reapplied to draw the buffer through as a precaution against the nitrocellulose membrane drying out and consequent inhibition of protein binding. Protein extracts made from each of 18 sequential 5mm transverse leaf sections (prepared as described in Section 2.8.1) were immediately pipetted into the wells (two wells per leaf section), with care taken to avoid bubble production and resultant inhibition of protein binding. Protein content of the extracts was previously determined (as described in Section 2.8.2) and, following preliminary experiments, it was found that loading 50μg protein per well was satisfactory. Crude extracts were appropriately diluted so that a volume of 100μl was loaded per well - a certain volume was required to prevent the membrane drying out, and in any case it was found that crude extract tended to fail to pass through the membrane fully. Four control wells were loaded with an equal volume of the same batch of whole protein extract of known protein content (again, 50μg protein per well in a 100μl volume per well), on all runs for all replicates. Unused wells were loaded with an equal volume of wash buffer to ensure equal suction across the nitrocellulose membrane - the two outer wells on each row of the apparatus were not used for protein loading as they occasionally did not respond to the pull of the vacuum. After the protein extracts had been drawn through, each well was loaded with 500μl wash buffer and the

vacuum increased to 1.30-1.70Bar to draw the buffer through. This was repeated twice more. At no point was the membrane allowed to dry out. The vacuum was then disconnected, and the nitrocellulose membrane removed from the apparatus for immediate immunostaining, or air-dried and stored at 4°C until required for up to several hours.

Twelve nitrocellulose blots were produced for each of five replicate sets of protein extracts, to allow for two blots (each with duplicate protein extracts) for each of the six mitochondrial proteins under investigation.

2.9.4 Immunostaining of Western and Slot Blots

2.9.4.1 Incubation with Primary Antibodies

In order to test the specificity of the antibodies used in this study, immunostaining was carried out using Western blots (Section 2.9.2) and indirect immunolabelling (see Section 1.3.1). The following procedure was also carried out on slot blots (see Section 2.9.3) to determine the comparative amounts of specific proteins in different tissue extracts, where antibody specificity had already been established. The nitrocellulose blots were briefly rinsed in Tris-buffered saline (TBS) (25mM Tris, 140mM NaCl, 2.6mM KCl, pH 8.0), then incubated for 1h in blocking buffer (10% (w/v) Marvel™ non-fat milk powder in TBS, pH 8.0) on a rotator at room temperature. The blots were then incubated in primary antibody, diluted as appropriate in TBS in 1% (w/v) Marvel™ (pH 7.3), for 1h, on a rotator at room temperature. The primary antibody working dilution was determined by initially testing a range of dilutions from 1:10 to 1:5000 for optimum results, along with a constant secondary antibody dilution - see Table 2.1 for the working dilutions used. For slot blots, the nitrocellulose membranes containing the control slots (see Section 2.9.3) were all incubated in an identical dilution of anti-GDC P-protein as a control. Excess primary antibody was then removed by washing the nitrocellulose blots in 0.1% (v/v) Tween-20 in TBS (pH 8.0) for 10mins and then in 0.5% (v/v) Tween-20 in TBS (pH 8.0) for 10mins on a rotator. The blots were then washed again in 0.1% (v/v) Tween-20 in TBS (pH 8.0) for 10mins on a rotator. Primary antibody solutions were reused only when previous experiments confirmed that no loss of antibody activity resulted from this, and solutions were only reused once.

Two different methods involving enzyme-labelled secondary antibodies were

used for visualisation of polypeptides, depending on the target protein. For Rubisco-LSU, alkaline phosphatase was used and for all other polypeptides (which were accepted to be present in smaller amounts in the leaf than Rubisco-LSU), the more sensitive horseradish peroxidase (HRP) with enhanced chemiluminescence (ECL) detection was used.

Target antigen	Antibody & working dilution for Western blots		Antibody & working dilution for slot blots		Tissue origin of primary antibody	Source of primary antibody	First published use of primary
	Primary	Secondary	Primary	Secondary			
Rubisco-LSU	rat mono-clonal 1:100	goat anti-rat 1:8000	not applicable	not applicable	wheat leaf Rubisco-LSU	Dr M.A.J. Parry IACR Rothamsted, U.K.	Parry & Gutteridge (1989)
PDC E1α	mouse mono-clonal 1:300	goat anti-mouse 1:100	mouse mono-clonal 1:800	goat anti-mouse 1:500	maize leaf mPDC E1α	Prof. D.D. Randall University of Missouri, U.S.A.	Luethy *et al.* (1995)
PDC E1β	rabbit poly-clonal 1:1000	goat anti-rabbit 1:5000	rabbit poly-clonal 1:1000	goat anti-rabbit 1:4000	recombinant *Arabidopsis* mPDC E1β	Prof. D.D. Randall University of Missouri, U.S.A.	Thelen *et al.* (1998)
PDC E2	rabbit poly-clonal 1:200	goat anti-rabbit 1:1000	rabbit poly-clonal 1:100	goat anti-rabbit 1:1000	potato tuber whole mPDC	Dr A.H. Millar University of Western Australia	Millar *et al.* (1999)
PDC E3	rabbit poly-clonal 1:5000	goat anti-rabbit 1:2000	rabbit poly-clonal 1:2000	goat anti-rabbit 1:2000	pea leaf mPDC E3	Prof. J.G. Lindsay University of Glasgow, U.K.	Conner *et al.* (1996)
GDC P-protein	rabbit poly-clonal 1:2000	goat anti-rabbit 1:1000	rabbit poly-clonal 1:800	goat anti-rabbit 1:1000	pea leaf GDC P-protein	Dr S. Rawsthorne John Innes Centre, Norwich, U.K.	Rawsthorne *et al.* (1988)
GDC L-protein	rabbit poly-clonal 1:500	goat anti-rabbit 1:1000	rabbit poly-clonal 1:500	goat anti-rabbit 1:2000	pea leaf GDC L-protein	Dr S. Rawsthorne John Innes Centre, Norwich, U.K.	Rawsthorne *et al.* (1988)

Table 2.1 Details of Antibodies used for Immunostaining of Wheat Primary Leaf Mitochondrial Proteins on Slot Blots and Western Blots. See Section 2.9.4. Secondary antibodies were conjugated to alkaline phosphatase for the Rubisco-LSU-specific antibody, and horseradish peroxidase (HRP) for all other primary antibodies.

2.9.4.2 Alkaline Phosphatase

In the case of Rubisco-LSU, an alkaline phosphatase detection method was used. Here, a colourless chromagen substrate is converted by the enzyme to a visible brown end-product at the reaction site (de Jong *et al.*, 1985).

Following primary antibody incubation and washing, nitrocellulose blots were incubated in secondary antibody (Sigma goat anti-rat IgG alkaline phosphatase conjugate) at a dilution of 1:8000, diluted in 1% (w/v) Marvel™ milk powder in TBS (pH 7.3), for 2h on a rotator at room temperature. Excess secondary antibody was removed by washing the blots in 0.1% (v/v) Tween-20 in TBS (pH 8.0) for 10mins; 0.5% (v/v) Tween-20 in TBS (pH 8.0) for 10mins; then bicarbonate buffer (0.1M $NaHCO_3$, 1mM $MgCl_2$, pH 9.8) for 10mins to adjust the pH, all on a rotator. In order to visualise the polypeptide bands, the nitrocellulose blots were incubated in filtered NBT/BCIP substrate solution (0.03% (w/v) nitroblue tetrazolium (NBT), 0.015% (w/v) bromochloroindoylphosphate (BCIP) in bicarbonate buffer), for minutes or seconds with agitation, until the polypeptide bands were visible, without the development of background staining. Nitrocellulose blots were immediately immersed in 20mM EDTA solution to terminate colour development, then air-dried and stored at 4°C in the dark.

2.9.4.3 Horseradish Peroxidase (HRP) and Enhanced Chemiluminescence (ECL)

In the case of target polypeptides other than Rubisco-LSU, the ECL detection method was used. This is far more sensitive than the alkaline phosphatase method and was used to detect polypeptides thought to be present in very small amounts in the leaf. The ECL method (Amersham International plc, Buckinghamshire, U.K.) is a chemiluminescence system which detects specific immobilised antigens, conjugated directly or indirectly to horseradish peroxidase (HRP) -labelled antibodies (in this study, the latter was the secondary antibody, and hence involved indirect immunolabelling - see Section 1.3.1). Chemiluminescence is defined as the emission of light resulting from the dissipation of energy from a substance in an excited state, and where the excitation is caused by a chemical reaction. Oxidised HRP catalyses the oxidation of luminol (a cyclic diacylhydrazide) under alkaline conditions. Immediately following oxidation, luminol is in an excited state and decays to ground state via a light-emitting pathway (Campbell, 1988). ECL Western blotting detection reagents contain luminol; hydrogen peroxide (which oxidises HRP); and chemical enhancers (phenols) which

increase the light output 1000-fold and extend the time of light emission. Light emission (maximum at λ 428nm) can be detected by a short exposure to a blue-light sensitive autoradiography film. Hence, when a protein blot is indirectly immunolabelled using an HRP-conjugated secondary antibody, then immersed in ECL reagents, chemiluminescence should occur at the sites of the target antigen only.

Following primary antibody incubation and washing, blots were incubated in secondary antibody (Sigma goat anti-rabbit or goat anti-mouse IgG horseradish peroxidase conjugate, for rabbit- and mouse-derived primary antibodies respectively) diluted as appropriate in TBS in 1% (w/v) Marvel™ (pH 7.3), for 2h on a rotator at room temperature. The secondary antibody working dilution was determined by initially testing a range of dilutions from 1:10 to 1:5000 for optimum results, along with the determined optimum primary antibody dilution - see Table 2.1 for the working dilutions used. Excess secondary antibody was removed by washing the blots in 0.1% (v/v) Tween-20 in TBS (pH 8.0) three times, each for 10mins on a rotator. Blots were then incubated in a darkroom in 6ml ECL Western blotting detection reagents for 1-5mins (depending on the strength of the signal obtained during test runs), mixed in equal amounts immediately prior to this according to the manufacturer's instructions. Blots were then placed in a G.R.I. Hi-Speed-X intensifying autoradiography cassette (Genetic Research Instruments Ltd., Dunmow, U.K.) between two sheets of Saran wrap (Dow Chemical Company, from: Viskase, Swansea, U.K.), and with a sheet of Kodak X-OMAT AR film (Eastman Kodak Company, New York, U.S.A.) or Hyperfilm ECL (Amersham International plc) placed on top, overlaying the blots. The position of the blots was marked on the film, and the cassette was closed for up to 2mins, exposing the film to the chemiluminescence emitted from the blots. The film negative was then developed in a Fuji RGII X-ray film processor (Fuji Photo Film Company Ltd, Tokyo, Japan). All film handling was performed under a safe-light in the darkroom.

2.9.5 Analysis of Polypeptide Band Intensity on Immunostained Blots

Following immunostaining using the ECL detection method on slot blots, the comparative intensities of polypeptide bands on developed film negatives were analysed using the AnalySIS image analysis system and software programme (Soft-Imaging Software GmbH, Münster, Germany) equipped with a CCD (charge-coupled device) monochrome video camera (Norfolk Analytical Ltd., Hilgay, U.K.). The image analyser

was initially calibrated to give pixel numbers per mm using the captured image of a ruler.

Captured images of the developed film negatives were then taken and stored as computer TIFF files. Images were corrected for brightness and contrast, then the image intensity calibrated so that the greyscale values of the control bands were always the same on all blots for each particular protein (so that any slight differences in film exposure time between different replicates would be accounted for). Greyscale values (in pixels) were then recorded at 20 random points on all the other bands, and summed to give a single greyscale value in each case.

Greyscale values corresponded to the intensity of the protein bands and therefore gave an indication of the relative amounts of protein per band. It was vital to ensure that a linear relationship existed between increasing band intensity and increasing protein concentration on the membrane, or else band intensity could not be related to protein concentration. This was confirmed by immunostaining slot blots containing a serial dilution of leaf protein extract with anti-PDC E1α antibody. Band intensity was found to increase linearly with increasing protein concentration when the film was exposed for the same time period as used in all experiments.

Per replicate, two slot blots (each with two bands representing each sequential leaf section) were analysed for each of the six proteins under investigation. Using the measurements of leaf protein per mesophyll cell previously obtained (Section 2.8.3), the data was converted to greyscale values per mesophyll cell (since it was known that 50μg protein was loaded per well in all cases). Greyscale values (intensity) per mesophyll cell were then expressed as a percentage of the maximum value obtained in each case, allowing comparisons of different mitochondrial proteins.

Detection of band intensity was also carried out in a similar way, using immunostained Western blots to detect the Rubisco-LSU, developed using the alkaline phosphatase method (Section 2.9.4). Here, lanes of pure Rubisco-LSU protein of known concentrations were included on the original gels as control bands. The density of immunostained leaf protein bands were compared with the control bands to indicate the amount of Rubisco-LSU protein present in the former.

2.9.6 Stripping of Used Immunostained Blots

Where nitocellulose blots were reused after immunostaining using the ECL method, they were stripped of antibodies and reagents by incubation in stripping buffer (62.5mM Tris, 100mM mercaptoethanol, 2% (w/v) SDS, pH 6.7) for 30mins at 60°C with occasional agitation. Blots were rinsed three times in 0.1% Tween-20 in TBS (pH 8.0), for 10mins each time, and were then ready to be reprobed with another antibody. Blots were reused only once.

2.10 Transmission Electron Microscopy (TEM) of Primary Leaf Tissue

For ultrastructural observation, tissue was embedded in Spurr's (1969) medium grade epoxy resin (TAAB Laboratories Ltd., Berkshire, U.K.), which gives excellent ultrastructural preservation. For immunolabelling, tissue was embedded in L.R. White medium grade acrylic resin (London Resin Company Ltd., Reading, U.K.), which does not give such good ultrastructural preservation, but does preserve antigenicity in the tissue, unlike Spurr's resin. There are slight differences in tissue processing for EM for each resin, described as follows.

2.10.1 Tissue Fixation

2.10.1.1 Fixation: Spurr's Resin

Transverse sections of 1mm were cut from approximately 50 leaves with a razor blade on a cold glass plate, at 0-1mm, 3-7mm, 11-12mm, 15-16mm, 20-21mm, and 30-31mm., 50-51mm, and 80-81mm from the basal meristem (sections were not taken right at the leaf tip as the extra unbroken cuticular surface area here was found to inhibit fixative and resin penetration to the inner tissue). Sections were immediately transferred to primary fixative (2.5% (v/v) glutaraldehyde in 0.1M sodium cacodylate buffer, pH 7.3) and vacuum infiltrated for 15mins to aid fixative penetration and therefore protein cross-linkage in the tissue. Sections were then transferred to fresh fixative and placed on a rotator (TAAB Laboratories Ltd.) at 2r.p.m., overnight at room temperature. Sections were subsequently washed in four changes of 0.1M sodium cacodylate buffer (pH 7.3) and incubated in secondary fixative (1% (w/v) osmium tetroxide in 0.1M sodium cacodylate buffer, pH 7.3) on a rotator at 2r.p.m. for 2h at room temperature to fix tissue lipids. Sections were then washed twice in 0.1M sodium cacodylate buffer (pH 7.3) for 5mins each time to remove excess osmium tetroxide.

2.10.1.2 Fixation: L.R. White Resin

Transverse sections of 1mm were cut from approximately 50 leaves with a razor blade on a cold glass plate, at 0-1mm, 7-8mm, 15-16mm, 50-51mm, and 80-81mm from the basal meristem (sections were not taken right at the leaf tip as the extra unbroken cuticular surface area here was found to inhibit fixative and resin penetration to the inner tissue). Sections were immediately transferred to primary fixative (2.5% (v/v) glutaraldehyde in 0.1M sodium cacodylate buffer, pH 7.3) and vacuum infiltrated for 15mins to aid fixative penetration and therefore protein cross-linkage in the tissue. Sections were then transferred to fresh fixative and placed on a rotator (TAAB Laboratories Ltd.) at 2r.p.m., overnight at 4°C. Sections were subsequently washed in four changes of 0.1M sodium cacodylate buffer (pH 7.3).

2.10.2 Tissue Dehydration

2.10.2.1 Dehydration: Spurr's Resin

Fixed sections were incubated sequentially in 30%, 50%, 70%, 90% and 100% (v/v) ethanol for 1h in each dilution at room temperature, and then in fresh 100% (v/v) ethanol for a further 1h. Sections were then en-bloc stained in 2% (w/v) uranyl acetate in 100% (v/v) ethanol on a rotator at 2r.p.m., overnight in darkness; then washed in 100% (v/v) ethanol for 1h at room temperature to remove excess uranyl acetate.

2.10.2.2 Dehydration: L.R. White Resin

Fixed sections were incubated in 30% (v/v) ethanol for 1h at 4°C, sequentially in 50%, 70%, 90% and 100% (v/v) ethanol for 1h in each dilution at -20°C, then in fresh 100% (v/v) ethanol for a further 1h.

2.10.3 Tissue Embedding

2.10.3.1 Embedding: Spurr's Resin

Tissue sections were embedded in Spurr's medium grade epoxy resin (TAAB Laboratories Ltd.), prepared according to the manufacturer's instructions. Dehydrated sections were placed on a rotator at 2r.p.m., for 1h in each of the following in series at room temperature:

2:1 100% (v/v) ethanol to Spurr's resin
1:1 100% (v/v) ethanol to Spurr's resin
1:2 100% (v/v) ethanol to Spurr's resin
Spurr's resin

Sections were transferred to fresh resin on a rotater at 2r.p.m., overnight at room temperature. Tissue was placed in fresh resin for a further 1h, and then polymerised in fresh resin in flat green silicone rubber AGAR moulds (AGAR Scientific Ltd., Essex, U.K.) at 60°C for 24h, producing blocks of approximately 170µl volume. Tissue sections were orientated in the moulds in an optimum position for subsequent transverse sectioning.

2.10.3.2 Embedding: L.R. White Resin

Tissue sections were embedded in L.R. White medium grade acrylic resin (London Resin Company Ltd.). Dehydrated sections were placed on a rotator at 2r.p.m., for 1h in each of the following in series at -20°C:

2:1 100% (v/v) ethanol to L.R. White resin
1:1 100% (v/v) ethanol to L.R. White resin
1:2 100% (v/v) ethanol to L.R. White resin
L.R. White resin

Polymerisation accelerator (0.05% (w/v) benzoin methyl ether) was added to the 100% resin incubations only. Sections were then transferred to fresh resin and placed on a rotator at 2r.p.m., overnight at -20°C. Tissue was placed in fresh resin for a further 1h, and then polymerised in size 0 gelatin capsules (AGAR Scientific Ltd.) at -20°C for 24h under an indirect UV light source, producing blocks of approximately 680 µl volume. Approximately five sections were placed in each of eight capsules (by this stage in the procedure, some of the original 50 sections may have been lost, damaged or removed due to poor quality). The UV lamp (AGAR Scientific Ltd.) emitted 360nm λ light from two 6W bulbs, and was placed approximately 20cm from the capsules. The polymerisation chamber was completely lined with tinfoil to provide a reflective environment, and capsules were shielded from direct UV light by tinfoil shields

attached to the lamp. Capsules were anchored onto the base of the polymerisation chamber with double-sided adhesive tape so that tissue sections were orientated in an optimum position for subsequent transverse sectioning (Figure 2.2).

2.10.4 Ultrathin Sectioning of Tissue Blocks

After roughly trimming the block with razor blades under a dissection microscope to obtain a small tissue face; transverse sections of leaf tissue were cut from polymerised Spurr's and L.R. White blocks using glass knives (freshly cut from plate glass strips using a LKB Knifemaker 7801B, Leica Microsystems U.K. Ltd., Milton Keynes, U.K.) on a Reichert-Jung Ultracut ultramicrotome (Leica U.K. Ltd.) at a knife angle of 5°, cutting angle of 0° and cutting speed of 2mm.s^{-1}. Thick sections of approximately 1μm were initially cut onto dH_2O, transferred to light microscope slides and dried in dH_2O on a hot plate at 80°C for 1min. Sections were stained with methylene blue (1% (w/v) methylene blue, 1% (w/v) sodium tetraborate in dH_2O) for 1min on a hot plate at 80°C, then rinsed with dH_2O. Sections were viewed under a light microscope (Nikon U.K. Ltd.) at ×100 magnification to confirm a satisfactory general standard of fixation, and to select a smaller area of tissue from which to cut sections. Ultrathin sections of approximately 95nm showing purple or copper/gold light interference when cut onto dH_2O, were expanded using 100% (v/v) chloroform vapour (producing sections with copper/gold or silver interference). Sections were mounted onto the coated (see Section 2.10.5) side of 3.05mm diameter Athene Old 400 mesh (45μm^2 holes) copper (for Spurr's resin) or nickel (for L.R. White resin) electron microscopy (EM) grids (AGAR Scientific Ltd.), by placing the grids flat onto the expanded sections, using forceps. EM grids were then transferred to Whatman No. 50 hardened filter paper to dry. See Section 2.13 for sampling of tissue blocks for sectioning.

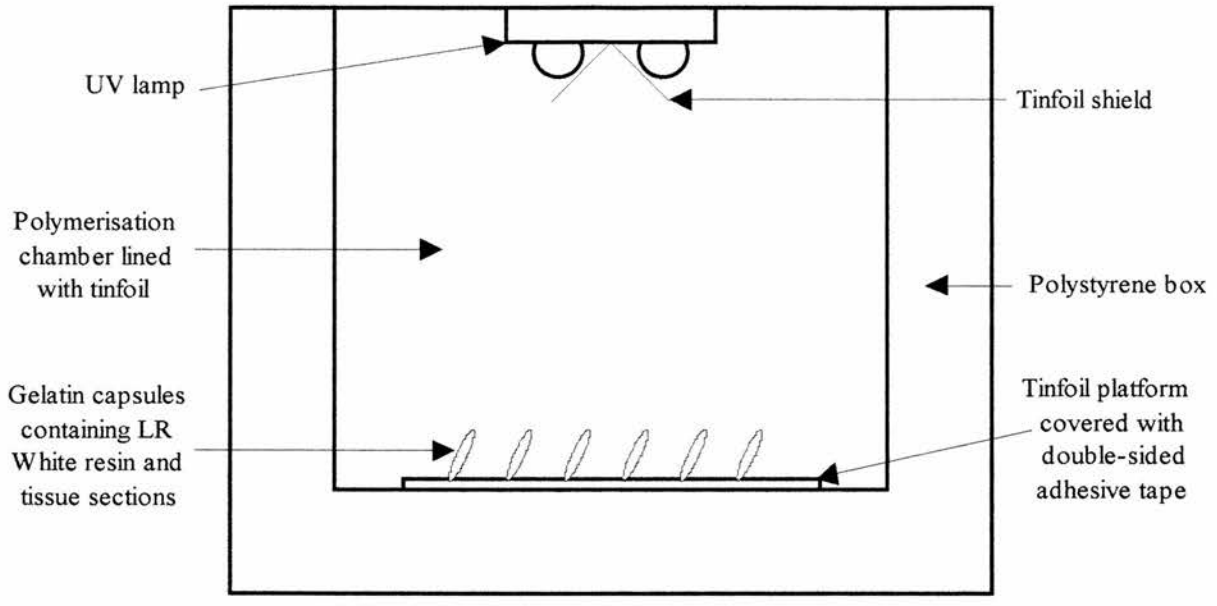

Figure 2.2 UV Light Apparatus used for Polymerisation of L.R. White Embedded Wheat Primary Leaf Tissue. See Section 2.10.3. Resin blocks containing fixed tissue sections were polymerised in gelatin capsules.

2.10.5 Coating EM Grids with Formvar and Carbon

Prior to use, EM grids were coated on one side with formvar plastic as a tissue support, then carbon to stabilise the tissue and formvar film under the electron beam of the EM. To create formvar films, glass slides were immersed in 1% formvar (previously oven-dried to remove any moisture) in chloroform for 1min; shaken and held above the solution in a covered container for 45s. Slides were then transferred onto a clean dH_2O surface in a small bowl by scoring the slides with a diamond pen and slowly dipping them at a 45° angle in the dH_2O so that the films came off onto the water surface. The % of formvar in chloroform used, and the time which the newly-immersed slides were held above this solution, were previously determined by testing a range of dilutions and times to obtain the thinnest films possible without compromising on strength - such films were observed as having silver light interference. EM grids were thoroughly cleaned by immersion in several changes of chloroform for a few minutes each time, dried on Whatman No. 50 hardened filter paper, then laid dull-side down onto the floating film (the dull sides of EM grids are rougher and provide a larger surface area for film adherence than the smoother polished sides). The film with adhered EM grids

was then transferred onto parafilm (Nescofilm, Bando Chemical Ind. Ltd., Kobe, Japan) by carefully rolling the latter on the dH_2O surface causing the film to adhere evenly to the parafilm. Where possible, formvar coating was carried out in conditions of minimum atmospheric moisture, i.e. a sunny day, since high moisture levels can produce unstable films (pers. com., J. Mackie, University of St Andrews). EM grids were then left to dry on Whatman No. 50 hardened filter paper before being carbon-coated on the same side using vacuum evaporation apparatus (Carbon Turbocoater, Bio-Rad Microscience Division), according to the manufacturer's instructions. Carbon coating thickness was controlled as it was found that where the carbon coating was too thick, the whole support film occasionally came off the grids during processing. Coated EM grids were stored on Whatman No. 50 hardened filter paper in a dust-free environment.

2.10.6 Heavy Metal Staining of Tissue

Following ultrathin sectioning, Spurr's sections on copper EM grids were stained with electron-dense heavy metals to enhance tissue contrast when viewed under the EM. L.R. White sections on nickel EM grids used for immunogold techniques (Section 2.12.2), were stained after the latter were performed.

Staining of tissue on EM grids was carried out on strips of parafilm in covered plastic petri-dishes by floating EM grids (with tissue side face-down) on 50µl droplets of the appropriate staining solutions. All solutions were centrifuged at 10,000*g* in an MSE Microcentaur bench-top centrifuge (MSE Ltd.) for 10mins, then filtered through a 0.2µm filter (Millipore Corporation, Bedford, U.K.) to minimise the incidence of artifacts on the EM grids. Between all the following transferrals, EM grids were blotted on Whatman No. 50 hardened filter paper to remove excess solution, and forceps washed. EM grids were stained in 2% (w/v) uranyl acetate (Hayat, 1975) in 70% (v/v) ethanol for 20mins in darkness, then rinsed in three changes of dH_2O for 5mins each time to remove excess uranyl acetate. EM grids were then stained in 0.3% (w/v) lead citrate (Reynolds, 1963) in 0.1 M NaOH for 3mins, in a moisture-free environment (maintained by placing several NaOH pellets within the covered petri-dishes). EM grids were then rinsed briefly in 0.1M NaOH, rinsed in three changes of dH_2O for 5mins each time, dried on Whatman No. 50 hardened filter paper, and stored in a dust-free environment.

2.10.7 Examination of Tissue Sections

Leaf sections were viewed under a Phillips 301 Transmission Electron Microscope (TEM) at 60kv (Phillips, Cambridge, U.K.) and photographed with Agfa-Gavaert EM film at magnifications of ×5000 (Spurr's sections) and ×15650 (L.R. White sections). Negatives were developed in Ilford Phenisol (Ilford Ltd., Mobberley, Cheshire, U.K.) for 3.5mins at 20°C and washed in running tap water for 2mins. Negatives were then fixed in Ilford Hypham (Ilford Ltd.) for 5mins, washed in running tap water for 2mins and left to air dry. Electron micrographs were analysed using the AnalySIS image analysis system and software programme (Soft-Imaging Software Gmb H) equipped with a CCD monochrome video camera (Norfolk Analytical Ltd.). See Section 2.13 for details of the measurements made from micrographs. Once prepared, EM grids with tissue sections (immunostained or not) can be stored for years with no deterioration, for repeated viewing.

2.11 Light Microscopy (LM) of Primary Leaf Tissue

Tissue sections embedded in Spurr's resin for electron microscopy, were also sampled for light microscopy by cutting 0.5 μm thick sections using a microtome (Leica U.K. Ltd.) as before (see Section 2.10.4). After cutting, sections were transferred to light microscope slides and dried in dH_2O on a hot plate at 80°C for 1min. Sections were then stained with methylene blue (1% (w/v) methylene blue, 1% (w/v) sodium tetraborate in dH_2O) for 1min on a hot-plate at 80°C, then rinsed with dH_2O. Sections were viewed under a Zeiss Axioplan Universal light microscope (Carl Zeiss Microscopy, Jena, Germany) equipped with a Pentax LX 35mm camera (Leica U.K. Ltd.), and photographed at magnifications of ×100 and ×300, using automatic exposure and Agfa-Gevaert 25 film (Agfa-Gevaert, Brentford, Middlesex, U.K.). Light micrograph negatives were analysed using the AnalySIS image analysis system and software programme (Soft-Imaging Software Gmb H) equipped with a mono-chrome CCD monochrome video camera (Norfolk Analytical Ltd.). See Section 2.13 for details of the measurements made from micrographs.

2.12 Immunogold Localisation of Mitochondrial Proteins in Primary Leaf Sections

Immunogold labelling was carried out on 1mm primary leaf sections taken at five locations along the leaf, using tissue sections on nickel EM grids (prepared as

described in Section 2.10), and an indirect immunolabelling technique (see Section 1.3.1.3). Nickel rather than copper EM grids were used for immunogold labelling procedures since the latter produce a chemical reaction with gold conjugates.

2.12.1 Optimisation of Immunogold Labelling Procedure

Although a large variety of protocols for indirect immunogold labelling exist, all consist of the same basic elements. These are the blocking of non-specific antibody sites, followed by incubation in primary antibody, then incubation in secondary antibody (with appropriate washing off of excess reagents between each stage). Different blocking buffers, antibody incubation times, etc. may be used depending on what produces optimal results in a particular experiment. The procedure used here was based on a protocol previously used successfully on cereals in our laboratory (Peat & Tobin, 1996), and was refined via preliminary experiments to produce optimal results in the present study. The primary antibody working dilution was determined by initially testing a range of dilutions from 1:10 to 1:5000 for the best results along with a constant secondary antibody dilution (1:100). The determined optimum primary antibody dilution was then used to test a range of secondary antibody dilutions from 1:10 to 1:5000. This was done individually for each mitochondrial protein investigated due to differences in antibody titre, specificity, affinity and so on; and due to possible differences in the amount of target protein present in the samples. Where necessary, further testing with narrower ranges of dilutions was carried out to more accurately determine optimum concentrations. Test EM grids used for these preliminary experiments included those with tissue sections representing three different developmental stages along the primary leaf (transverse sections of 0-1mm, 15-16mm, and 80-81mm from the basal meristem).

2.12.2 Immunogold Labelling Procedure

Immunolabelling of tissue on EM grids was carried out at room temperature on strips of parafilm in covered plastic petri-dishes by floating EM grids (with tissue side face-down - the dull sides of the EM grids) on 50µl droplets of the appropriate solutions. For the longer antibody incubations, moist filter paper was placed in the petri-dishes below the parafilm to prevent the droplets drying out. All solutions except the antibodies were filtered through 0.2µm filters (Millipore Corporation) to minimise the

incidence of artifacts on the EM grids. Between all the following transferrals, excess solution from the last incubation was removed from the EM grids by carefully blotting the rims on Whatman No. 50 hardened filter paper (avoiding any direct contact with the tissue sections), and forceps washed.

EM grids were initially incubated in 0.5M NH_4Cl for 1h to remove any free aldehydes from the surface of the sections induced by fixation (which can otherwise bind to antibodies); then transferred to blocking buffer (10mM Na-phosphate buffer, 3% (w/v) NaCl, 1% (w/v) globulin-free bovine serum albumin (BSA), 0.1% (v/v) Tween-20) for 1h to block nonspecific sites with protein. EM grids were then transferred to primary antibody solution, appropriately diluted in blocking buffer, for 2h. EM grids were rinsed of excess primary antibody by incubation in three changes of blocking buffer for 5mins each time. EM grids were then transferred to secondary antibody solution - goat anti-rabbit or goat anti-mouse IgG 15nm gold conjugate (British Biocell International, Cardiff, U.K.), for rabbit and mouse derived primary antibodies respectively - appropriately diluted in blocking buffer, for 2h. EM grids were then rinsed again in three changes of blocking buffer for 5mins each time, and then in three changes of dH_2O for 5mins each time. The tissue sections were then stained with heavy metals, as described in Section 2.10.6. Details and working dilutions of the antibodies used in this study for detection of the individual proteins under investigation, are shown in Table 2.2.

To test the specificity of the secondary antibodies used, a negative control was included in each experiment, where the primary antibody was substituted for blocking buffer. Absence of gold labelling indicated that the secondary antibody had not non-specifically attached to tissue factors such as basic proteins and aldehyde groups. For experiments involving polyclonal antibodies, another negative control was included where the primary antibody was replaced by non-immune serum (i.e. serum from an non-immunised animal of the same species in which the primary antibody was raised), was also included in each experiment to check whether the primary antiserum contained any antibodies which might react with similar antigens or tissue factors, and in turn be recognized by the secondary antibody. Absence of gold labelling in both negative controls indicated that the antiserum contained antibodies which were only specific for the antigen of interest.

Target antigen	Primary antibody & working dilution	Secondary antibody & working dilution	Tissue origin of primary antibody	Source of primary antibody	First published use of primary antibody
PDC E1α	mouse monoclonal 1:5	goat anti-mouse 1:10	maize leaf mPDC E1α	Prof. D.D. Randall University of Missouri, U.S.A.	Luethy *et al.* (1995)
PDC E1β	rabbit polyclonal 1:600	goat anti-rabbit 1:100	recombinant *Arabidopsis* mPDC E1β	Prof. D.D. Randall, University of Missouri, U.S.A.	Thelen *et al.* (1998)
PDC E2	rabbit polyclonal 1:300	goat anti-rabbit 1:100	potato tuber whole mPDC	Dr A.H. Millar University of Western Australia	Millar *et al.* (1999)
PDC E3	rabbit monoclonal 1:100	goat anti-rabbit 1:500	pea leaf mPDC E3	Prof. J.G. Lindsay University of Glasgow, U.K.	Conner *et al.* (1996)
GDC P-protein	rabbit poly-clonal 1:300	goat anti-rabbit 1:600	pea leaf GDC P-protein	Dr S. Rawsthorne John Innes Centre, Norwich, U.K.	Rawsthorne *et al.* (1988)
GDC L-protein	rabbit poly-clonal 1:200	goat anti-rabbit 1:100	pea leaf GDC L-protein	Dr S. Rawsthorne John Innes Centre, Norwich, U.K.	Rawsthorne *et al.* (1988)

Table 2.2 Details of Antibodies used for Immunogold Labelling of Wheat Primary Leaf Mitochondrial Proteins on Transverse Tissue Sections. See Section 2.12.2. Secondary antibodies were gold conjugates with a particle size of 15nm.

2.13 Sampling for Microscopy Studies

Microscopy was carried out at four different magnifications, using light microscopy (LM) and transmission electron microscopy (TEM). For each of three replicates, one LM slide or EM grid was made from each of ten resin-embedded transverse leaf sections for each of five (for L.R. White tissue blocks) or nine (for Spurr's tissue blocks) leaf developmental stages. This was done for each magnification, except that the same slides were used to take light micrographs at ×100 and ×300. For immunogold labelling experiments at ×15650, this was repeated six times to produce six different sets of grids, for use with the six different mitochondrial proteins under investigation. For L.R. White blocks, the five developmental stages were represented by 1mm transverse sections cut at the following distances from the basal meristem: 0-1mm (leaf base), 7-8mm (middle of leaf elongation zone), 15-16mm (end of leaf elongation zone), 50-51mm (approximately halfway along leaf), and 80-81mm (near leaf tip). In addition to these five developmental stages, Spurr's blocks also included four other

developmental stages represented by 1mm transverse sections taken at the following distances from the basal meristem: 3-4mm, 10-11mm, 20-21mm, and 30-31mm. Table 2.3 shows the various stereological measurements made at each magnification. Two micrographs were taken from each LM slide or EM grid at each magnification. For immunogold labelling observation at ×15650, two sets of micrographs were taken from the LR White grids, one of mesophyll tissue, and one of vascular tissue (companion cells). So, in each individual case a total of 20 micrographs were produced per developmental stage. Extra grids were also produced as controls for immunogold localisation experiments, and in case of damage to other grids during processing.

Embedded leaf sections were chosen randomly after any poorly-embedded or damaged sections had been discarded. Unsatisfactory embedding occasionally occurred in some tissue sections, due to poor resin penetration or trapped air bubbles next to the tissue during resin polymerisation. Any sections which were poorly-orientated in the resin were also eliminated, for ease of transverse sectioning.

A sample size of 20 micrographs was calculated for all the measurements made at the EM level, from the sampling errors inherent in the stereological methods used. This was done by plotting the cumulative standard errors of the data for an increasing number of micrographs (Bolender, 1978). The point at which the graph plateaued indicated the number of micrographs required to reduce the standard error to ≤ 10% of the mean (Blouin *et al.*, 1977) - see Section 1.3.2 for further information on the principles of stereology. Hence, a plot was made for comparative quantification of immunogold labelling for each developmental stage, mitochondrial protein under investigation and cell type (mesophyll or companion cell); and for mitochondrial transverse area (TA) and volume fraction (V_v) measurements at each developmental stage. The calculated figures ranged from between 15 and 20 micrographs, and 20 were taken in each case for uniformity. It was not necessary to make cumulative standard error plots for measurements made at the LM level, however for uniformity 20 micrographs were taken in these cases also, at each developmental stage. For light micrographs, two different regions of tissue were chosen via systematic random sampling from a single section on each LM slide. For electron micrographs, two different grid squares were chosen via systematic random sampling from a single section on each EM grid, and the micrograph taken from the region of cytoplasm nearest to the top right hand corner of the grid square. Producing only one LM slide/EM

grid per tissue section avoided the same area of tissue being sampled more than once, providing that micrographs were taken via systematic random sampling, and taken from a single section per LM slide/EM grid.

For cellular V_v measurement, the total tissue area of interest on each micrograph was measured, and expressed as a % of the total transverse leaf area for each developmental stage. Numbers of individual mesophyll, vascular and epidermal cells within the whole transverse leaf area were counted on each micrograph for each developmental stage, and the frequency expressed as a % of total cell frequency in the leaf. For vacuolar V_v measurement, total vacuolar area on each micrograph was measured, and expressed as a % of total mesophyll cell area. To measure mitochondrial TA (μm^2), 100 mitochondrial profiles were measured from each sample of 20 micrographs. For mitochondrial V_v measurement, total mitochondrial area on each micrograph was measured, and expressed as a % of total cytoplasmic area, inclusive of any cellular compartments within the cytoplasm except vacuoles and nuclei. For immunogold analysis, total mitochondrial area on each micrograph was measured, the gold particles located there counted, and the data expressed as gold particles per μm^2 mitochondrial area.

The magnifications used for microscopy were the lowest which gave satisfactory resolution of the objects being observed and measured, while giving the largest possible tissue area for examination, e.g. below a magnification of $\times$15650, 15nm gold particles could not be adequately resolved for comparative quantification.

Magnification	Measurements made from micrographs	Embedding resin used
LM ×100	volume fraction (Vv) of primary leaf occupied by mesophyll cells, vascular cells, epidermal cells, and air spaces (%) at different stages of leaf development	Spurr's
	frequency of mesophyll, vascular and epidermal cells in primary leaf (%) at different stages of leaf development	
LM ×300	volume fraction (Vv) of mesophyll cell occupied by vacuole (%) at different stages of leaf development	Spurr's
TEM ×5000	mitochondrial transverse area (TA) (μm^2) at different stages of leaf development	Spurr's
	volume fraction (Vv) of mesophyll cell cytoplasm occupied by mitochondria (%) at different stages of leaf development	
TEM ×15650	comparative quantification of immunogold labelling at different stages of leaf development (gold particles. μm mitochondrial $area^{-2}$) in both mesophyll and companion cells	L.R.White

Table 2.3 Stereological Measurements made from Micrographs taken during Light Microscopy (LM) and Transmission Electron Microscopy (TEM) Studies of Developing Wheat Primary Leaves. See Section 2.13. Measurements were made at nine different leaf developmental stages for Spurr's-embedded tissue, and at five different leaf developmental stages for L.R. White embedded-tissue.

CHAPTER 3: CHARACTERISATION OF THE NATURAL DEVELOPMENTAL GRADIENT OF WHEAT PRIMARY LEAVES, FOR USE AS A MODEL IN THE STUDY OF PLANT MITOCHONDRIAL BIOGENESIS

3.1 Introduction

3.1.1 Studies of Wheat Primary Leaf Development

There has been extensive study of the growth and development of *Triticum aestivum* (wheat), and of the development of cereals and the Gramineae in general. The economic importance of cereals and in particular wheat - the most important arable crop in the world with 16.5 million tonnes produced in the U.K. in 2000 (FAO Agricultural Production Statistical Database, 2001) - has partly fuelled this large body of research. However, there are particular reasons which make grasses especially suitable for leaf developmental studies.

3.1.2 The Natural Developmental Gradient of Monocot Leaves

As described in Chapter 1, in monocot plants such as wheat, all cell division in the young leaf occurs near the base within the basal intercalary meristem. This generates a developmental gradient along the leaf from base to tip, and provides a useful model for leaf developmental studies. The youngest cells are located just above the meristem with cells increasing in age distal to this, and with the most functionally mature cells occurring at the leaf tip (Nelson & MacAdam, 1989; Tobin & Rogers, 1992). This means that developmental studies conducted at any point along the leaf, are concerned with cells of known age. In wheat for example, primary leaves are best studied when approximately seven days old (as in the present study), since at this time, the developmental gradient along the leaf is at its greatest (Tobin, Ridley & Stewart 1985).

Many leaf developmental studies have been carried out on a wide range of dicot species however, e.g. *Nicotiana tabacum* (tobacco) (Richards & Kavanagh, 1943), *Xanthium italicum* (cocklebur) (Maksymowych & Erickson, 1973), *Pisum sativum* (pea) (Azcon-Bieto, Lambers & Day, 1983; Lennon *et al.*, 1995), *Phaseolus vulgaris* (bean) (Castrillo, 1999) and *Arabidopsis thaliana* (Donnelly *et al.*, 1999). For dicots, methods of distinguishing tissue of different developental stages have included the comparison of

etiolated and green leaves; and the use of seedlings of different ages, as in pea (Miernyk, Camp & Randall, 1985).

An extensive amount of plant developmental research though, has utilised the natural developmental gradient of the Gramineae. These studies include *Triticum aestivum* (wheat) (Dean & Leech, 1982a, 1982b; Topping & Leaver, 1990; Rogers *et al.*, 1991; Tobin & Rogers, 1992; Beemster & Masle, 1996; Hu, Camp & Schmidhalter, 2000), *Hordeum vulgare* (barley) (Dale, 1972; Owen, Laybourn-Parry & Wellburn, 1986; Thompson, Bowsher & Tobin, 1998), *Zea mays* (maize) (Darvill, Smith & Hall, 1978; Hernandez, Passas & Smith, 1999), *Oryza sativa* (rice) (Dai *et al.*, 1995; Lorbiecke & Sauter, 1998), *Lolium temulentum* (rye grass) (Ougham, Jones & Evans, 1987) and *Festuca arundinacea* (tall fescue grass) (Schnyder & Nelson, 1988; Maurice, Gastal & Durand, 1997). These studies encompass morphological, ultrastructural, physiological, biochemical and molecular aspects of leaf development.

3.1.3 Aims of Chapter

The aims of this chapter are to characterise the growth of wheat primary leaves, and to identify the presence of a developmental gradient between the leaf base and tip. This gradient has been well characterised in wheat (Tobin & Rogers, 1992), and was investigated here for characterisation under the particular growth conditions of this study. Such a natural developmental gradient is an excellent model for the study of many aspects of leaf development, and therefore this chapter provides an essential basis for the study of wheat primary leaf metabolic development under the same growth conditions, presented in later chapters.

3.2 Results

3.2.1 Wheat Primary Leaf Growth

3.2.1.1 Primary Leaf Length

Mean primary leaf length significantly increased ($p \leq 0.05$) with time linearly from 24.8mm to 111.1mm between 4d and 8d post-imbibition, corresponding to a mean growth rate of 21.6 $mm.d^{-1}$ during this time period (Figure 3.1). From 8d to 10d post-imbibition, mean primary leaf growth rate declined to 10.4 $mm.d^{-1}$, and leaf length remained virtually constant from 10d to 11d post-imbibition.

3.2.1.2 Primary Leaf Fresh and Dry Weight

Mean primary leaf fresh weight significantly increased ($p \leq 0.05$) with time from 15.8mg to 71.7mg between 4d and 7d post-imbibition in a virtually linear trend, corresponding to a mean weight increase of 18.6 $mg.d^{-1}$ during this time period (Figure 3.2). Primary leaf dry weight significantly increased ($p \leq 0.05$) with time linearly from 2.1mg to 7.9mg over the same time period, corresponding to a mean weight increase of 1.9 $mg.d^{-1}$. Mean primary leaf dry weight was approximately 12% of fresh weight over the whole time period so that at the time of harvest, mean primary leaf water content was constant at approximately 88%. Dry weight is generally accepted to be a more accurate measurement than fresh weight as it avoids the possibility of short-term fluctuations in tissue water-content.

3.2.1.3 Primary Leaf Segmental Elongation Rate (SER)

Mean primary leaf Segmental Elongation Rate (SER), i.e. the elongation rate of a specified leaf segment relative to elongation of the whole leaf, is shown in Figure 3.3. SER values are plotted at the distance corresponding to the midpoint of each leaf segment examined within the basal region of the primary leaf. SER significantly increased ($p \leq 0.05$) from zero to a maximum of 0.13 $mm.mm\ leaf\ length^{-1}.h^{-1}$ between a distance of 0mm and 6mm from the basal meristem. From here, SER significantly declined ($p \leq 0.05$) back to zero up to a distance of 16mm from the basal meristem. Although the leaf piercing method of measuring SER reduced leaf growth by approximately 30% compared to controls, Schnyder, Nelson & Coutts (1987) evaluated the technique and found that all segments are affected by any growth reduction to the same extent. Hence, comparisons between segments on the same leaf are valid. The

equations used to calculate SER account for the overall difference in growth between pierced and control plants (see Section 2.5.3).

3.2.1.4 Primary Leaf Velocity of Displacement (V_D)

Mean primary leaf Velocity of Displacement (V_D), i.e. the velocity at which a specified leaf segment is displaced away from the leaf base, was calculated from SER data (Sections 2.5.3 and 3.2.1.3) and is shown in Figure 3.4. V_D values are plotted at a distance corresponding to the midpoint of each leaf segment examined within the basal region of the primary leaf. V_D initially increased from zero to 0.08 $mm.h^{-1}$ between a distance of 0mm and 4mm from the basal meristem, and then continued to increase linearly between this point and 12mm from the basal meristem, where V_D was 0.86 $mm.h^{-1}$. Between this point and a distance of 16mm from the basal meristem, V_D attained a maximum value of 0.93 $mm.h^{-1}$.

3.2.1.5 Primary Leaf Cell Age

The mean cell age within the primary leaf increased rapidly between a distance of 0mm and 5mm from the basal meristem, with cells being approximately 20h old at 5mm (Figure 3.5). From here, cell age increased linearly towards the leaf tip accompanied by a slower rate of cell displacement, with cells ageing approximately 7.5h with every 5mm displacement from the basal meristem.

3.2.1.6 Primary Leaf Mesophyll Cell Number

Mean primary leaf mesophyll cell number in transverse sections taken at intervals along the leaf, is shown in Figure 3.6 - plotted values are means for each particular leaf segment examined, e.g. the value plotted at 5mm represents the leaf segment 0-5mm from the basal meristem. Mean mesophyll cell number significantly decreased ($p \leq 0.05$) from a maximum value of 2.90 $\times 10^4$cells.g fresh $weight^{-1}$ at a distance of 0-5mm from the basal meristem; to a value of 0.68 $\times 10^4$ cells.g fresh $weight^{-1}$ at a distance of 15-20mm from the basal meristem. From here, mesophyll cell number remained constant along the leaf to the tip at an average of 0.56 $\times 10^4$ cells.g fresh $weight^{-1}$ between 15mm and 90mm from the basal meristem.

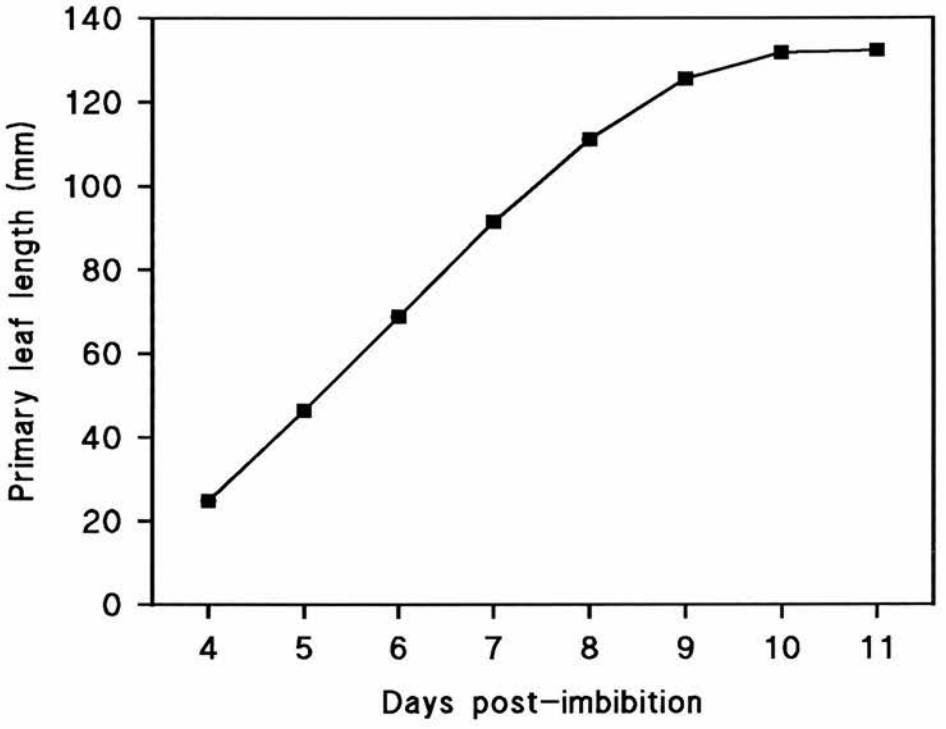

Figure 3.1 Increase in Wheat Primary Leaf Length with Time. See Section 3.2.1.1. Values represent the mean of five replicates, each from a different batch of plants ± standard errors. Standard errors are in the range 0.03-0.08 and are too small to be visible on this graph.

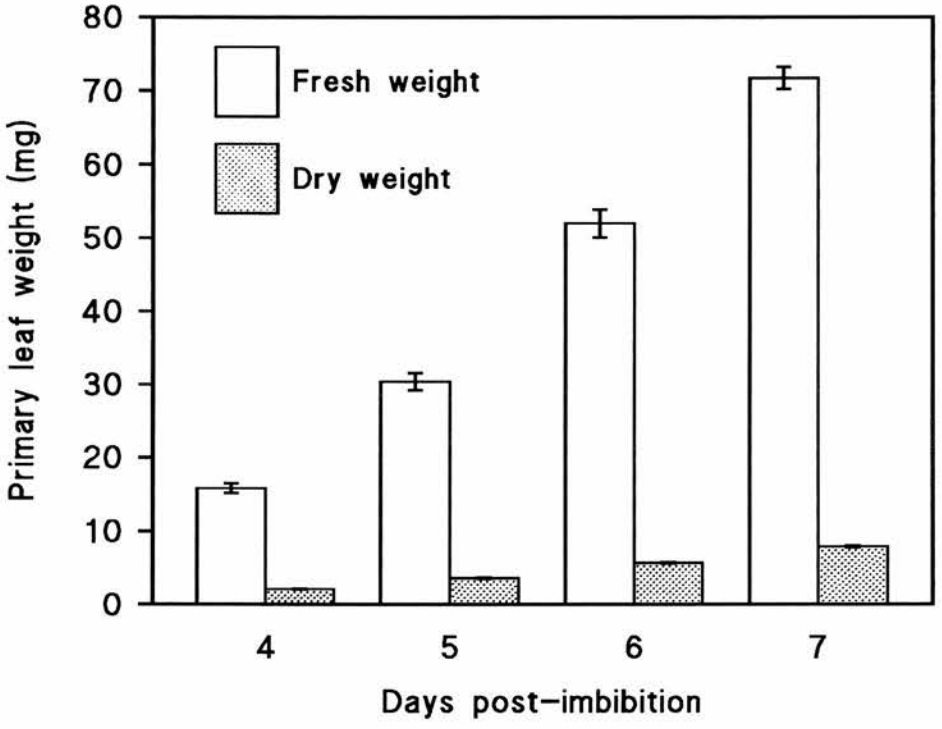

Figure 3.2 Increase in Wheat Primary Leaf Fresh and Dry Weight with Time. See Section 3.2.1.2. Bars represent the mean of five replicates, each from a different batch of plants ± standard errors.

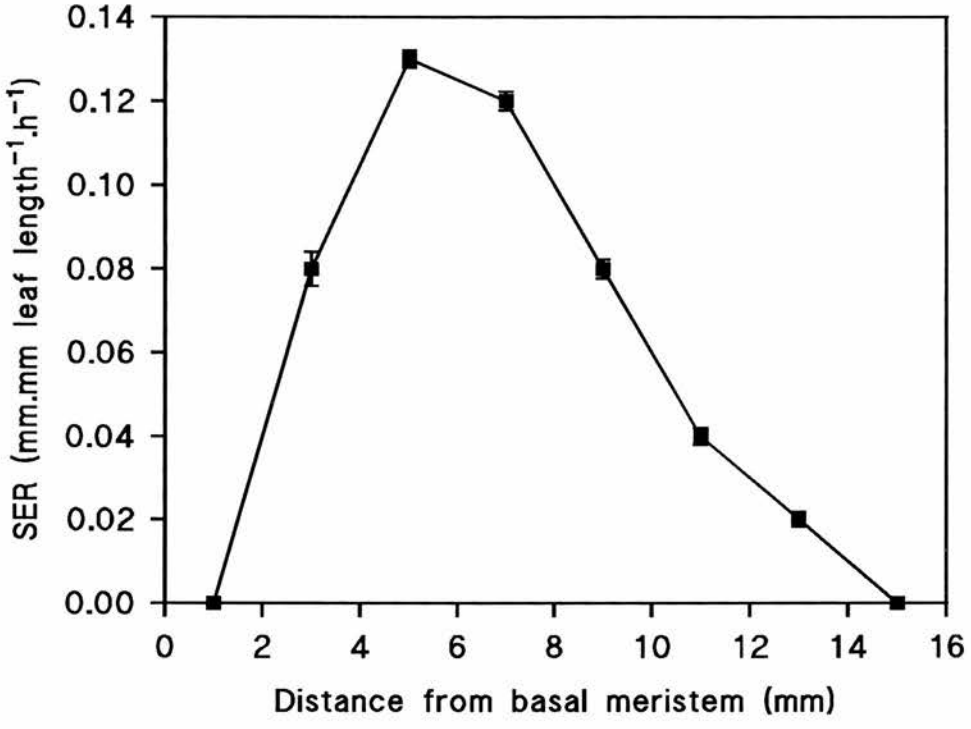

Figure 3.3 Segmental Elongation Rate (SER) of Leaf Segments along the Basal Region of Wheat Primary Leaves. See Section 3.2.1.3. Values represent the mean of five replicates, each from a different batch of plants ± standard errors. SER was measured between 6d and 7d post-imbibition, and values are plotted at the distance corresponding to the midpoint of each leaf segment examined (see Section 2.5.3).

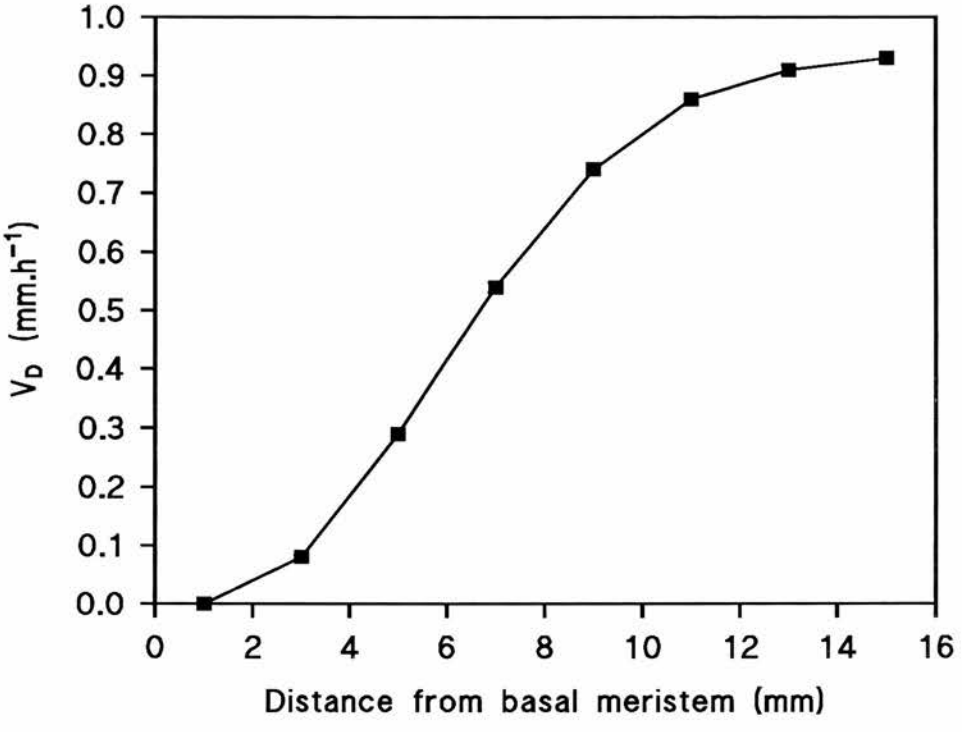

Figure 3.4 Velocity of Displacement (V_D) of Leaf Segments along the Basal Region of Wheat Primary Leaves. See Section 3.2.1.4. Values represent the mean of five replicates, each from a different batch of plants. V_D values were calculated from SER values measured between 6d and 7d post-imbibition, and are plotted at a distance corresponding to the midpoint of each leaf segment examined (see Section 2.5.3).

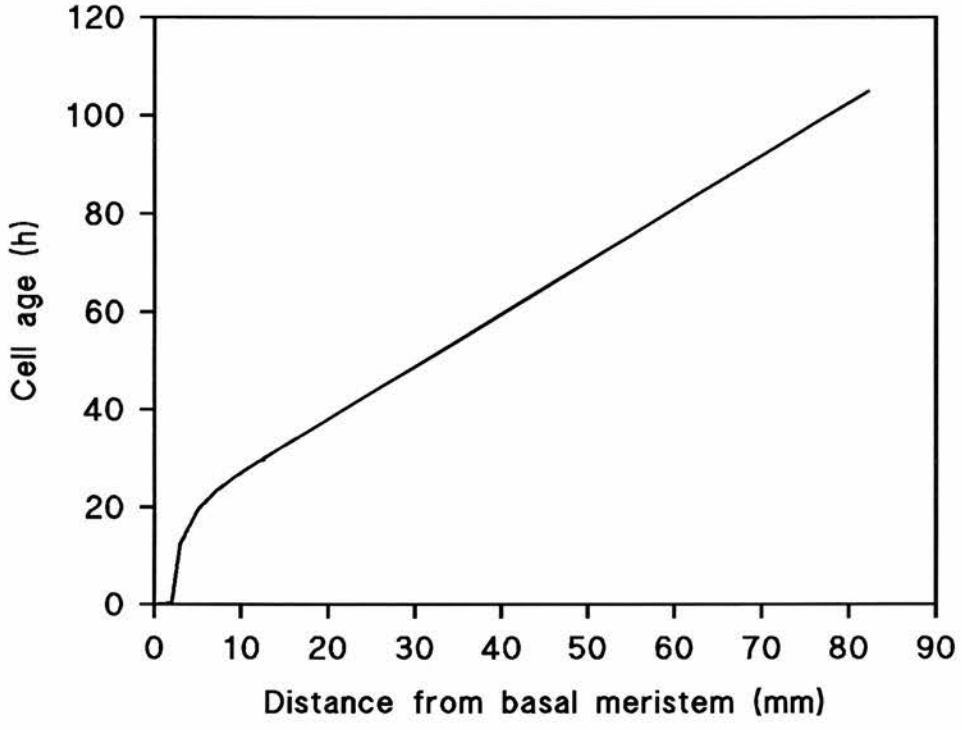

Figure 3.5 Cell Age Gradient along 7d-old Wheat Primary Leaves. See Section 3.2.1.5. Values represent the mean of five replicates, each from a different batch of plants. Cell age values were calculated from V_D data (see Section 2.5.3).

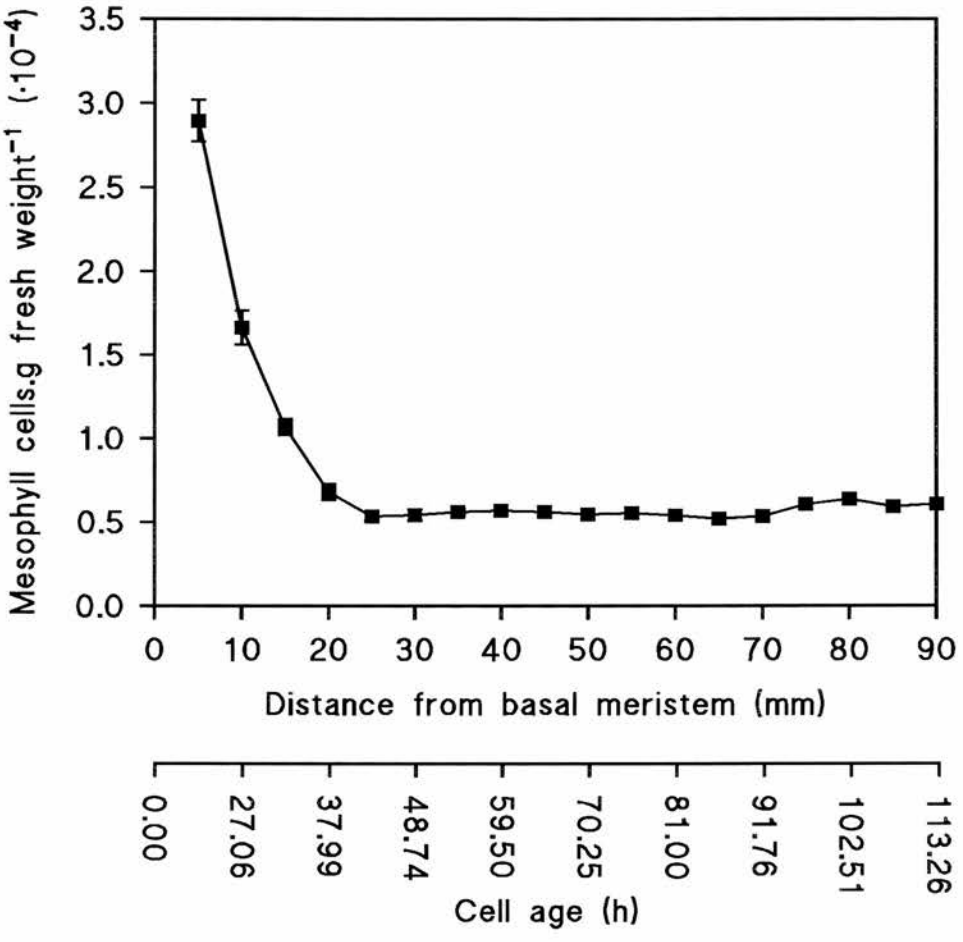

Figure 3.6 Mesophyll Cell Number along 7d-old Wheat Primary Leaves. See Section 3.2.1.6. Values represent the mean of five replicates, each from a different batch of plants ± standard errors. Standard errors are in the range 0.01-0.05 and some are too small to be visible on this graph. Measurements were made from sequential 5mm transverse sections along the leaf. Values are averages for each particular leaf segment under examination, e.g. the value plotted at 5mm represents the leaf segment 0-5mm from the basal meristem. The cell age corresponding to distance from the basal meristem is also shown (see Section 2.5.3).

3.2.2 Examination of Wheat Primary Leaf Sub-Structure

3.2.2.1 Light Microscopical Observation of Primary Leaf Sub-Structure

Observation of primary leaf transverse tissue sections was carried out at nine different distances - i.e. developmental stages - from the basal meristem, viewed at magnifications of ×100 and ×300. Observation of leaf sub-structure was made from Spurr's resin-embedded tissue. Light micrographs of five different developmental stages are shown in Figure 3.7, taken at a magnification of ×100. As well as allowing structural observation, micrographs also provided a means of assessing the standard of tissue fixation and sectioning, and of tissue orientation for sectioning. Poor tissue fixation might result in shrinkage of the cytoplasm from the cell wall, and poor sectioning might be evident in knife marks across the tissue face. In some cases, the particular orientation of the tissue made transverse sectioning difficult.

Changes in leaf sub-structure were observed in transverse sections taken at intervals along the leaf. Figure 3.7 shows transverse wheat primary leaf sections, indicating the upper and lower epidermis, and the internal mesophyll cells and vascular bundles. Stomata are visible in the lower epidermis on some micrographs. Figure 3.7(A) shows a transverse section taken at 0-1mm distal to the basal meristem and mesophyll cells here appear densely-packed together. With increasing distance from the basal meristem - Figure 3.7(B), (C), (D) and (E) - mesophyll cells are observed to become less tightly-packed together, resulting in the formation of more pronounced intercellular spaces. Cells also become less uniform in shape with increasing age, with some appearing more elongated with age.

3.2.2.2 Volume Fraction (V_v) of Primary Leaf Occupied by Different Tissue Types

Figure 3.8 shows the mean volume fraction (V_v) of wheat primary leaves in transverse section occupied by mesophyll tissue, vascular tissue, epidermal tissue and intercellular spaces; with increasing distance from the basal meristem (expressed as a % of total leaf volume). Mesophyll tissue V_v showed a small significant decrease ($p \leq 0.05$) between a distance of 0mm and 16mm from the basal meristem, then remained virtually constant between this point and the leaf tip. Mean mesophyll tissue V_v of the whole leaf volume was approximately 55% (i.e. the mean of all mesophyll tissue V_v measurements from all leaf sections). Vascular tissue V_v remained relatively constant with increasing distance from the basal meristem, at approximately 7% of whole leaf volume.

Epidermal tissue Vv showed a slight significant increase ($p \leq 0.05$) between a distance of 0mm and 21mm from the basal meristem, then a slight significant decrease ($p \leq 0.05$) between this point and the leaf tip. Average epidermal tissue Vv of the whole leaf volume was approximately 25%. Intercellular space Vv significantly increased ($p \leq 0.05$) between the leaf base and leaf tip, and occupied an average of approximately 13% of the whole leaf volume. This increase in intercellular spaces was generally observed from light micrographs (Section 3.2.2.1 and Figure 3.7). The mesophyll tissue : vascular tissue : epidermal tissue : intercellular space volume ratio within the leaf as a whole was approximately 8 : 1 : 4 : 2.

3.2.2.3 Frequency of Cell Types in Primary Leaf

Figure 3.9 shows the numbers (frequency) of individual cells of mesophyll, vascular and epidermal cells (expressed as a % of total cell number in leaf section), counted on wheat primary leaf transverse sections taken at increasing distances from the basal meristem. Mesophyll cell frequency showed a small significant increase ($p \leq 0.05$) between a distance of 0mm and 12mm from the basal meristem, and then remained relatively constant between this point and the leaf tip. The mean frequency of cells in the whole leaf (i.e. the mean of all mesophyll cell counts from all sections examined along the leaf) was approximately 37% of total leaf cells (with total leaf cells being the mean of total cell counts from all sections examined along the leaf).

Vascular cell frequency significantly decreased ($p \leq 0.05$) in mirror image to the mesophyll cell number increase between 0mm and 12mm from the basal meristem, and then remained fairly constant between this point and the leaf tip. The mean frequency of vascular cells was approximately 50% of total leaf cells. Epidermal cell frequency showed a small significant decrease ($p \leq 0.05$) between a distance of 0mm and 21mm from the basal meristem; a significant increase ($p \leq 0.05$) between a distance of 20mm and 31mm from the basal meristem; then remained relatively constant between 31mm and the leaf tip. The mean frequency of epidermal cells was approximately 13% of total leaf cells. The cell frequency ratio of mesophyll cells : vascular cells : epidermal cells within the leaf as a whole was approximately 3 : 4 : 1.

3.2.2.4 Volume Fraction (V*v*) of Mesophyll Cell Occupied by Vacuole

The mean volume fraction (V*v*) of primary leaf mesophyll cells occupied by vacuoles, with increasing distance from the basal meristem, is shown in Figure 3.10 (expressed as a % of total mesophyll cell volume). Mean vacuolar V*v* remained relatively constant at approximately 73% of mesophyll cell volume, with increasing distance from the basal meristem.

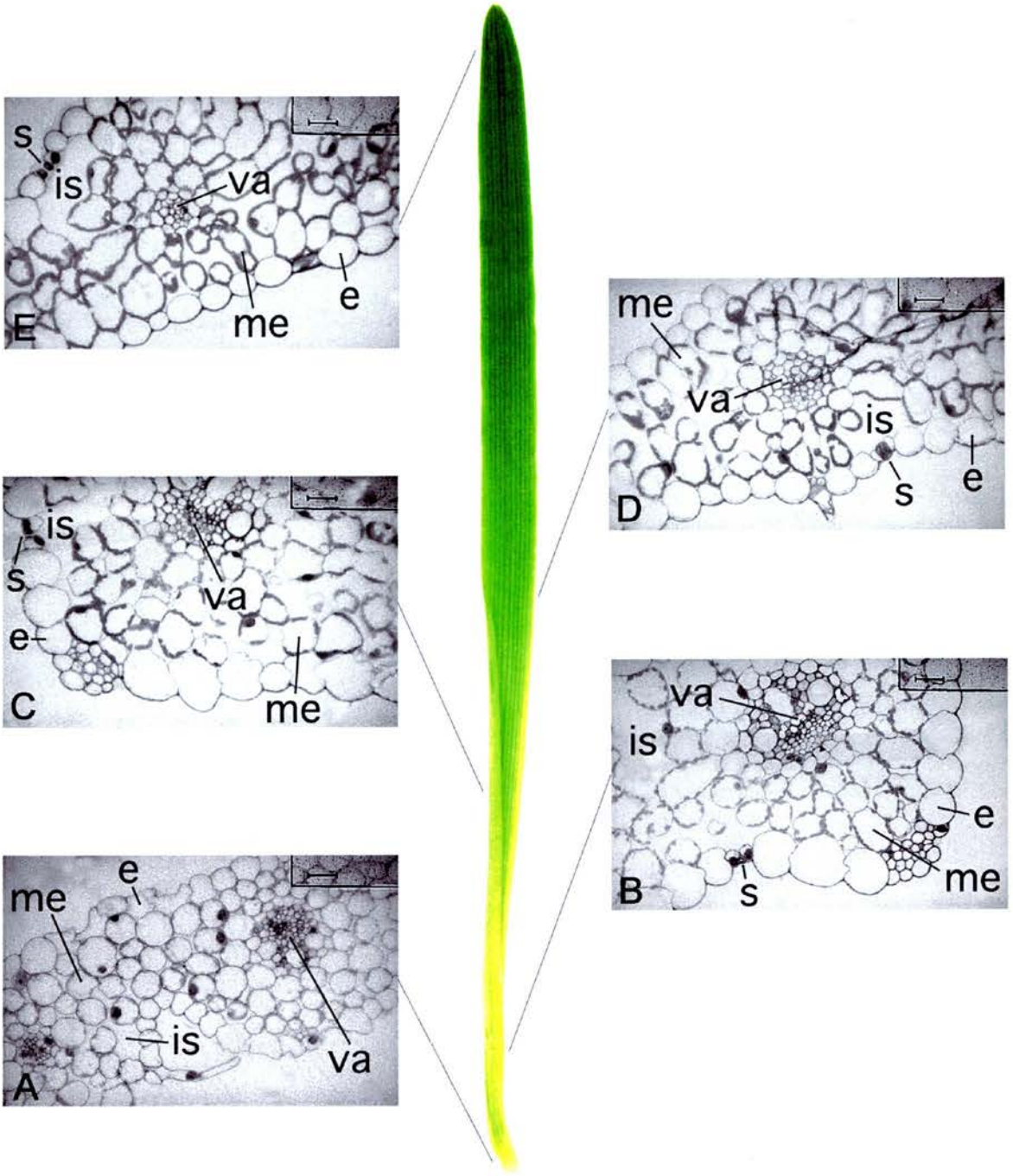

Figure 3.7 Sub-Structure of Developing Wheat Primary Leaves. Light micrographs of Spurr's resin embedded tissue from a 7d-old leaf, transversely sectioned at the following distances from the basal meristem: 0-1mm (A), 15-16mm (B), 30-31mm (C), 50-51mm (D) and 80-81mm (E). Micrographs were taken at a magnification of ×100 (bar represents 24μm). Mesophyll tissue (me), vascular tissue (va), epidermal tissue (e), intercellular space (is), stoma (s).

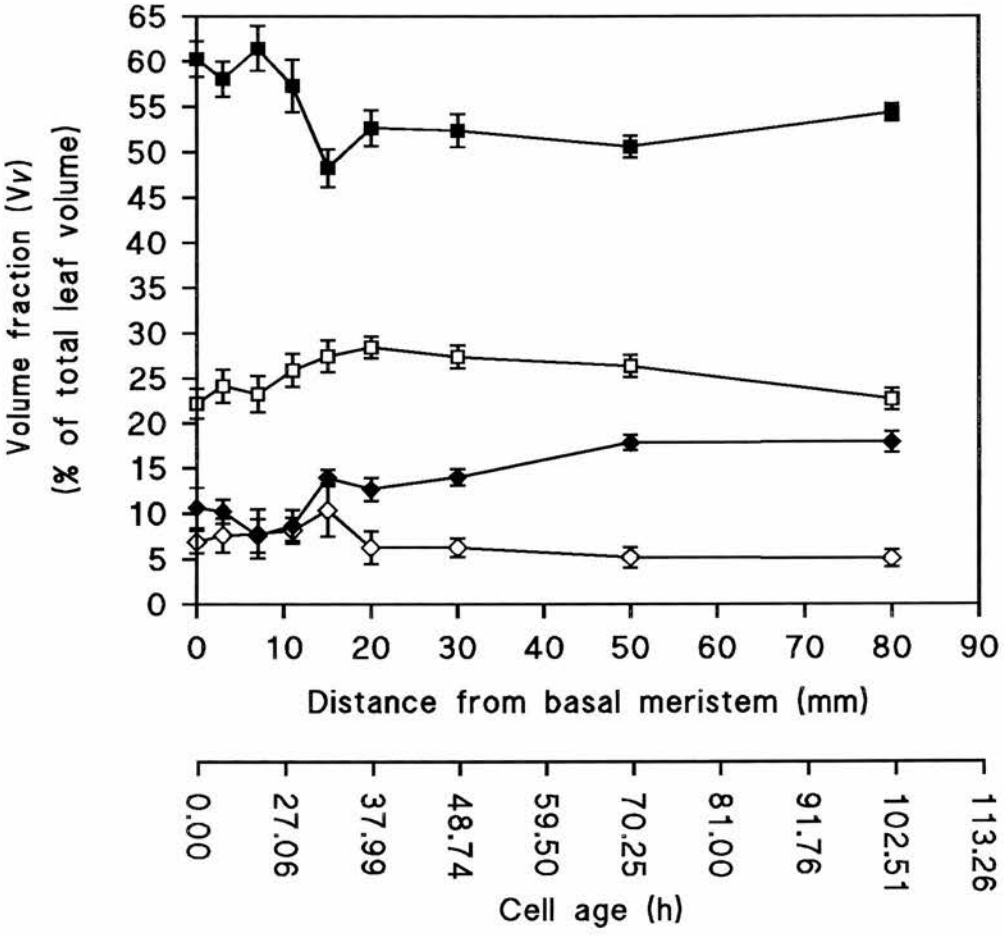

Figure 3.8 Volume Fraction (V*v*) of Leaf Tissue Occupied by Mesophyll Tissue, Vascular Tissue, Epidermal Tissue and Intercellular Spaces, along 7d-old Wheat Primary Leaves. See Section 3.2.2.2. Values represent the mean of three replicates, each from a different batch of plants ± standard errors. Measurements were made from 1mm transverse sections at nine different developmental stages along the leaf. The cell age corresponding to distance from the basal meristem is also shown (see Section 2.5.3). ■ mesophyll tissue; ◇ vascular tissue; □ epidermal tissue; ◆ intercellular spaces.

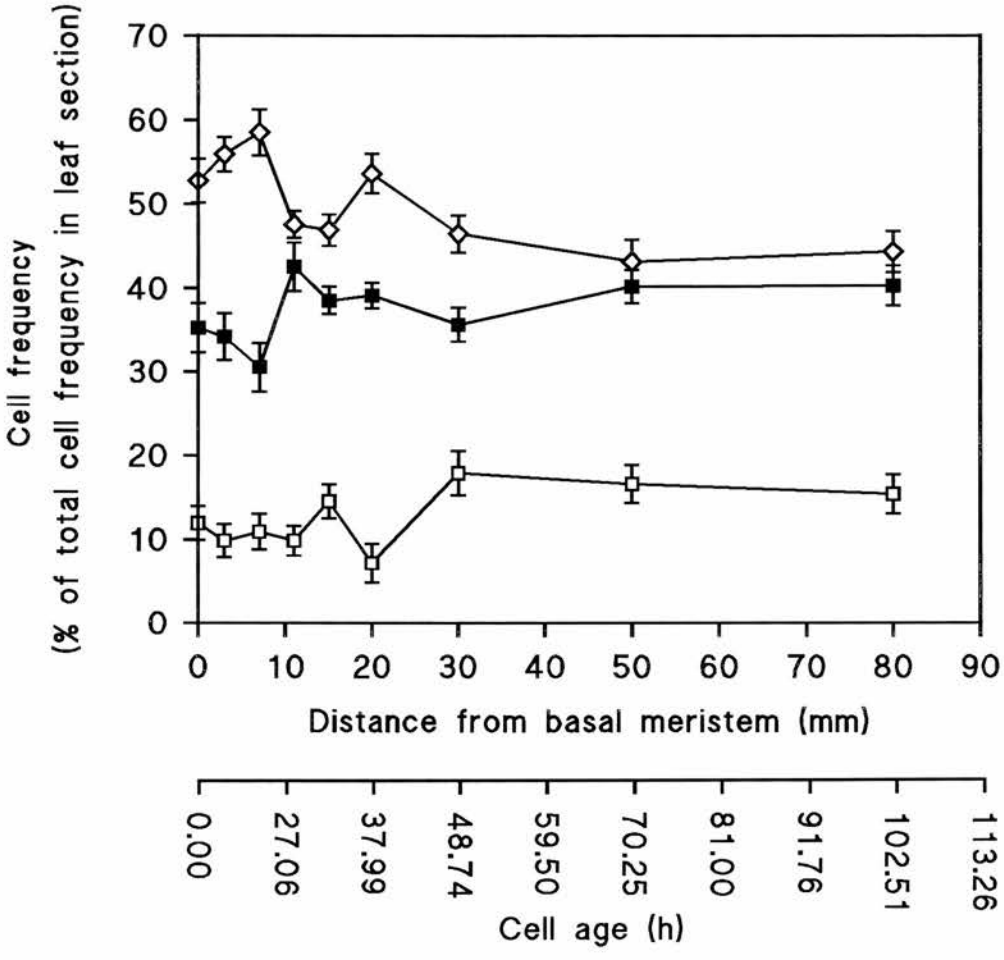

Figure 3.9 Frequency of Mesophyll Cells, Vascular Cells and Epidermal Cells along 7d-old Wheat Primary Leaves. See Section 3.2.2.3. Values represent the mean of three replicates, each from a different batch of plants ± standard errors. Measurements were made from 1mm transverse sections at nine different developmental stages along the leaf. The cell age corresponding to distance from the basal meristem is also shown (see Section 2.5.3). ■ mesophyll tissue; ◇ vascular tissue; □ epidermal tissue.

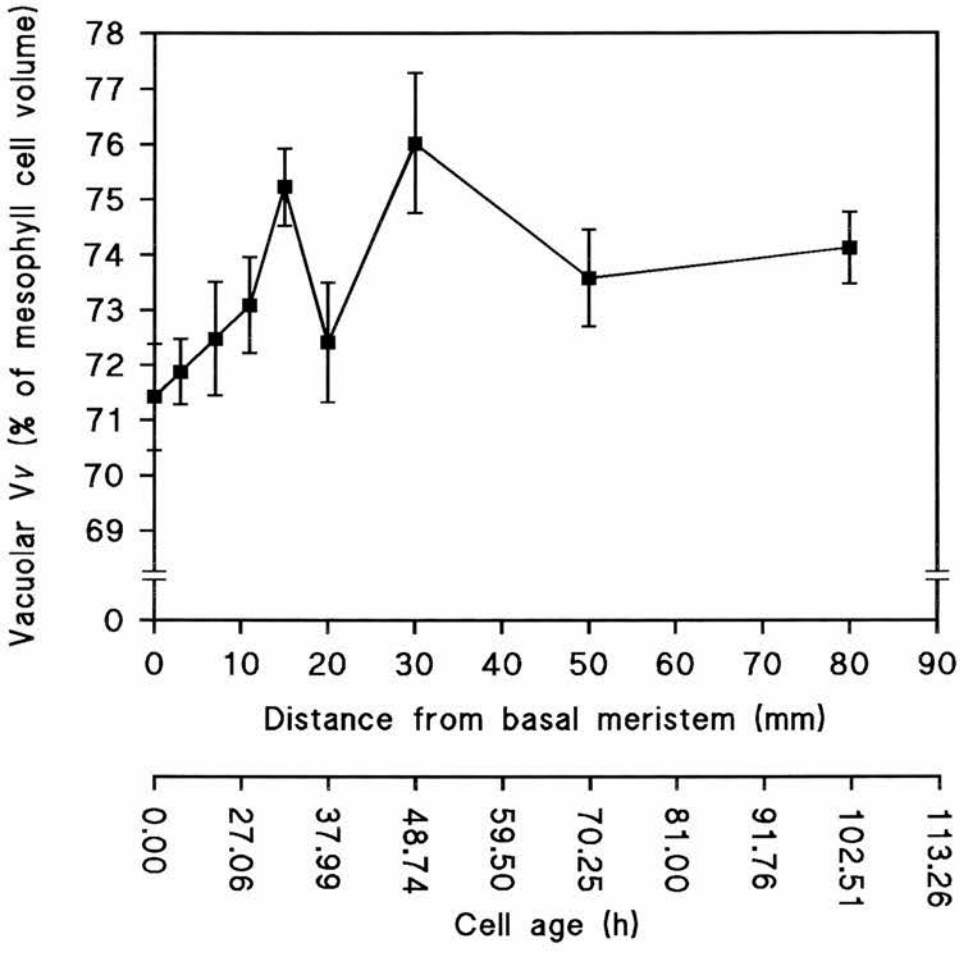

Figure 3.10 Volume Fraction (V*v*) of Mesophyll Cells Occupied by Vacuoles along 7d-old Wheat Primary Leaves. See Section 3.2.2.4. Values represent the mean of three replicates, each from a different batch of plants ± standard errors. Measurements were made from 1mm transverse sections at nine different developmental stages along the leaf. The cell age corresponding to distance from the basal meristem is also shown (see Section 2.5.3).

3.2.3 Examination of Wheat Primary Leaf Mesophyll Cell Ultrastructure

3.2.3.1 Electron Microscopical Observation of Mesophyll Cell Ultrastructure

Observation of primary leaf transverse tissue sections taken at nine different distances - i.e. developmental stages - from the basal meristem, revealed changing mesophyll cell ultrastructure with increasing cell age when viewed at a magnification of ×5000. Ultrastructural observation was made from Spurr's resin-embedded tissue. Electron micrographs of five different developmental stages are shown in Figure 3.11.

Figure 3.11A shows a mesophyll cell from immature tissue taken in the region 0-1mm distal to the basal meristem, i.e. recently produced from the meristematic tissue of the basal intercalary meristem. Here, cells appear to contain a large volume of cytoplasm with many small vacuoles (bound by the single unit membrane of the tonoplast), some of which are probably interconnected in the 3-D cell. Small immature chloroplasts are present, bound by double-unit membranes, containing relatively simple thylakoid membrane systems within the fluid stroma. A large nucleus is present, and the visible dense nucleolous within is another indication of immature tissue. Mitochondria are visible though it is difficult to discern internal cristae at this magnification. The whole cell contents are bound by a single-unit membrane (the plasmalemma), which is pushed outwards against the cellulose cell wall.

At 15-16mm distal to the basal meristem (Figure 3.11B), the small numerous vacuoles observed at the leaf base form one large central vacuole within each mesophyll cell, a typical indication of more mature cells. Chloroplasts appear to be larger, and contain more complex thylakoid membrane systems within the stroma than those at the base, with more individual granal sacs per granum. With further increasing distance from the leaf base, the large single vacuole remains and chloroplasts appear to become even larger, with increasing complexity of the thylakoid membrane systems, and large grana near the leaf tip: Figure 3.11C, D and E. Figure 3.11F and G were taken at a lower magnification and show this clear difference between immature and mature cells.

Mitochondria are visible at all stages of development, and Figure 3.12A shows a mitochondrion from near the leaf base, showing the mitochondrial double-unit membrane, cristae and internal fluid matrix. Figure 3.12 also shows other cellular organelles and structures observed at higher magnifications. In transverse sections of mesophyll cells, mitochondria were typically present in groups of one to three in-

between the chloroplasts. It was useful to become familiar with general cell ultrastructure and with the location of mitochondria in Spurr's resin-embedded tissue, in preparation for later viewing of L.R. White resin-embedded tissue, which does not give the same clarity of ultrastructural preservation as Spurr's resin.

3.2.3.2 Mesophyll Cell Mitochondrial Transverse Area (TA)

In order to sample enough electron micrographs for analysis of mitochondrial transverse area (TA) within primary leaf mesophyll cells, the cumulative standard errors of the data were plotted for an increasing number of electron micrographs, for each developmental stage examined (see Section 2.13). For example, the resulting plot for leaf base tissue (0-1mm from the basal meristem) is shown in Figure 3.13. The graph plateaued at 20 micrographs, indicating this number to be a statistically sound sample size per replicate for this developmental stage. For the other developmental stages, the graphs plateaued between 16 and 20 micrographs.

The primary axis of Figure 3.15 shows mean mitochondrial TA (μm^2) with distance from the basal meristem. Mean mitochondrial TA significantly increased ($p \leq 0.05$) between a distance of 0mm and 10mm from the basal meristem, then significantly decreased ($p \leq 0.05$) between 11mm and 16 mm to a minimum value of 0.26 μm^2. TA then significantly increased again ($p \leq 0.05$) with increasing distance from the basal meristem, reaching a maximum value of 0.65 μm^2 near the leaf tip.

3.2.3.3 Volume Fraction (*Vv*) of Mesophyll Cell Occupied by Mitochondria

In order to sample enough electron micrographs for analysis of mitochondrial volume fraction (*Vv*) of primary leaf mesophyll cells, the cumulative standard errors of the data were plotted for an increasing number of electron micrographs, for each developmental stage examined (see Section 2.13). For example, the resulting plot for leaf base tissue (0-1mm from the basal meristem) is shown in Figure 3.14. The graph plateaued at 20 micrographs, indicating this number to be a statistically sound sample size per replicate for this developmental stage. For the other developmental stages, the graphs plateaued between 18 and 20 micrographs.

The secondary axis of Figure 3.15 shows primary leaf mitochondrial *Vv* expressed as a % of total cytoplasmic volume, with increasing distance from the basal meristem. Since it was found that vacuolar *Vv* remained constant at 73% of total

mesophyll volume (Section 3.2.2.4), mitochondrial V_v of mesophyll cells along the leaf was measured indirectly as a % of cytoplasmic volume. Mean mitochondrial V_v remained virtually constant along the length of the leaf, at an average value of 5.42% of cytoplasmic volume - this corresponded to a constant mitochondrial V_v value of 1.46% of mesophyll cell volume.

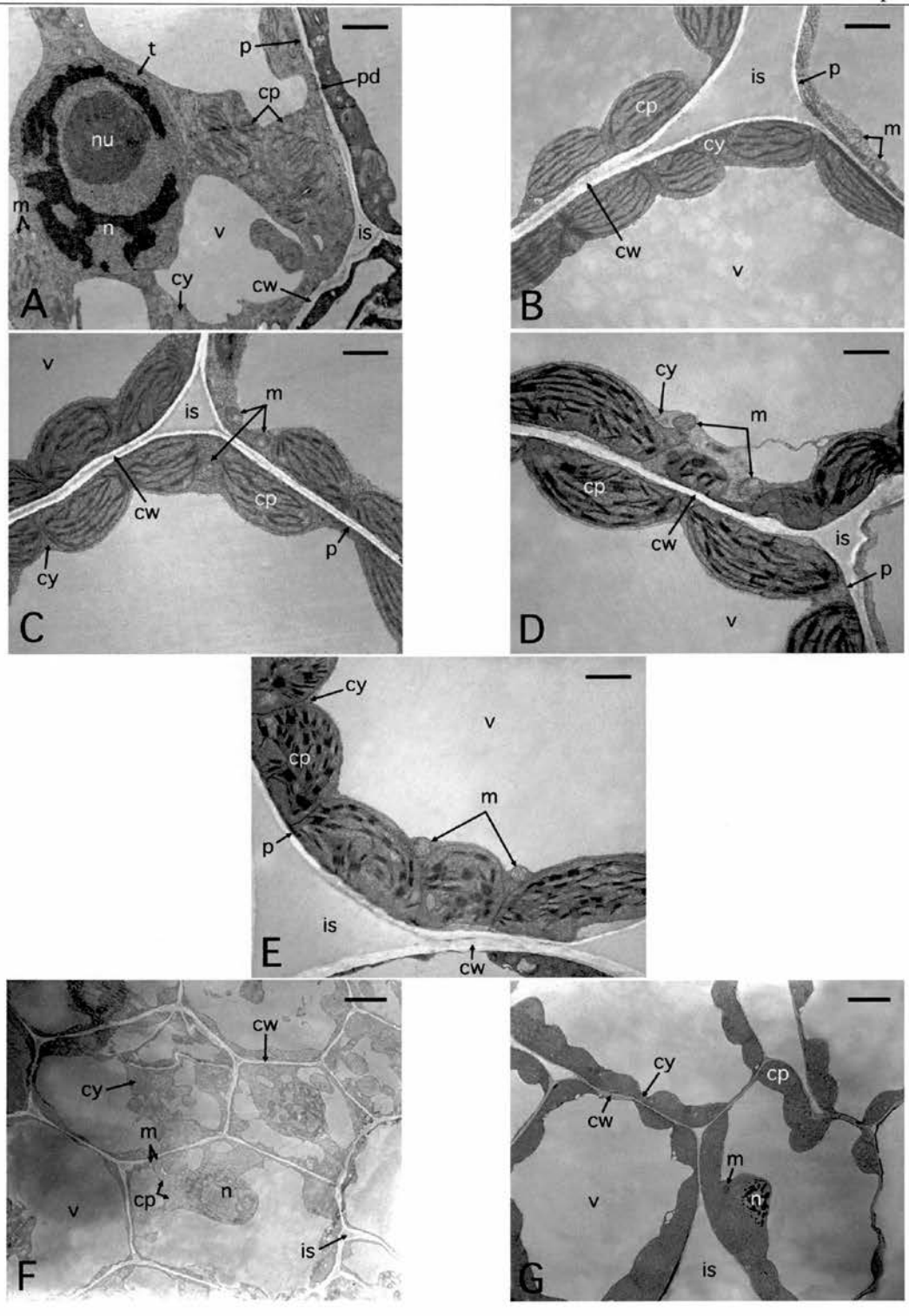

Figure 3.11 Changes in Wheat Primary Leaf Mesophyll Cell Ultrastructure with Development. Electron micrographs of Spurr's resin embedded tissue from a 7d-old leaf, transversely sectioned at the following distances from the basal meristem: 0-1mm (A and F), 15-16mm (B), 30-31mm (C), 50-51mm (D) and 80-81mm (E and G). Micrographs A-E were taken at a magnification of ×5000 (bar represents 2μm), and micrographs F and G were taken at ×1820 (bar represents 5 μm). Cell wall (cw), plasmalemma (p), cytosol (cy), nucleus (n), nucleolus (nu), vacuole (v), tonoplast (t), chloroplast (cp), mitochondrion (m), plasmodesmata (pd), intercellular space (is).

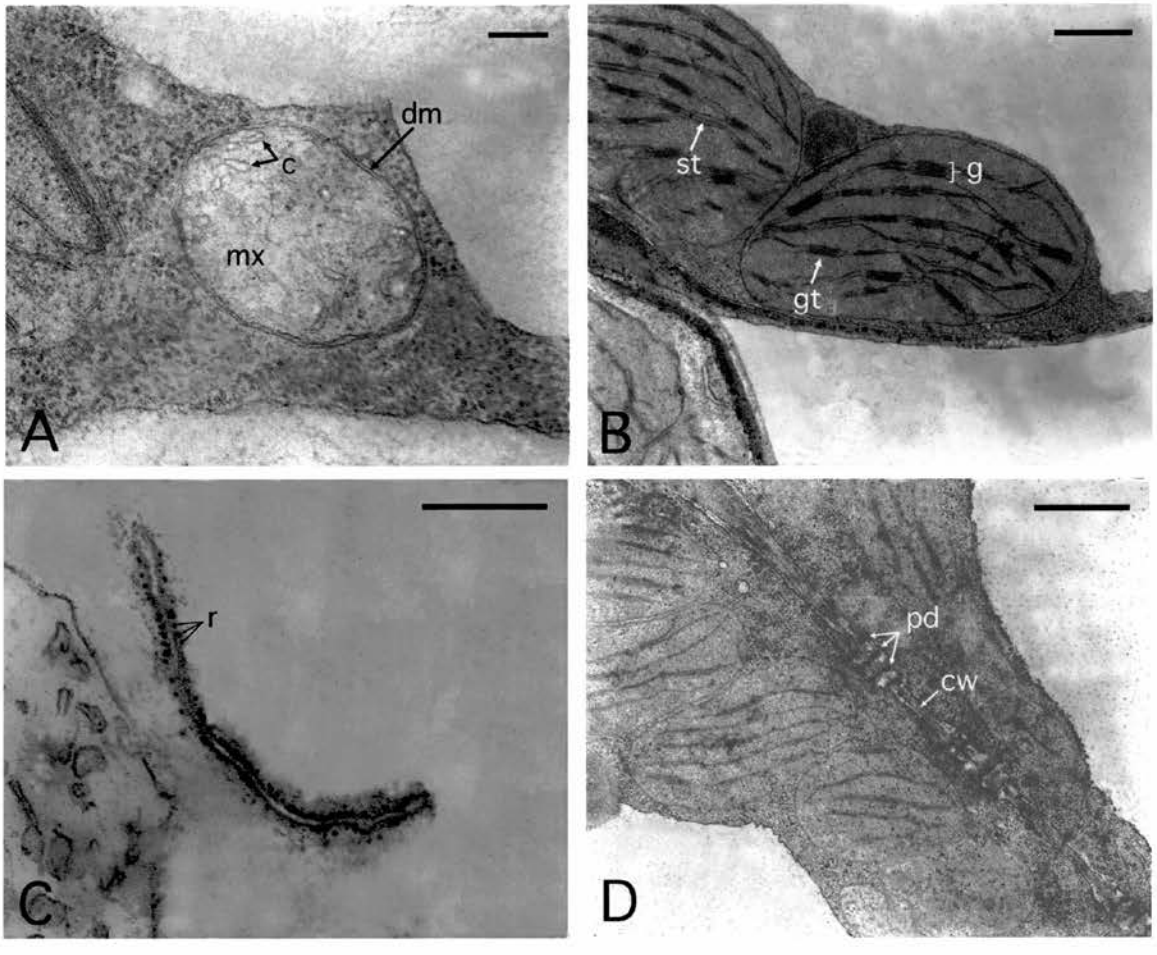

Figure 3.12 Ultrastructural Features of Wheat Primary Leaf Mesophyll Cells. Electron micrographs of transversely sectioned Spurr's resin embedded tissue from a 7d-old leaf, showing different cellular organelles and features. A: mitochondrion taken at a magnification of ×45600 (bar represents 0.2μm), showing a double-unit membrane (dm), cristae (c), and the matrix (mx); B: chloroplasts taken at ×12000 (bar represents 1μm), showing internal stromal thylakoid membranes (st), granal thylakoid membranes (gt) and grana (g); C: rough endoplasmic reticulum taken at ×38400 (bar represents 0.5 μm), with ribosomes (r); D: plasmodesmata (pd) taken at × 15650 (bar represents 1μm) within the cell wall (cw) separting two mesophyll cells.

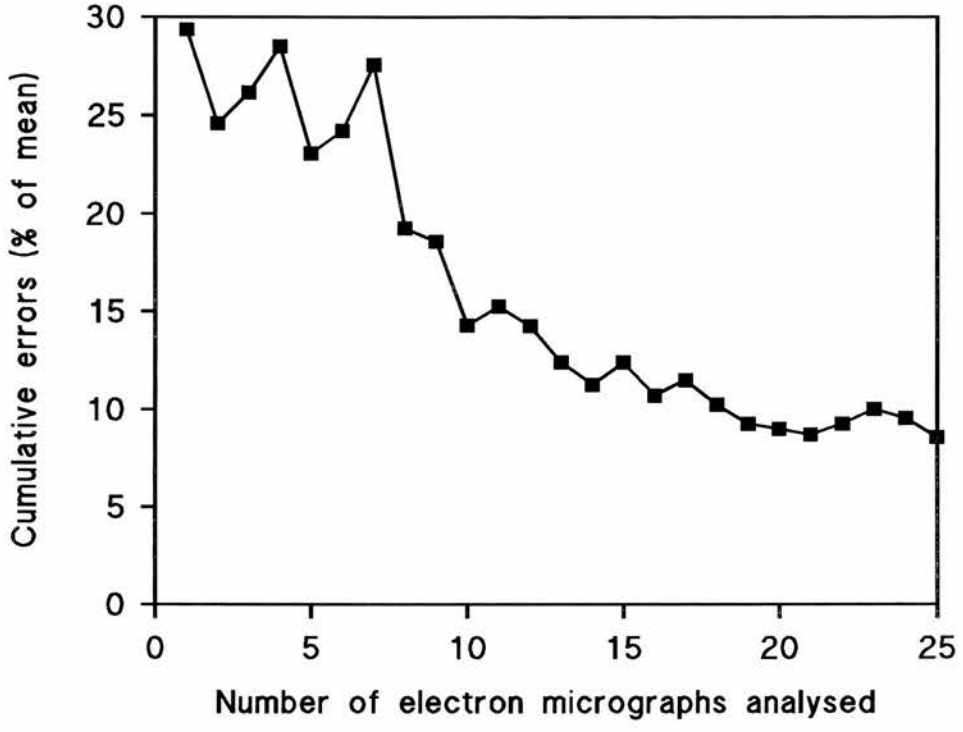

Figure 3.13 Example of a Cumulative Standard Error Plot for Electron Micrograph Sampling: Analysis of Mesophyll Cell Mitochondrial Transverse Area (TA) at the Leaf Base of 7d-old Wheat Primary Leaves. See Section 3.2.3.2.

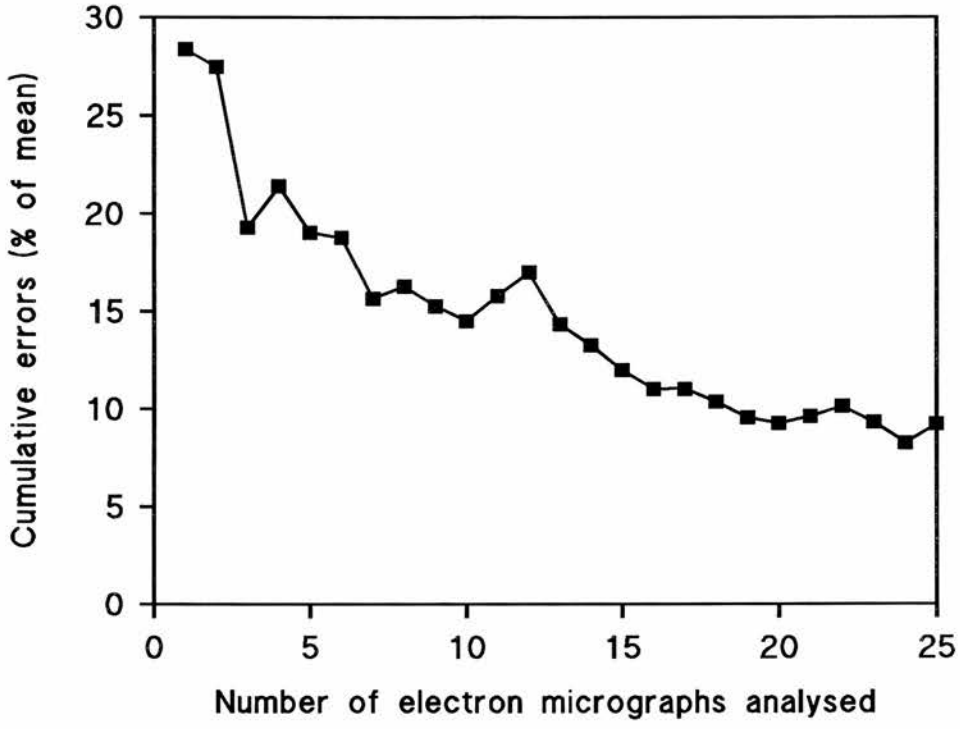

Figure 3.14 Example of a Cumulative Standard Error Plot for Electron Micrograph Sampling: Analysis of Mesophyll Cell Mitochondrial Volume Fraction (V*v*) at the Leaf Base of 7d-old Wheat Primary Leaves. See Scetion 3.2.3.3.

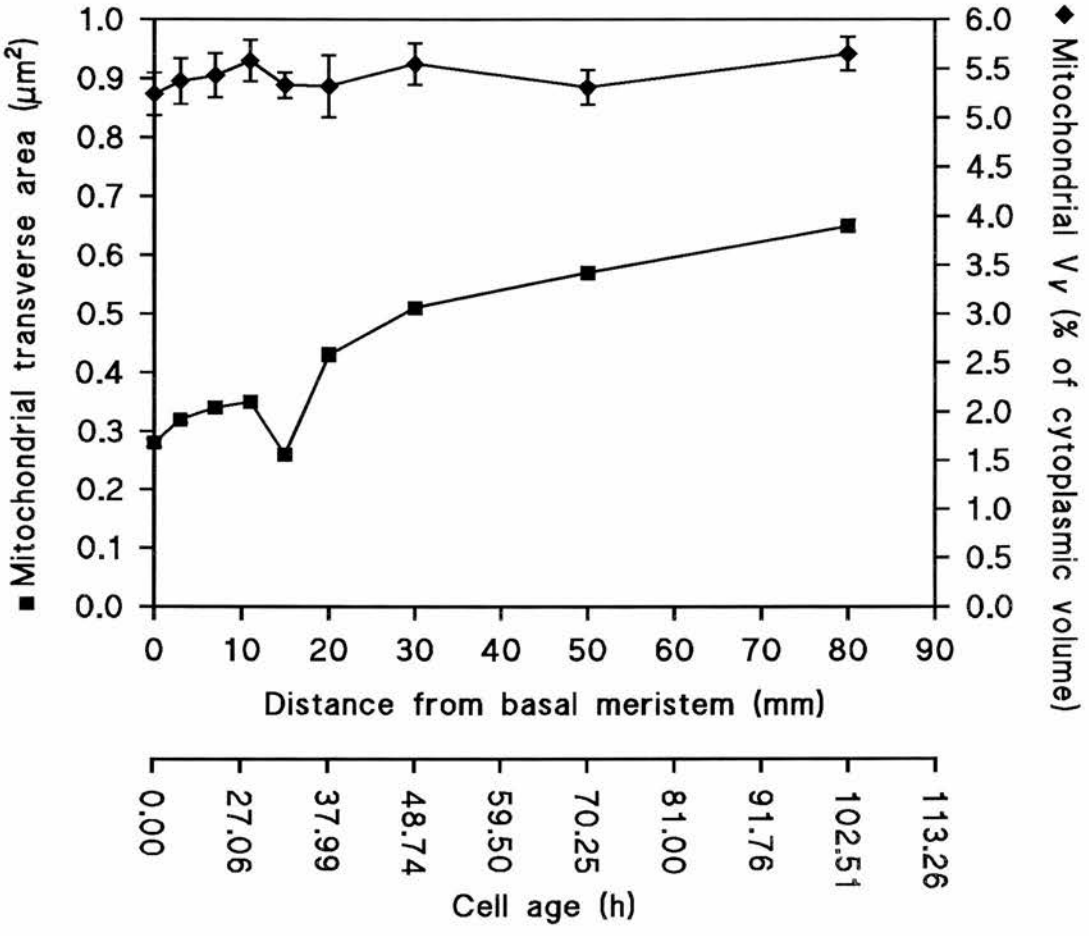

Figure 3.15 Mesophyll Cell Mitochondrial Transverse Area and Mitochondrial Volume Fraction (V*v*) along 7d-old Wheat Primary Leaves. See Sections 3.2.3.2 and 3.2.3.3. Values represent the mean of three replicates, each from a different batch of plants ± standard errors. Measurements were made from 1mm transverse sections at nine different developmental stages along the leaf. The cell age corresponding to distance from the basal meristem is also shown (see Section 2.5.3).

3.3 Discussion

3.3.1 Wheat Primary Leaf Growth and Development

The increases observed in wheat primary leaf length and primary leaf fresh and dry weight with time (Figures 3.1 and 3.2), were comparable to previous studies on wheat (Boffey *et al.*, 1979; Tobin & Rogers, 1992). Maximum leaf growth rate was maintained up to 7d post-imbibition, and therefore a maximum gradient of leaf cell development existed at this point. Hence, in this study, all leaves were harvested at 7d post-imbibition - leaves harvested before or after this would not have exhibited as large a range of cell age between the leaf base and the tip.

The spatial distributions of SER and V_D (Figures 3.3 and 3.4) obtained were comparable to that found in previous studies of wheat (L. Hopkins, 1997) and other Gramineae, e.g. *Festuca arundinacea* (Schnyder & Nelson, 1988), *Lolium perenne* (Schnyder *et al.*, 1990). The data indicated that the primary leaf cell elongation zone extended between 0-14mm distal to the basal meristem, since cell elongation ceased beyond this point. This cell elongation at the leaf base of the leaf occurs mainly via water-uptake by mesophyll cells via turgor-pressure driven expansion of the cell walls (Ray, Green & Cleland, 1972), and is highly vertically polarized due to the particular orientation of the cell wall cellulose fibres (Dale, 1988).

Cells are displaced away from the leaf base towards the tip, as younger cells form in the leaf base and expand, pushing the cells above further away. The observed increase in cell age - calculated from V_D data - with time (Figure 3.5) highlights this cell displacement away from the leaf base, resulting in a developmental gradient with the youngest cells at the leaf base, and the most mature cells at the leaf tip. From mitotic index measurements, it was previously found that in wheat, all cell division is located in the basal 5mm of the primary leaf, with the highest rate occurring in the basal intercalary meristem (L. Hopkins, 1997). In the present study, the maximum rate of cell elongation was observed within the basal 6mm of the leaf, increasing as cell division is declining. The observed decrease in mesophyll cell number per g fresh weight with distance from the basal meristem (Figure 3.6) was consistent with the observed SER data - the highest cell numbers were found at the leaf base, with a sharp decline in the basal 10mm of the leaf as cells elongated resulting in fewer cells present per g fresh weight. Mesophyll cell number then declined to a constant minimum from the end of the elongation zone to the leaf tip, indicating cessation of cell elongation.

3.3.2 Wheat Primary Leaf Sub-Structural Development

The natural developmental gradient present in wheat primary leaves was evident from leaf sub-structural observation (Figure 3.7). Elongating mesophyll cells became more irregular in shape (whole intact cells were observed microscopically during cell number measurement - Sections 2.8.3 and 3.2.1.6) and therefore less densely packed as they grew larger. The increase in total intercellular space found as leaf tissue developed was a direct measurement of this (Figure 3.8). Similarly, the small decrease in the proportion of the leaf occupied by mesophyll cells at the leaf base (Figure 3.8) corresponds with the observation on light micrographs of densely-packed mesophyll cells in this region, which become less densely-packed with increasing distance from the basal meristem (i.e. resulting in less total mesophyll cell volume per unit leaf tissue volume). This change in internal leaf anatomy increases the rate of transfer of atmospheric CO_2 to mesophyll cells as they mature and become fully photosynthetic (Leech & Baker, 1983).

It is more difficult to draw conclusions from the cell frequency data (Figure 3.9), especially regarding mesophyll cells, since the latter become more irregular in shape, growing longer and more lobed with maturity. Hence, counting mesophyll cells on more mature tissue sections may in fact result in the same cell being counted more than once, due to separate parts of the cell appearing as two different cells on 2-dimensional tissue sections. However, near the leaf base, this is unlikely to be the case, and the frequencies of different cell types can be compared. With vascular and epidermal cells, this does not create such a problem, since from personal observation, they do not generally become so lobed, and tend to elongate in a single longitudinal plane.

The unit volume of leaf tissue (Vv) occupied by vascular cells remains virtually constant with increasing cell age, while the number of vascular cells per unit tissue volume decreases from base to tip. Hence, vascular cells must be becoming relatively larger with age. Similarly, in the basal 20mm of the leaf, the volume of leaf tissue occupied by epidermal cells increases, again suggesting expansion of these cells with age. In this same region, the number of epidermal cells per unit tissue volume decreases, and it therefore appears that epidermal cells are expanding at a greater rate than vascular cells, as the leaf matures.

3.3.3 Wheat Primary Leaf Mesophyll Cell Ultrastructural Development

The changes in leaf mesophyll cell ultrastructure with increasing maturity (Figure 3.11) were similar to that found previously in wheat and other higher plants, and such changes are well characterised (Robards, 1975; Tobin & Rogers, 1992). The formation of a large central vacuole from the many small vacuoles present in young cells at the leaf base, can be explained by the onset of cell elongation at the leaf base. The intake of water into the mesophyll cells drives cell elongation, increases turgor, and pushes the cytoplasm out towards the cell wall, with the collection of fluid inside a rapidly expanding vacuole. However, the actual proportion of mesophyll cell volume occupied by the vacuole remains constant throughout cell elongation, in this study at 73% (Figure 3.10).

Under the electron microscope, chloroplasts were seen to increase in size with cell age, and previous studies have shown that the proportion of wheat leaf mesophyll cell cytoplasm occupied by chloroplasts increases with cell age (Ellis & Leech, 1985) increasing from 5.7% at a distance of 1mm from the basal meristem to 13% at 55mm (J.R. Thorpe, W.J. Rogers & A.K. Tobin, unpublished) (see Tobin & Rogers, 1992). Chloroplast number has been found to increase with cell development in wheat from the base to about 40mm along the primary leaf (at 40mm, chloroplast division ceases), then remain constant from this point to the leaf tip (Boffey *et al.*, 1979; Tobin, Ridley & Stewart, 1985), and the increase in total chloroplastic volume of the cell with time is due to both an increase in chloroplast size and number. The internal thylakoid membrane systems of chloroplasts appeared to become visibly more complex with cell maturity under the electron microscope, and an increase in general complexity and in the number of individual sacs per thylakoid granum has been found previously in wheat (L. Hopkins, 1997) and other Graminaceous plants such as *Zea mays* (Baker & Leech, 1977) and *Hordeum vulgare* (Robertson & Laetsch, 1974). The increase in total chloroplastic volume and thylakoid complexity, indicates an increase in the photosynthetic capacity of mesophyll cells with time – the rate of photosynthesis of developing wheat primary leaf tissue is investigated and discussed in Chapter 4.

Individual mitochondria were found to increase in volume with cell age (since mitochondrial transverse area increased), but the total proportion of the cytoplasm occupied by mitochondria was found to remain constant throughout cell development. This was in accordance with previous studies in wheat (Tobin & Rogers, 1992; L.

Hopkins, 1997), and suggests that mitochondria must be decreasing in number with increasing cell age; and that total mitochondrial volume is increasing in proportion with mesophyll cell volume. The initial decrease in mitochondrial volume fraction in the leaf elongation zone was probably due to mitochondrial division in this region - J.R Thorpe, W.J. Rogers & A.K. Tobin (unpublished) found an increase in mitochondrial numbers in the basal 0-15mm of the wheat primary leaf (see Tobin & Rogers, 1992). As to the apparent decrease in mitochondrial number beyond the elongation zone, mitochondria appear to fuse together to create larger organelles (Tobin & Rogers, 1992), perhaps prompted by the increasing restriction of expanding chloroplast volume in the cytoplasm, as cells develop. Specific measurement of changing mitochondrial numbers in developing leaves is an area requiring further investigation. Mitochondria had visible internal cristae at all stages of development, suggesting a respiratory role from early development, and changes in mitochondrial populations and structure have been shown to be linked with tissue respiratory activity (Simon & Chapman, 1961; Geronimo & Beevers, 1964; Solomos *et al.*, 1972). The respiratory rate of developing wheat leaf tissue is investigated in Chapter 4, with the aim of determining whether functional as well as structural changes occur during development.

3.3.4 Summary and Conclusions

This chapter has established the presence of a natural developmental gradient within wheat primary leaves, and has characterised this gradient in a number of ways. In Graminaceous leaves such as wheat, all cell division takes place at the leaf base - mainly within the basal intercalary meristem - with cells being gradually displaced towards the leaf tip as they age, generating a developmental gradient with the youngest cells at the leaf base and the most mature at the leaf tip. Evidence of this gradient was reported in the form of changes in leaf growth, and microscopical observation and stereological measurement at the leaf sub-structural and cell ultrastructural levels. This was achieved using 7d-old wheat primary leaves in which the developmental gradient was at a maximum under the growth conditions of this study. Figure 3.16 shows a summary of the changes taking place during development of the wheat primary leaf.

The primary leaf elongation zone was shown to be located between 0mm and 14mm from the basal meristem from leaf segment elongation rate measurements, and from an observed decrease in mesophyll cell number in this region. A gradient of cell

age was calculated for the primary leaf from leaf segment elongation measurements, equating each point along the leaf with a particular cell age (see Figure 3.16).

Leaf sub-structural changes with development were evident in changing proportions of different leaf cell types with development, and in changes in cell type frequency. The proportion of the leaf occupied by intercellular spaces increased between the leaf base and leaf tip, and this was also visible on light micrographs. The volume ratio of mesophyll tissue : vascular tissue : epidermal tissue : intercellular spaces within the whole primary leaf was approximately 8 : 1 : 4 : 2. The cell frequency ratio of mesophyll cells : vascular cells : epidermal cells within the whole leaf was approximately 3 : 4 : 1. The volume fraction of mesophyll cells occupied by vacuole remained constant throughout leaf development.

Changes in leaf mesophyll cell ultrastructure were evident with leaf development. Mitochondrial transverse area increased, while the total proportion of mesophyll cells occupied by mitochondria remained constant, indicating a decrease in mitochondrial number with development. Under the electron microscope, chloroplasts appeared visibly larger with development.

In living organisms, the complex relationship between structure and function cannot be over-emphasised, whether it be at the whole-organ or ultrastructural level. This chapter has highlighted wheat leaf structure and compartmentation at various levels, and the changes that occur in these compartments with development. Since form is intrinsically linked with function, any changes in structure and compartmentation are likely to be related to a changing metabolic role. Cell metabolism for example relies on the compartmentation of chemical reactions within specific organelles and cellular structures, allowing the cell to carry out many different essential functions simultaneously (Beevers, 1991). Various levels of compartmentation within the cell contribute to metabolic control along with enzyme regulation, so that metabolism is regulated in both space and time. Any change in organelle structure and population could therefore be related to changing metabolism in that organelle. This chapter has established the presence of a developmental gradient and has characterised some of the structural and stereological changes occurring along the leaf. This raises the question of possible changing metabolism as wheat leaf cells develop. The next two chapters investigate possible metabolic changes with leaf development, and concentrate on the study of changing mitochondrial metabolism with wheat primary leaf cell development.

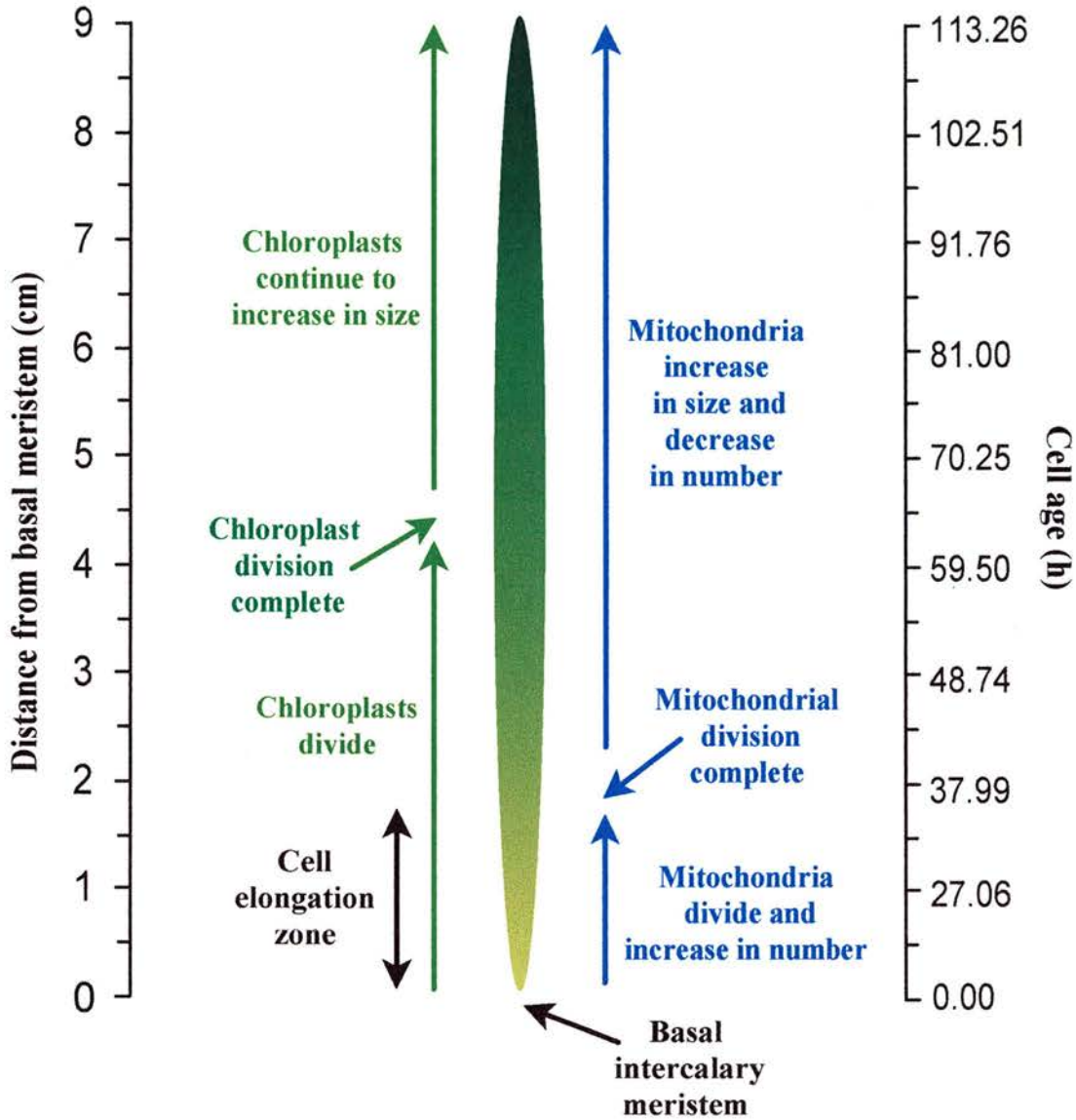

Figure 3.16 Summary of the Changes in Growth and Organelle Populations along the Natural Developmental Gradient of 7d-old Wheat Primary Leaves. Data are from the present study, and summarised from Tobin & Rogers (1992); Rogers, Thorpe & Tobin (unpublished).

CHAPTER 4: IMMUNOLOGICAL LOCALISATION OF THE MITOCHONDRIAL PYRUVATE DEHYDROGENASE COMPLEX (PDC) AND GLYCINE DECARBOXYLASE COMPLEX (GDC) IN WHEAT PRIMARY LEAVES BY IMMUNOSTAINING OF SLOT BLOTS

4.1 Introduction

4.1.1 The Study of Plant Proteins

The changes in ultrastructure with wheat primary leaf development reported in Chapter 3, are intrinsically associated with metabolic changes within leaf cells, and the fundamental relationship between structure and function has already been emphasised. An important way of monitoring metabolic change in living organisms is to observe any changes in protein concentration and composition. Proteins occupy a central role in the functioning of all living cells, and constitute more than 50% of the dry weight of most tissues. In plants, proteins are involved in virtually every biochemical and physiological process taking place, including structural support, storage, transport and - as enzymes - catalysis of biochemical reactions (Ko, 1998).

4.1.2 Aims of Chapter

Having characterised the natural developmental gradient of wheat primary leaves in Chapter 3, the aim of this chapter was to use this developmental model to investigate protein development in wheat primary leaves as a means of examining changing leaf metabolism with increasing cell age. This was approached by making a general study of total leaf proteins, and of two central metabolic processes via the measurement of respiration and photosynthesis rates in leaf tissue. This was followed by the more specific study of the development of six particular mitochondrial proteins in wheat leaf tissue, detected using specific antibodies: the E1α, E1β, E2 and E3 subunits of the pyruvate dehydrogenase complex (PDC), and the P-protein and L-protein subunits of the glycine decarboxylase complex (GDC).

In a study of changing mitochondrial metabolism during leaf development, the PDC complex is an obvious choice due to its important role at the entry point of the TCA cycle. The GDC complex provides an interesting comparison with the PDC

complex with its involvement in photorespiration - in addition to aerobic respiration of course, mitochondria are also involved in photorespiration in plant cells. The role of these complexes, and the reasons why they were chosen for investigation in this study are discussed in more detail in Section 1.4. The aim of detecting particular developmental patterns of mitochondrial proteins was to contribute to the current understanding of the control and co-ordination of mitochondrial biogenesis in relation to leaf development.

4.2 Results

For all the following results where measurements are with reference to increasing distance from the basal meristem, plotted values are averages for each particular leaf segment under examination, e.g. the value plotted at 5mm represents the leaf segment 0-5mm from the basal meristem.

4.2.1 General Study of Changing Metabolism in Wheat Primary Leaves

4.2.1.1 Primary Leaf Soluble Protein Content

The change observed in total wheat leaf soluble protein content with increasing distance from the basal meristem, is shown in Figure 4.1, and is expressed per unit leaf fresh weight and per leaf mesophyll cell.

On a leaf fresh weight basis (Figure 4.1, primary axis), soluble protein content significantly decreased ($p \leq 0.05$) from approximately 19 mg.g fresh weight^{-1} to approximately 8 mg.g fresh weight^{-1} between 0mm and 10mm from the basal meristem. From here, soluble protein significantly increased ($p \leq 0.05$) in a virtually linear trend, reaching 30.5 mg.g fresh weight^{-1} at the leaf tip.

When the data are expressed on a per mesophyll cell basis (Figure 4.1, secondary axis), a more steady significant increase ($p \leq 0.05$) in leaf soluble protein content was observed between the leaf base and tip, and a maximum value of approximately 5 μg.mesophyll cell^{-1} was attained at the leaf tip.

4.2.1.2 SDS-PAGE of Primary Leaf Polypeptides

Soluble proteins extracted from sequential 5mm leaf sections along the wheat primary leaf from base to tip were separated by SDS-PAGE (see Section 2.9.1), and an example of a gel stained with Coomassie Blue is shown in Figure 4.2, where 50μg leaf protein was loaded per well. Various general differences in the polypeptide bands at each developmental stage can be observed. In particular, an increase in a large polypeptide band at approximately 50kDa can be observed with increasing distance from the basal meristem. This corresponds to the molecular weight of the large subunit (LSU) of the enzyme ribulose 1,5-biphosphate carboxylase/oxygenase (Rubisco), which has a molecular weight of 52-55kDa in most photosynthetic organisms (Keys & Parry, 1990).

Rubisco-LSU was localised via immunostaining of Western blots using a specific antibody (see Section 2.9.4), confirming that this large band represented this

enzyme. In addition to 16μg leaf protein loaded per well on the original gels, three lanes of pure Rubisco-LSU protein were also included, of known amounts: 0.1μg, 1μg and 5μg. Analysis of the changing band density on the immunostained blots (see Section 2.9.5), comparing the density of the leaf protein bands with the density of the pure Rubisco-LSU protein bands; revealed a virtually linear increase in cellular Rubisco-LSU content along the primary leaf, increasing from approximately 18-fold between the base and tip (Figure 4.3).

4.2.1.3 Primary Leaf Respiration Rate

The rate of primary leaf respiration at increasing distances from the basal meristem is shown in Figure 4.4, and is expressed per unit leaf soluble protein and per leaf mesophyll cell.

Respiration rate, expressed as oxygen consumption per mg leaf soluble protein, decreased rapidly between 0mm and 20mm from the basal meristem. From here, respiration rate continued to decrease more slowly, reaching a minimum value of 3.5 mol $\times 10^{-6}$. mg protein^{-1}. min^{-1} at the leaf tip (Figure 4.4, primary axis). When expressed on a per mesophyll cell basis, a more constant trend was obtained overall along the length of the leaf as a whole (Figure 4.4, secondary axis) at an average value of 19.1 mol $\times 10^{-6}$. mesophyll cell^{-1}. min^{-1}; though with a slight peak approximately halfway along the leaf.

4.2.1.4 Primary Leaf Photosynthesis Rate

The rate of primary leaf net photosynthesis at increasing distances from the basal meristem is shown in Figure 4.5, and is expressed per unit leaf soluble protein and per leaf mesophyll cell.

Following an initial rapid increase in CO_2-dependent O_2 evolution per mg leaf protein in the basal 0-10mm of the leaf, rate per mg leaf protein continued to increase steadily beyond this point, then levelled off near the leaf tip (Figure 4.5, primary axis). When the data were expressed per mesophyll cell, a more linear increase was observed between the leaf base and approximately 70mm from the basal meristem. The trend levelled of after this, reaching a maximum of 75.6 mol $\times 10^{-9}$. mesophyll cell^{-1}. min^{-1} at the leaf tip (Figure 4.5, secondary axis).

When the cellular rates of respiration and photosynthesis were added together, the gross rate of photosynthesis per cell was obtained (Figure 4.6). The trend was

similar to that of net photosynthesis (Figure 4.5), but with oxygen evolution at all stages of leaf development.

When gross cellular photosynthesis rate was plotted against Rubisco-LSU content, the trend shown in Figure 4.7 was produced. An increase in oxygen evolution was observed up until Rubisco-LSU protein constituted approximately 1μg per mesophyll cell. From this point, photosynthetic rate levelled off, despite increasing accumulation of cellular Rubisco-LSU.

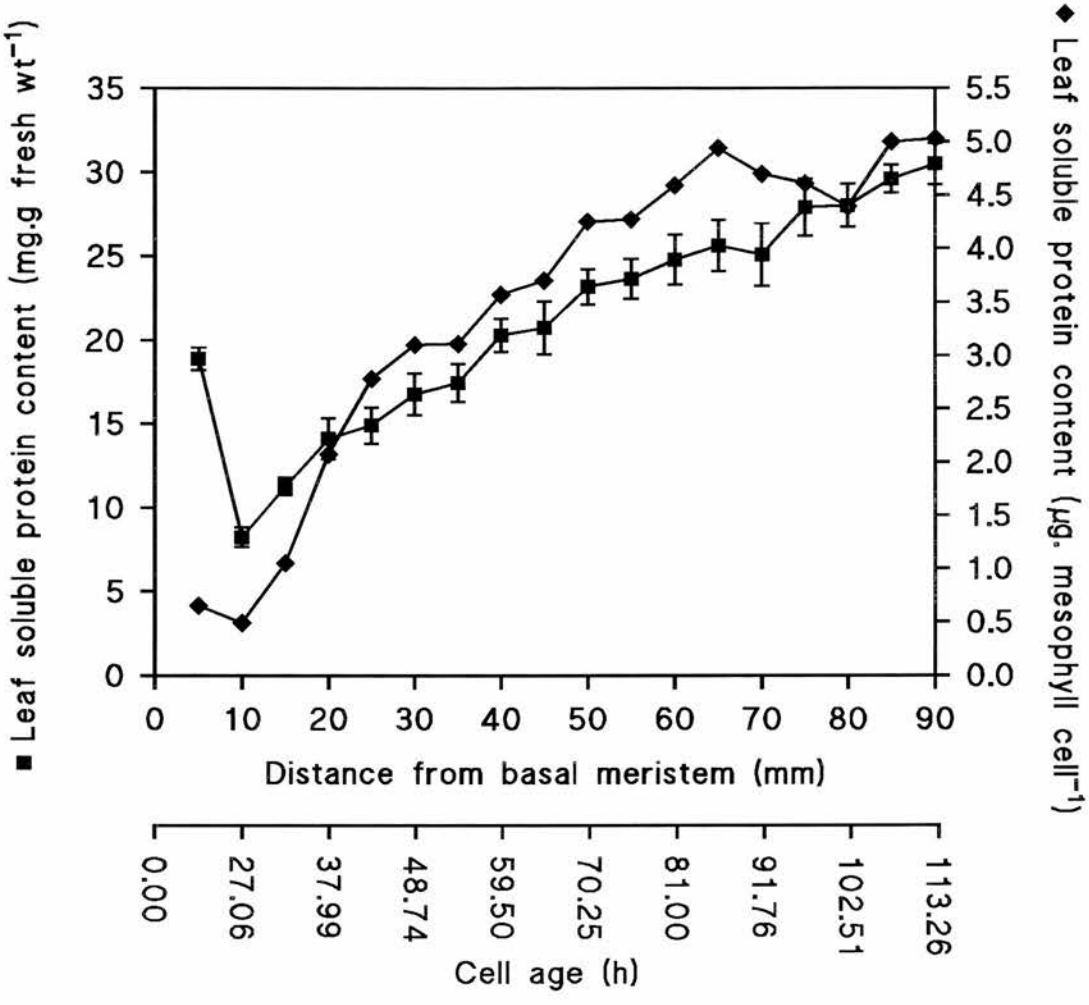

Figure 4.1 Soluble Protein Content along 7d-old Wheat Primary Leaves. See Section 4.2.1.1. Values represent the mean of five replicates, each from a different batch of plants ± standard errors. Data are expressed per unit fresh weight and per mesophyll cell (see Section 2.8). Measurements were made from sequential 5mm transverse sections along the leaf. Values are means for each particular leaf segment under examination, e.g. the value plotted at 5mm represents the leaf segment 0-5mm from the basal meristem. The cell age corresponding to distance from the basal meristem is also shown (see Section 2.5.3).

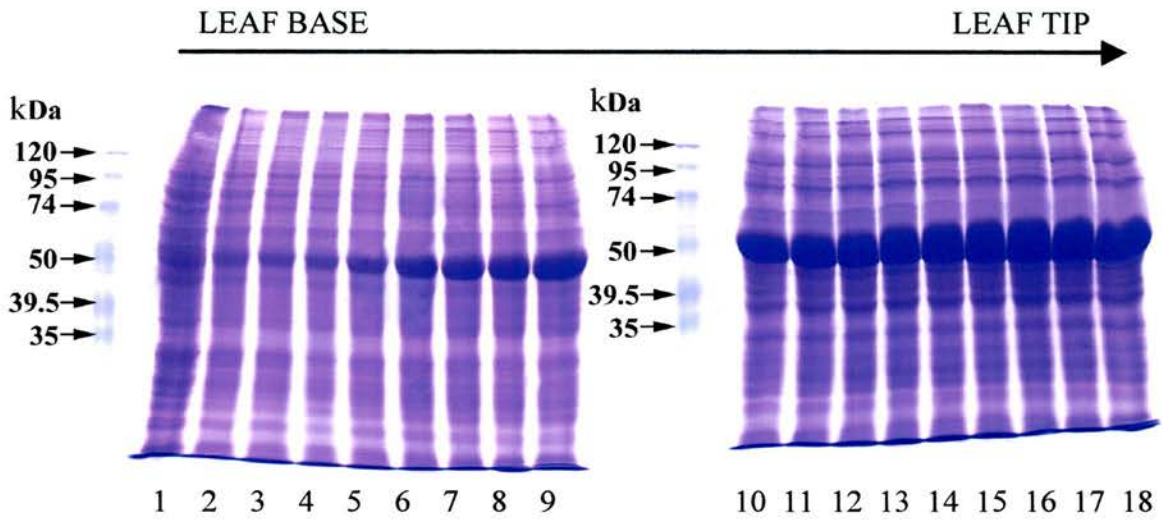

Figure 4.2 SDS-PAGE of Polypeptides from 7d-old Wheat Primary Leaves. See Section 4.2.1.2. Soluble protein was extracted from sequential 5mm leaf sections (1 to 18 on figure) from the leaf base to the tip. Lane 1 represents leaf sections taken from 1-5mm from the leaf base, lane 2 represents leaf sections taken from 5-10mm from the leaf base, and so on. 50μg protein was loaded per well, and the gel was stained with Coomassie blue to visualise polypeptide bands (see Section 2.9.1). 10μl prestained molecular weight markers were loaded per well (Sigma prestained SDS-PAGE standard solution, molecular weight range 35-120 kDa).

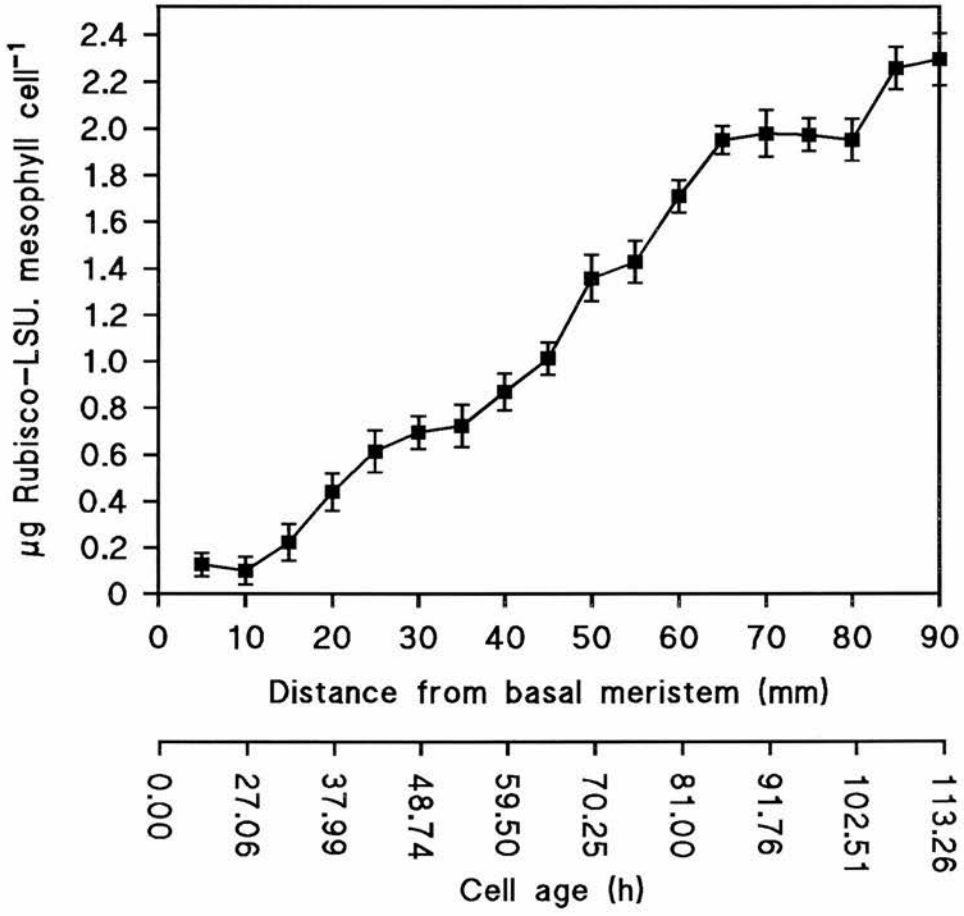

Figure 4.3 Increase in the Cellular Concentration of the Large Subunit of Rubisco along 7d-old Wheat Primary Leaves. See Section 4.2.1.2. Values represent the mean of five replicates, each from a different batch of plants ± standard errors. See Figure 4.1 for details of leaf section sampling. Whole leaf protein extract was probed on Western blots with a specific antibody, and the bands visualised using horseradish peroxidase (see Section 2.9.4). The cell age corresponding to distance from the basal meristem is also shown (see Section 2.5.3).

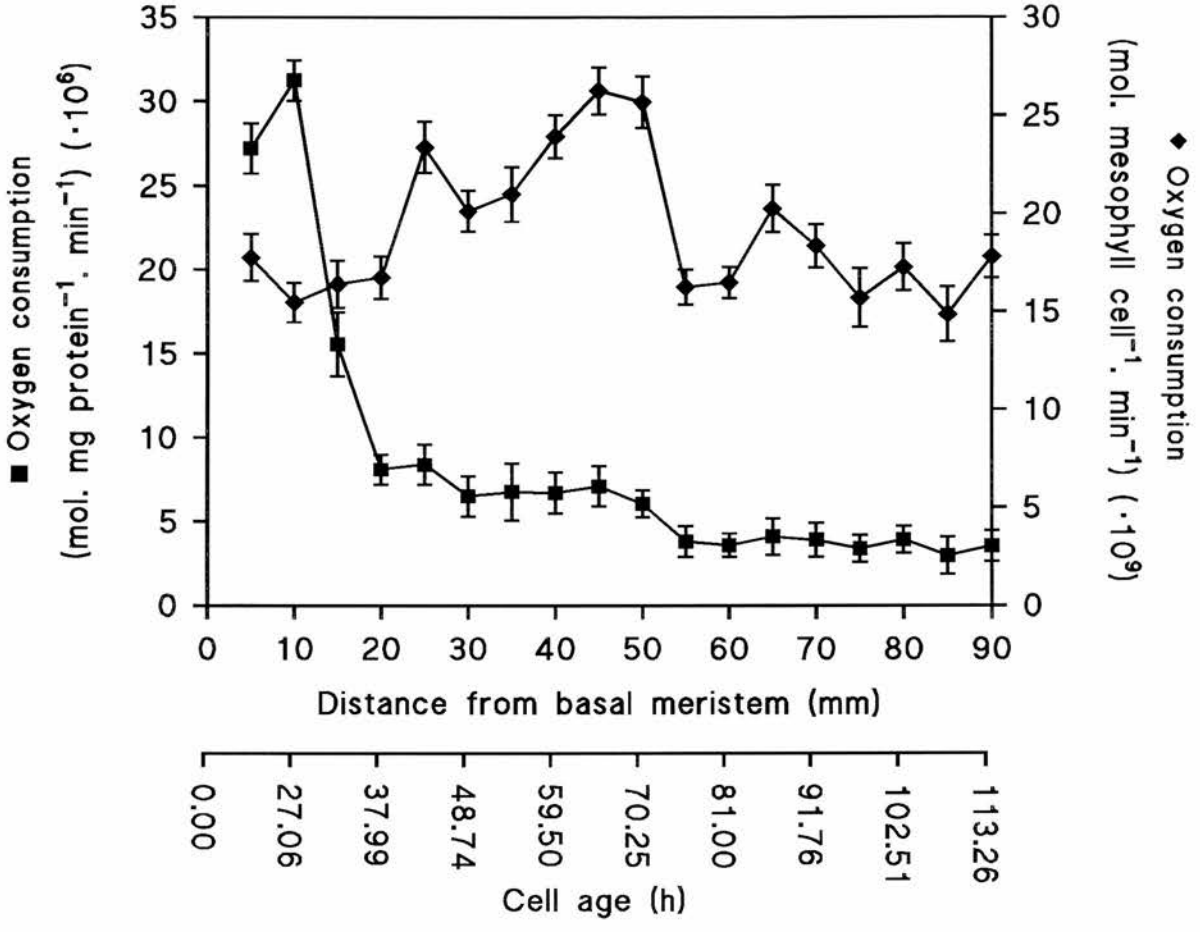

Figure 4.4 Rate of Respiration along 7d-old Wheat Primary Leaves. See Section 4.2.1.3. Values represent the mean of five replicates, each from a different batch of plants ± standard errors. Data are expressed per mg soluble protein and per mesophyll cell. See Figure 4.1 for details of leaf section sampling. The cell age corresponding to distance from the basal meristem is also shown (see Section 2.5.3).

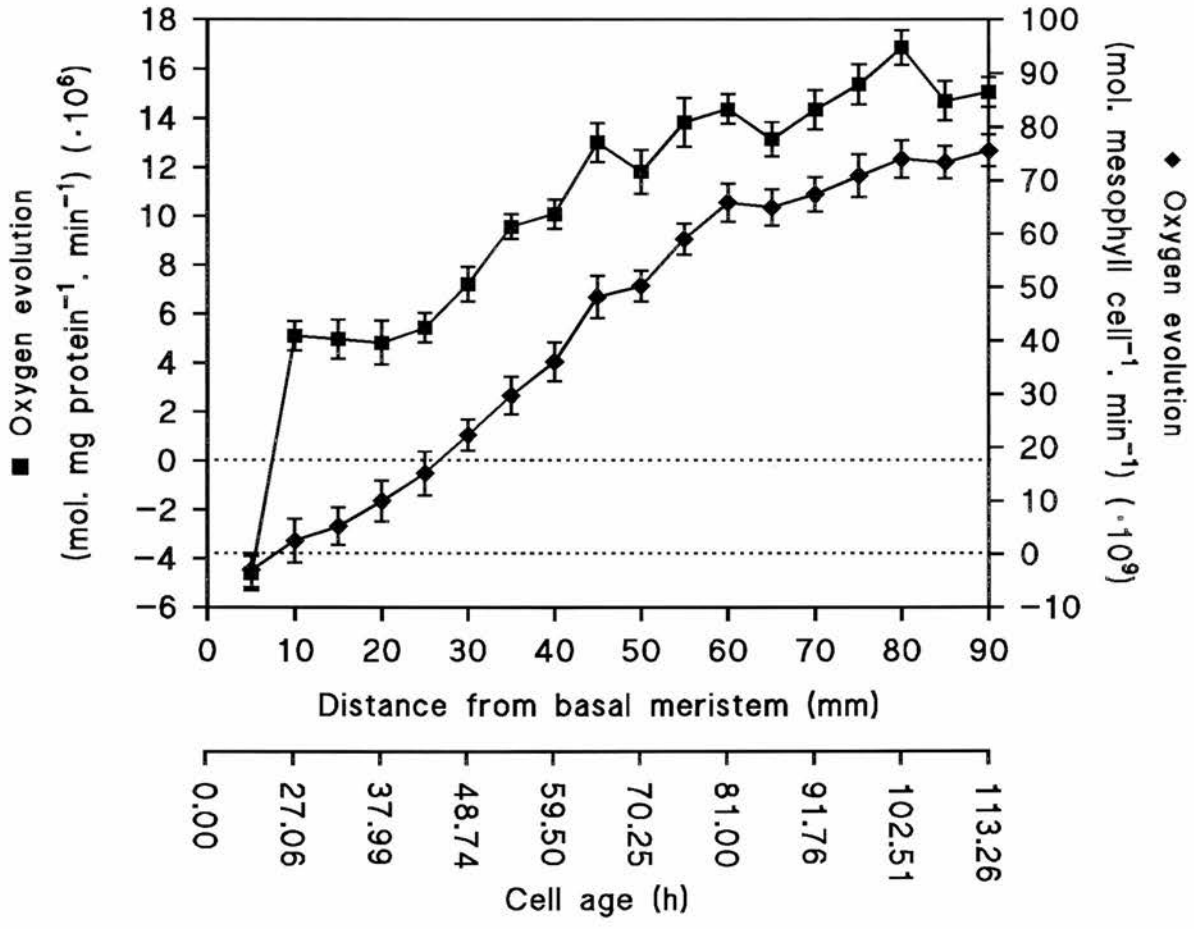

Figure 4.5 Net Rate of Photosynthesis along 7d-old Wheat Primary Leaves. See Section 4.2.1.4. Values represent the mean of five replicates, each from a different batch of plants ± standard errors. Data are expressed per mg soluble protein and per mesophyll cell. See Figure 4.1 for details of leaf section sampling. The cell age corresponding to distance from the basal meristem is also shown (see Section 2.5.3).

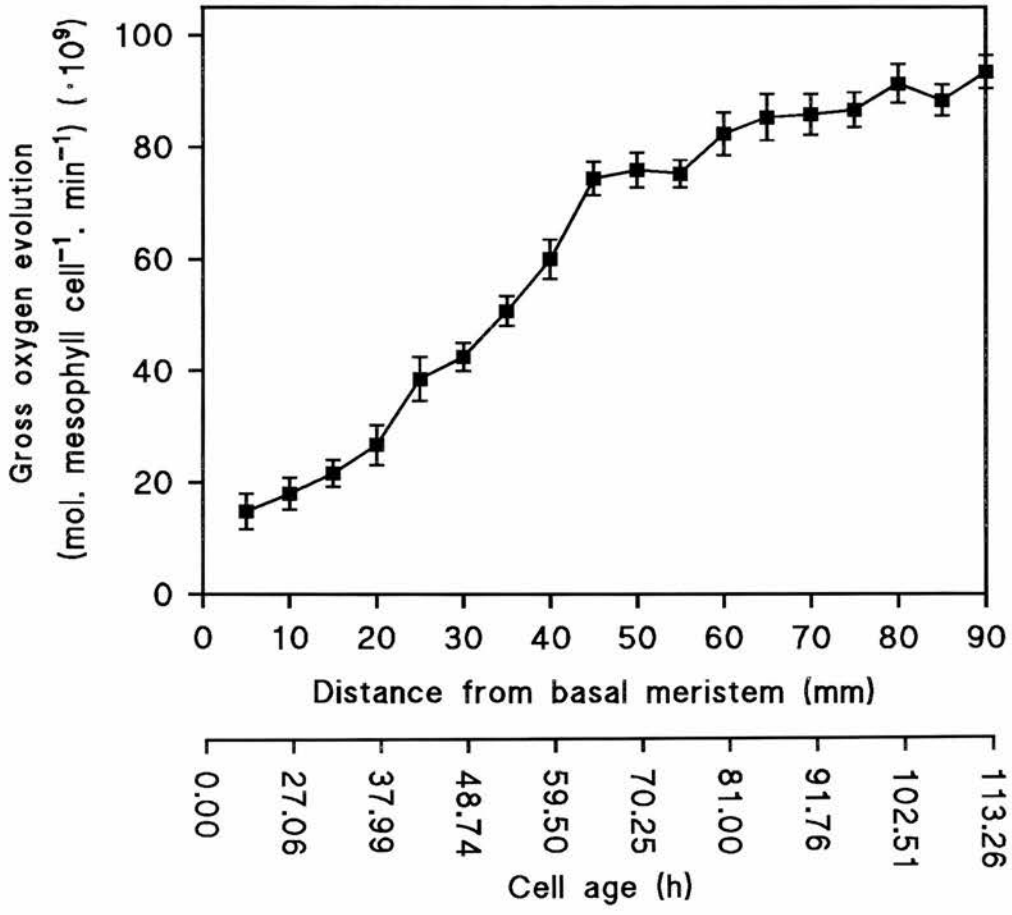

Figure 4.3 Increase in the Cellular Concentration of the Large Subunit of Rubisco along 7d-old Wheat Primary Leaves. See Section 4.2.1.2. Values represent the mean of five replicates, each from a different batch of plants ± standard errors. See Figure 4.1 for details of leaf section sampling. Whole leaf protein extract was probed on Western blots with a specific antibody, and the bands visualised using horseradish peroxidase (see Section 2.9.4). The cell age corresponding to distance from the basal meristem is also shown (see Section 2.5.3).

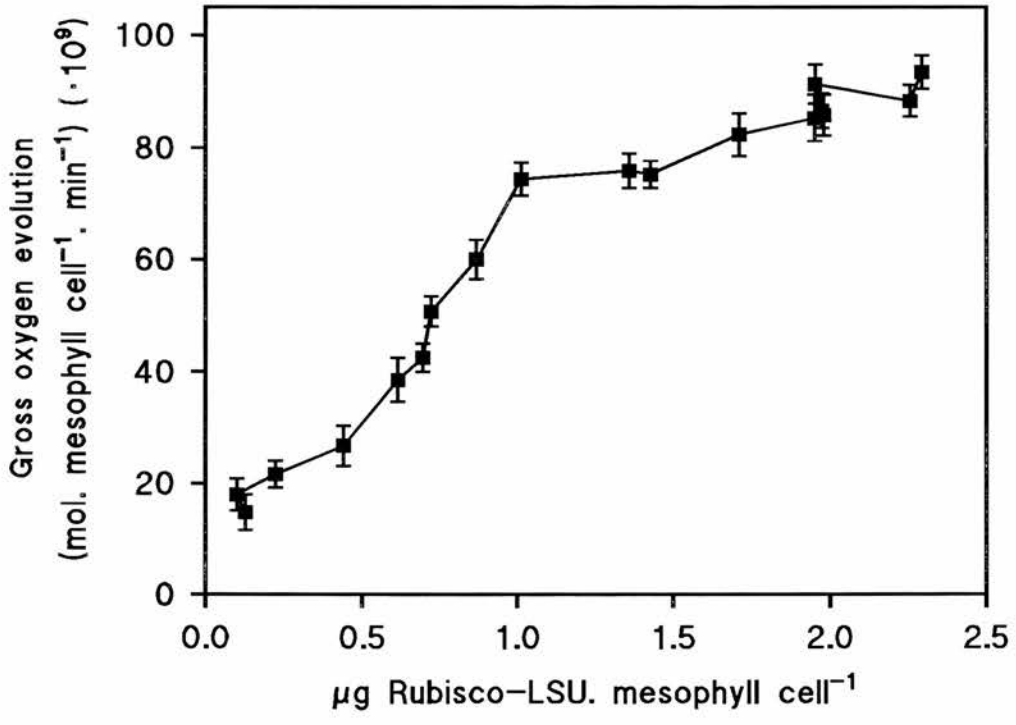

Figure 4.7 Gross Rate of Photosynthesis with Increasing Cellular Rubisco-LSU Content, in 7-d old Wheat Primary Leaves. See Section 4.2.1.4. Values represent the mean of five replicates, each from a different batch of plants ± standard errors, and are calculated from the data of Figures 4.3 (cellular Rubisco-LSU content) and 4.6 (gross cellular rate of photosynthesis).

4.2.2 Immunostaining of Wheat Primary Leaf Mitochondrial PDC and GDC Complex Proteins, using Crude Protein Extracts

4.2.2.1 Immunostaining of Primary Leaf Proteins on Western Blots

The six mitochondrial proteins under investigation were identified using specific antibodies to immunostain Western blots produced via SDS-PAGE of whole leaf soluble protein extract (see Section 2.9). In each case, a single band was visible, verifying the presence of the protein in the leaf, and also indicating that the antibodies used were specific only for that protein (especially in the case of PDC, where a chloroplastic PDC exists in addition to the mitochondrial form) and therefore suitable for use in this study. The position of the immunostained bands reconfirmed the identity of the polypeptides in question, along with evidence from previous studies using these particular antibodies. The exact size of the polypeptides in question vary depending on species, and studies on higher plant species including pea, maize, barley and potato have reported molecular weights in the order of: 41-43 kDa (E1α), 37-40 kDa (E1β), 50-80 kDa (E2), 56-67 kDa (E3), 97-105 kDa (GDC P-protein) and 50-61kDa (GDC L-protein) (Vauclare *et al.*, 1996; Millar, Leaver & Hill, 1999). The exact size of polypeptide bands could not be determined in this study via fractionation on mini-gels, and in any case, the aim of immunostaining the Westerns was simply to confirm the presence of the proteins and to confirm antibody specificity. Figure 4.8 shows the six polypeptides immunostained on Western blots.

4.2.2.2 Immunostaining of Primary Leaf Proteins on Slot Blots

Slot blots were produced using soluble protein extracts from sequential 5mm transverse sections taken from the leaf base to the tip (Section 2.9), and immunostaining with specific antibodies revealed the presence of the six mitochondrial proteins under investigation, at each of these different leaf developmental stages. Figures 4.9 to 4.14 show the developmental patterns of each protein with leaf development, revealed by measuring differences in slot blot band intensity between the leaf base and tip for each protein (see Section 2.9.5 for procedure). The results are expressed as a % of the maximum band intensity in each case, and describe relative protein concentration per cell with increasing distance from the basal meristem (it was essential to confirm a linear relationship between increasing band intensity and increasing protein concentration with this technique, and this was done initially - see Section 2.9.5). Since the data were derived from summed greyscale values (see Section 2.9.5), standard errors

are not applicable on the graphs. The technique assumed that antibodies did not discriminate between separate populations of mitochondria which might be present at different stages of development (e.g. mitochondria of different sizes or shapes), and that the epitope recognised by the antibody did not change throughout leaf development.

Figure 4.9 shows changing polypeptide band intensity of the PDC E1α subunit along the primary leaf. Relative protein concentration increased steadily from a minimum value at the leaf base to a maximum at 45mm from the basal meristem. From here, protein concentration decreased towards the leaf tip, reaching 40% of the maximum concentration at this point.

Figure 4.10 shows changing polypeptide band intensity of the PDC E1β subunit along the primary leaf. Relative protein concentration increased sharply between 0mm and 15mm from the basal meristem, then decreased to a minimum at 50mm from the basal meristem. Protein concentration then remained fairly constant between this point and the leaf tip.

Figure 4.11 shows changing polypeptide band intensity of the PDC E2 subunit along the primary leaf. Relative protein concentration increased in a fairly linear manner from the leaf base to the leaf tip, plateuing towards the leaf tip from approximately 70mm from the basal meristem. Maximum protein concentration occurred at 80mm from the basal meristem.

Figure 4.12 shows changing polypeptide band intensity of the PDC E3 subunit along the primary leaf. Relative protein concentration increased within the elongation zone (0-15mm from the basal meristem), then platcaucd from hcrc to 45mm from the basal meristem. From here, protein concentration continued to increase linearly towards the leaf tip, reaching a maximum value at 85mm from the basal meristem.

Figure 4.13 shows changing polypeptide band intensity of GDC P-protein along the primary leaf. Relative protein concentration increased in a fairly linear manner between the leaf base and the tip, reaching a maximum value at 85mm from the basal meristem.

Figure 4.14 shows changing polypeptide band intensity of GDC L-protein along the primary leaf. Relative protein concentration increased in a fairly linear manner between the leaf base and the tip (more linearly than GDC P-protein, Figure 4.13), reaching a maximum value at 90mm from the basal meristem.

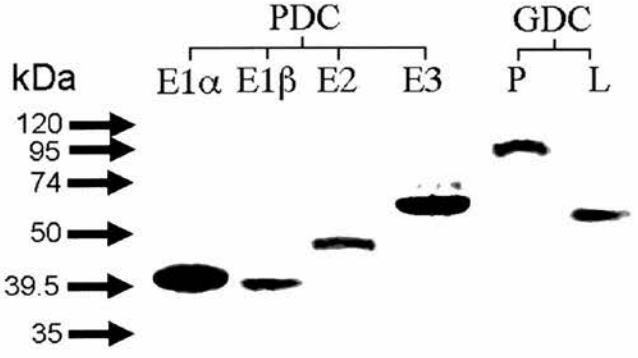

Figure 4.8 Immunostaining of Wheat Primary Leaf Mitochondrial PDC and GDC Subunits on Western Blots. See Section 4.2.2.1. Whole leaf protein extracts from 7d-old leaves were probed on Western blots with specific antibodies, and the polypeptide bands visualised using the ECL detection method (Section 2.9.4). 50μg protein was loaded per well on the original gels together with 10μl prestained molecular weight markers (Sigma prestained SDS-PAGE standard solution, molecular weight range 35-120 kDa).

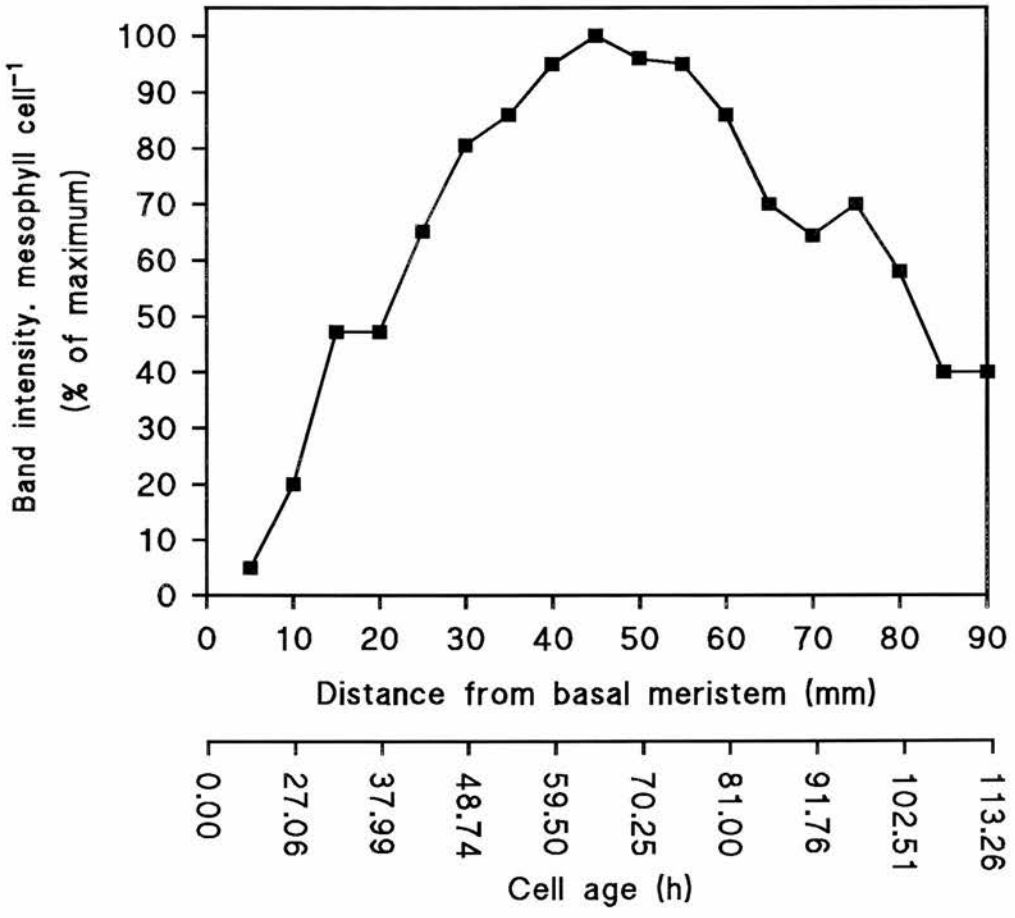

Figure 4.9 Development of the PDC E1α Subunit along 7d-old Wheat Primary Leaves: Slot Blot Analysis. See Section 4.2.2.2. Values represent the mean of five replicates, each from a different batch of plants ± standard errors. See Figure 4.1 for details of leaf section sampling. The cell age corresponding to distance from the basal meristem is also shown (see Section 2.5.3).

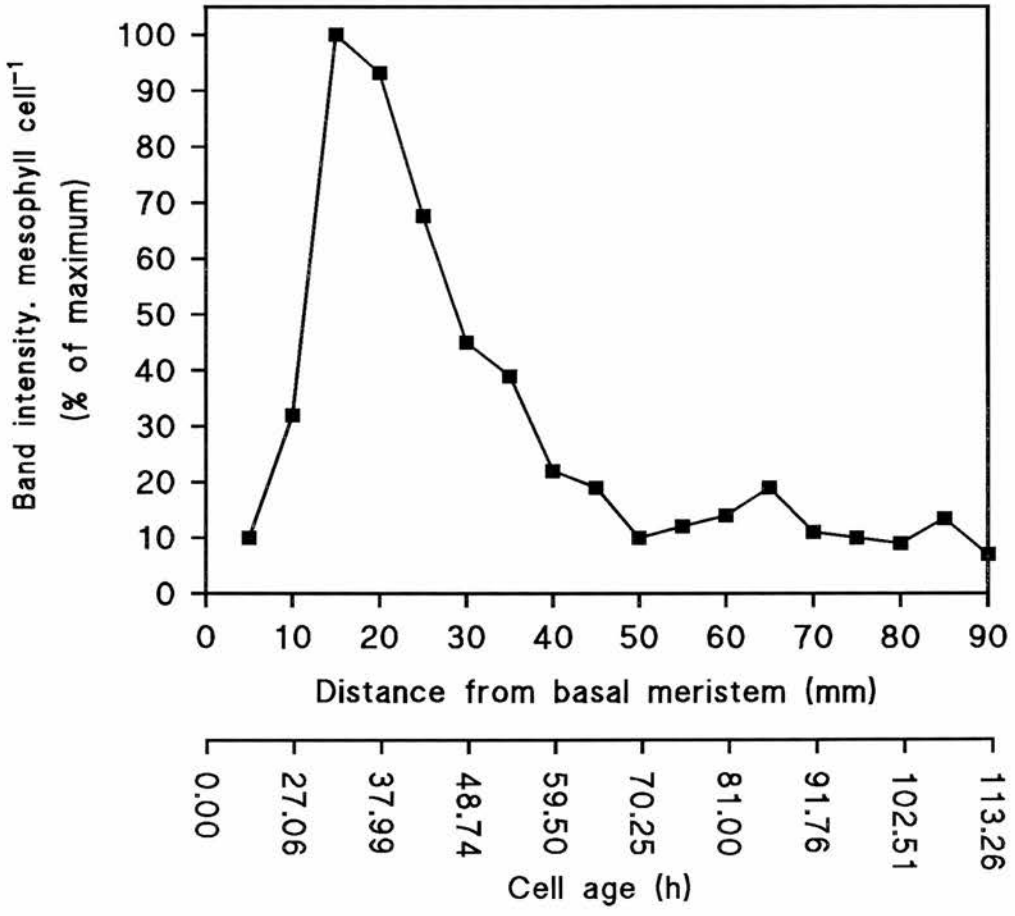

Figure 4.10 Development of the PDC E1β Subunit along 7d-old Wheat Primary Leaves: Slot Blot Analysis. See Section 4.2.2.2. Values represent the mean of five replicates, each from a different batch of plants ± standard errors. See Figure 4.1 for details of leaf section sampling. The cell age corresponding to distance from the basal meristem is also shown (see Section 2.5.3).

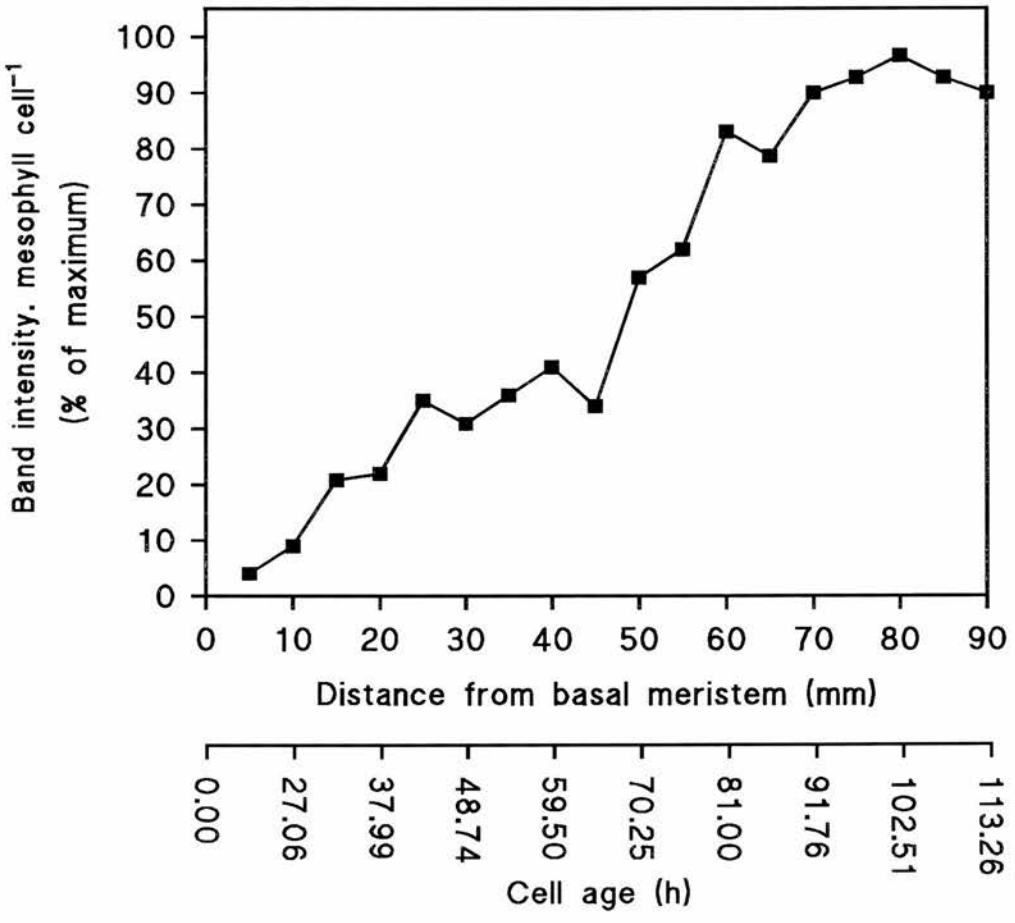

Figure 4.11 Development of the PDC E2 Subunit along 7d-old Wheat Primary Leaves: Slot Blot Analysis. See Section 4.2.2.2. Values represent the mean of five replicates, each from a different batch of plants ± standard errors. See Figure 4.1 for details of leaf section sampling. The cell age corresponding to distance from the basal meristem is also shown (see Section 2.5.3).

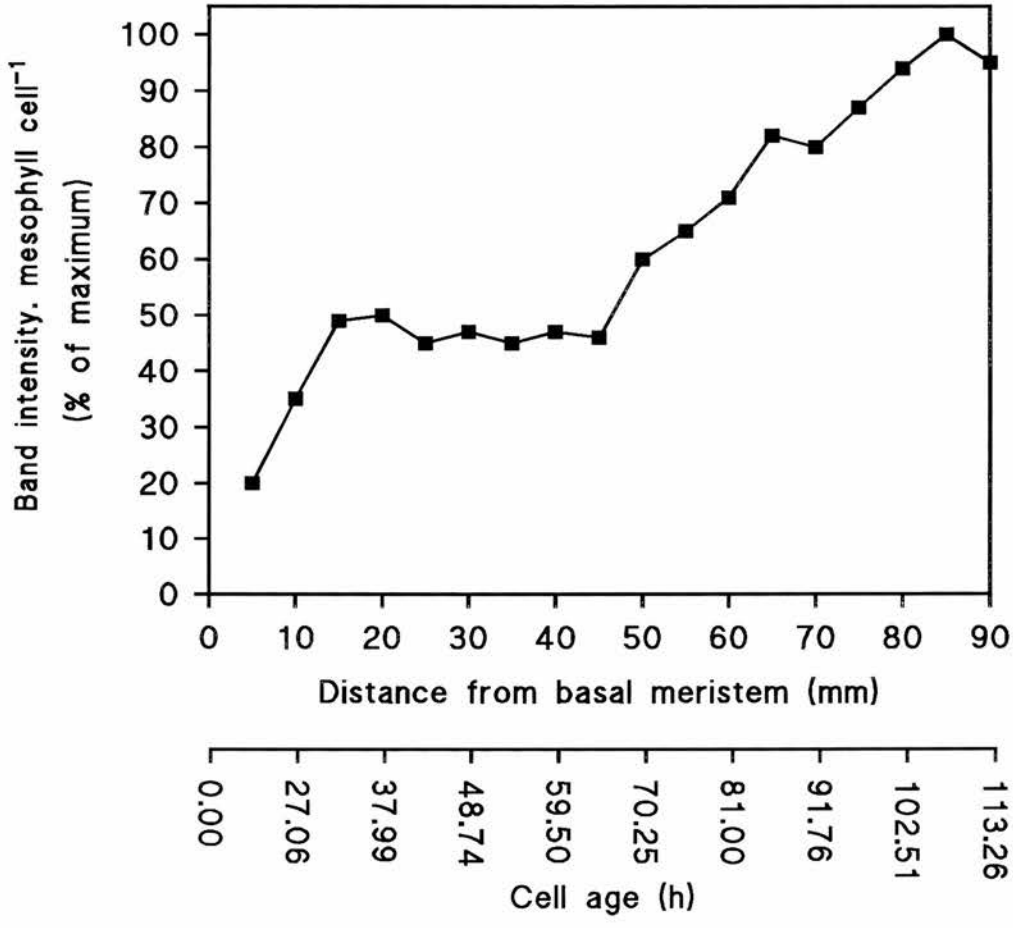

Figure 4.12 Development of the PDC E3 Subunit along 7d-old Wheat Primary Leaves: Slot Blot Analysis. See Section 4.2.2.2. Values represent the mean of five replicates, each from a different batch of plants ± standard errors. See Figure 4.1 for details of leaf section sampling. The cell age corresponding to distance from the basal meristem is also shown (see Section 2.5.3).

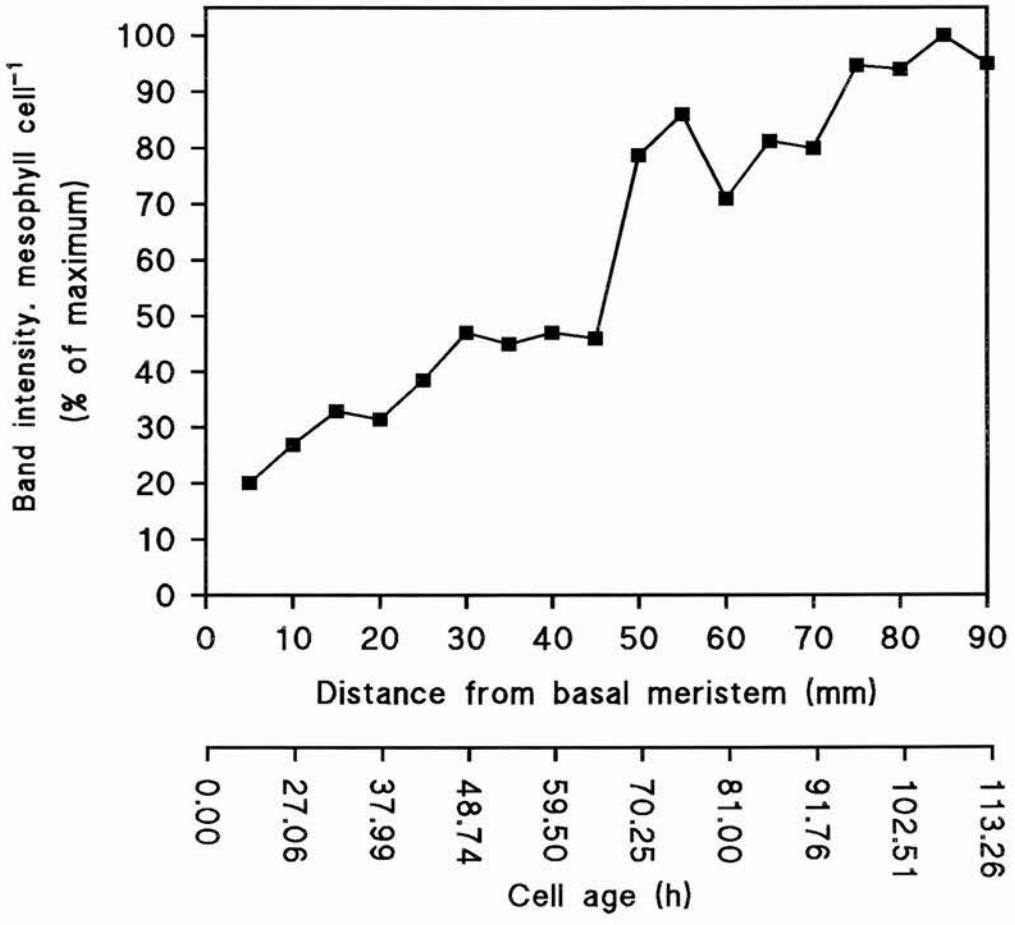

Figure 4.13 Development of the GDC P-protein Subunit along 7d-old Wheat Primary Leaves: Slot Blot Analysis. See Section 4.2.2.2. Values represent the mean of five replicates, each from a different batch of plants ± standard errors. See Figure 4.1 for details of leaf section sampling. The cell age corresponding to distance from the basal meristem is also shown (see Section 2.5.3).

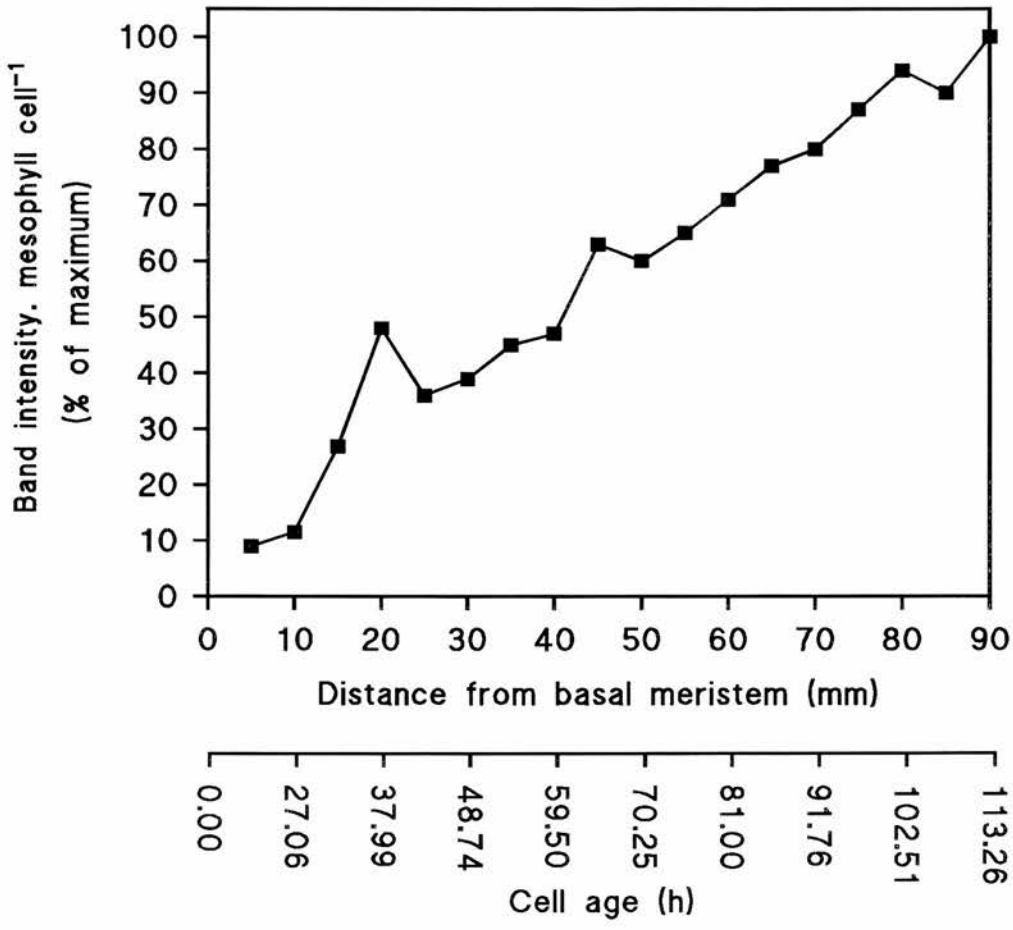

Figure 4.14 Development of the GDC L-protein Subunit along 7d-old Wheat Primary Leaves: Slot Blot Analysis. See Section 4.2.2.2. Values represent the mean of five replicates, each from a different batch of plants ± standard errors. See Figure 4.1 for details of leaf section sampling. The cell age corresponding to distance from the basal meristem is also shown (see Section 2.5.3).

4.3 Discussion

4.3.1 Changes in Wheat Primary Leaf Metabolism with Development

Given the vital role that proteins occupy in all living cells, the observed changes in total soluble protein composition and in amounts of protein present between the base and tip of the developing wheat leaf are important indicators of changing metabolism with increasing cell age. Leaf soluble protein per unit fresh weight decreased initially in the elongation zone, and then increased steadily towards the leaf tip. This initial sharp decrease corresponds to the decrease in cell number as cells elongate within this region reported in Chapter 3. When expressed per mesophyll cell, a steady increase in leaf mesophyll cell soluble protein content between the leaf base and tip was observed, in accordance with the findings of previous studies on wheat (Dean & Leech, 1982a; Topping & Leaver, 1990) and barley (Viro & Kloppstech, 1980; Thompson, Bowsher & Tobin, 1998).

Rubisco-LSU was clearly observed to increase with cell age on stained gels and Western blots (Figures 4.3 and 4.4), and the 18-fold increase in μg Rubisco per cell between the leaf base and tip found in this study, is similar to the 20-fold increase found in a previous study of developing wheat mesophyll cells (Dean & Leech, 1982a). Rubisco may in fact constitute 50% of the total protein in mature wheat leaf tissue (Ostareck & Lieckfeldt, 1989), and is therefore responsible for a large proportion of the observed increase in total soluble protein content with increasing cell age.

The increase in soluble protein content must also include other proteins, and in addition to Rubisco-LSU, other photosynthetic enzymes as well as photorespiratory enzymes have been shown to increase with cereal leaf cell development. For example, the photorespiratory enzymes chloroplastic glutamine synthetase, glycollate oxidase and glycine decarboxylase activities develop in a similar pattern along the developing wheat leaf as Rubisco (Tobin, Ridley & Stewart, 1985; Tobin *et al.*, 1988; Tobin *et al.*, 1989), indicating a co-ordination between photosynthesis and photorespiration.

The cellular increase in rate of net photosynthesis observed with leaf cell development was similar to that found previously in wheat (Tobin *et al.*, 1988). Immature cells at the leaf base are primarilly heterotrophic, and rely mainly on carbon imported from the seed or from mature leaf tissue (Dale, 1985), even although the presence of Rubisco is detectable at low levels in very immature tissue (Dean & Leech, 1980). As cells mature and are displaced away from the leaf base, they develop increasing photosynthetic capacity and convert to a more autotrophic metabolism,

resulting in the observed linear increase in rate of photosynthesis along the leaf. This is in accordance with the dramatic increase in occurrence of the important photosynthetic enzyme Rubisco noted, and suggests increases in other photosynthetic enzymes, and an increase in rate of photorespiration. Increased rate of photosynthesis with development also concurs with increasing chloroplast development. As discussed in Chapter 3, chloroplasts increase in number and individual size with leaf development, exhibit a more complex internal thylakoid membrane system, and take up a greater total proportion of the cell (Tobin, Ridley & Stewart, 1985). In the present study, the gross rate of photosynthesis per cell showed that photosynthesis was taking place at all stages of development, even in the young basal tissue; and when compared with the rate of net photosynthesis, showed that in the basal tissue, the rate of respiratory oxygen uptake exceeded that of photosynthetic oxygen evolution.

When gross cellular photosynthesis rate was plotted against cellular Rubisco-LSU protein content, a linear increase in photosynthesis was observed with increasing Rubisco-LSU concentration up to approximately 1μg Rubisco-LSU per mesophyll cell. This linear relationship indicates that Rubisco-LSU concentration is a major limiting factor in determining photosynthetic activity in young and developing leaf cells. In more mature tissue, where Rubisco-LSU content exceeds 1μg protein per mesophyll cell, rate of photosynthesis does not increase with further increases in cellular Rubisco-LSU content. This suggests that either Rubisco-LSU is not fully active in this older tissue, or that other factors are more limiting to photosynthesis than the presence of Rubisco, e.g. light-harvesting reactions or other Calvin cycle enzymes may exert more control over photosynthesis.

On a per cell basis, 'dark' respiration rate peaked slightly halfway along the leaf, but remained relatively constant along the leaf as a whole. When expressed relative to total protein per unit fresh weight, respiration rate decreased towards the leaf tip in a similar trend to that found previously (Azcón-Bieto, Lambers & Day, 1983; Thompson, Bowsher & Tobin, 1998). This again emphasises an increase in photosynthetic and photorespiratory proteins compared to respiratory proteins with cell development.

4.3.2 Development of Wheat Primary Leaf Mitochondrial Proteins

Young leaf cells convert from mainly a heterotrophic to a more autotrophic role with increasing cell age and the development of photosynthesis and photorespiration, and it follows that mitochondrial protein composition will alter with

leaf development, adjusting to suit functional requirements.

The six mitochondrial proteins under investigation were found to develop in different patterns between the leaf base and tip. The data in these graphs have been expressed as percentages of the maximum value, so that any differences in protein development can be seen clearly with increasing distance from the basal meristem, and so that different trends exhibited by different proteins can be easily compared. However, only the *trends* between graphs can be compared - it is impossible to compare actual amounts of protein between graphs as each protein was localised by a different antibody, producing different signal intensities when immunostained. It is therefore only possible to compare amounts *within* each graph (assuming that the increasing amounts of soluble protein have not significantly altered relative protein proportions along the leaf- see later), and here only relative comparisons can be made, i.e. comparative quantification. In order to obtain actual amounts of protein, known amounts of pure samples of the proteins in question would have to have been included on the slot blots, and the band intensities of these measured and compared with the crude extract band intensities. It was not possible to obtain pure samples of all the proteins analysed in this study, and this was not necessary in any case – the point of these experiments was to observe any differences in the developmental patterns of the enzymes in question.

The developmental trends observed between the leaf base and tip for PDC E1α, PDC E1β, and GDC L-protein were very similar to those obtained in a previous study of barley in our laboratory, using the same technique (Thompson, Bowsher & Tobin, 1998). The trend obtained for GDC P-protein was not so similar, although it did exhibit the same general increase from base to tip as the barley study, although it was a more steady increase in the present study. PDC E2 and PDC E3 were not included in the barley study. The similarity in the results between the study on barley and the present one, is perhaps not surprising due to the similarity of the two species, and the fact that PDC and GDC have well-established roles in higher plants, and an initial conclusion might be that they probably perform identical roles in both wheat and barley. The similarity in the results of the two studies also increases confidence in the slot blot technique used.

In general, it is interesting that amounts of mitochondrial proteins change with development, and that different proteins appear to have different developmental patterns. All six proteins increased within the elongation zone, between the leaf base

and approximately 15mm from the basal meristem. From here, three different developmental patterns were evident.

Following an increase in the leaf elongation zone, PDC E1α increased between the base and approximately halfway along the leaf before decreasing towards the leaf tip. This is a similar trend to that of cellular respiration rate along the leaf. PDC E1β exhibited a sharp decrease at the end of the elongation zone, then adopted a trend similar to that of cellular respiration rate along the remaining length of the leaf. PDC E2, PDC E3, GDC P-protein and GDC L-protein showed very similar developmental trends along the whole length of the leaf, with a steady increase from the base to the tip, reaching a maximum at or near the leaf tip. This developmental trend parallels that of photosynthetic development along the leaf, though is similar to that of cellular respiration rate along the first half of the leaf. It is perhaps less surprising that enzymes of different protein complexes might show different developmental trends, but it is particularly interesting that three different developmental trends are exhibited by the four subunits of PDC.

The interpretation of the developmental patterns of the mitochondrial proteins is complicated by the observed increase in the total amount of leaf soluble proteins between the leaf base and tip, with amounts of some proteins increasing more than others, in particular Rubisco, so that the relative proportions of different proteins change. Since equal amounts of whole leaf protein extract were loaded onto slot blots for each developmental stage, an increase in the amount of Rubisco would result in less mitochondrial protein A being detected at the tip than the base. This would not necessarily be because mitochondrial protein A has decreased per cell, but because there would be a smaller proportion of all mitochondrial proteins in each whole leaf protein sample at the tip than at the base, due to the increased proportion of Rubisco in the sample.

To overcome this, data would have to be obtained revealing the exact amounts of photosynthetic (and for that matter, all other) proteins present per unit whole leaf protein extract at each developmental stage under the particular growth conditions of this study, so that they could be subtracted from the total, and extra whole leaf protein extract loaded onto slot blots as necessary for the particular developmental stage. This was not feasible in the present study, and would probably result in introducing enough errors to make the whole procedure pointless.

However, since this study involved the comparison of mitochondrial proteins –

all constituting a similar small proportion at the leaf tip compared to Rubisco, a simple comparison of developmental trends could still be carried out, involving no reference to differences in actual amounts of protein between the leaf base and the tip from approximately 20mm from the basal meristem. In any case, presence of a protein does not necessarily reflect activity. Between 0mm and 20mm from the basal meristem, Rubisco does not increase significantly enough to severely alter relative proportions of leaf proteins (Dean & Leech, 1982a), and therefore in this region reference to comparative changes in amounts of protein can be made within each graph. For example, PDC E1β (Figure 4.10) can be said to increase in amount between 0mm and 20mm from the basal meristem. However, beyond 20mm, the sharp decrease shown on the graph might equate to a levelling off of the amount of protein, due to the decreasing proportion of the protein sample examined occupied by E1β with increasing distance from the leaf base. Even so, comparing this trend with that of E1α (Figure 4.9), it can still be concluded that more E1α than E1β accumulates in leaf mesophyll cells between approximately 20mm and 50mm from the basal meristem, even though the relative amounts cannot be obtained from the data.

So, why do different mitochondrial proteins (especially if belonging to the same complex) exhibit different developmental patterns?

In the region 0mm to 20mm from the basal meristem, cells enlarge in the elongation zone, resulting in a decrease in cell number per unit fresh weight (see Chapter 3). In addition, wheat mitochondria divide and increase in number in this region, reaching a maximum near the end of the elongation zone (Tobin & Rogers, 1992; see Chapter 3). This might be in accordance with a general increase in the cellular concentration of mitochondrial proteins along the elongation zone, even although the respiratory rate per cell was observed to remain constant along the same region of the leaf, and that with increasing cell enlargement, the same proportion of the volume of each mesophyll cell is occupied by mitochondria at all developmental stages (Tobin & Rogers, 1992). However, there are other possible factors which influence respiratory rate such as substrate availability and adenylate control (Moore *et al.*, 1992).

The difference in developmental patterns between the E1α and E1β subunits is difficult to account for, since the two are so closely associated and are bound together in all eukaryote PDCs characterised to date (Miernyk, Thelen & Randall, 1998). PDC catalyses the oxidative decarboxylation of pyruvate to form acetyl-CoA and NADH, and the E1 subunit catalyses the decarboxylation of pyruvate and the transfer of the

remaining acetyl moiety to the cofactor thiamine pyrophosphate (TPP) (Thelen, Miernyk & Randall, 1998) (see Figure 1.2 in Chapter 1). Both E1α and E1β are involved in this, but one difference is that E1α is regulated by phosphorylation via PDC-kinase and phospho-PDC phosphatase (Budde & Randall, 1988), while E1β is not. It was not possible in this study to know the phosphorylation status of the enzyme throughout development, and whether this would have some impact on the developmental pattern - it would be interesting to observe the developmental patterns of the two regulating enzymes (both of which have two subunits in mammals, Stepp *et al.*, 1983), and perhaps the developmental pattern of E1α has a greater association with the development of these regulatory proteins, than with the E1β subunit.

PDC E2 and PDC E3 have different functions to PDC E1α and E1β, and therefore it is less difficult to accept that they show different developmental patterns to E1. E2 catalyses the transfer of the acetyl moiety from TPP to coenzyme A, with the reduction of a covalently bound lipoamide cofactor; while E3 reoxidises the lipoamide residue and converts NAD^+ into its reduced form, via a bound flavin adenine nucleotide cofactor (Hill, 1998). Even so, all the PDC subunits contribute to the overall reaction of the oxidative decarboxylation of pyruvate which cannot take place without all its component parts. For all four PDC subunits however, a co-ordinated increase was observed in the elongation zone, concurring with the attainment of maximum cell size and cessation of mitochondrial division at the end of the elongation zone. Beyond this region, with the required amounts of all PDC components having been synthesised, it could be that the levels of activity exhibited by the components bear no relation to the developmental trends of the proteins. Enzyme activity was not measured in this study, but in a previous study of barley it was found that overall mitochondrial PDC activity per cell remains constant along the developing leaf (Lernmark & Gardestrom, 1994).

The two subunits of GDC examined in this study, showed the same developmental trend, i.e. an increase between the leaf base and tip (which will in reality be even more pronounced than the graphs suggest, due to the changing protein proportions of samples, as previously discussed). The same trends were found in a previous similar study of barley, and in the latter, GDC H-protein and GDC T-protein were also analysed and a similar developmental trend was found for all four subunits (Thompson, Bowsher & Tobin, 1998). GDC is a photorespiratory enzyme and catalyses the oxidation of glycine (Walker & Oliver, 1986). The rate of photorespiration increases with cell age (Tobin & Rogers, 1992), and an accompanying increase in

photorespiratory enzymes therefore concurs with this. In pea, the GDC L-protein and the PDC E3 subunit have been found to be exactly the same enzyme within both complexes (Conner, Krell & Lindsay, 1996). The similar developmental trends observed for these two proteins are in accordance with this, and it could be that in wheat they are one and the same protein, though this has not been confirmed to date. Certainly, the similarity in band sizes obtained on Western blots for the two proteins, might suggest this to be the case.

4.3.3 Summary and Conclusions

An important way of monitoring metabolic change in organisms is to observe any changes in the amount or developmental patterns of proteins with increasing cell age. Following the ultrastructural and stereological findings of Chapter 3, this chapter has continued to characterise the natural developmental gradient of primary wheat leaves between the leaf base and tip, via the study of metabolic changes with increasing cell age. In accordance with previous studies on wheat and other cereal primary leaves, total leaf soluble protein per mesophyll cell was found to increase linearly between the leaf base and tip, together with changes in protein complement (visualised via Western blotting), highlighting the various metabolic changes that must occur as the leaf tissue converts from a heterotrophic status to a more autotrophic role. The similar linear increase in rate of photosynthesis observed, together with the increase in amount of Rubisco with cell age, is further evidence for this change. Again in accordance with previous studies, respiration rate per mesophyll cell remained relatively constant with increasing cell age. When expressed relative to total soluble protein per unit fresh weight, respiration rate decreased between the leaf base and tip, emphasising the increase in photorespiratory enzymes compared to respiratory enzymes with cell development. This information, together with that of Chapter 3, provided a general characterisation of the developmental gradient present in wheat primary leaves under the particular growth conditions of this study, and provided a basis for carrying out the more specific study of the development of the two major mitochondrial protein complexes.

Six mitochondrial proteins were analysed in this chapter: the E1α, E1β, E2 and E3 subunits of the PDC complex, and the P-protein and L-protein subunits of the GDC complex, via localisation on slot blots using specific antibodies. Three different protein developmental patterns were evident. An increase in the presence of all the proteins

within the elongation zone concurred with accompanying increases in rates of respiration, photosynthesis and photorespiration with increasing cell age. Only two of the PDC subunits are comparable to cellular respiration rate along the leaf, while the other two show trends more similar to that of photosynthesis rate. It is perhaps easier to understand the developmental patterns of the GDC subunits, owing to their similarity to that of photosynthesis and photorespiration. Differences in developmental patterns between different subunits of the PDC complex are difficult to explain, although ultimately only limited conclusions can be drawn from the data as it does not indicate levels of enzyme activity, and therefore it cannot be concluded whether the observed changes affect mitochondrial function. The general conclusion however, is that development of mitochondrial proteins in wheat appears to be heterogeneous, and this is a useful basis for the work described in the next chapter.

In chapter 5, the study of the six mitochondrial proteins discussed in the present chapter is investigated in much more detail using a different immunological approach. The slot blot technique described in the present chapter was useful in revealing general developmental patterns, but gave no indication of the location of the proteins in the leaf tissue examined, e.g. of any differences in protein levels between different cell types. Proteins with specific photosynthetic or photorespiratory functions may be specifically localised in photosynthetic mesophyll cells, and hence heterogeneity may occur at a spatial level within the leaf. The next chapter will examine protein development at the microscopical level, relating protein levels to mitochondrial area, rather than crude protein extracts from leaf sections, as in the slot blot technique; and investigate differences in mitochondrial biogenesis between different cell types.

CHAPTER 5: IMMUNOLOGICAL LOCALISATION OF THE MITOCHONDRIAL PYRUVATE DEHYDROGENASE COMPLEX (PDC) AND GLYCINE DECARBOXYLASE COMPLEX (GDC) IN WHEAT PRIMARY LEAF MESOPHYLL AND VASCULAR CELLS BY IMMUNOGOLD LABELLING

5.1 Introduction

5.1.1 The Study of Plant Proteins Using Immunogold Localisation

As described in Chapter 1, immunogold labelling is a widely used immunohistochemical technique involving the localisation of proteins on tissue sections, via the attachment of specific gold-labelled antibodies (Polak & Van Noorden, 1997). The gold particles can then be visualised using transmission electron microscopy (TEM) and the exact ultrastructural location of the proteins observed.

In the present study, this technique was utilised to investigate the development of mitochondrial proteins, using the same specific primary antibodies used for the slot blot procedure of the previous chapter, in addition to specific secondary antibodies conjugated to colloidal gold particles. Again, the six proteins under investigation were the E1α, E1β, E2 and E3 subunits of the pyruvate dehydrogenase complex (PDC), and the P-protein and L-protein subunits of the glycine decarboxylase complex (GDC). Immunogold labelling has been previously used in various studies to localise plant proteins, e.g. Rawsthorne *et al.*, 1988; Tobin *et al.*, 1989; Brangeon, Hirel & Forchioni, 1989; Datta *et al.*, 1991; Peat & Tobin, 1996; Rylott, Metzlaff & Rawsthorne, 1998; Hayakawa *et al.*, 1999; Brugière *et al.*, 1999; Neubohn *et al.*, 2000.

5.1.2 Tissue Under Investigation in this Study

The ultrastructural element of the immunogold technique allowed the comparison of different tissue types in the wheat leaf, and in this study, mesophyll and phloem tissue were compared. Since only half the number of cells of mature wheat leaves may be unspecialised mesophyll parenchyma (Jellings & Leech, 1982), it is appropriate to examine other cell types as well as mesophyll tissue. From a metabolic point of view, it is interesting to compare mitochondrial development in different tissue types which may have different metabolic requirements.

In this study, mesophyll cells were easily identified under the TEM. Vascular cell types were generally more difficult to identify under the TEM and isolate on slides (due to the smaller volume fraction of leaf section occupied by vascular cells than mesophyll, the smaller individual size of vascular cells, and the complexity of vascular tissue). Among the vascular cells, phloem companion cells were easily identified, and were chosen as a comparison to mesophyll cells due to the large mitochondrial presence.

Phloem tissue functions to transport photosynthetically-produced molecules around the plant, from sites of production to those of consumption. Specialised elongated cells known as sieve elements are aligned end to end with pore-filled sieve plates inbetween, forming long conducting sieve tubes for this purpose (Fahn, 1990). The same mother cells from which sieve elements are formed, also produce companion cells. While mature sieve elements contain minimal cytoplasm and organelles, and contain no nucleus; companion cells retain a full cytoplasm, nucleus and complement of organelles (and in fact tend to have a denser cytoplasm than e.g. unspecialised phloem parenchyma cells). Each sieve element exists in close association with at least one companion cell, and abundant plasmodesmata are located in the walls between the two cell types, branched on the side of the companion cell (Gunning & Steer, 1975; Robards, 1970). The exact function of companion cells still remains unclear, but it is generally accepted that they perform many of the metabolic functions of the sieve elements, transport photosynthates in and out of the sieve elements, and maintain the pressure gradient in the sieve tubes (Turgeon, 2000). This functional connection is emphasised by the fact that companion cells die when the associated sieve elements do. They tend to have a high complement of mitochondria, suggesting the need for extra energy production to maintain both the companion cell and the associated sieve element (Gunning & Steer, 1975).

5.1.3 Aims of Chapter

As in Chapter 4, the aim of this chapter was to investigate mitochondrial protein development in wheat primary leaves as a means of examining changing leaf metabolism with increasing cell age. Following the results of Chapter 4 which indicated a heterogeneity of mitochondrial protein development, this chapter aimed to follow on from this and take a more direct and specific approach by examining protein development at the microscopical level, while still using an immunohistochemical

technique with the same specific antibodies. This allowed the relation of protein concentration to mitochondrial area - with the slot blot studies of the previous chapter using crude leaf extracts, this was not possible. Measurements had a stereological basis, and therefore could be related to other measured stereological parameters in the leaf. In addition, this technique allowed the comparison of mitochondrial protein development between mesophyll and vascular cells.

This chapter aimed to build on the data obtained from Chapter 4, and produce a more specific contribution to the current understanding of the control and co-ordination of mitochondrial biogenesis in relation to leaf development.

5.2 Results

5.2.1 Identification of Companion Cells

Companion cells were identified under the TEM by their close proximity to sieve elements (the latter being readily identifiable, e.g. by the minimal cytoplasm and often thickened cell walls), the presence of abundant plasmodesmata between them and sieve elements; dense cytoplasms and prominent nuclei; and the presence of many mitochondria. Care was taken not to confuse companion cells with the less specialised phloem parenchyma, though the latter were generally much larger. Figure 5.1 shows electron micrographs of phloem companion cells, taken from wheat primary leaf tissue sections used in this study. Micrograph A shows part of a vascular bundle, with phloem, xylem and bundle sheath cells. Micrograph B is of a higher magnification, and shows a phloem companion cell with adjacent sieve elements. The minimal cytoplasm in the sieve elements is clear. Micrograph C shows a dense grouping of mitochondria in the cytoplasm of a companion cell. Here, the mitochondrial cristae and double-unit membranes are clearly visible.

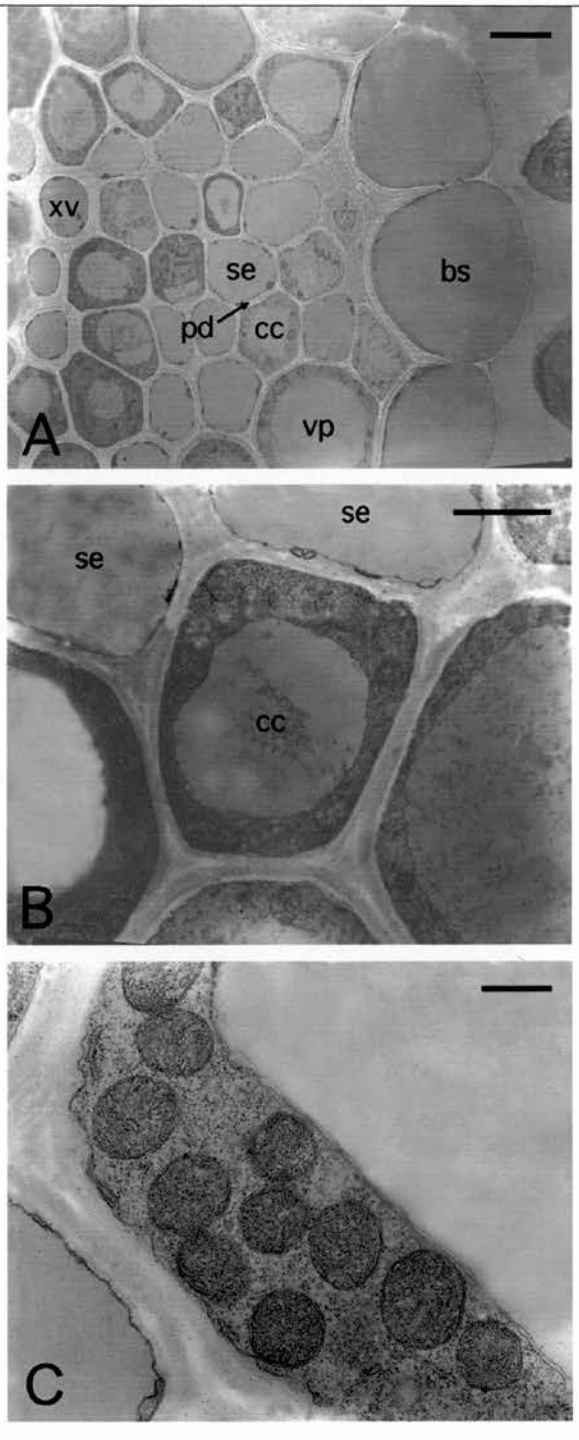

Figure 5.1 Wheat Primary Leaf Phloem Companion Cell Ultrastructure. Electron micrographs of Spurr's resin embedded tissue from a 7d-old leaf, transversely sectioned. A: vascular bundle showing bundle sheath cells (bs), companion cells (cc), plasmodesmata (pd), sieve elements (se), vascular parenchyma (vp) and xylem vessels (xv), taken at a magnification of ×1820 (bar represents 5μm). B: phloem companion cell (cc) in the centre with adjacent sieve elements (se), taken at ×7450 (bar represents 2 μm). C: mitochondria within companion cell cytoplasm, taken at ×21200 (bar represents 0.5 μm).

5.2.2 Determination of Optimum Antibody Dilutions for Immunogold Labelling of Wheat Primary Leaf Tissue

Before conducting immunogold labelling procedures, initial experiments were carried out to determine the optimum primary and secondary antibody dilutions required for efficient localisation of each mitochondrial protein under investigation. Tissue sections were incubated in a range of primary antibody dilutions from 1:10 to 1:5000 to determine which dilution produced an optimum level of immunogold labelling following image analysis of the sections. Based on this result, a narrower range of primary antibody dilutions was tested in the same way, and the optimum dilutions observed here were used in immunogold labelling experiments. Following this, and using the previously obtained optimum primary antibody dilutions, similar experiments were conducted to determine the optimum secondary antibody dilution for localisation of each mitochondrial protein. The details of this are given in Section 2.12.1, and the final antibody dilutions used are listed in Table 2.2.

Figures 5.2 to 5.7 show the results of these initial labelling density experiments, and compare the density of gold labelling on different cellular compartments: the cytosol, the cell wall, chloroplasts, mitochondria and the vacuole. In all cases, optimum antibody dilutions describe those which produced a density of mitochondrial gold labelling that was significantly higher than background labelling on other cellular compartments. Where more than one dilution produced this, the dilution which produced the highest density of mitochondrial labelling was preferred.

Figure 5.2 for example, shows the results of experiments to determine the optimum primary and secondary antibody dilutions for immunogold localisation of mitochondrial PDC E1α on leaf tissue sections. It can be seen on Figure 5.2A that a primary antibody dilution of 1:10 provided the greatest level of labelling, but more importantly, that the mitochondrial labelling was significantly higher than that on other cellular compartments. Further testing (Figure 5.2B) concluded that a primary antibody dilution of 1:5 was even more useful as it produced a greater density of mitochondrial labelling, while still maintaining a significantly higher labelling density than that of other cellular compartments. Figure 5.2 also shows the results of experiments to determine the optimum secondary antibody dilutions for this protein. Initially, a dilution of 1:10 was optimum in producing a high level of mitochondrial labelling that was significantly different from that of other cellular compartments (Figure 5.2C), and further testing with a narrower range of dilutions confirmed this (Figure 5.2D).

This approach was taken in all cases to determine optimum primary and secondary antibody dilutions, and the results for PDC E1β, PDC E2, PDC E3, GDC P-protein and GDC L-protein are showed in Figures 5.3 to 5.7 respectively, where the optimum dilutions are indicated in each case.

Figure 5.8 shows electron micrographs of leaf tissue which was labelled with immunogold for localisation of PDC E1β. With high levels of background labelling produced by using an excessively high primary antibody concentration, virtually every part of the cell is labelled (Figure 5.8A). Cell walls can be particularly prone to non-specific labelling, and this is evident on the micrograph. With optimum primary and secondary antibody dilutions on the other hand (Figure 5.8B), a low level of background labelling is still present, but not to the extent as to obscure any differences in mitochondrial labelling between different tissue samples.

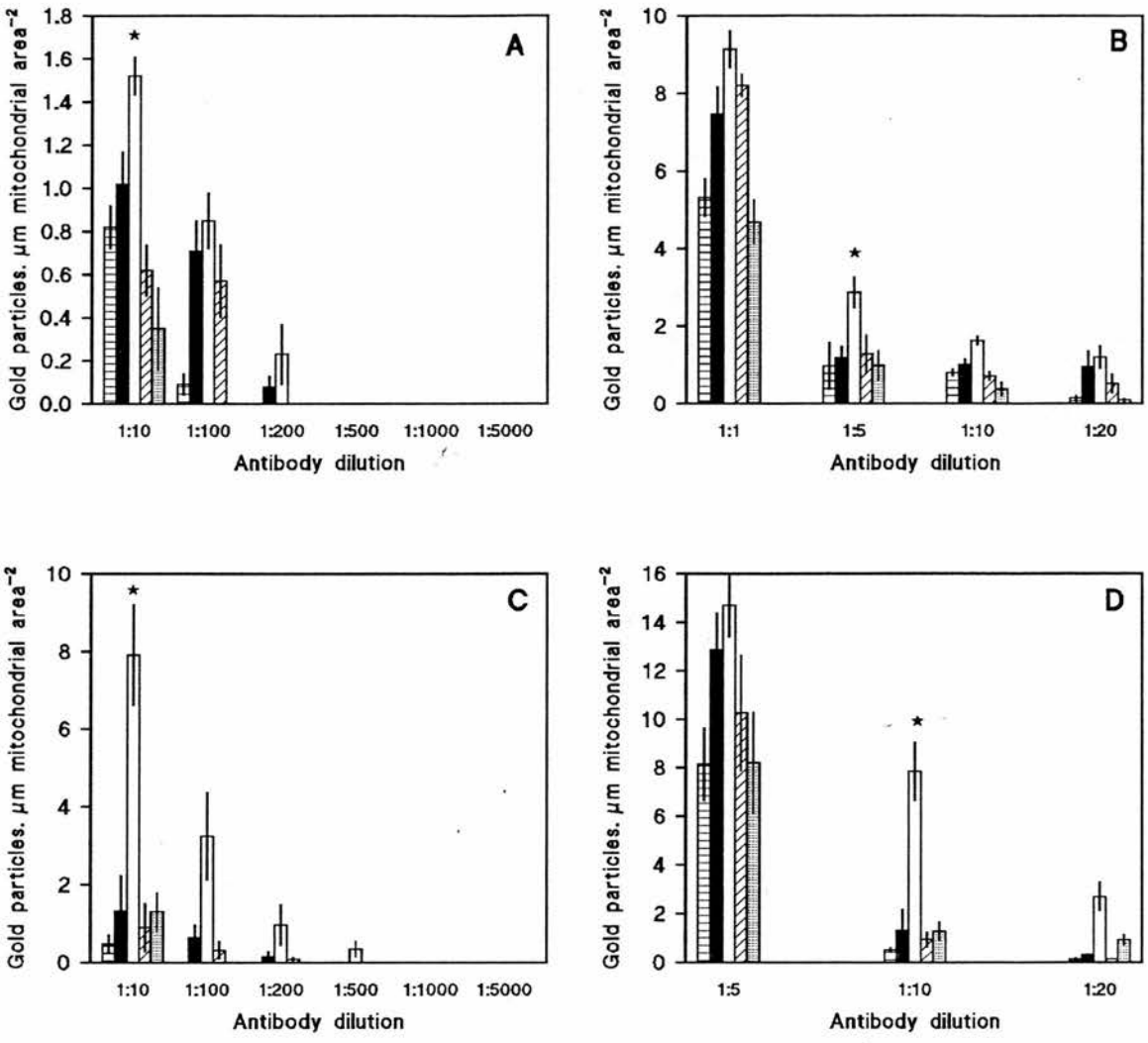

Figure 5.2 Determination of Optimum Primary and Secondary Antibody Dilutions for Immunogold Labelling of the Wheat Primary Leaf Mitochondrial PDC E1α Subunit. See Section 5.2.2. Values represent the mean of three replicates, each from a different batch of plants ± standard errors. Tissue sections were incubated in a range of primary antibody dilutions from 1:10 to 1:5000 to determine which produced the optimum level of gold labelling (A). Based on this, further testing was carried out using a narrower range of dilutions (B), to determine the dilution for use in immunogold experiments. Optimum secondary antibody dilution was determined similarly (C and D). The optimum antibody dilution in each case, is indicated by ★. Cytoplasm ▤, cell wall ■, mitochondria □, chloroplasts ▨, vacuole ▩.

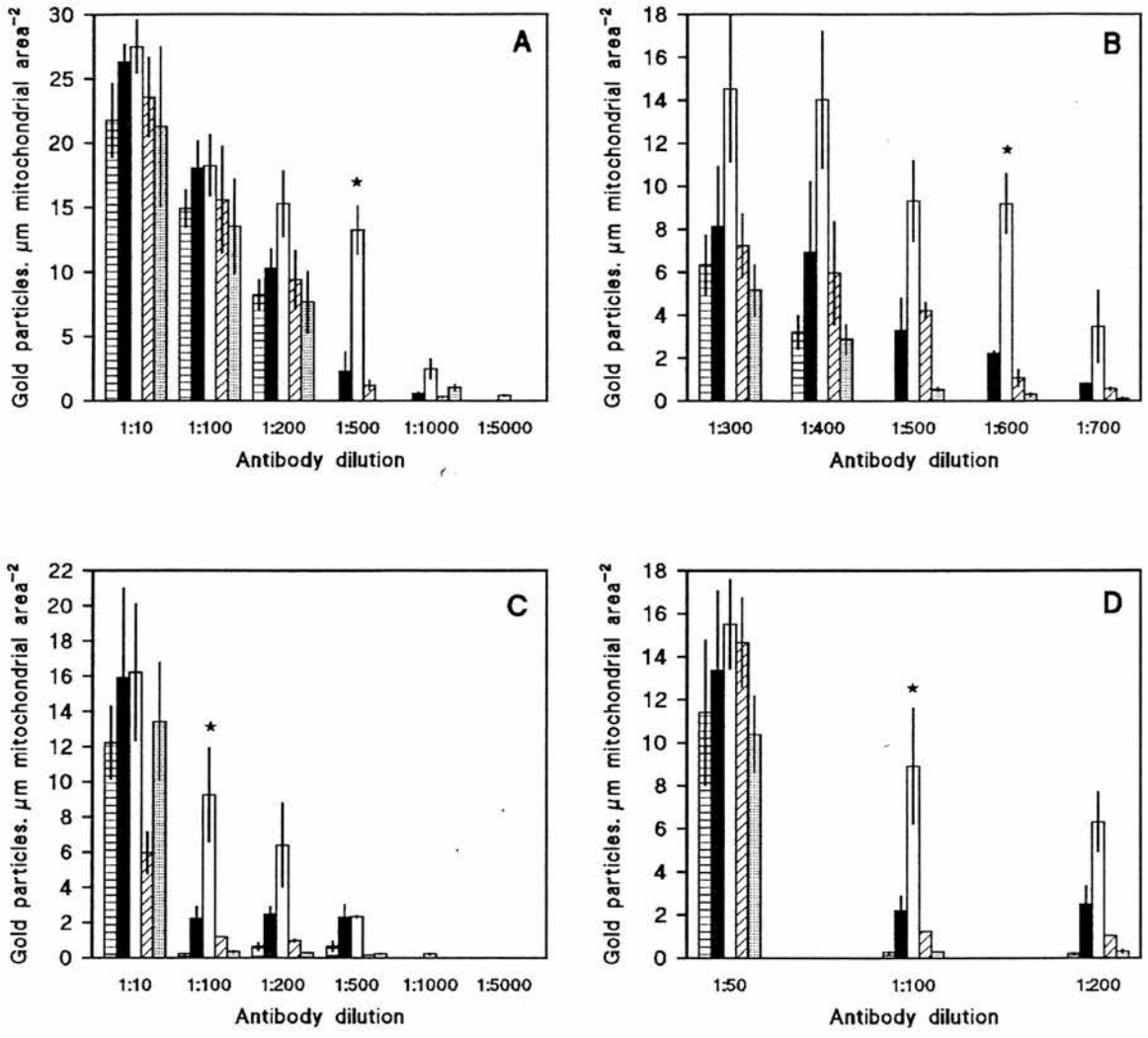

Figure 5.3 Determination of Optimum Primary and Secondary Antibody Dilutions for Immunogold Labelling of the Wheat Primary Leaf Mitochondrial PDC E1β Subunit. See Section 5.2.2. Values represent the mean of three replicates, each from a different batch of plants ± standard errors. See Figure 5.2 for method of dilution determination. The optimum antibody dilution in each case, is indicated by ⋆. Cytoplasm ▤, cell wall ■, mitochondria □, chloroplasts ▨, vacuole ▩.

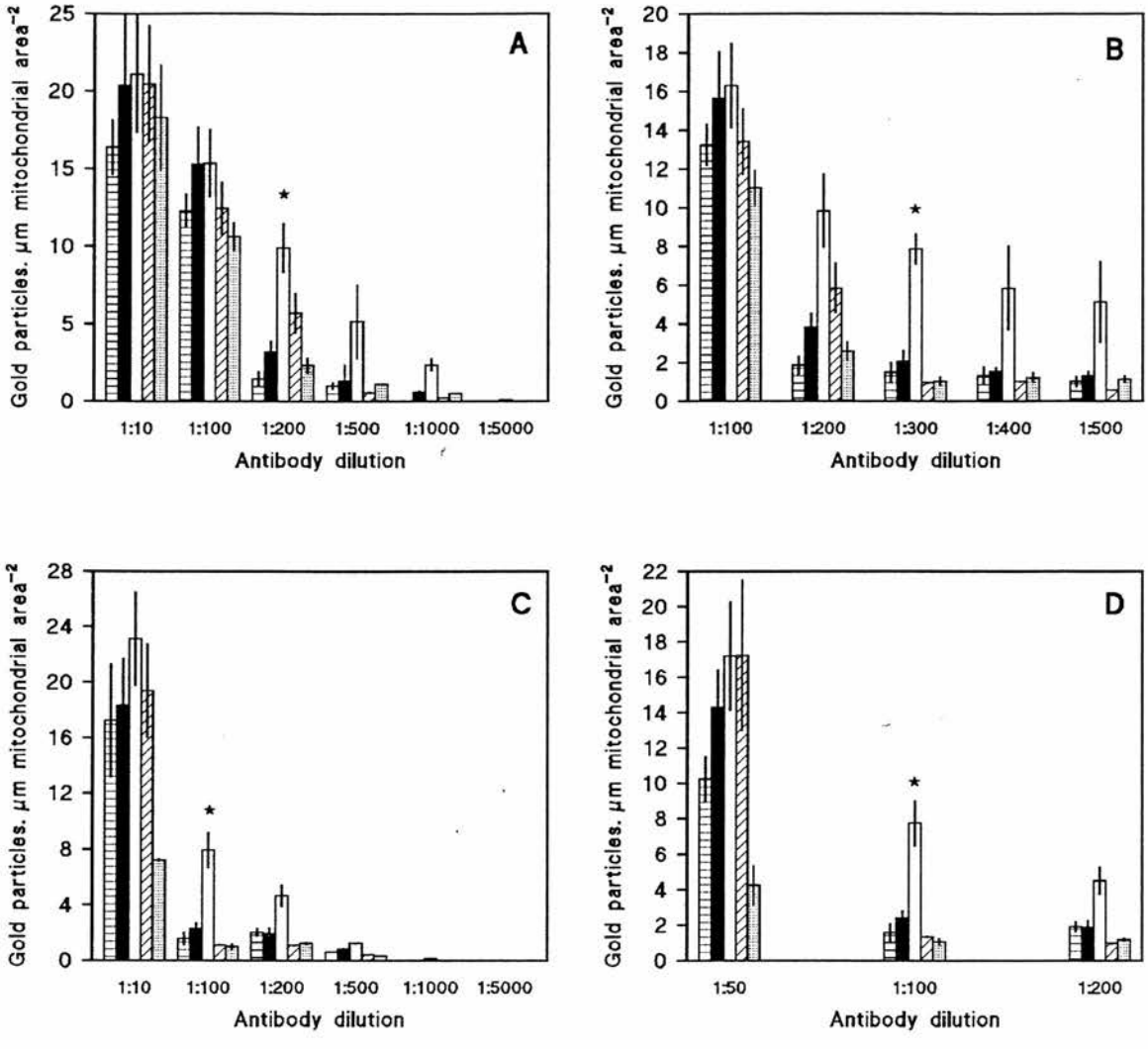

Figure 5.4 Determination of Optimum Primary and Secondary Antibody Dilutions for Immunogold Labelling of the Wheat Primary Leaf Mitochondrial PDC E2 Subunit. See Section 5.2.2. Values represent the mean of three replicates, each from a different batch of plants ± standard errors. See Figure 5.2 for method of dilution determination. The optimum antibody dilution in each case, is indicated by ⋆. Cytoplasm ▤, cell wall ■, mitochondria □, chloroplasts ▨, vacuole ▩.

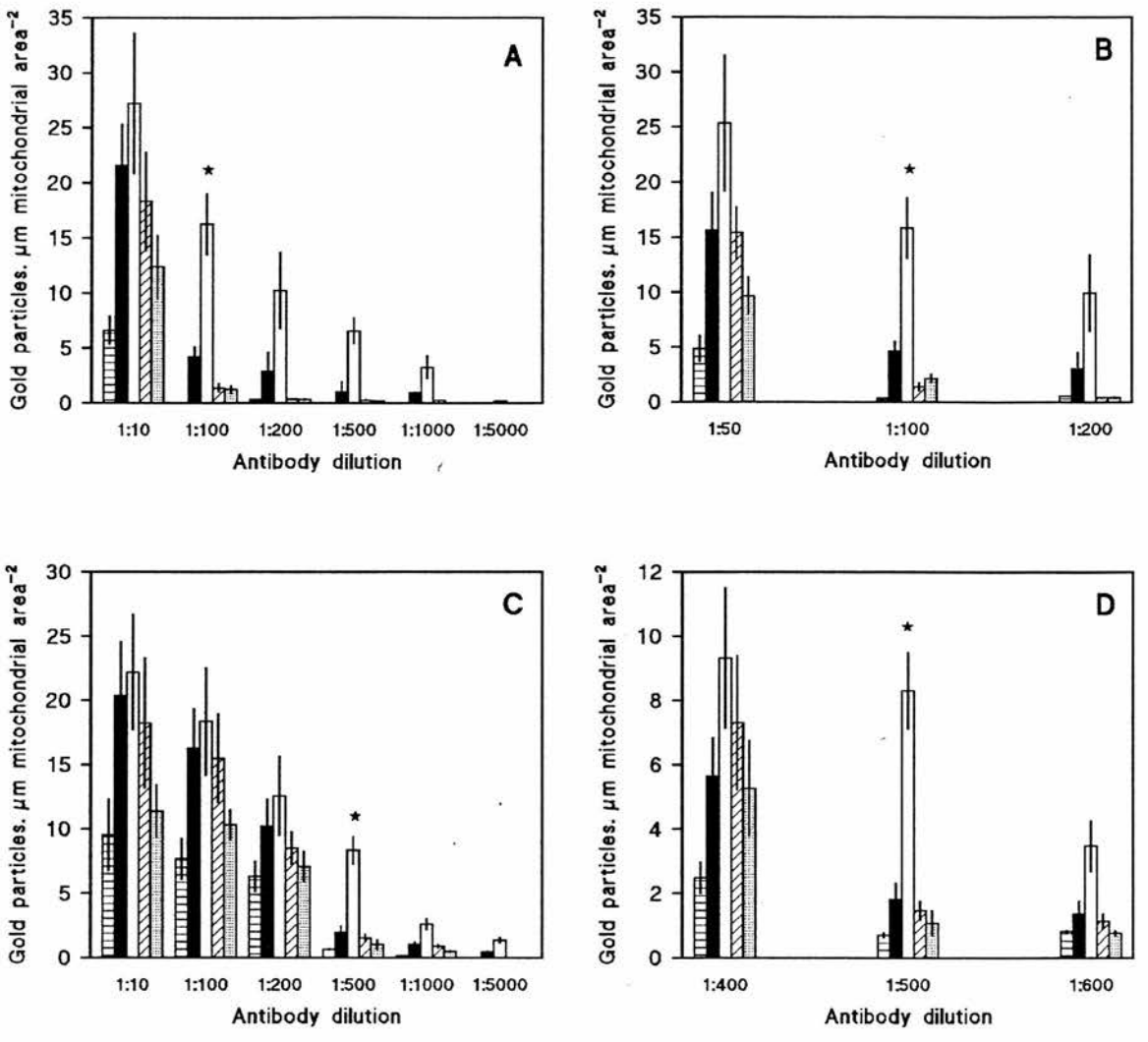

Figure 5.5 Determination of Optimum Primary and Secondary Antibody Dilutions for Immunogold Labelling of the Wheat Primary Leaf Mitochondrial PDC E3 Subunit. See Section 5.2.2. Values represent the mean of three replicates, each from a different batch of plants ± standard errors. See Figure 5.2 for method of dilution determination. The optimum antibody dilution in each case, is indicated by ⋆. Cytoplasm ▤, cell wall ■, mitochondria □, chloroplasts ▨, vacuole ▩.

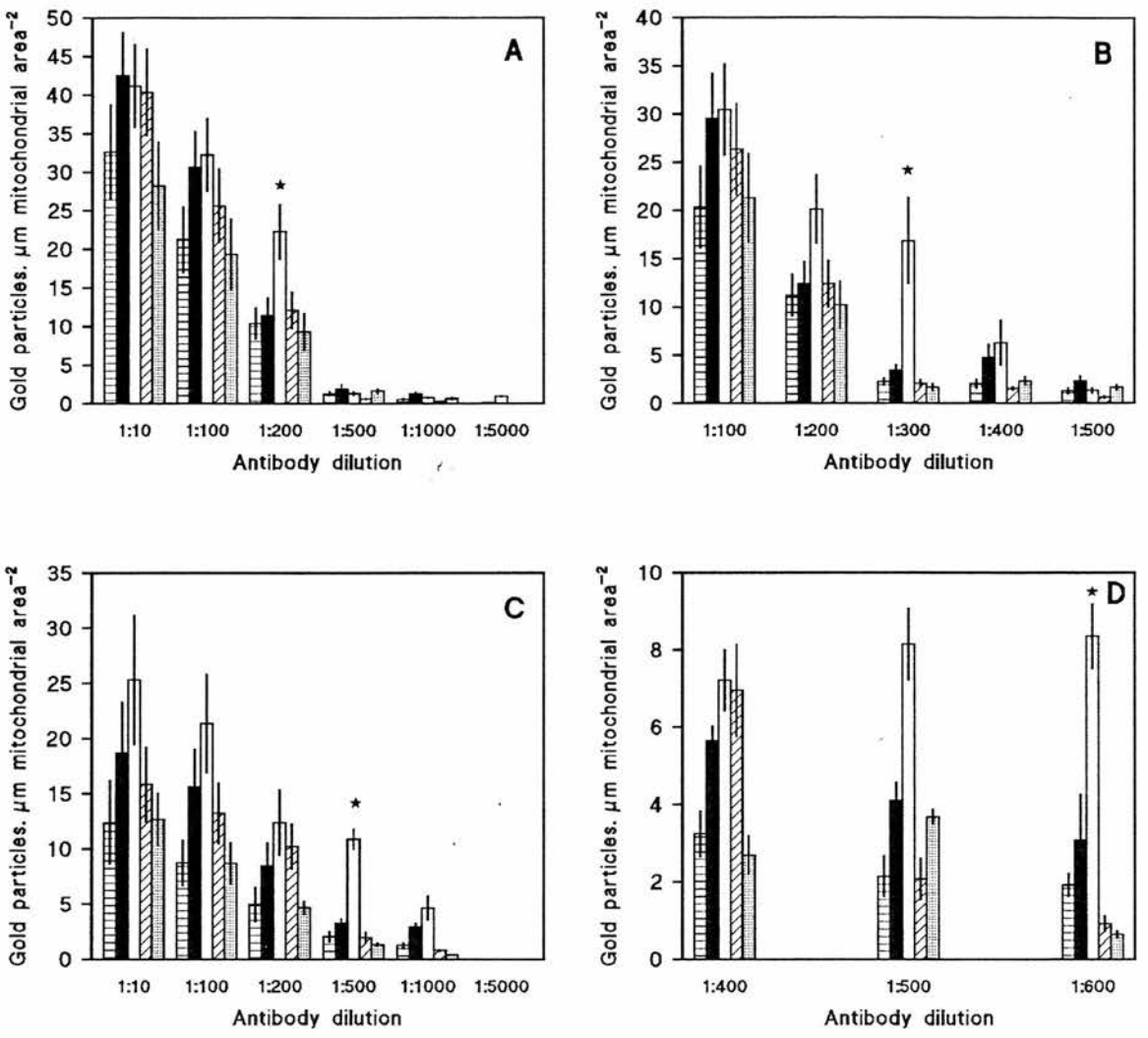

Figure 5.6 Determination of Optimum Primary and Secondary Antibody Dilutions for Immunogold Labelling of the Wheat Primary Leaf Mitochondrial GDC P-protein. See Section 5.2.2. Values represent the mean of three replicates, each from a different batch of plants ± standard errors. See Figure 5.2 for method of dilution determination. The optimum antibody dilution in each case, is indicated by ⋆. Cytoplasm ▤, cell wall ■, mitochondria □, chloroplasts ▨, vacuole ▩.

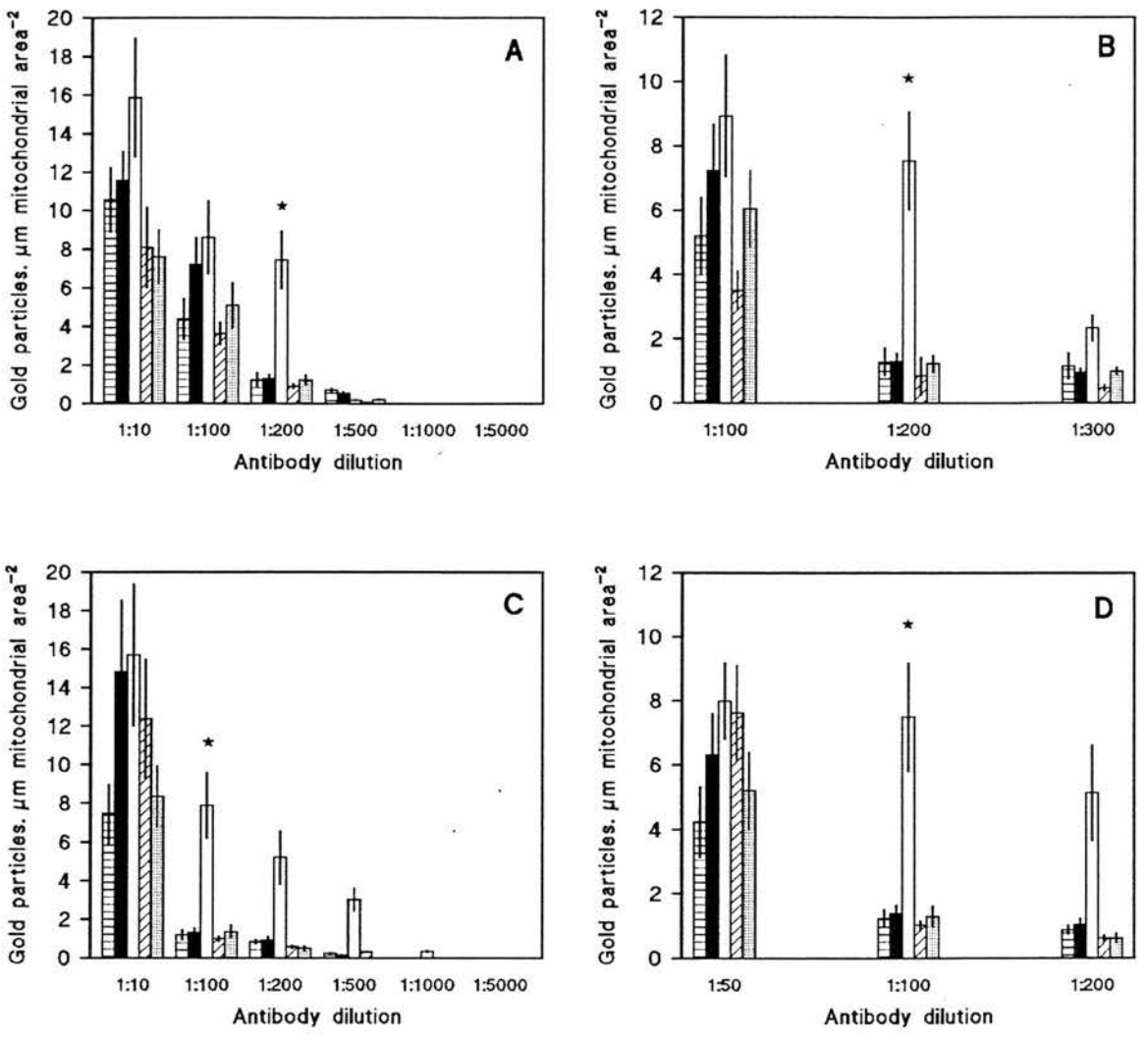

Figure 5.7 Determination of Optimum Primary and Secondary Antibody Dilutions for Immunogold Labelling of the Wheat Primary Leaf Mitochondrial GDC L-protein. See Section 5.2.2. Values represent the mean of three replicates, each from a different batch of plants ± standard errors. See Figure 5.2 for method of dilution determination.The optimum antibody dilution in each case, is indicated by ⋆. Cytoplasm ▤, cell wall ■, mitochondria □, chloroplasts ▨, vacuole ▩.

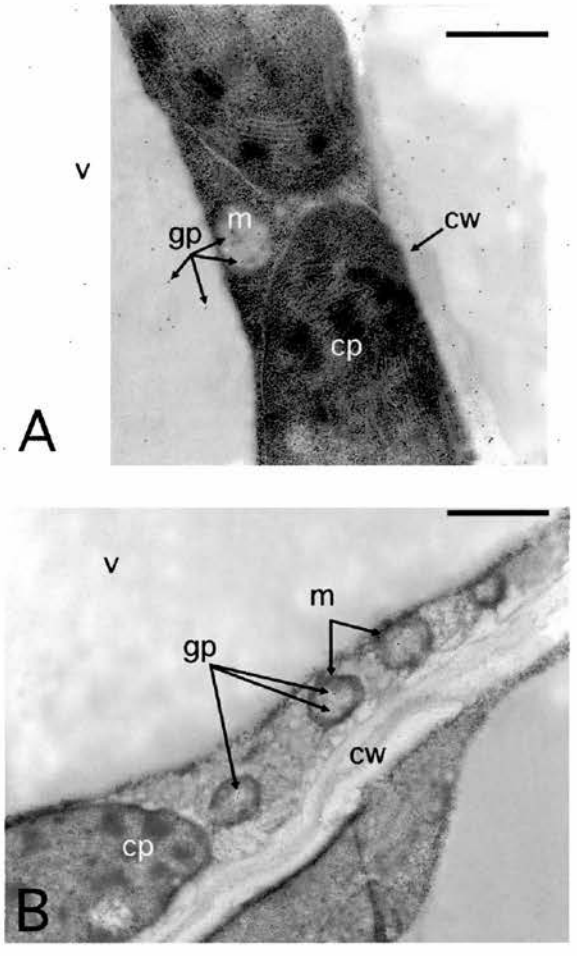

Figure 5.8 Achieving Optimum Immunogold Labelling Density on Wheat Leaf Tissue Sections. Electron micrographs of L.R. White resin embedded tissue from a 7d-old leaf, transversely sectioned. Sections were treated for immunogold localisation of PDC E1β (magnification × 15650, bar represents 1μm). A: high levels of background labelling produced by using a very high primary antibody concentration. B: optimum level of labelling, produced by using optimum primary and secondary antibody dilutions. Gold particles (gp), chloroplasts (cp), cell wall (cw), mitochondria (m), vacuole (v).

5.2.3 Immunogold Localisation of Mitochondrial Proteins in Wheat Primary Leaf Mesophyll Tissue

Figures 5.9 to 5.14 show the localisation of mitochondrial proteins via immunogold labelling of wheat leaf mesophyll cells. The graphs show any changes in labelling density with increasing distance from the basal meristem, representing changes in mitochondrial protein presence with increasing cell age. Data are presented as the number of gold particles present per μm^2 mitochondrial area, and the corresponding cell age to distance from the leaf base is also shown.

Figure 5.9 shows the immunogold localisation of PDC E1α. Intensity of labelling of this subunit significantly increased ($p \leq 0.05$) between the leaf base and 16mm from the basal meristem, then plateaued between this point and 51mm from the basal meristem. Labelling density then significantly decreased ($p \leq 0.05$) between this point and the leaf tip, reaching a level similar to that observed at the leaf base.

Presence of the PDC E1β subunit along the leaf is shown in Figure 5.10. Labelling density of the enzyme remained fairly constant along the whole length of the leaf with a slight - but not significant - peak in immunogold labelling density at approximately 8mm from the basal meristem.

Figure 5.11 shows the immunogold localisation of PDC E2. The graph shows a virtually linear significant increase ($p \leq 0.05$) between the leaf base and tip.

Mitochondrial immunolabelling of the PDC E3 subunit significantly increased ($p \leq 0.05$) between the leaf base and 16mm from the basal meristem, then remained constant between this point and the leaf tip (Figure 5.12).

Figure 5.13 shows the immunogold localisation of GDC P-protein. Labelling density of this subunit significantly decreased ($p \leq 0.05$) between the leaf base and 8mm from the basal meristem. From this point, labelling intensity of the enzyme significantly increased ($p \leq 0.05$) in a virtually linear trend towards the leaf tip.

Figure 5.14 shows the immunogold localisation of GDC L-protein. Immunolabelling of this enzyme significantly increased ($p \leq 0.05$) between the leaf base and 16mm from the basal meristem. From this point, labelling density of significantly increased ($p \leq 0.05$) towards the leaf tip, reaching a maximum at 81mm from the basal meristem.

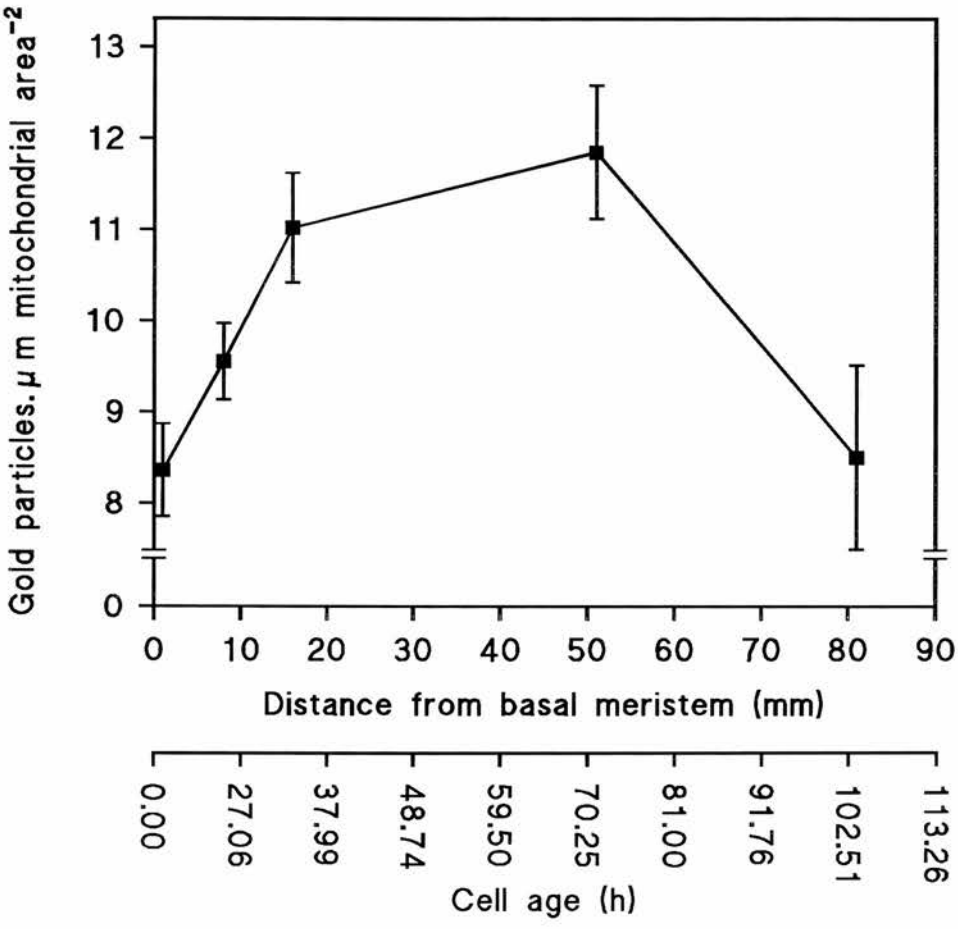

Figure 5.9 Immunogold Localisation of the PDC E1α Subunit in Mesophyll Cell Mitochondria, along 7d-old Wheat Primary Leaves. See Section 5.2.3. Values represent the mean of four replicates, each from a different batch of plants ± standard errors. Tissue was analysed from 1mm transverse sections taken at five different developmental stages along the leaf: 0-1mm, 7-8mm, 15-16mm, 50-51mm, and 80-81mm from the basal meristem. Values are averages for each particular leaf segment under examination, e.g. the value plotted at 1mm represents the leaf segment 0-1mm from the basal meristem. The cell age corresponding to distance from the basal meristem is also shown (see Section 2.5.3).

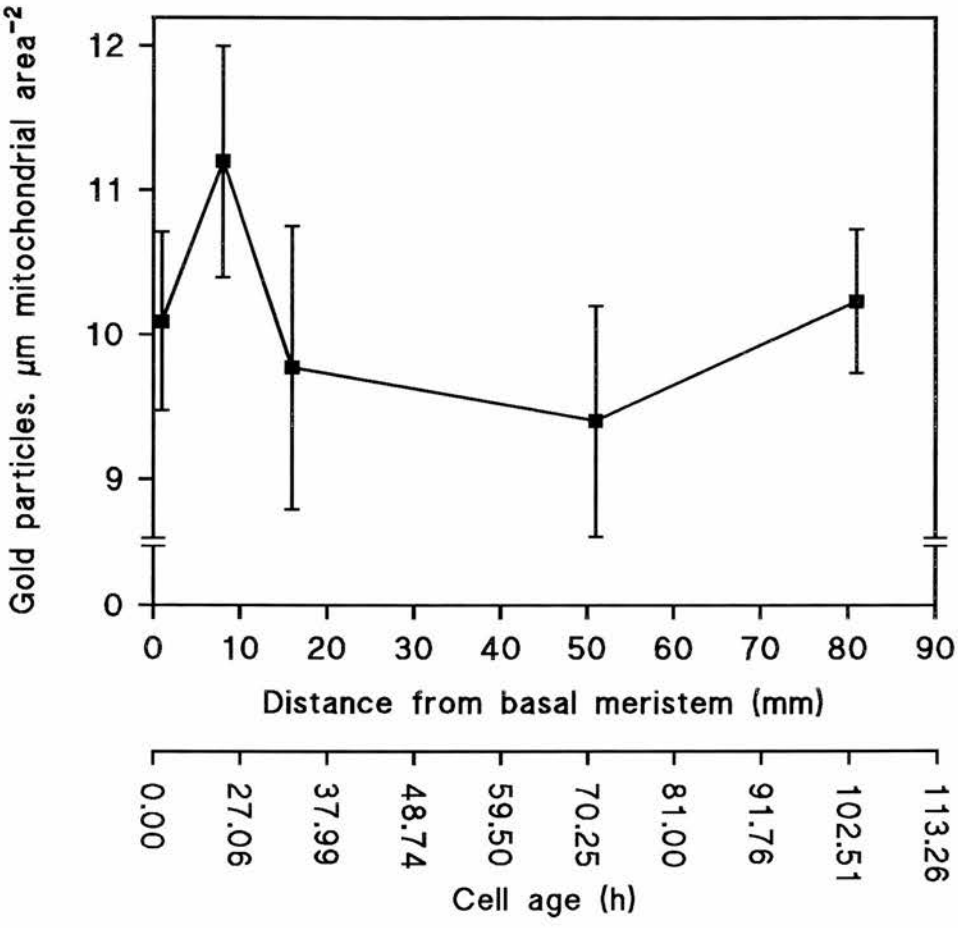

Figure 5.10 Immunogold Localisation of the PDC E1β Subunit in Mesophyll Cell Mitochondria, along 7d-old Wheat Primary Leaves. See Section 5.2.3. Values represent the mean of four replicates, each from a different batch of plants ± standard errors. See Figure 5.9 for details of leaf section sampling. The cell age corresponding to distance from the basal meristem is also shown (see Section 2.5.3).

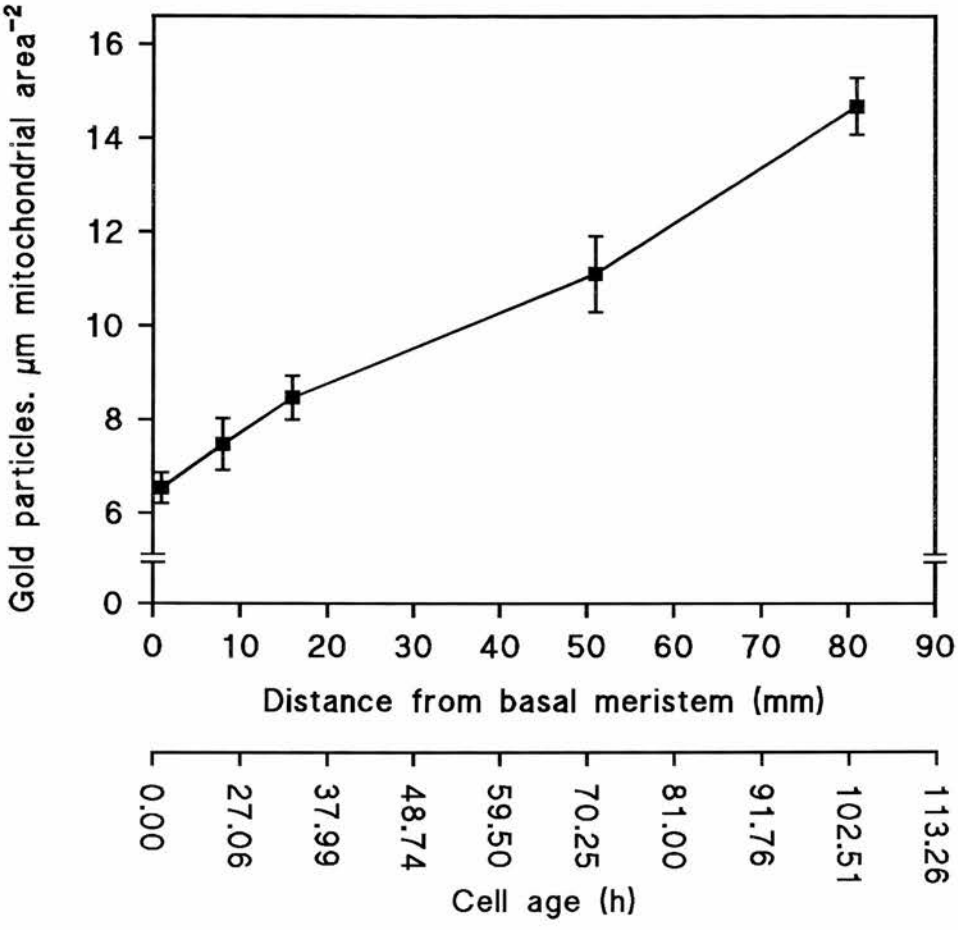

Figure 5.11 Immunogold Localisation of the PDC E2 Subunit in Mesophyll Cell Mitochondria, along 7d-old Wheat Primary Leaves. See Section 5.2.3. Values represent the mean of four replicates, each from a different batch of plants ± standard errors. See Figure 5.9 for details of leaf section sampling. The cell age corresponding to distance from the basal meristem is also shown (see Section 2.5.3).

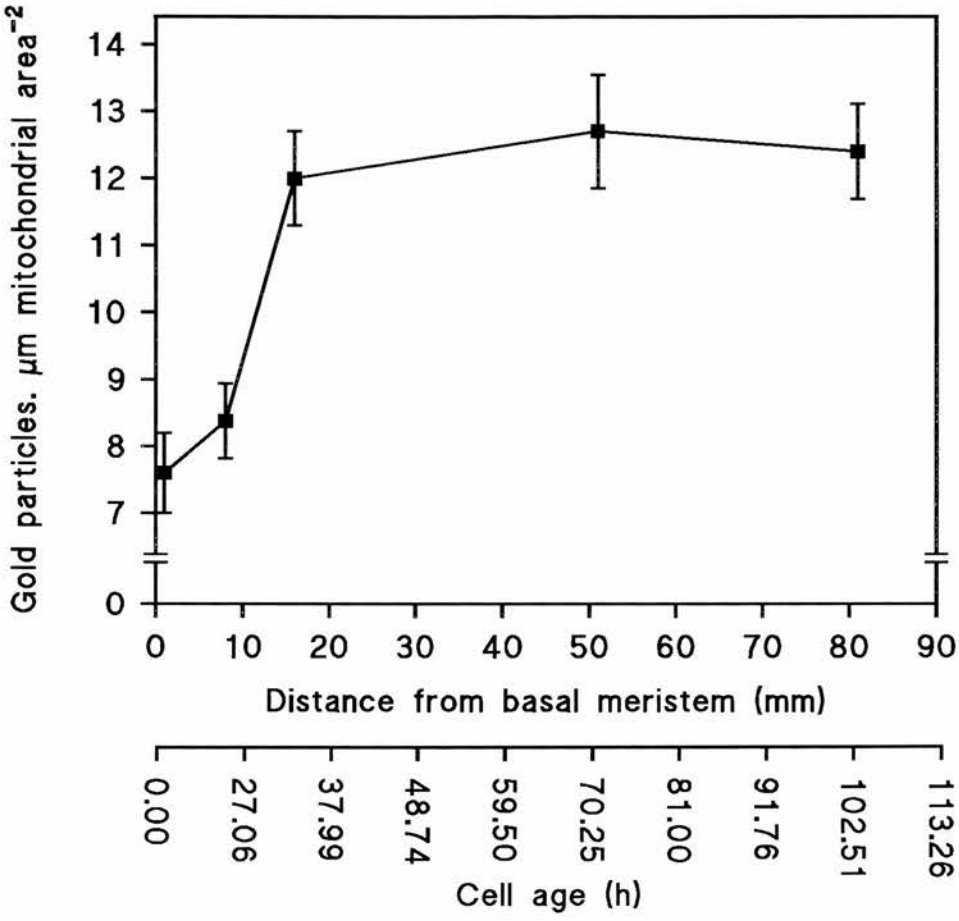

Figure 5.12 Immunogold Localisation of the PDC E3 Subunit in Mesophyll Cell Mitochondria, along 7d-old Wheat Primary Leaves. See Section 5.2.3. Values represent the mean of four replicates, each from a different batch of plants ± standard errors. See Figure 5.9 for details of leaf section sampling. The cell age corresponding to distance from the basal meristem is also shown (see Section 2.5.3).

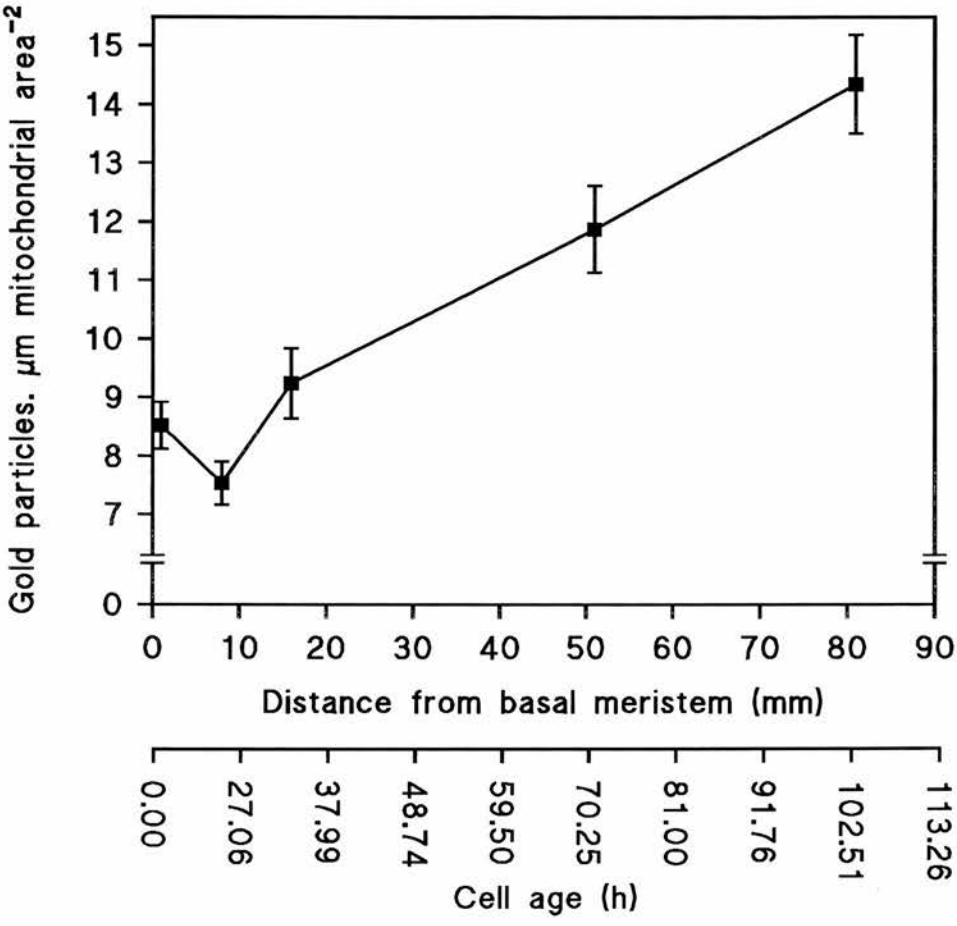

Figure 5.13 Immunogold Localisation of the GDC P-protein Subunit in Mesophyll Cell Mitochondria, along 7d-old Wheat Primary Leaves. See Section 5.2.3. Values represent the mean of four replicates, each from a different batch of plants ± standard errors. See Figure 5.9 for details of leaf section sampling. The cell age corresponding to distance from the basal meristem is also shown (see Section 2.5.3).

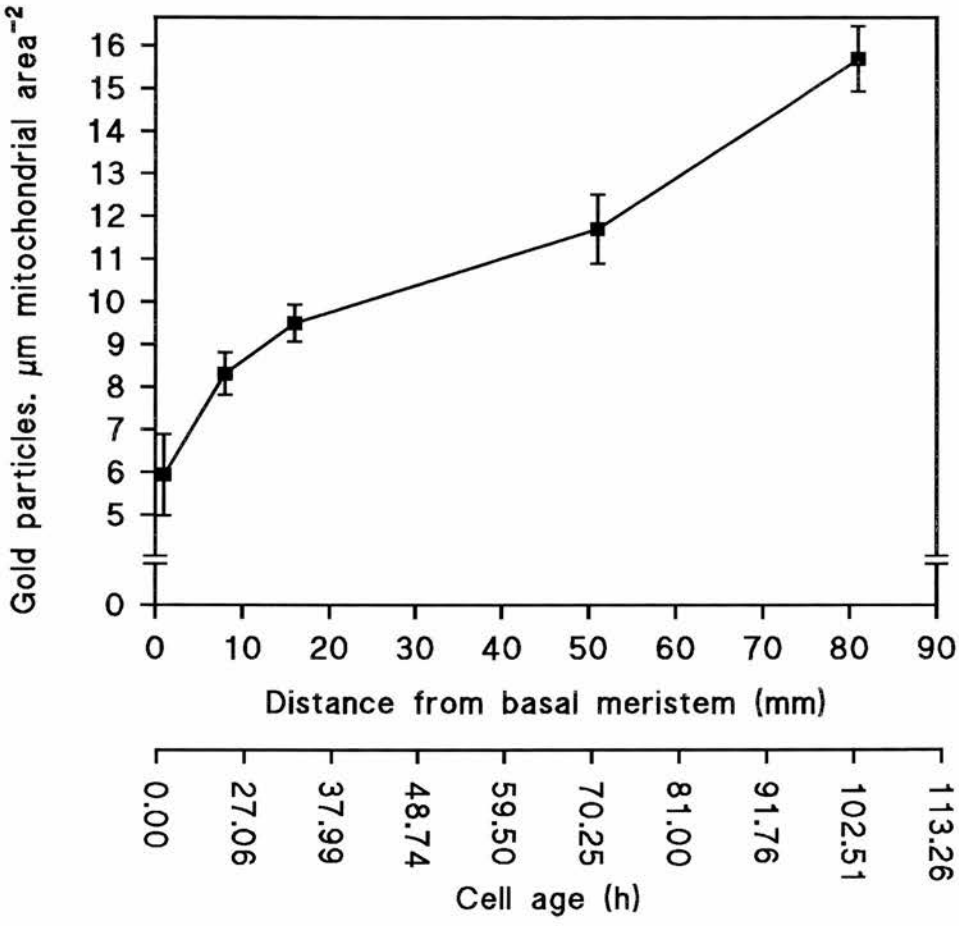

Figure 5.14 Immunogold Localisation of the GDC L-protein Subunit in Mesophyll Cell Mitochondria, along 7d-old Wheat Primary Leaves. See Section 5.2.3. Values represent the mean of four replicates, each from a different batch of plants ± standard errors. See Figure 5.9 for details of leaf section sampling. The cell age corresponding to distance from the basal meristem is also shown (see Section 2.5.3).

5.2.4 Immunogold Localisation of Mitochondrial Proteins in Wheat Primary Leaf Vascular Tissue

Figures 5.15 to 5.20 show the localisation of mitochondrial proteins via immunogold labelling of wheat leaf phloem companion cells. The graphs show the changes in labelling density with increasing distance from the basal meristem, equating to the changes in protein presence with increasing cell age. Data are presented as the number of gold particles present per μm^2 mitochondrial area, and the corresponding cell age to distance from the leaf base is also shown.

Figure 5.15 shows the immunogold localisation of PDC E1α. The labelling intensity for this enzyme significantly increased ($p \leq 0.05$) between the leaf base and 51mm from the basal meristem. Labelling density then significantly decreased ($p \leq 0.05$) between this point and the leaf tip, reaching a level similar to that observed at the leaf base.

The labelling of PDC E1β remained constant along the whole length of the leaf, as indicated by the similar density of immunogold labelling observed between the leaf base and tip (Figure 5.16).

Figure 5.17 shows the immunogold localisation of PDC E2. Presence of this enzyme significantly increased ($p \leq 0.05$) between the leaf base and 16mm from the basal meristem, then remained constant between this point and the leaf tip.

A significant linear decrease ($p \leq 0.05$) in labelling density of PDC E3 was observed between the leaf base and tip (Figure 5.18).

Figure 5.19 shows the immunogold localisation of GDC P-protein. Labelling of this enzyme remained fairly constant within the elongation zone, then was observed to significantly decrease ($p \leq 0.05$) linearly between approximately 80mm from the basal meristem, and the leaf tip.

The change in immunogold labelling density of GDC L-protein with increasing distance from the basal meristem is shown in Figure 5.20. Labelling density remained constant within the elongation zone, then significantly decreased ($p \leq 0.05$) in a virtually linear trend between approximately 80mm from the basal meristem, and the leaf tip.

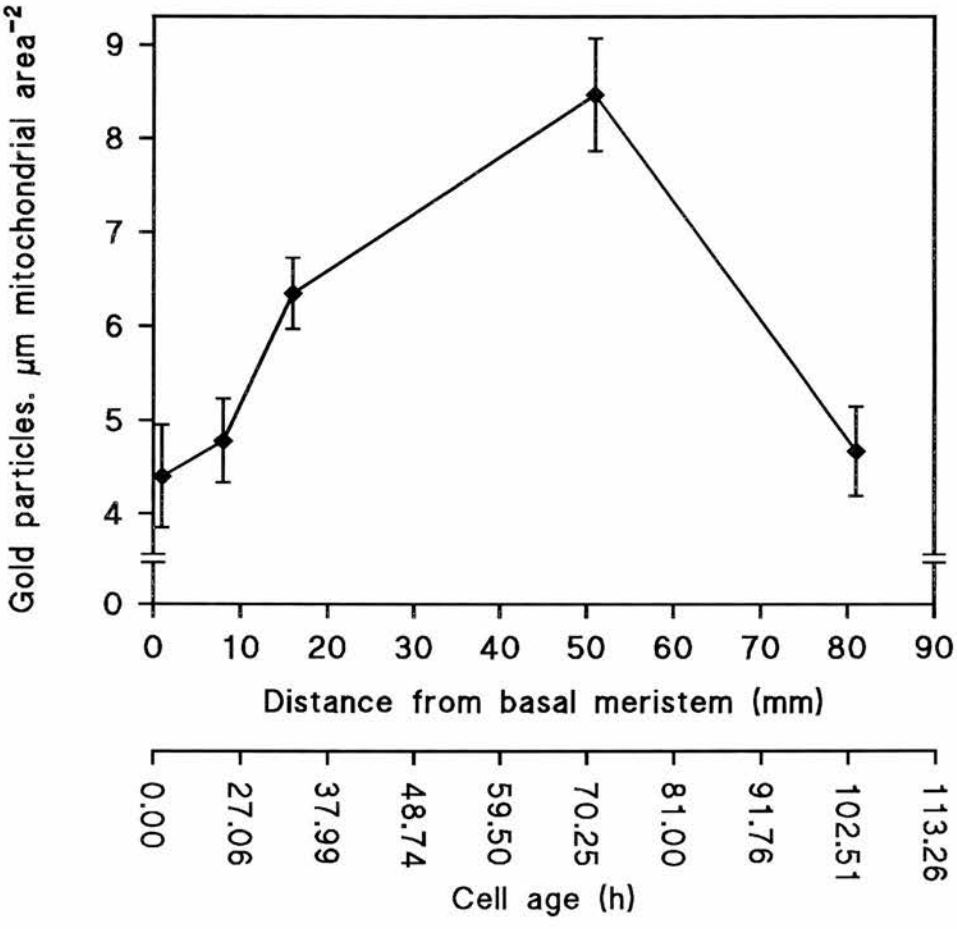

Figure 5.15 Immunogold Localisation of the PDC E1α Subunit in Companion Cell Mitochondria, along 7d-old Wheat Primary Leaves. See Section 5.2.4. Values represent the mean of four replicates, each from a different batch of plants ± standard errors. See Figure 5.9 for details of leaf section sampling. The cell age corresponding to distance from the basal meristem is also shown (see Section 2.5.3).

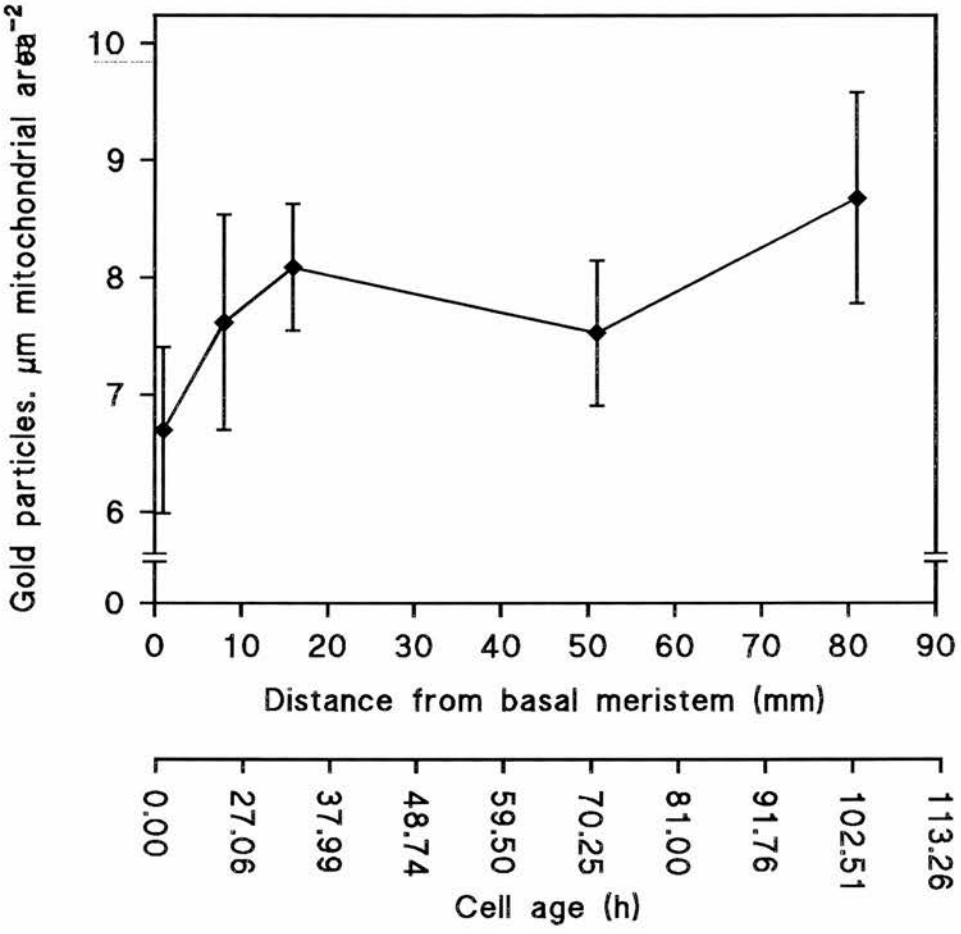

Figure 5.16 Immunogold Localisation of the PDC E1β Subunit in Companion Cell Mitochondria, along 7d-old Wheat Primary Leaves. See Section 5.2.4. Values represent the mean of four replicates, each from a different batch of plants ± standard errors. See Figure 5.9 for details of leaf section sampling. The cell age corresponding to distance from the basal meristem is also shown (see Section 2.5.3).

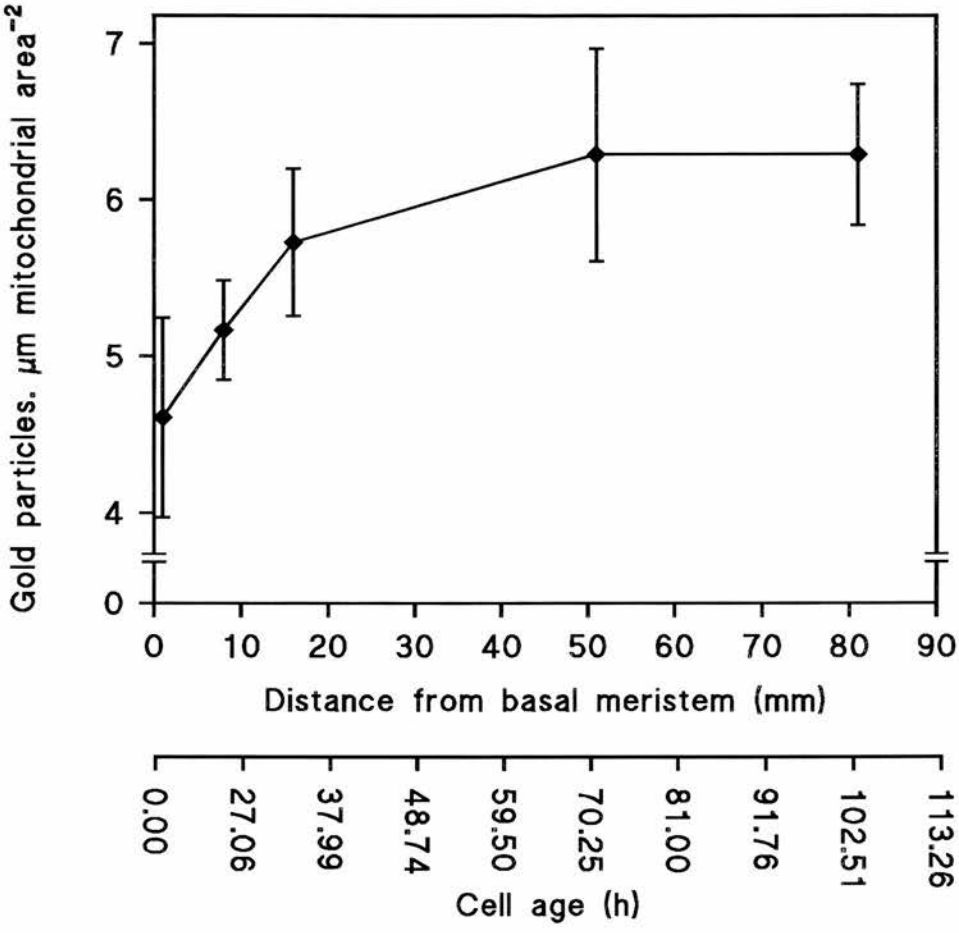

Figure 5.17 Immunogold Localisation of the PDC E2 Subunit in Companion Cell Mitochondria, along 7d-old Wheat Primary Leaves. See Section 5.2.4. Values represent the mean of four replicates, each from a different batch of plants ± standard errors. See Figure 5.9 for details of leaf section sampling. The cell age corresponding to distance from the basal meristem is also shown (see Section 2.5.3).

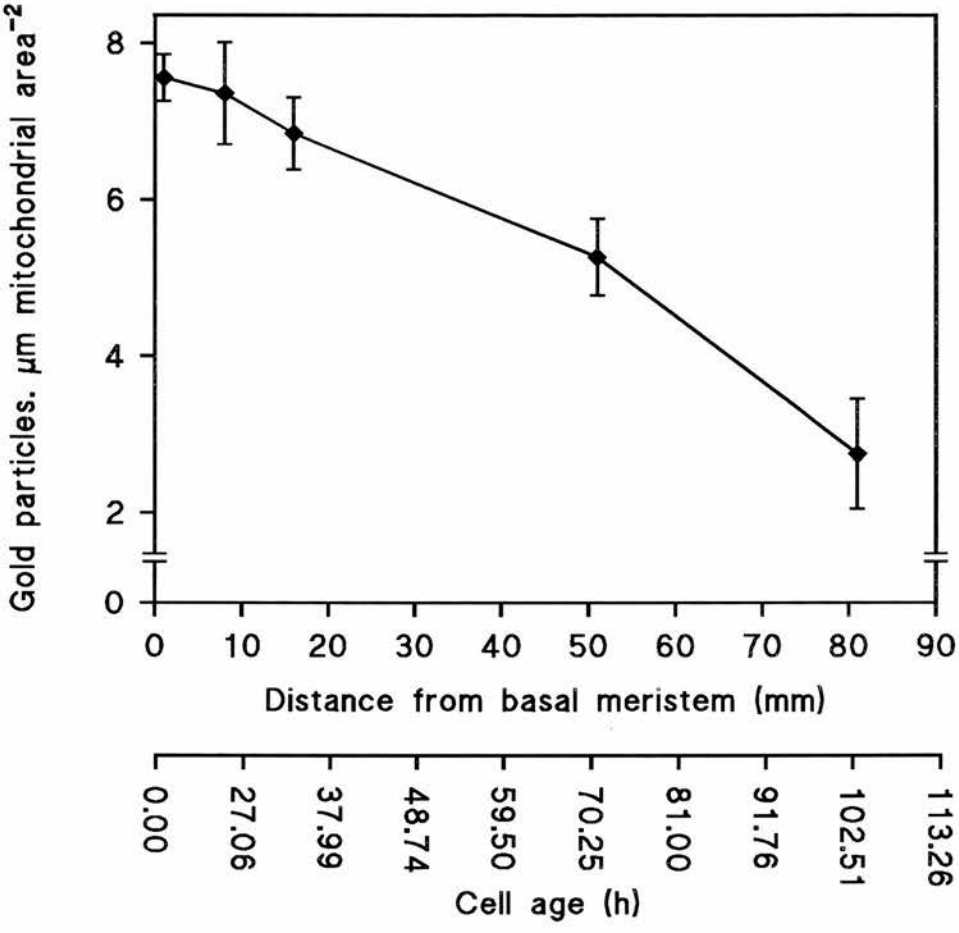

Figure 5.18 Immunogold Localisation of the PDC E3 Subunit in Companion Cell Mitochondria, along 7d-old Wheat Primary Leaves. See Section 5.2.4. Values represent the mean of four replicates, each from a different batch of plants ± standard errors. See Figure 5.9 for details of leaf section sampling. The cell age corresponding to distance from the basal meristem is also shown (see Section 2.5.3).

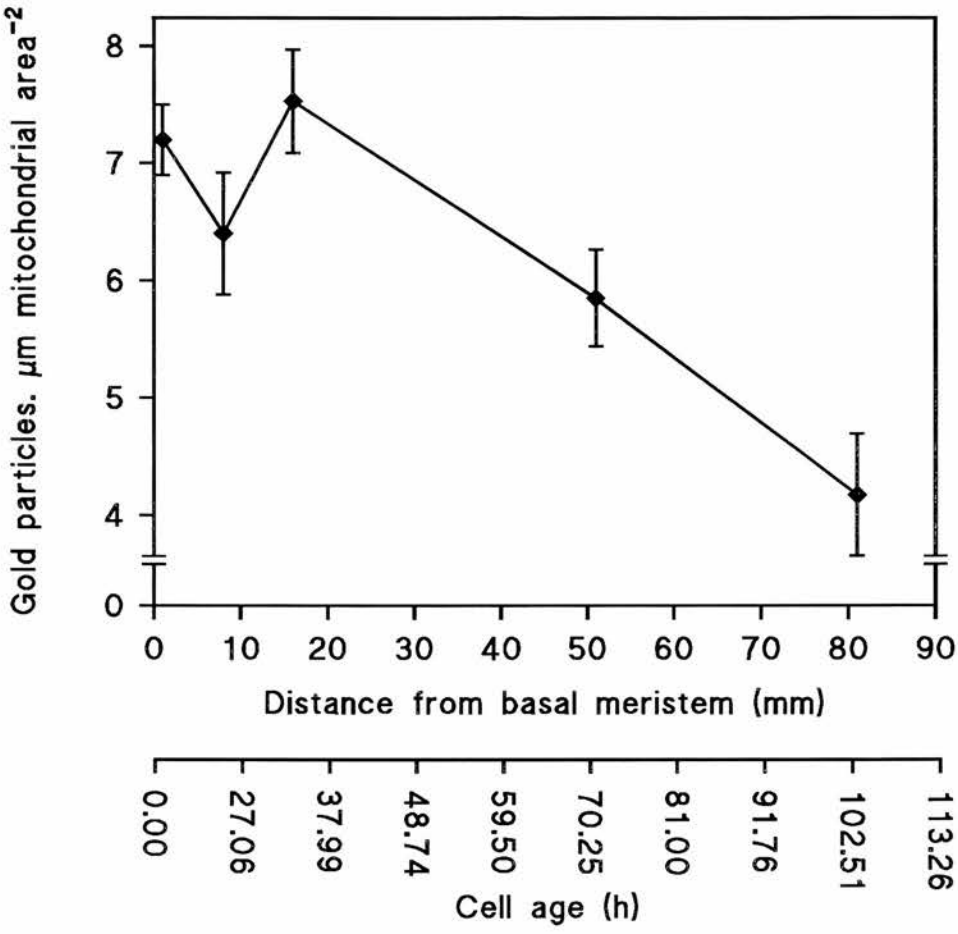

Figure 5.19 Immunogold Localisation of the GDC P-protein Subunit in Companion Cell Mitochondria, along 7d-old Wheat Primary Leaves. See Section 5.2.4. Values represent the mean of four replicates, each from a different batch of plants ± standard errors. See Figure 5.9 for details of leaf section sampling. The cell age corresponding to distance from the basal meristem is also shown (see Section 2.5.3).

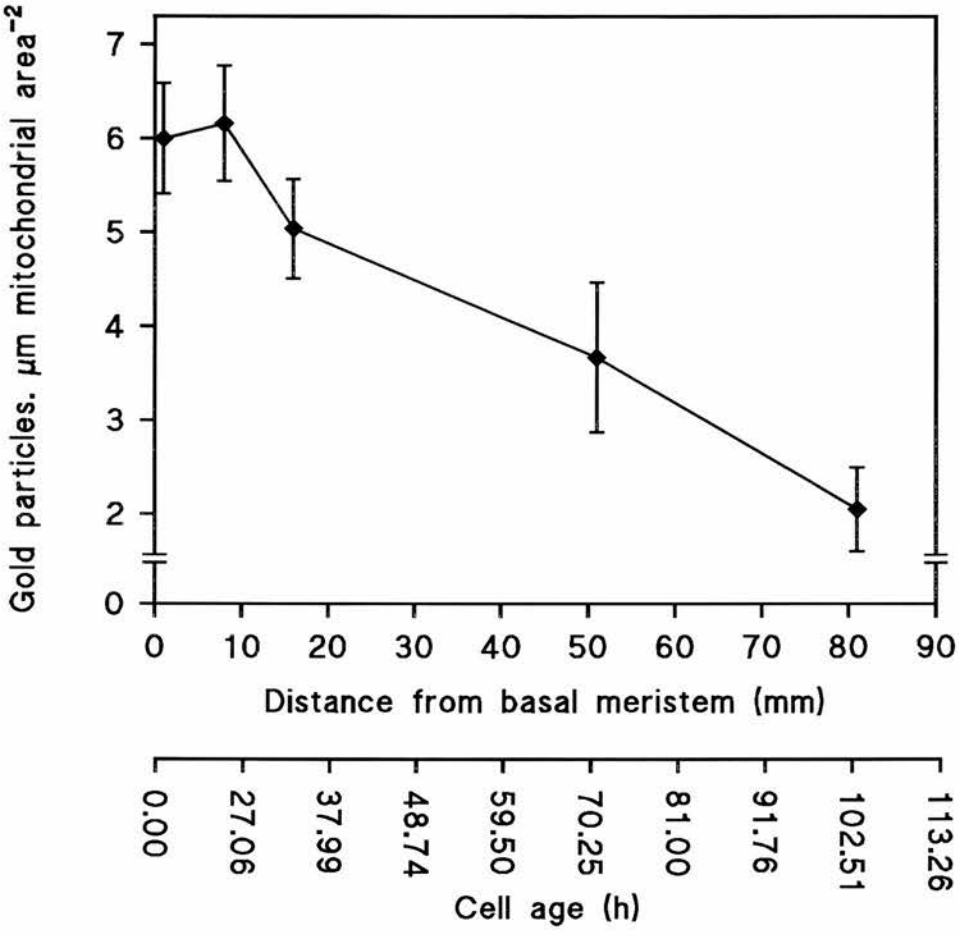

Figure 5.20 Immunogold Localisation of the GDC L-protein Subunit in Companion Cell Mitochondria, along 7d-old Wheat Primary Leaves. See Section 5.2.4. Values represent the mean of four replicates, each from a different batch of plants ± standard errors. See Figure 5.9 for details of leaf section sampling. The cell age corresponding to distance from the basal meristem is also shown (see Section 2.5.3).

5.3 Discussion

5.3.1 Determination of Optimum Antibody Dilutions

Tissue sections were considered optimally labelled, where the immunogold labelling on the mitochondria was significantly different to any other background labelling, i.e. on the cell walls, chloroplasts, or anywhere else on the tissue sections, other than mitochondria.

Background labelling on fixed plant tissue sections can be caused by a number of factors. Non-specific binding of antibodies may occur due to tissue factors such as positively-charged tissue components which attract negatively-charged antibodies (including binding to basic tissue proteins); antigen-mimicking aldehyde sites left in the tissue from fixation; and hydrophobic reactions between tissue components and immunoreagents. Background labelling can also be caused by antibody factors: where polyclonals are used, other antibodies in the antiserum might specifically bind to unknown antigens in the tissue or non-specifically to tissue factors, and in turn be recognised by the secondary antibody. Cross-reaction of the primary antibody with related antigens in the tissue might also occur (Van Noorden, 1993).

In this study, certain negative controls were carried out in order to isolate the source of background labelling. When experiments were run replacing the primary antibody with blocking buffer (i.e. the antibody dilutent), zero labelling was obtained on sections, confirming that the secondary antibody was not a source of non-specific binding via tissue factors. A further negative control substituting the primary antibody for non-immune serum also produced zero labelling, confirming that the secondary antibody was not reacting with any of the other antibodies present in the polyclonal antiserum. In addition to these controls, immunostaining of Western blots (see Section 4.2.2.1) confirmed that in each case, only a single band was detectable, i.e. that only one antigen was being recognised by the secondary antibody. Hence, in the present study, the low level of background labelling observed must have been due to the binding of the primary antibody to tissue factors. Although the immunostaining procedure includes various steps which minimise the presence of tissue factors, these obviously did not completely eliminate the phenomenon.

Although the presence of background labelling should not theoretically affect the comparison of mitochondrial labelling on two different tissue sections, it was necessary to eliminate background labelling to the extent that mitochondrial labelling was not at saturation point. If two different tissue sections were labelled to saturation

point, any differences in protein presence between the two sections would not be detected. For all the proteins under investigation, background labelling was reduced to a very low level. It was also a consideration that the primary antibodies used were donated by other workers and did not constitute an infinite supply. Using the smallest amounts of antibodies possible for an optimum result, was therefore economically sensible.

At the same time, and as already outlined in Chapter 1, complete removal of background labelling was unnecessary and undesirable for comparative quantification of immunogold labelling where zero background was accompanied by zero labelling in some of the structures of interest. If the latter occurred, the scale of any differences observed between different tissue samples might be lost since two different mitochondria showing no labelling might show different labelling densities following experimental procedures that allowed a much higher labelling density. So, it was important to prevent background labelling being reduced to the point where all gold labelling on mitochondria was completely removed, so that comparative quantification of gold labelling density between mitochondria on different transverse leaf sections was possible.

5.3.2 Development of Mitochondrial Proteins in Wheat Primary Leaf Mesophyll and Vascular Tissue

5.3.2.1 Interpreting the Immunogold Data

As already stated, given that young leaf cells convert from a mainly heterotrophic to a more autotrophic role with increasing cell age and the increasing development of photosynthesis and photorespiration, it follows that mitochondrial protein composition will alter with leaf development, adjusting to suit functional requirements. The results of the immunogold labelling experiments of this chapter, are in accordance with the findings of chapter 4 in indicating that different mitochondrial proteins are heterogeneous in their developmental patterns.

As with the slot blot data of Chapter 4, it must be noted that only the *trends* between graphs can be compared - it is impossible to compare actual amounts of protein between graphs as each protein was localised by a different antibody, producing different immunogold labelling densities. It is therefore only possible to compare amounts *within* each graph, and here only relative comparisons can be made, i.e. comparative quantification.

Although mitochondria increase in size and decrease in number with wheat primary leaf development, the total mesophyll cell volume fraction (Vv) occupied by mitochondria remains constant throughout leaf development (Section 3.2.3.3 of present study; Tobin & Rogers, 1992). Any changes in the amount of immunogold labelling of mitochondrial enzymes with leaf development must therefore indicate relative changes in mitochondrial concentration of the localised enzymes in mesophyll cells. However, no data are available regarding possible changes in mitochondrial Vv in phloem companion cells, and it has been assumed that in these cells, mitochondrial Vv also remains constant throughout development. Given that the Vv of the cytoplasm occupied by mitochondria remains constant throughout development, this means that mitochondria always contribute the same proportion of cytoplasmic and therefore mesophyll cell volume. Hence if a protein remains at the same mitochondrial concentration, it also remains at the same cellular concentration with increasing cell age.

5.3.2.2 Relating Immunogold and Slot Blot Data

The results of this chapter indicate that the four subunits of PDC show different developmental patterns in mesophyll cells. This is in accordance with crude-extract analyses such as the results of Chapter 4 and previous studies (Thompson, Bowsher & Tobin, 1998), where a heterogeneous pattern of development was also exhibited. These results also indicate that the concentration of the P-protein and L-protein of GDC increase with leaf mesophyll cell development. Again, this is in accordance with crude-extract analyses such as the results of Chapter 4 and previous studies which indicated an increase in all four subunits of GDC with increasing cell age. In addition, the results indicate different patterns of PDC and GDC development between mesophyll and vascular cells.

In most cases, the patterns of development exhibited by immunogold labelling of mesophyll cells are similar to those of the slot blot data, while the developmental patterns in immunogold-labelled vascular cells generally differ from the slot blot trends. Since the slot blot graphs represent all cell types present in a crude extract, it is possible that these graphs are masking more subtle developmental trends in different cell types. At all stages of development, the volume fraction (Vv) of leaf tissue occupied by mesophyll cells is much greater than that occupied by vascular cells (by a ratio of 8:1, see Section 3.2.2.2), so it follows that the slot blot developmental trend should more closely resemble that of mesophyll cells than that of the vascular cells. Even so, it is

difficult to explain why the mesophyll immunogold and slot blot trends should be so similar, since both were measured in a different way: slot blots relative to cell protein content, and immunogold relative to mitochondrial/cellular concentration.

5.3.2.3 Development of PDC

Each of the four PDC subunits carry out a specific function, and all four must be present and functional in order to catalyse the oxidative decarboxylation of pyruvate at the start of the TCA cycle (Bourguinon *et al.*, 1996). Considering this individual nature of the subunits (see Chapter 1 for a description of subunit functions), it is perhaps not surprising that they exhibit different developmental patterns. As stated before, immunogold localisation indicates the presence and not the activity of the enzymes, but even so, there must be reasons for this heterogeneous development of the amounts of the different PDC subunits with leaf development.

PDC E1α and E1β develop similarly in both mesophyll and vascular cells, peaking and then decreasing in cellular concentration with increasing cell age; whereas PDC E2 and E3 development differs between the two cell types, significantly in the case of E3. The developmental patterns of PDC E1α and E1β in mesophyll cells are in fact similar to the rate of respiration per mesophyll cell along the leaf (relatively constant, but with a slight peak halfway along the leaf - see Section 4.2.1.3), though the peak occurs earlier with E1β. This suggests involvement in respiration. The developmental patterns of PDC E2 and E3 in mesophyll cells however do show similarities with respiration rate per cell, but only in the first half of the leaf. They tend to show a greater similarity to the development of photosynthetic and photorespiratory enzymes, exhibiting an increase in cellular concentration with increasing cell age and development of photosynthetic function, in parallel with the increase in rate of cellular photosynthesis with increasing cell age (see Section 4.2.1.4). While E2 in mesophyll cells showed an increase between the leaf base to tip, the pattern in companion cells showed an increase near the leaf base, which then levelled off along the remaining length of the leaf. PDC E3 showed a notably different pattern of development in companion cells than in mesophyll, decreasing in cellular concentration between the leaf base and tip. If PDC E2 and E3 subunits are involved in photosynthesis or photorespiration, it is acceptable that the developmental patterns in the vascular cells are different from those in mesophyll cells and would not mimic photosynthetic development due to the largely non-photosynthetic nature of vascular cells. It is

therefore possible that these two subunits have dual functions in plant mitochondria, being in some way involved in photosynthetic or photorespiratory pathways as well as respiratory metabolism.

Studies of pea (Miernyk, Camp & Randall, 1985) barley (Lernmark & Gardeström, 1994) and maize (Thelen *et al.*, 1999) reveal that mPDC activity is greatest in young leaf tissue. This relates to high respiratory rates (per unit leaf protein) in young tissue and a high demand for biosynthetic intermediates in developing cells. Only E1α (mesophyll and companion cells), E1β (mesophyll cells) and E3 (companion cells) exhibit a pattern similar to this, though this could be of no consequence since presence of a protein does not necessarily indicate enzyme activity. The trends shown by these three subunits can also be related to rate of respiration per cell, which remains fairly constant along the leaf as a whole, with increasing cell age (though there is a slight peak in respiration rate per cell halfway along the leaf, which relates more to the developmental patterns of PDC E1α). Immunogold labelling indicates cellular protein concentration, and in the zone of elongation when cells are increasing in size, a constant concentration of a particular protein would still equate to an increase in total protein content per cell. Hence, immunogold trends showing a decrease in protein concentration between the leaf base and the tip would perhaps equate to a constant rate of respiration per cell along the leaf, assuming that there was a direct relationship between protein presence and rate of respiration.

In the case of PDC E3, a different developmental pattern to that of the other three subunits might be explained by the possibility that this subunit co-exists as the L-protein of GDC and as a component of the α-oxo acid dehydrogenase complexes. This is the case in pea (Bourguignon *et al.*, 1996), but it has not been established as a rule for all higher plants. In this study though, the developmental trends of PDC E3 and GDC L-protein are very similar in both mesophyll and companion cells. GDC activity has been found to increase with leaf development due to an increase in photorespiratory capacity (Tobin *et al.*, 1989), and if PDC E3 is a component of GDC, an increase in the amount of the subunit in mitochondria with increasing cell age would therefore not be surprising.

In pea, Randall and co-workers have identified various modes of regulation of mitochondrial PDC, including product and metabolite inhibition, compartmentation and reversible phosphorylation (Randall *et al.*, 1989). The results of this chapter indicate that PDC in wheat appears to develop in a heterogeneous manner, and support the

evidence that developmental regulation of PDC in wheat is one factor in the overall regulation and control of this complex.

5.3.2.4 Development of GDC

In mesophyll cells, cellular GDC P-protein and L-protein concentrations increase between the base and the tip in a similar manner to other photorespiratory and photosynthetic enzymes, and parallel the increase in rate of photosynthesis and photorespiration with inceasing cell age (Section 4.2.1.4). In vascular cells, the developmental trend is the opposite, with cellular protein concentration decreasing between the leaf base and tip for both subunits. As with PDC E2 and E3, if the GDC subunits are involved in photosynthesis or photorespiration, it would be expected that different developmental trends would occur in the vascular tissue, where these processes do not occur. GDC is of course involved in photorespiration in plants, and this most likely explains the difference in GDC development between the two cell types examined. Of course GDC is not solely a photorespiratory enzyme, since it exists in animal cells. It is likely however, that in plant cells the primary occupation of this enzyme is in the photorespiratory pathway.

The expression and activity of GDC appears to be light-regulated. Non-photosynthetic or etiolated tissues show low levels of glycine oxidation (Gardeström, Bergman & Ericson, 1980), whereas green tissue shows high levels (Dry & Wiskich, 1985). Furthermore, in wheat, mature leaf tissue has been shown to contain higher levels of GDC activity than younger tissue - since wheat leaf tissue increases in photosynthetic capacity with increasing age, this indicates a positive relationship between GDC activity and cellular photosynthetic activity (Tobin *et al.*, 1989). However, etiolated photosynthetic tissue still shows higher levels of glycine oxidation than etiolated non-photosynthetic tissue (Lernmark *et al.*, 1991). Indeed, in etiolated leaves, up to 70% of GDC L-protein and 25-30% of the P-, H- and T-proteins (Rogers *et al.*, 1991) are retained. The presence of relatively high concentrations of GDC, and relatively high GDC activity in etiolated tissues suggests that light is not the only regulatory factor in the development of this complex (Tobin & Rogers, 1992), and that regulation is also tissue-specific.

The results of the present study further support tissue-specific regulation of GDC expression. While the total mitochondrial concentration of P protein and L protein increased in leaf mesophyll cells, both subunits were found to decrease in concentration

in phloem companion cells. This tissue-specific heterogeneity of GDC is in accordance with previous immunogold localisation studies of GDC. Tobin *et al.* (1989) similarly found that the concentration of GDC P-protein increased in wheat leaf mesophyll cells, and decreased in vascular parenchyma cells, the first demonstration of a heterogeneity in the development of GDC P-protein in wheat leaves. It is not surprising that different cell types with different functions might show differing patterns of enzymatic development, and the most obvious basis for an explanation of the decrease in GDC concentration in vascular cell mitochondria, is the lower photorespiratory activity of these cells, compared to that in photosynthetic mesophyll tissue. In C_4 plants, GDC activity is only present in those cells which contain Rubisco (bundle sheath and not the mesophyll) (Ohnishi & Kanai, 1983). In C_3-C_4 intermediate plants, GDC is confined to the bundle sheaths, even although Rubisco is present in both the bundle sheath and mesophyll (Hylton *et al.*, 1988, Rawsthorne *et al.*, 1988).

This raises the question as to what the function of GDC is in companion cells. If GDC had no particular function, it might be expected that the cellular concentration of thr subunits might remain constant throughout cell development, but in this study it was found that the concentraton of P-protein and L-protein actually decreases with an increase in cell age. Even though photorespiration might not be taking place in these cells, it is possible that glycine oxidation is still taking place, with glycine being transported from elsewhere, e.g. from photosynthetic cells. Assimilation of NH_4^+ (released from glycine oxidation) could be occurring given that both glutamine synthetase and glutamate synthase have both been detected in vascular cells (Tobin & Yamaya, 2001). GDC might therefore be involved in amino-acid synthesis and turnover in companion cells.

5.3.3 Summary and Conclusions

The results of this chapter indicate the existence of a heterogeneity in the total mitochondrial cellular concentration of individual subunits of PDC and GDC present at different leaf developmental stages. This suppors the evidence that developmental regulation contributes to the overall regulation of these two enzyme complexes. In addition, a number of the proteins examined showed different developmental patterns in vascular cells than in mesophyll, suggesting tissue-specific developmental control in these cases also.

This differential development of the subunits can be related to respiratory and

photosynthetic function, and the results suggest that those subunits showing a pattern similar to the development of either respiration or photorespiration, are involved in that pathway.

CHAPTER 6: GENERAL DISCUSSION

6.1 Leaf Growth Studies

The aim of this study was to use the natural developmental gradient of wheat primary leaves as a model to investigate the development of mitochondrial proteins in relation to leaf development. An extensive amount of research has utilised the developmental gradient in leaves of the Gramineae, e.g. in wheat (Dean & Leech, 1982a, 1982b; Topping & Leaver, 1990; Rogers *et al.*, 1991; Tobin & Rogers, 1992; Beemster & Masle, 1996; Hu, Camp & Schmidhalter, 2000), barley (Dale, 1972; Owen, Laybourn-Parry & Wellburn, 1986; Thompson, Bowsher & Tobin, 1998), and various other species.

Before investigating mitochondrial protein biogenesis, the leaf developmental gradient which exists in monocot leaves, was identified and characterised in wheat primary leaves under the particular growth conditions of this study. In Chapter 3, growth studies were conducted involving measurement of leaf growth rate, leaf elongation rate, mesophyll cell number and cell age, with increasing distance from the leaf base. Various stereological measurements were also made between the leaf base and tip, characterising changes in the proportion (V_v) of leaf volume occupied by different tissue types, the frequency of different cell types in the leaf, the proportion (V_v) of mesophyll cell volume occupied by vacuole, mitochondrial transverse area, and the proportion (V_v) of mesophyll cell volume occupied by mitochondria. In addition, microscopical observation of developing leaves (LM) and mesophyll cells (EM), revealed various changes in leaf, tissue and cell morphology with increasing cell age.

In accordance with previous studies on cereal leaves (Tobin, Ridley & Stewart, 1985; Tobin & Rogers, 1992, Thompson, Bowsher & Tobin, 1998) these studies confirmed that a developmental gradient exists in wheat primary leaves between the leaf base and tip. All new cells are produced in the basal intercalary meristem, and are displaced towards the leaf tip as they elongate and develop and cells continue to divide at the leaf base (Nelson & MacAdam, 1989). Cell age increases with distance from the basal meristem so that the youngest cells are located at the base and the most mature cells at the leaf tip. With increasing distance from the leaf base, various changes in leaf tissue and cell morphology take place with increasing cell age. In this study, each stage of development could be equated with a particular cell age, presenting an ideal model for all kinds of developmental studies.

6.2 Changes in Leaf Metabolism with Increasing Cell Age

In living organisms, structure is intrinsically linked with function. Observation of changing cell ultrastructure and compartmentation with increasing cell age therefore suggest that such changes are in association with metabolic changes. In Chapter 4, general metabolic changes along the leaf developmental gradient were also investigated.

The primary leaf soluble protein content per mesophyll cell was found to increase between the leaf base and tip, in accordance with previous studies in wheat (Dean & Leech, 1982a; Topping and Leaver, 1990). SDS-PAGE of leaf polypeptides showed that the protein composition changed with increasing cell age. Given the vital role that proteins play in the functioning of living organisms, this change in cellular concentration and composition of soluble protein suggests metabolic change with development. Indeed, young leaf cells convert from a mainly heterotrophic to a more autotrophic role with age (Tobin *et al.*, 1992), and it follows that cellular protein composition will alter with leaf development, adjusting to suit functional requirements.

In addition, and in accordance with previous studies in cereals, the rate of photosynthesis per mesophyll cell was found to increase (Tobin *et al*, 1988), and rate of cellular respiration remained relatively constant, but with a slight peak halfway along the leaf (Thompson, Bowsher & Tobin, 1998). Rubisco-LSU concentration per cell increased linearly with increasing distance from the leaf base, as found previously in wheat (Dean & Leech, 1982a). These studies served to confirm that metabolic changes take place along with the changing cell ultrastructure and compartmentation found in Chapter 3.

6.3 Investigation of Mitochondrial Protein Development

Having characterised the primary wheat leaf developmental gradient in terms of leaf cell ultrastructure and general metabolism, it was used as a model to investigate mitochondrial protein biogenesis. Mitochondrial biogenesis has received comparatively little attention in recent years, compared to cellular organelles such as chloroplasts. In order to investigate mitochondrial metabolic development, two mitochondrial enzyme complexes were investigated – the pyruvate dehydrogenase complex (PDC) and the glycine decarboxylase complex (GDC). In particular, development of the E1α, E1β, E2 and E3 subunits of PDC, and the P-protein and L-protein of GDC were investigated. These two complexes have important functions in plants.

PDC is a respiratory complex located at a crucial point at the intersection of several metabolic pathways, making it an important site for regulation of carbon metabolism (Miernyk, Thelen & Randall, 1998). With involvement in the entry of carbon into the TCA cycle, it is potentially important in understanding the control of respiratory metabolism (Millar, Knorpp, Leaver & Hill, 1998). GDC, on the other hand, is involved in photorespiration, and provides an interesting comparison to PDC. Since this study involved the examination of both mesophyll and vascular cells, it was interesting to look at two complexes with different functions, with the possibility of different developmental patterns in cell types with different dominant metabolic pathways.

6.4 Detection of PDC and GDC in Crude Leaf Extracts

The investigation of the development of PDC and GDC was initially approached by comparing the relative cellular concentrations of the individual subunits in crude protein extracts taken from whole tissue sections at nine different developmental stages along the primary leaf, between the base and tip. Specific antibodies were used to localise the proteins on slot blots of the protein extracts, and the relative intensities (expressed per mesophyll cell) of the localised polypeptide bands for each developmental stage were compared for each mitochondrial protein.

The six mitochondrial proteins examined were found to exhibit different developmental patterns, which were similar to those obtained using the same technique in barley, where PDC E1α, PDC E1β, GDC P-protein and GDC L-protein were examined (Thompson, Bowsher & Tobin, 1998). Four of the proteins (PDC E2 and E3; GDC P- and L-proteins) showed a developmental trend similar to that of photosynthesis, i.e. an increase between the leaf base and tip, and might suggest involvement in photosynthesis. This is not surprising in the case of the two GDC subunits, but it is interesting that PDC E2 and E3 - apparently involved in respiration - also show this trend. PDC E1α and E1β showed a developmental pattern more similar to that of cellular respiration. With no comparable enzyme activity data, it is difficult to draw conclusions from the results of Chapter 4, but the general finding that the development of these proteins appears to be heterogeneous was a useful basis for the immunogold analysis of Chapter 5.

6.5 Immunogold Localisation of PDC and GDC

Following the immunolocalisation of mitochondrial proteins in crude leaf extracts in Chapter 4, Chapter 5 involved immunogold localisation of the six proteins in tissue from five different leaf developmental stages, using the same specific antibodies. Two cell types were examined – mesophyll and phloem companion cells, so that not only could protein concentration be measured per unit mitochondrial area, but such measurements could be compared in different cell types, impossible with the slot blot technique. The results indicated the relative mitochondrial and cellular concentration of the proteins. Since PDC and GDC are involved in respiration and photorespiration, respectively, it was interesting to see if there would be any difference in protein development between mesophyll cells, where both respiration and photosynthesis take place, and companion cells, which have a minor photosynthetic function.

In mesophyll cells, most of the developmental trends were similar to that of the slot blot data, whereas in companion cells, they were generally different. Since the slot blot results represent all cell types present in a crude protein extract, it is possible that the trends are masking more subtle developmental changes within different cell types, only revealed by the immunogold results. All the proteins examined were present in leaf tissue at all stages of development, as emphasised in Table 6.1 which shows the mean gold particle counts obtained from immunogold studies.

Immunogold localisation showed PDC E1α and E1β to develop similarly in both mesophyll and companion cells, peaking and then decreasing in cellular concentration with increasing cell age. PDC E2 and E3 development, however, differed between the two cell types. The developmental changes in PDC E1α and E1β in mesophyll cells were similar to the rate of cellular respiration along the leaf, as might be expected of a respiratory enzyme. It might be suggested that the contrast in the developmental trends of E1α and E1β in this study was related to differences in the stability of the two subunits (Leuthy *et al*, 2001). However, the fact that the difference in development was supported by two different techniques – slot blot analysis of crude protein extracts and immunogold localisation on tissue sections – suggests tht this is not the case.

The developmental patterns of PDC E2 and E3 in mesophyll cells, showed greater similarities to the development of photosynthetic and photorespiratory enzymes and rates than with the rate of cellular respiration, increasing in cellular concentration with increasing cell age and increased photosynthetic function. If PDC E2 and E3

Distance from basal meristem	PDC								GDC			
	E1α		E1β		E2		E3		P-protein		L-protein	
	M	C	M	C	M	C	M	C	M	C	M	C
0-1mm	8.4	4.4	10.1	6.7	6.5	4.6	7.6	7.6	8.5	7.2	5.9	6.1
7-8mm	9.6	4.8	11.2	7.6	7.5	5.2	8.4	7.4	7.5	6.4	8.3	6.2
15-16mm	11.0	6.4	9.8	8.1	8.5	5.7	12.0	6.9	9.2	7.5	9.5	5.0
50-51mm	11.9	8.5	9.4	7.5	11.1	6.3	12.7	5.3	11.9	5.9	11.7	3.7
80-81mm	8.5	4.7	10.2	8.7	14.7	6.3	12.4	2.8	14.3	4.2	15.7	2.1

Table 6.1 Summary of Immunogold Counts obtained from Localisation of Mitochondrial PDC and GDC in Primary Wheat Leaves. Values are mean gold particle counts per μm mitochondrial area, at each of five developmental stages for both mesophyll (M) and companion (C) cells. Values represent the mean of three replicates, each from a different batch of plants.

subunits are involved in photosynthesis or photorespiration, it follows that the developmental patterns in the companion cells would be different from those in mesophyll cells and would not mimic photosynthetic development since companion cells do not have a significant photosynthetic role. Indeed, the developmental pattern of these two proteins did differ between mesophyll and vascular cells. While mesophyll cell E2 increased from base to tip, the developmental trend in vascular cells showed an increase near the leaf base, and then a levelling off along the remaining length of the leaf. PDC E3 showed a completely different pattern of development in vascular cells than in mesophyll, decreasing between the leaf base and tip in companion cells. It is therefore possible that these two subunits have dual functions in plant mitochondria, being in some way involved in photosynthesis or photorespiration as well as the respiratory pathway.

In mesophyll cells, GDC P-protein and L-protein increased in cellular

concentration between the base and the tip in a similar manner to other photorespiratory and photosynthetic enzymes, and paralleled the increase in rate of photosynthesis and photorespiration with increasing cell age. In vascular cells, the developmental pattern was the opposite, with the cellular protein concentration of both subunits decreasing along the leaf. As with PDC E2 and E3, if the GDC subunits are involved in photosynthesis or photorespiration, it would be expected that different developmental trends would occur in the vascular tissue, where these processes do not occur. GDC is involved in photorespiration in plants, and this most likely explains the difference in GDC development between the two cell types examined. A summary of the results obtained from immunogold localisation studies is shown in Figure 6.1

6.6 Conclusions

The natural developmental gradient present in wheat primary leaves provided a simple and useful model for the investigation of mitochondrial protein biogenesis in this species. Slot blot analysis of mitochondrial protein development, revealed heterogeneity in the development of subunits of PDC and GDC, and subsequent immunogold localisation confirmed this with reference to mitochondrial and cellular protein concentration. These results suggest a change in mitochondrial function with development in wheat, and that this change can depend on cell type and function. As speculated by Tobin & Rogers (1992), changes in mitochondrial protein concentration may be a reflection of a changing role for mitochondria as leaf cells develop. In immature cells with low rates of photosynthesis and photorespiration, respiration rate is high and mitochondria are likely to be the main providers of cytosolic ATP. As cells mature and photosynthesis develops however, chloroplasts could be indirectly providing ATP, diminishing the role of mitochondria in this. In addition, with an increase in rate of photorespiration with increasing cell age, mitochondria become more in demand as sites of glycine oxidation via the catalytic activity of GDC. Measurements of enzyme activity would have been useful in interpreting the results further. This study has contributed to the evidence that changes in leaf and mitochondrial compartmentation occur in association with metabolic changes.

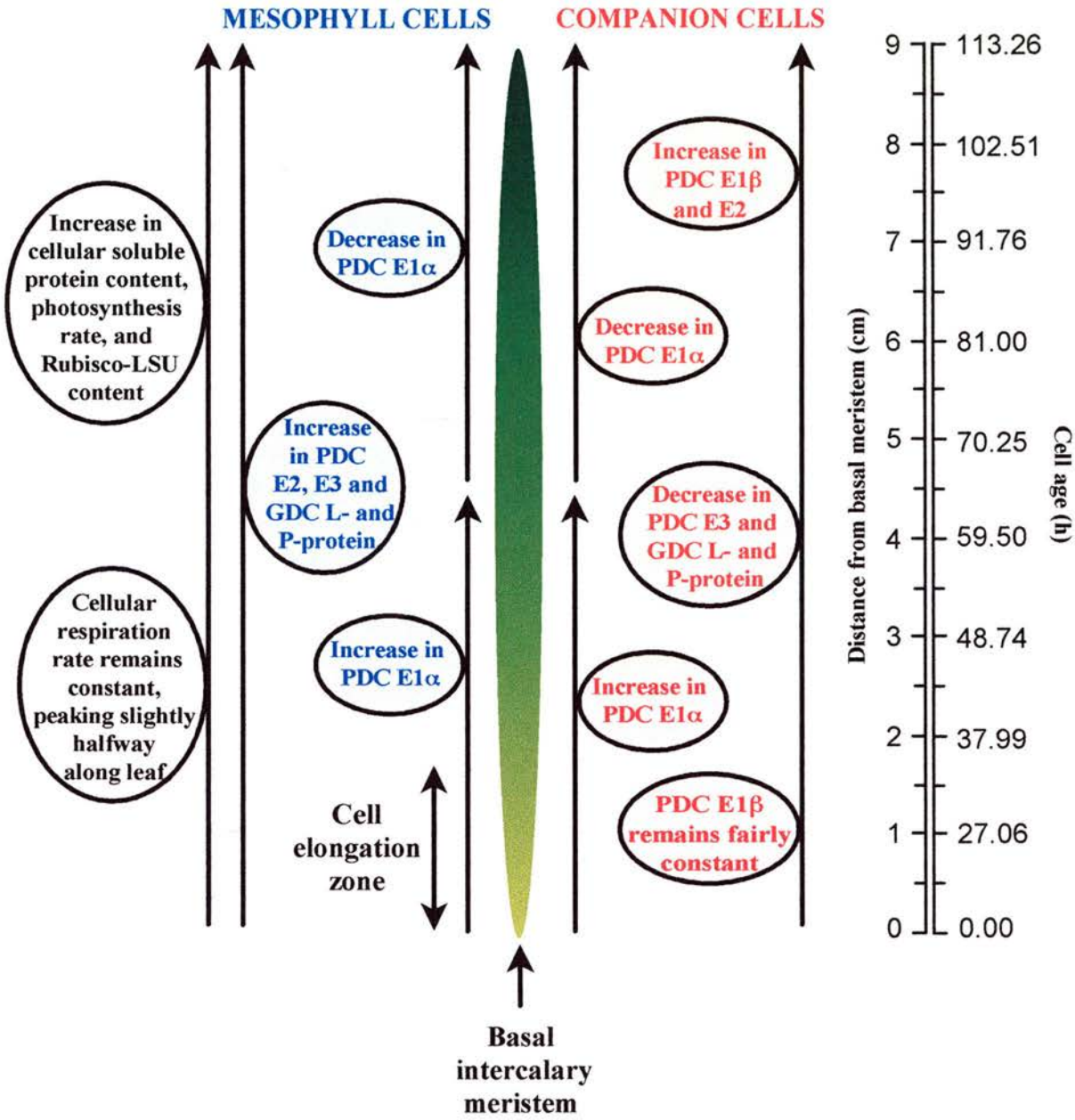

Figure 6.1 Summary of the Results obtained from Immunogold Localisation of Mitochondrial PDC and GDC in Primary Wheat Leaves. Information for mesophyll and companion cells refer to relative cellular protein concentration.

REFERENCES

Affourtit, C., Krab, K. & Moore, A.L. (2001). Control of plant mitochondrial respiration. *Biochimica et Biophysica Acta-Bioenergetics* **1504**: 58-69.

ap Rees, T. (1985). The organisation of glycolysis and the oxidative pentose phosphate pathway in plants. In: *Higher Plant Cell Respiration, Encyclopedia of Plant Physiology, New Series, Vol. 8*, R. Douce & D.A. Day (eds.). Springer-Verlag, Berlin, Germany, 391-417.

ap Rees, T. (1988). Hexose phosphate metabolism by nonphotosynthetic tissues of higher plants. In: *The Biochemistry of Plants, Vol. 14*, P.K. Stumpf & E.E. Conn (eds.). Academic Press, San diego, U.S.A., 1-30.

Avrameas, S. & Uriel, B. (1978). Méthode de marquage d'antigène et d'anticorps avec des enzymes et son application en immunodiffusion. *Comptes Rendus l'Acadamie de Sciences Paris, Series D* **262**: 2543-2545.

Azcon-Bieto, J., Lambers, H. & Day, D.A. (1983). Respiratory properties of developing bean and pea leaves. *Australian Journal of Plant Physiology* **10**: 237-245.

Bagshaw, V., Brown, R. & Yeoman, M.M. (1969). Changes in the mitochondrial complex accompanying callus growth. *Annals of Botany* **33**: 35-44.

Baker, N.R. & Leech, R.M. (1977). Development of photosystem I and photosystem II activities in leaves of light-grown maize (*Zea mays* L.). *Plant Physiology* **60**: 640-644.

Beemster, G.T.S. & Masle, J. (1996). The role of apical development around the time of leaf initiation in determining leaf width at maturity in wheat seedlings (*Triticum aestivum* L.) with impeded roots. *Journal of Experimental Botany* **47**: 1679-1688.

Beesley, J.E. (1993). *Immunocytochemistry: A Practical Approach*. IRL Press, Oxford, U.K.

Beevers, H. (1991). Metabolic compartmentation in plant cells. In: *Compartmentation of Plant Metabolism in Non-Photosynthetic Tissues, Society for Experimental Biology Seminar Series 42*, M.J. Emes (ed.). Cambridge University Press, Cambridge, U.K., 1-21.

Behal, R.H., Browning, K.S., Hall, T.B. & Reed, L.J. (1989). Cloning and nucleotide sequence of the gene for protein X from *Saccharomyces cerevisiae. Proceedings of the National Academy of Sciences of the U.S.A.* **86**: 8732-8736.

Blouin, A., Bolender, R. P. & Weibel, E. R. (1977). Distribution of organelles and membranes between hepatocytes and nonhepatocytes in the rat liver parenchyma: a stereological study. *Journal of Cell Biology* **72**: 441-455.

Boffey, S.A., Ellis, J.R., Sellden, G. & Leech, R.M. (1979). Chloroplast division and DNA synthesis in light-grown and etiolated wheat seedlings. *Plant Physiology* **64**: 502-505.

Bolender, R.P. (1978a). Correlation of morphometry and stereology with biochemical analysis of cell fractions. *International Review of Cytology* **55**: 247-289.

Bolender, R.P. (1978b). Integrated stereological and biochemical studies in hepatic membranes: membrane recovery in subcellular fractions. *Journal of Cell Biology* **77**: 565-583.

Bonen, L. & Gray, M.W. (1997). The mitochondrial genome and its expression. In: *Plant Metabolism*, D.T. Dennis, D.H. Turpin, D.D. Lefebvre & D.B. Layzell (eds.). Addison Wesley Longman Ltd., Harlow, U.K., 166-180.

Bourguignon, J., Merand, V., Rawsthorne, S., Forest, E. & Douce, R. (1996). Glycine decarboxylase and pyruvate dehydrogenase complexes share the same dihydrolipoamide dehydrogenase in pea leaf mitochondria: evidence from mass spectrometry and primary-structure analysis. *Biochemistry Journal* **313**: 229-234.

Bowsher, C.G. & Tobin, A.K. (2001). Compartmentation of metabolism within mitochondria and plastids. *Journal of Experimental Botany* **52**:513-527.

Bradford, M. (1976). A rapid and sensitive method for the quantification of microgram quantities of protein utilizing the principle of protein-dye binding. *Analytical Biochemistry* **72**: 248-252.

Brangeon, J., Hirel, B., and Forchioni, A. (1989) Immunogold localisation of glutamine synthetase in soybean leaves, roots and root nodules. *Protoplasma* **151**: 88-97.

Briarty, L. G. (1975). Stereology: methods for quantitative light and electron microscopy. *Science Progress Oxford* **62**: 1-32.

Brown, T.L. & LeMay, H.E. (1988). *Chemistry: The Central Science,* 4th edition. Prentice Hall Inc., New Jersey, U.S.A.

Brugière, N., Dubois, F., Limami, A.M., Lelandais, M., Roux, Y., Sangwan, R.S. & Hirel, B. (1999). Glutamine synthetase in the phloem plays a major role in controlling proline production. *Plant Cell* **11**: 1995-2012.

Budde, R.J.A. & Randall, D.D. (1988). Regulation of steady state pyruvate dehydrogenase complex activity in plant mitochondria. Reactivation constraints. *Plant Physiology* **88**: 1026-1030.

Campbell, A.K. (1988). *Chemiluminescence: Principles and Applications in Biology and Medicine*. Horwood/VCH, Chichester, U.K.

Canvin, D.T. & Salon, C. (1997). Photorespiration and CO_2-concentrating mechanisms. In: *Plant Metabolism*, D.T. Dennis, D.H. Turpin, D.D. Lefebvre & D.B. Layzell (eds.). Addison Wesley Longman Ltd., Harlow, U.K., 314-340.

Castrillo, M. (1999). Sucrose metabolism at three leaf developmental stages in bean plants. *Photosynthetica* **36**: 519-524.

Coggi, G., Dell'Orto, P. & Viale, G. (1986). Avidin-biotin methods. In: *Immunocytochemistry: Modern Methods and Applications*, 2nd edn., J.M. Polak & S. Van Noorden (eds.). Butterworth Heinemann, Oxford, U.K., 54-70.

Conner, M., Krell, T. & Lindsay, J.G. (1996). Identification and purification of a distinct dihydrolipoamide dehydrogenase from pea chloroplasts. *Planta* **200**: 195-202.

Coons, A.H., Creech, H.J. & Jones, R.N. (1941). Immunological properties of an antibody containing a fluorescent group. *Proceedings of the Society of Experimental Biology and Medicine* **47**: 200-202.

Coons, A.H. & Kaplan, M.H. (1950). Localisation of antigen in tissue cells. *Journal of Experimental Medicine* **91**: 1-13.

Coons, A.H., Leduc, E.H. & Connolly, J.M. (1955). Studies on antibody production. I: A method for the histochemical demonstration of specific antibody and its application to a study of the hyperimmune rabbit. *Journal of Experimental Medicine* **102**: 49-60.

Croxdale, J.G. & Pappas, T. (1987). Activity of glyceraldehyde-3-phosphate dehydrogenase-NADP in developing leaves of light-grown *Dianthus chinensis* L. *Plant Physiology* **84**: 1427-1430.

Dai, H., Lo, Y.-S., Jane, W.-N. & Chiang, K.-S. (1998). Population heterogeneity of higher plant mitochondria in structure and function. *European Journal of cell Biology* **75**: 198-209.

Dai, H., Lo, Y.-S., Wang, T.S. & Chiang, K.-S. (1995). Variation in protein and RNA synthesis activity in isolated mitochondria of the developing rice (*Oryza sativa* L.) panicle. *Theoretical and Applied Genetics* **90**: 1112-1118.

Dale, J.E. (1972). Growth and photosynthesis in the first leaf of barley: the effect of time and application of nitrogen. *Annals of Botany* **36**: 967-979.

Dale, J.E. (1985). The carbon relations of the developing leaf. In: *Control of Leaf Growth. Society for Experimental Biology Seminar Series, No. 27*, N.R Baker, W.J. Davies & C.K. Ong (eds.). Cambridge University Press, Cambridge, U.K., 135-153.

Dale, J.E. (1988). The control of leaf expansion. *Annual Review of Plant Physiology* **39**: 267-295.

Darvill, A.G., Smith, C.J. & Hall, M.A. (1978). Cell wall structure and elongation growth in *Zea mays* coleoptile tissue. *New Phytologist* **80**: 503-516.

Datta, D.B., Cai, X., Wong, P.P. & Triplett, E.W. (1991). Immunocytochemical localisation of glutamine synthetase in organs of *Phaseolus vulgaris* L. *Plant Physiology* **96**: 507-512.

Dean, C. & Leech, R.M. (1980). The co-ordinated synthesis of the large and small subunits of ribulose biphosphate carboxylase during early cellular development within a 7-day-old wheat leaf. *Federation of European Biochemical Societies Letters* **140**: 113-116.

Dean, C. & Leech, R.M. (1982a). Genome expression during normal leaf development. I. Cellular and chloroplast numbers and DNA, RNA and protein levels in tissues of different ages within a seven-day old wheat leaf. *Plant Physiology* **69**: 904-910.

Dean, C. & Leech, R.M. (1982b). Genome expression during normal leaf development. II. Direct correlation between ribulose biphosphate carboxylase content and nuclear ploidy in a polyploidy series of wheat. *Plant Physiology* **70**: 1605-1608.

de Jong, A.S.H., Van Kesse-Van Mark, M. & Raap, A.K. (1985). Sensitivity of various visualisation methods for peroxidase and alkaline phosphatase activity in immunoenzyme histochemistry. *Histochemical Journal* **17**: 1119-1130.

Delesse, M.A. (1847). Procédé mecanique pour déterminer la composition des roches. *Comptes Rendus de l'Academie de Sciences Paris* **25**: 544-545.

De Mey, J. (1986). The preparation and use of gold probes. In: *Immunocytochemistry, Modern Methods and Applications*, J.M. Polak & S. Van Noorden (eds.). John Wright & Sons Ltd., Bristol, U.K., 115-145.

Dengler, N. & Kang, J. (2001). Vascular patterning and leaf shape. *Current Opinion in Plant Biology* **4**: 50-56.

Doerner, P.W. (1994). Cell cycle regulation in plants. *Plant Physiology* **106**: 823-827.

Donnelly, P.M., Bonetta, D., Tsukaya, H., Dengler, R.E. & Dengler, N.G. (1999). Cell cycling and cell enlargement in developing leaves of *Arabidopsis*. *Developmental Biology* **215**: 407-419.

Douce, R., Bourguignon, J., Macherel, D. & Neuberger, M. (1994). The glycine decarboxylase system in higher plant mitochondria - structure, function and biogenesis. *Biochemical Society Transactions* **22**: 184-188.

Douce, R., Bourguignon, J., Neuberger, M. & Rebeille, F. (2001). The glycine decarboxylase system: a fascinating complex. *Trends in Plant Science* **6**: 167-176.

Dry, I.B. & Wiskich, J.T. (1985). Characteristics of glycine and malate oxidation by pea leaf mitochondria: evidence of differential access to NAD and respiratory chain. *Australian Journal of Plant Physiology* **12**: 329-339.

Ebbeson, S.O.E. & Tang, D. (1967). A comparison of sampling procedures in a structured cell population. In: *Stereology, Proceedings of the 2nd International Congress for Stereology*, H. Elias, (ed.). Springer-Verlag, Berlin, Germany, 131-145.

Ebbighausen, H., Jia, C. & Heldt, H.W. (1985). Oxaloacetate translocator in plant mitochondria. *Biochimica et Biophysica Acta* **47**: 184-199.

Elias, H., Henning, A. & Schwartz, D.E. (1971). Stereology: applications in biomedical research. *Physiological Reviews* **51**: 158-200.

Ellis, J.R. & Leech, R.M. (1985). Cell size and chloroplast size in relation to chloroplast replication in light-grown wheat leaves. *Planta* **165**: 120-125.

Fahn, A. (1990). *Plant Anatomy*, 4th edn. Pergamon Press, Oxford, U.K.

Faraday, M. (1857). The Bakerian Lecture: Experimental relations of gold (and other metals) to light. *Philosophical Transactions of the Royal Society of London* **147**: 145-181.

Faulk W.R. & Taylor, G.M. (1971). An immunocolloid method for the electron microscope. *Immunohistochemistry* **8**: 1081-1083.

Food and Agriculture Organisation (FAO) of the United Nations (2001). Agricultural Production statistical database: http://www/fao.org.

Fosket, D.E. (1994). *Plant Growth and Development: A Molecular Approach*. Academic Press, San Diego, U.S.A.

Francis, D. (1992). Tansley Review No. 38: The cell cycle in plant development. *New Phytologist* **122**: 1-20.

Frey, T.G. & Mannella, C.A. (2000). The internal structure of mitochondria. *Trends in Biochemical Sciences* **25**:319-324.

Gardeström, P., Bergman, A. & Ericson, I. (1980). Oxidation of glycine via the respiratory chain in mitochondria prepared from different parts of spinach. *Plant Physiology* **65**: 389-391.

Gemel, J. & Randall, D.D. (1992). Light regulation of leaf mitochondrial pyruvate dehydrogenase complex. *Plant Physiology* **100**: 908-914.

Geoghegan, W.D., Scillian, J.J. & Ackerman, G.A. (1978). The detection of human B-lymphocytes by both light and electron microscopy utilizing colloidal gold-labelled anti-immunoglobulin. *Immunological Communications* **7**: 1-12.

Geronimo, J. & Beevers, H. (1964). Effects of aging and temperature on respiratory metabolism of green leaves. *Plant Physiology* **39**: 786-793.

Giege, P. & Brennicke, A. (2001). From gene to protein in higher plant mitochondria. *Comptes Rendus de l'Academie des Sciences Serie III: Sciences de la Vie* **324**: 209-217.

Glagolev, A.A. (1933). On the geometrical methods of quantitative mineralogic analysis of rocks. *Transactions of the Institute of Economics, Moscow* **59**: 1-14.

Gopalakrishnan, S., Rahmatullah, M., Radke, G.A., Powers-Greenwood, S. & Roche, T.E. (1989). Role of protein X in the function of the mammalian pyruvate dehydrogenase complex. *Biochemical and Biophysical Research Communications* **160**: 715-721.

Gottlob-M^{c}Hugh, S.G., Sangwan, R.S., Blakely, S.D., Vanlerberghe, G.C., Ko, K., Turpin, D.H., Plaxton, W.C., Miki, B.L. & Dennis, D.T. (1992). Normal growth of transgenic tobacco plants in the absence of cytosolic pyruvate kinase. *Plant Physiology* **100**: 820-825.

Grierson, J. & Covey, F. (1988). *Plant Molecular Biology*. Blackie, London, U.K.

Griffiths, G. & Hoppeler, H. (1986). Quantitation in immunocytochemistry: correlation of immunogold labelling to absolute number of membrane antigens. *Journal of Histochemistry and Cytochemistry* **34**: 1389-1398.

Gundersen, H.J.G. & Østerby, R. (1980). Optimising sampling efficiency of stereological studies in biology: or 'Do more less well!' *Journal of Microscopy* **121**: 65-73.

Gunning, B.E.S. & Steer, M.W. (1975). *Plant Cell Biology: an Ultrastructural Approach*. Edward Arnold Ltd., London, U.K.

Hanson, M.R. & Folkerts, O. (1992). Structure and function of the higher plant mitochondrial genome. *International Review of Cytology* **141**: 129-172.

Harlow, E. & Lane, D, (1988). *Antibodies: A Laboratory Manual*. Cold Spring Harbor Laboratory Press, New York, U.S.A.

Hawkesford, M.J. & Leaver, C.J. (1987). Structure and biogenesis of the plant mitochondrial inner membrane. In: *Plant Mitochondria: Structural, Functional and Physiological Aspects*, A.L. Moore & R.B. Beechey (eds.). Plenum Press, London, U.K., 251-263.

Hayakawa, T., Hopkins, L., Peat, L.J., Yamaya, T. & Tobin A.K. (1999). Quantitative intercellular localisation of NADH-dependent glutamate synthase protein in different types of root cells in rice plants. *Plant Physiology* **119**: 409-416.

Hayat, M.A. (1975). *Positive Staining For Electron Microscopy*. Van Nostrand Reinhold, New York, U.S.A.

Hayat, M.A. (1992). Quantitation of immunogold labelling. *Micron and Microscopica Acta* **23**: 1-16.

Heineke, D., Bykova, N., Gardeström, P. & Bauwe. H. (2001). Metabolic response of potato plants to an antisense reduction of the P-protein of glycine decarboxylase. *Planta* **212**: 880-887.

Hernandez, M.L., Passas, H.J. & Smith, L.G. (1999). Clonal analysis of epidermal patterning during maize leaf development. *Developmental Biology* **216**: 646-658.

Hill, S.A. (1997). Carbon metabolism in mitochondria. In: *Plant Metabolism*, D.T. Dennis, D.H. Turpin, D.D. Lefebvre & D.B. Layzell (eds.). Addison Wesley Longman Ltd., Harlow, U.K., 181-199.

Holgate, C.S., Jackson, P., Cowen, P.N. & Bird, C.C. (1983). Immunogold-silver staining - new method of immunostaining with enhanced sensitivity. *Journal of Histochemistry and Cytochemistry* **31**: 938-944.

Hopkins, L. (1997). PhD thesis, University of St Andrews, U.K.

Horisberger, M. (1981). Colloidal gold: a cytochemical marker for light and fluorescent microscopy and for transmission and scanning electron microscopy. In: *Scanning Electron Microscopy II*, O. Johari (ed.). SEM Inc., AMF O'Hare, Illinois, U.S.A., 9-31.

Horisberger, M. & Rosset, J. (1977). Colloidal gold, a useful marker for transmission and scanning electron microscopy. *Journal of Histochemistry and Cytochemistry* **25**: 295-305.

Horisberger, M., Rosset, J. & Bauer, H. (1975). Colloidal gold granules as markers for cell surface receptors in the scanning electron microscope. *Experientia* **31**: 1147-1149.

Howell, K.E., Reuter-Carlson, U., Devaney, E., Luzio, J.P. & Fuller, S.D. (1987). One antigen, one gold? A quantitative analysis of immunogold labelling of plasma membrane 5' nucleotidase in frozen thin sections. *European Journal of Cell Biology* **44**: 318-327.

Hu, Y.C., Camp, K.H. & Schmidhalter, U. (2000). Kinetics and spatial distribution of leaf elongation of wheat (*Triticum aestivum* L.) under saline soil conditions. *International Journal of Plant Sciences* **161**: 575-582.

Hylton, C.M., Rawsthorne, S., Smith, A.M., Jones, D.A. & Woolhouse, H.W. (1988). Glycine decarboxylase is confined to the bundle-sheath cells of leaves of C_3-C_4 intermediate species. *Planta* **175**: 452-459.

Jellings, A.J. & Leech, R.M. (1982). The importance of quantitative anatomy on the interpretation of whole leaf biochemistry in species of *Triticum*, *Hordeum* and *Avena*. *New Phytologist* **92**: 39-48.

Johnstone, A. & Thorpe, R. (1996). *Immunocytochemistry in Practise*, 3rd edn. Blackwell Scientific Publications, Oxford, U.K.

Kellenberger, E. & Hayat, M.A. (1991). Some basic concepts for the choice of methods. In: *Colloidal Gold: Principles, Methods and Applications*, M.A. Hayat (ed.). Academic Press Inc., San Diego, U.S.A., 1-30.

Keys, A.J. & Parry, M.A.J. (1990). Ribulose 1,5-biphosphate carboxylase/ oxygenase and carbonic anhydrase. In: *Methods in Plant Biochemistry Vol. 3: Enzymes of Primary Metabolism*, P.J. Lea (ed.). Academic Press, London, U.K., 1-14.

Ko, K. (1998). Protein synthesis in plant cells. In: *Plant Metabolism*, D.T. Dennis, D.H. Turpin, D.D. Lefebvre & D.B. Layzell (eds.). Addison Wesley Longman Ltd., Harlow, U.K., 17-25.

Köhler, G. & Milstein, C. (1975). Continuous cultures of fused cells producing antibodies of predefined specificity. *Nature* **256**: 495-497.

Köhler, R.H., Zipfel, W.R., Webb, W.W. & Hanson, M.R. (1997). The green fluorescent protein as a marker to visualise plant mitochondria *in vivo*. *Plant Journal* **11**: 613-621.

Krömer, S. (1995). Respiration during photosynthesis. *Annual Review of Plant Physiology and Plant Molecular Biology* **46**: 45-70.

Kruger, N.J. (1997). Carbohydrate synthesis and degradation. In: *Plant Metabolism*, D.T. Dennis, D.H. Turpin, D.D. Lefebvre & D.B. Layzell (eds.). Addison Wesley Longman Ltd., Harlow, U.K., 83-104.

Laemmli, U.K. (1970). Cleavage of structural proteins during the assembly of the head of bacteriophage T4. *Nature* **227**: 680-685.

Lambers, H. (1997). Oxidation of mitochondrial NADH and the synthesis of ATP. In: *Plant Metabolism*, D.T. Dennis, D.H. Turpin, D.D. Lefebvre & D.B. Layzell (eds.). Addison Wesley Longman Ltd., Harlow, U.K., 200-219.

Lambers, H. Day, D.A. & Azcón-Bieto, J. (1983). Cyanide-resistant respiration in roots and leaves. Measurements with intact tissues and isolated mitochondria. *Physiologia Plantarum* **58**: 148-154.

Leech, R.M. (1984). Chloroplast development in angiosperms:current knowledge and future prospects. In: *Topics in Photosynthesis, Vol. 5*, N.R. Baker & J. Barber (eds.). Elsevier, Amsterdam, The Netherlands, 1-21.

Leech, R.M. & Baker, N.R. (1983). The development of photosynthetic capacity in leaves. In: *The Growth and Functioning of Leaves*, J.E. Dale & F.L. Milthorpe (eds.). Cambridge University Press, Cambridge, U.K., 271-307.

Leech, R.M., Rumsby, M.G. & Thomson, W.W. (1973). Plastid differentiation, acyl lipid and fatty acid changes in developing green maize leaves. *Plant Physiology* **52**: 240-245.

Lennon, A.M., Pratt, J., Leach, G. & Moore, A.L. (1995). Developmental regulation of respiratory activity in pea leaves. *Plant Physiology* **107**: 925-932.

Lernmark, U. & Gardeström, P. (1994). Distribution of pyruvate dehydrogenase complex activities between chloroplasts and mitochondria from leaves of different species. *Plant Physiology* **106**: 1633-1638.

Lernmark, U., Henricson, D., Wigge, B. & Gardeström, P. (1991). Glycine oxidation in mitochondria from light grown and etiolated plant tissue. *Physiologia Plantarum* **82**: 339-344.

Logan, D.C. & Leaver, C.J. (2000). Mitochondria-targeted GFP highlights the heterogeneity of mitochondrial shape, size and movement within living plant cells. *Journal of Experimental Botany* **51**: 865-871.

Lorbiecke, R. & Sauter, M. (1998). Induction of cell growth and cell division in the intercalary meristem of submerged deepwater rice (*Oryza sativa* L.). *Planta* **204**: 140-145.

Lorimer, G.H. (1981). The carboxylation and oxygenation of ribulose 1,5-biphosphate: the primary events in photosynthesis and photorespiration. *Annual Review of Plant Physiology* **32**: 349-383.

Luethy, M.H., David, N.R., Elthon, T.E., Miernyk, J.A. & Randall, D.D. (1995). Characterisation of a monoclonal antibody recognizing the E1α subunit of plant mitochondrial pyruvate dehydrogenase. *Journal of Plant Physiology* **145**: 443-449.

Luethy, M.H., Gemel, J., Johnston, M.L., Mooney, B.P., Miernyk, J.A. & Douglas D. Randall, D.D. (2001). Developmental expression of the mitochondrial pyruvate dehydrogenase complex in pea (*Pisum sativum*) seedlings. *Physiologia Plantarum* **112**: 559-566.

Luethy, M.H., Miernyk, J.A. & Randall, D.D. (1996). Plant pyruvate dehydrogenase complexes. In: *Alpha-Keto Acid Dehydrogenase Complexes*, Patel. M.S., Roche, T.E. & Harris, R.A. (eds.). Birkhauser Verlag AG, Basel, Switzerland, 71-92.

Lyndon, R.F. (1983). The mechanism of leaf initiation. In: *The Growth and Functioning of Leaves*, J.E. Dale & F.L. Milthorpe (eds.). Cambridge University Press, Cambridge, U.K., 3-24.

Lyndon, R.F. (1990a). Root and shoot meristems: structure and growth. In: *Plant Development, the Cellular Basis*. Unwin Hyman Ltd., London, U.K., 28-37.

Lyndon, R.F. (1990b). The problems of development: embryogenesis. In: *Plant Development, the Cellular Basis*. Unwin Hyman Ltd., London, U.K., 1-27.

Mahdihassan S. (1984). Outline of the beginnings of alchemy and its antecedents. *American Journal of Chinese Medicine* **12**: 32-42.

Maksymowych, R. & Erickson, R.O. (1973). Analysis of leaf development. Cambridge University Press, Cambridge, U.K.

Margulis, L. (1970). *Origin of Eukaryote Cell.* Yale University Press, New Haven, U.S.A.

Mason, D.Y. & Sammons, R.E. (1978). Alkaline phosphatase and peroxidase for double immunoenzymatic labelling of cellular constituents. *Journal of Clinical Pathology* **31**: 454-462.

Maurice, I., Gastal, F. & Durand, J.L. (1997). Generation of form and associated mass deposition during leaf development in grasses: a kinematic approach for non-steady growth. *Annals of Botany* **80**: 673-683.

McBride, J.T. (1995). Quantitative immunocytochemistry. In: *Image Analysis in Histology, Conventional and Confocal Microscopy*, R. Wooton, D.R. Springall, & J.M. Polak (eds.). Cambridge University Press, Cambridge, U.K., 339-354.

Mettler, I.J. & Beevers, H. (1980). Oxidation of NADH in glyoxisomes by a malate-aspartate shuttle. *Plant Physiology* **66**: 555-560.

Miernyk, J.A., Camp, P.J. & Randall, D.D. (1985). Regulation of plant pyruvate dehydrogenase complexes. *Current Topics in Plant Biochemistry and Physiology* **4**: 175-190.

Miernyk, J.A., Thelen, J.J. & Randall, D.D. (1998). Reversible phosphorylation as a mechanism for regulating activity of the mitochondrial dehydrogenase complex. In: *Plant Mitochondria: from Gene to Function*, I.M. Møller, P. Gardeström, K. Glimelius & E. Glaser (eds.). Backhuys Publishers, Leiden, The Netherlands, 321-327.

Millar, A.H., Knorpp, C., Leaver, C.J. & Hill, S.A. (1998). Plant mitochondrial pyruvate dehydrogense complex: purification and identification of catalytic components in potato. *Biochemistry Journal* **334**: 571-576

Millar, H.A., Leaver, C.J. & Hill, S.A. (1999). Characterisation of the dihydrolipoamide acetyltransferase of the mitochondrial pyruvate dehydrogenase complex from potato and comparisons with similar enzymes in diverse plant species. *European Journal of Biochemistry* **264**: 973-981.

Miranda, V., Baker, N.R. & Long, S.P. (1981). Limitations of photosynthesis in different regions of the *Zea mays* leaf. *New Phytologist* **89**: 165-178.

Mitchell, P. (1985). The correlation of chemical and osmotic forces in biochemistry. *Journal of Biochemistry* **97**: 1-18.

Moore, A.L., Siedow, J.N., Fricaud, A.C., Vojnikov, V., Walters, A.J. & Whitehouse, D.G. (1992). Regulation of mitochondrial respiratory activity in photosynthetic systems. In: *Plant Organelles. Compartmentation of Metabolism in Photosynthetic Tissue. Society for Experimental Biology Seminar Series No. 50*, A.K. Tobin (ed.). Cambridge University Press, Cambridge, U.K., 188-210.

Moore, A.L., Wood, C.K. & Watts, F.Z. (1994). Protein import into plant mitochondria. *Annual Review of Plant Physiology and Plant Molecular Biology* **45**: 545-575.

Munn, E.A. (1974). *The Structure of Mitochondria.* Academic Press, London, U.K.

Nelson, C.J. & MacAdam, J.W. (1989). Cellular dynamics in the leaf growth zone. *Current Topics in Plant Biochemistry and Physiology* **8**: 207-223.

Neubohn B., Gubatz S., Wobus U. & Weber H. (2000). Sugar levels altered by ectopic expression of a yeast-derived invertase affect cellular differentiation of developing cotyledons of *Vicia narbonensis* L. *Planta* **211**: 325-334.

Oda, K., Yamato, K., Ohta, E., Nakamura, Y., Takemura, M., Nozato, N., Akashi, K., Kanegae, T., Ogura, Y., Kohchi, T. & Ohyama, K. (1992). Gene organisation deduced from the complete sequence of liverwort *Marchantia polymorpha* mitochondrial DNA. *Journal of Molecular Biology* **223**: 1-7.

Ogren, W.L. (1984). Photorespiration: pathways, regulation, and modification. *Annual Review of Plant Physiology* **35**: 415-442.

Ohnishi, J. & Kanai, R. (1983). Differentiation of photorespiratory activity between mesophyll and bundle-sheath cells of C_4 plants. I. Glycine oxidation by mitochondria. *Plant Cell Physiology* **24**: 1411-1420.

Oliver, D.J. (1987). Glycine uptake by pea leaf mitochondria: a proposed model for the mechanism of glycine-serine exchange. In: *Plant Mitochondria: Structural, Functional and Physiological Aspects*, A.L. Moore & R.B. Beechey (eds.). Plenum Press, New York, U.S.A., 219-222.

Oliver, D.J. (1994). The glycine decarboxylase complex from plant mitochondria. *Annual Review of Plant Physiology and Plant Molecular Biology* **45**: 323-337.

Oliver, D.J. & Sarojini, G. (1987). Regulation of glycine decarboxylation by serine. In: *Progress in Photosynthesis Research*, J. Biggins (ed.). Nijhoff, The Hague, The Netherlands, 573-576.

Ostareck, D. & Lieckfeldt, E. (1989). Ribulose-1,5-biphosphate carboxylase/oxygenase and gas-exchange characteristics during the development of primary wheat leaves (*Triticum aestivum* L.). *Photosynthetica* **23**: 486-493.

Ougham, H.J., Jones, T.W.A. & Evans, M.L. (1987). Leaf development in *Lolium temulentum* L.: progressive changes in soluble polypeptide complement and isoenzymes. *Journal of Experimental Botany* **38**: 1689-1696.

Owen, J.H., Laybourn-Parry, J.E.M. & Wellburn, A.R. (1986). Leaf respiration during early plastidogenesis in light-grown barley seedlings. *Physiologia Plantarum* **68**: 100-106.

Palade, G.E. (1953). An electron microscope study of the mitochondrial structure. *Journal of Histochemistry and Cytochemistry* **1**: 188-193.

Parry, M.A.J. & Gutteridge, S. (1989). Variation in the specificity factor of C-3 higher plant Rubisco determined by the total consumption of ribulose-P-2. *Journal of Experimental Botany* **40**: 317-320.

Patel, M.S. & Roche, T.E. (1990). Molecular biology and biochemistry of pyruvate dehydrogenase complexes. *Federation of the American Society of Experimental Biologists (FASEB) Journal* **4**: 3224-3233.

Peat, L.J. & Tobin, A.K. (1996). The effect of nitrogen nutrition on the cellular localisation of glutamine synthetase isoforms in barley roots. *Plant Physiology* **111**: 1109-1117.

Plaxton, W.C. (1996). The organisation and regulation of plant glycolysis. *Annual Review of Plant Physiology and Plant Molecular Biology* **47**: 185-214.

Polak, J.M. & Van Noorden, S. (1997). *Introduction to Immunocytochemistry, RMS Microscopy Handbook No. 37*, 2nd edn. Bios Scientific Publishers Ltd., Oxford, U.K.

Possingham, J.V. (1980). Plastid replication and development in the life cycle of higher plants. *Annual Review of Plant Physiology* **31**: 113-129.

Proseus, T.E., Ortega, J.K.E. & Boyer, J.S. (1999). Separating growth from elastic deformation during cell enlargement. *Plant Physiology* **119**: 775-784.

Randall, D.D., Miernyk, J.A., David, N.R., Gemel, J. & Luethy, M.H. (1995). Regulation of leaf mitochondrial pyruvate dehydrogenase complex activity by reversible phosphorylation. *Proceedings of the Phytochemical Society of Europe* **37**: 87-103.

Randall, D.D., Miernyk, J.A., Fang, T.K., Budde, R.J.A. & Schuller, K.A. (1989). Regulation of pyruvate dehydrogenase complexes in plants. *Annals of the New York Academy of Sciences* **573: 192**-205.

Rawsthorne, S., Hylton, C.M., Smith, A.M. & Woolhouse, H.W. (1988). Photorespiratory metabolism and immunogld localisation of photorespiratory enzymes in leaves of C-3 and C-4 intermediate species of *Moricandia. Planta* **173**: 298-308.

Ray, P.M., Green, P.B. & Cleland, R.E. (1972). Role of turgor in plant cell growth. *Nature* **239**: 163-164.

Read, N.G. & Rhodes, P.C. (1993). Techniques for image analysis. In: *Immunocytochemistry, A Practical Approach*, J.E. Beesley (ed.). Oxford University Press, Oxford, U.K., 127-149.

Reynolds, E.S. (1963). The use of lead citrate at high pH as an electron-opaque stain in electron microscopy. *Journal of Cell Biology* **17**: 208-212.

Rhines, F.N. (1968). Introduction. In: *Quantitative Microscopy*, R. T. DeHoff & F. N. Rhines (eds.). McGraw-Hill, New York, U.S.A.

Richards, O.W. & Kavanagh, A.J. (1943). The analysis of the relative growth gradients and changing form of growing organisms illustrated by the tobacco leaf. *American Naturalist* **77**: 385-399.

Robards, A.W. (1970). *Electron Microscopy and Plant Ultrastructure*. M^{c}Graw-Hill Ltd., Maidenhead, U.K.

Robertson, D. & Laetsch, W.M. (1974). Structure and function of developing barley plastids. *Plant Physiology* **54**: 148-159.

Rogers, W.J., Jordan, B.R., Rawsthorne, S. & Tobin, A.K. (1991). Changes to the stoichiometry of glycine decarboxylase subunits during wheat (*Triticum aestivum* L.) and pea (*Pisum sativum* L.) leaf development. *Plant Physiology* **96**: 952-956.

Roth, J. (1983). The colloidal gold marker for light and electron microscopic cytochemistry. In: *Techniques in Immunocytochemistry, Vol. 2*, G.R. Bullock & P. Petruz (eds.). Academic Press, London, U.K., 219-284.

Rylott, E.L., Metzlaff, K. & Rawsthorne, S. (1998). Development and environmental effects on the expression of the C3-C4 intermediate phenotype in *Moricandia arvensis*. *Plant Physiology* **118**: 1277-1284.

Salisbury, F.B. & Ross, C.W. (1992). *Plant Physiology*, 4th edition. Wadsworth, Belmont, USA.

Schnyder, H. & Nelson, C.J. (1988). Diurnal growth of tall fescue leaf blades. I. Spatial distribution of growth, deposition of water, and assimilate import in the elongation zone. *Plant Physiology* **86**: 1070-1076.

Schnyder, H., Nelson, C.J. & Coutts, J.H. (1987). Assessment of spatial distribution of growth in the elongation zone of grass leaf blades. *Plant Physiology* **85**: 290-293.

Schnyder, H., Seo, S., Rademacher, I.F. & Kühbauch, W. (1990). Spatial distribution of growth rates and of epidermal cell lengths in the elongation zone during leaf development in *Lolium perenne* L. *Planta* **181**: 423-431.

Schurer, J.W., Hoedemaeker, P.J. & Molenaar, I. (1977). Polyethyleneimine as tracer particle for (immuno) electron microscopy. *Journal of Histochemistry and Cytochemistry* **25**: 384-387.

Schuster, W. & Brennicke, A. (1994). The plant mitochondrial genome: physical structure, information content, RNA editing and gene migration into the nucleus. *Annual Review of Plant Physiology and Plant Molecular Biology* **45**: 61-78.

Schwabe, W.W. (1984). Phylotaxis. In: *Positional Controls in Plant Development*, P.W. Barlow & D.J. Carr (eds.). Cambridge University Press, Cambridge, U.K., 403-440.

Silk, W.K. & Wagner, K.K. (1980). Growth sustaining water potential distributions in the primary corn root. *Plant Physiology* **66**: 859-863.

Simon, E.W. & Chapman, J.A. (1961). The development of mitochondria in *Arum* spadix. *Journal of Experimental Botany* **12**: 414-420.

Slot, J.W., Posthuma, G., Chang, L.-Y., Crapo, J.D. & Geuze, H.J. (1989). Quantitative assessment of immunogold labelling in cryosections. In: *Immunogold Labelling in Cell Biology*, A.J. Verkleij & J.L.M. Lueunissen (eds.). CRC Press, Boca Raton, Florida, U.S.A., 49-60.

Solomos, T., Malhotra, S.S., Prasad, S., Malhotra, S.K. & Spencer, M. (1972). Biochemical and structural changes in mitochondria and other cellular components of pea cotyledons during germination. *Canadian Journal of Biochemistry* **50**: 725-737.

Spurr, A.R. (1969). A low-viscosity epoxy resin embedding medium for electron microscopy. *Journal of Ultrastructure Research* **26**: 31-35.

Stepp, L.R., Pettit, F.H., Yeaman, S.J. & Reed, L.J. (1983). Purification and properties of pyruvate dehydrogenase kinase from bovine kidney. *Journal of Biological Chemistry* **258**: 9454-9458.

Sternberger, L.A., Hardy, Jr. P.H., Cuculis, I.J. & Mayer, H.G. (1970). The unlabelled antibody-enzyme method of immunohistochemistry. Preparation and properties of soluble antigen-antibody complex (horseradish peroxidase-anti-horseradish peroxidase) and its use in identification of spirochetes. *Journal of Histochemistry and Cytochemistry* **18**: 315-333.

Stierhof, Y.D., Schwarz, H. & Gordon, J. (1986). Transverse sectioning of plastic embedded immunolabelled cryosections: morphology and permeability to protein A-colloidal gold complexes. *Journal of Ultrastructure and Molecular Structure Research* **97**: 187-196.

Stoops, J.K., Cheng, R.H., Yazdi, M.A., Maeng, C.Y., Schroeter, J.P., Klueppelberg, U., Kolodziej, S.J., Beker, T.S. & Reed, L.J. (1997). On the unique structural organisation of the *Saccharomyces cerevisiae* pyruvate dehydrogenase complex. *Journal of Biological Chemistry* **272**: 5757-5764.

Suzuki, S., Nakomoto, H., Ku, M.S.B. & Edwards, G.E. (1987). Influence of cell age on photosynthesis, enzyme activity and metabolite levels in wheat. *Plant Physiology* **84**: 1244-1248.

Tardieu, F., Reymond, M., Hamard, P., Granier, C. & Muller, B. (2000). Spatial distribution of expansion rate, cell division rate and cell size in maize leaves: a synthesis of the effects of soil water status, evaporative demand and temperature. *Journal of Experimental Botany* **51**: 1505-1514.

Taylor, A.E., Cogdell, R.J. & Lindsay, J.G. (1992). Immunological comparison of the pyruvate dehydrogenase complexes from pea mitochondria and chloroplasts. *Planta* **188**: 225-231.

Terry, N., Waldron, L.J. & Taylor, S.E. (1983). Environmental influences on leaf expansion. In: *The Growth and Functioning of Leaves*, J.E. Dale & F.L. Milthorpe, (eds.). Cambridge University Press, Cambridge, U.K., 179-205.

Thelen, J.J., Miernyk, J.A. & Randall, D.D. (1998). Partial purification and characterisation of the maize mitochondrial pyruvate dehydrogenase complex. *Plant Physiology* **116**: 1443-1450.

Thelen, J.J., Muszynski, M.G., David, N.R., Luethy, M.H., Elthon, T.E., Miernyk, J.A. & Randall, D.D. (1999). The dihydrolipoamide acetyltransferase subunit of the mitochondrial pyruvate dehydrogenase complex from maize contains a single lipoyl domain. *Journal of Biological Chemistry* **274**: 21769-21775.

Thompson, P., Bowsher, C.G. & Tobin, A.K. (1998). Heterogeneity of mitochondrial protein biogenesis during primary leaf development in barley. *Plant Physiology* **118**: 1089-1099.

Tobin, A.K., Ridley, S.M. & Stewart, G.R. (1985). Changes in the activity of chloroplast and cytosolic isoenzymes of glutamine synthetase during normal leaf development in wheat. *Planta* **163**: 544-548.

Tobin, A.K. & Rogers, W.J. (1992). Metabolic interactions of organelles during leaf development. In: *Plant Organelles. Compartmentation of Metabolism in Photosynthetic Tissue. Society for Experimental Biology Seminar Series No. 50*, A.K. Tobin (ed.). Cambridge University Press, Cambridge, U.K., 293-323.

Tobin, A.K., Sumar, N., Patel, M., Moore, A.L. & Stewart, G.R. (1988). Development of photorespiration during chloroplast biogenesis in wheat leaves. *Journal of Experimental Botany* **39**: 833-843.

Tobin, A.K., Thorpe, J.R., Hylton, C.M. & Rawsthorne, S. (1989). Spatial and temporal influences on the cell-specific distribution of glycine decarboxylase in leaves of wheat (*Triticum aestivum* L.) and pea (*Pisum sativum* L.). *Plant Physiology* **91**: 1219-1225.

Tobin, A.K., Thorpe, J.R. Jordan, B.R. & Rogers, W.J. (1992). Development and distribution of mitochondrial enzymes in leaves. In: *Molecular, Biochemical and Physiological Aspects of Plant Respiration*, H. Lambers & L.H.W.van der Plas (eds.). SPB Academic Publishing, The Hague, The Netherlands, 177-193.

Tobin, A.K. & Yamaya, T. (2001). Cellular compartmentation of ammonium assimilation in rice and barley. *Journal of Experimental Botany* **52**: 591-604.

Tolbert, N.E. (1997). The C_2 oxidative photosynthetic carbon cycle. *Annual Review of Plant Physiology and Plant Molecular Biology* **48**: 1-25.

Topping, J.F. & Leaver, C.J. (1990). Mitochondrial gene expression during wheat leaf development. *Planta* **182**: 399-407.

Toth, R. (1982). An introduction to morphometric cytology and its application to botanical research. *American Journal of Botany* **69**: 1694-1706.

Towbin, H., Staehelin, T. & Gordon, H. (1979). Electrophoretic transfer of proteins from polyacrylamide gels to nitrocellulose sheets: procedure and some applications. *Proceedings of the National Academy of Sciences of the U.S.A.* **76**: 4350-4354.

Turgeon, R. (2000). Plasmodesmata and solute exchange in the phloem. *Australian Journal of Plant Physiology* **27**: 521-529.

Tzagoloff. A. (1982). *Mitochondria*. Plenum Press, New York, U.S.A.

Umbach, A.L. & Siedow, J.N. (1997). Changes in the redox state of the alternative oxidase regulator sylfhydryl/disulphide system during mitochondrial isolation: implications for inferences of activity *in vivo. Plant Science* **123**: 19-28.

Underwood, E.E. (1969). Stereology, or the quantitative evaluation of microstructures. *Journal of Microscopy* **89**: 161-180.

Unseld, M., Marienfeld, J.R., Brandt, P. & Brennicke, A. (1997). The mitochondrial genome of *Arabidopsis thaliana* contains 57 genes in 366,924 nucleotides. *Nature Genetics* **15**: 57-61

Van Noorden, S. (1993). Problems and solutions. In: *Immunocytochemistry: A Practical Approach*, J.E. Beesley (ed.). Oxford University Press, Oxford, U.K., 208-239.

Van Volkenburgh, E. (1999). Leaf expansion - an integrating plant behaviour. *Plant Cell and Environment* **22**: 1463-1473.

Vauclare, P., Diallo, N., Bourguignon, J., Macherel, D. & Douce, R. (1996). Regulation of the expression of the glycine decarboxylase complex during pea leaf development. *Plant Physiology* **112**: 1523-1530.

Viro, M. & Kloppstech, K. (1980). Differential expression of the genes for ribulose 1,5-biphosphate carboxylase and light-harvesting chlorophyll a/b protein in the developing barley leaf. *Planta* **150**: 41-45.

Walker, J.L. & Oliver, D.J. (1986). Glycine decarboxylase multienzyme complex. Purification and partial characterisation from pea leaf mitochondria. *Journal of Biological Chemistry* **261**: 2214-2221.

Wang, B.L. & Larsson, L.-I. (1985). Simultaneous demonstration of multiple antigens by indirect immunofluorescence or immunogold staining. Novel light and electron microscopical double and triple staining method employing primary antibodies from the same species. *Histochemistry* **83**: 47-56.

Wareing, P.F. & Phillips, I.D.J. (1981). The plant cell in development. In: *Growth and Differentiation in Plants*. Pergamon Press Ltd., Oxford, U.K., 1-20.

Weibel, E.R. (1969). Stereological principles for morphometry in electron microscopic cytology. *International Review of Cytology* **26**: 235-302.

Weibel, E.R. (1973). Stereological techniques for electron microscopic morphometry. In: *Principles and Techniques of Electron Microscopy: Biological Applications, Vol. 3*, M. A. Hayat (ed.). Van Nostrand Rheinhold Co., New York, U.S.A., 237-296.

Weibel, E.R. (1979). *Stereological Methods, Vol. 1: Practical Methods for Biological Morphometry.* Academic Press, London, U.K.

Whatley, J.B. (1974). Chloroplast development in primary leaves of *Phaseolus vulgaris. New Phytologist* **73**: 1097-1100.

Wiskich, J.T. & Dry, I.B. (1985). The tricarboxylic acid cycle in plant mitochondria. In: *Higher Plant Cell Respiration, Encyclopedia of Plant Physiology, New Series, Vol.8*, R. Douce & D.A. Day (eds.). Springer-Verlag, Berlin, Germany, 281-313.